UNITED KINGDOM • CHINA • MALAYSIA

MICROFLUIDIC SYSTEMS FOR NEURONAL CELL CULTURE

Alex Johnstone

Thesis submitted to the University of Nottingham
for the degree of Doctor of Philosophy

November 2015

Abstract

At a high level of abstraction, the brain is a system for analysing sensory information, and responding appropriately. That information is encoded and stored in the millions of neural circuits that comprise the brain. Deciphering this code is essential to understanding how memories are implemented in physiologically normal brain tissue, and to inferring the nature of some neurological disorders affecting memory such as Alzheimer's disease, in which the neural encoding is aberrant or unsuccessful.

One approach to this problem is to reduce the complexity of the brain functionality to three elements: stimuli, response, and reinforcement. The electrical activity of individual neurons can be recorded with electrodes, capturing the pathways of signal propagation in a network of cells. Individual neurons can be also induced to reliably respond to electrical or optical stimuli, so that they initiate, relay, or even block a signal.

If the stimuli to a finite network of cells can be made heterogeneous so that only a sub-population of cells is targeted, then the network can be trained to react in a repeatable way to a given stimulus, testing the concept that the higher order functions of the brain can emerge from a simple set of underlying computational rules.

Training however requires a mechanism for reinforcing only some of the possible pathways, in synchrony with stimuli and in response to the recorded network activity. In the intact brain, this mechanism is pharmacological: a neuromodulator such as dopamine is released throughout the brain, but as it only coincides with some but not all neuronal activity, the reinforcement is temporally selective.

The key task of this project is to emulate this selective neuromodulator reinforcement *in vitro* in a finite neuronal network. The project must also provide capacity for heterogeneous stimulation and individual cell recording, which can be coordinated with the reinforcement under computer control.

The strategy used was to develop microscale chambers to house a small network of cultured neurons. The chambers were integrated with existing cell recording and stimulating technologies, so that specific connections between neurons could be both monitored and induced. Neuronal cultures of a few hundred cells were successfully grown in microchannels, on substrates capable of recording their electrical activity. Thus it was possible to create a small cultured network in which complete network activity could be detected, subject to a sufficiently precise recording technique.

Additionally, a fluid-handling system was developed in order to emulate the continual replenishment of nutrients and soluble gases that are essential to cell survival. The system is intended to deliver soluble chemicals that modulate neuronal activity, on a timescale that is consistent with neuromodulator delivery in the body.

The fluid handling system comprises a set of pressure driven pumps under automated computer control. This system has the capacity to deliver neuromodulator in solution with high spatiotemporal precision. The ability to reliably deliver and wash off precise volumes of drugs in a matter of seconds, with no dilution of the intended concentration, will be of great benefit to researchers investigating the response of various cell types to different agonists.

Acknowledgements

I would like to thank my supervisors Dr Noah Russell and Dr Tomas Bellamy for their support and guidance throughout this journey, and for giving the opportunity to be involved in such a fascinating and challenging project.

I would also like to thank all my colleagues in the Neurophotonics Laboratory Research Group who helped me in so many ways, and for all the great times we have shared.

In particular I would like to thank Solomon Idinyang and Bo Fu for their expertise in LabVIEW programming and their advice in system control.

Thanks to Chris Towlson, Tim Smith, Nitzan Herzog, Paul Goodwin, Wayne Croft and Katharina Reusch for sharing their expertise in cell biology and *in vitro* cell culture.

Thanks to Houda Sahaf, Hala Dhowre, Sebastiaan Van Nuffel and Sunil Rajput for their assistance and advice in surface chemistry.

And thanks to Carmel Howe and Jamie Williams who kept me sane towards the end.

Thanks also to John Hinchliffe and the Engineering Workshop who helped me turn so many of my designs into working prototypes, and to Jas Chauhan, David Taylor, and Chris Mellor for their assistance and advice in cleanroom fabrication.

Finally I would like to thank all my family for their unwavering support and encouragement throughout this PhD.

Table of Contents

Glossary of Abbreviations

AP	Action Potential, a characteristic voltage change associated with neuronal inter-cell signalling. Also called a *spike*
APTMS	*(3-Aminopropyl) trimethoxysilane*, an aminosilane that permits cell growth on glass
Au	Gold (element)
AUT	*11-amino-1-undecanethiol (AUT)*, an aminothiol permitting cell growth on gold surfaces
BBB	Blood-Brain Barrier, a selective membrane separating the brain from the vascular environment
BPRS	Shipley BPR™ positive photoresist, used here to create gold patterns on glass
Ca^{2+}	Calcium ion
CAD	Computer Aided Design
CCD	Charge-Coupled Device, used to convert electrical charge into a digital value, as for camera images
CHO	Chinese Hamster Ovary (cell line type)
Cl^-	Chloride ion
CO_2	Carbon Dioxide (typically gas)
COMSOL	A multiphysics modelling software
CSF	Cerebrospinal Fluid
DAQ	Data Acquisition (card), a signal processing unit permitting parallel computer control of laboratory apparatus
DI / dH_2O	Deionised / distilled water

div	Days *in vitro*, time cultured cells have been growing post-removal from the original organism
.dxf	Drawing Exchange Format, an image file type
EPSP	Excitatory Post-Synaptic Potential
FEM	Finite Element Modelling
FEP	Fluorinated Ethylene Propylene, a plastic
FET	Field Effect Transistor
FITC	*Fluorescein isothiocyanate*, a fluorophore
fMRI	Functional Magnetic Resonance Imaging
GPTMS	*(3-Glycidyloxypropyl) trimethoxysilane*, an epoxysilane
HEK	Human Embryonic Kidney (cell line type)
HPLC	High Pressure/Performance Liquid Chromatography
Hz, kHz, MHz	Hertz, kilohertz, megahertz (frequency)
IPA	Isopropyl Alcohol, a solvent
IPSP	Inhibitory Post-Synaptic Potential
K^+	Potassium ion
LabVIEW	Laboratory Virtual Instrument Engineering Workbench, a visual programming language
LED	Light Emitting Diode
LTD	Long Term Depression
LTP	Long Term Potentiation
mA	milliamp
mbar	millibar, a pressure unit
MEA	Micro-Electrode Array
mg, µg	milligram, microgram: masses
MIF	Metal Ion Free
MPTS	*(3-mercaptopropyl) trimethoxysilane (MPTS)*, a ligand
mPa	milli-Pascal, a pressure unit

mL, µL, nL, pL	millilitre, microlitre, nanolitre, picolitre: volumes
mm, µm, nm	millimetre, micrometre (micron), nanometre: lengths
mM, µM, nM	Millimolar, micromolar, nanomolar: molecular concentrations
ms	Millisecond
mV	milliVolt
MWCO	Molecular weight cut-off
N_2	Nitrogen (typically gas)
Na^+	Sodium ion
NTC	Negative Temperature Coefficient
O_2	Oxygen (typically gas)
OSTE	*Off-stochiometry thiol-ene*, a thiol-allyl polymer
PCB	Printed Circuit Board
PCTE	Polycarbonate
PDMS	poly(dimethylsiloxane), an elastomer
PE	Polyester
PEEK	Polyethylethylketone, a plastic
PEI	Polyethylenimine, a ligand
PET	Polyethylene Terephthalate, a plastic
PID method	Proportional-Integral-Derivative, a feedback control
PDL / PLL	Poly-D-Lysine and Poly-L-Lysine, cell attachment ligands
PS	Polystyrene
PVA	Polyvinyl Alcohol
PWM	Pulse Width Modulation
RMS	Root mean square
ROI	Region of Interest (in an image)
RPM	Revolutions per minute

SH-SY5Y	Human-derived cell line
SiN	Silicon Nitride
SiO_2	Silicon Dioxide
SLAB	Simple Living Artificial Brain
SLM	Spatial Light Modulator
SNR	Signal to Noise Ratio
SPR	Surface Plasmon Resonance
STD	Standard Deviation
STDP	Spike Timing Dependent Plasticity
Ti	Titanium (element)
TiN	Titanium Nitride
UV	Ultraviolet, wavelengths in the range 100 to 400nm
VI	Virtual Instrument, a LabVIEW program element

1 Introduction and literature review

1.1 Motivation: a new system for analysing learning mechanisms in neuronal circuits

One of the outstanding mysteries of brain function is the nature of the encoding and discrimination of information transmitted between neurons, and how this may be related to known phenomena, both ‘higher order’ (learning and behaviour in a complete organism such as a laboratory animal) and ‘lower order’ (physiologically detectable on the order of a single cell).

Top-down theories of learning and behaviour identify areas of the brain according with neurological function, often by damaging a region and noting any detrimental effect. But this does not describe how the functionality is implemented, or how the information imparted is processed (computation). An alternative, bottom-up approach posits that decision-making and memory formation is encoded in the transfer of electrochemical cues between cells. Understanding how this encoding is successfully implemented (or unsuccessfully, in the case of some neurological disorders) is critical.

Signalling mechanisms for the transfer of information in the brain are generally agreed upon: propagation of action potentials along neuronal axons, and synaptic transmission between connected neurons. However, an explicit understanding of how these signals are encoded and interpreted is still unresolved.

One approach to this problem is to reduce the complexity of the system to three elements: stimuli, response, and reinforcement. This would allow for a defined network of neurons to be induced to “learn” a particular pattern of activity in response to a pattern on inputs imposed by the experimenter, testing the concept that the higher order functions of the brain can emerge from a simple set of underlying computational rules. To achieve this goal, it is necessary to devise new experimental tools that can control the number, density, connectivity and activity of neurons, with the further capacity to

modulate activity with external stimuli that can be applied with a speed and spatiotemporal precision that is comparable to signalling mechanisms present in the intact brain. The development of such a system, within the context of a larger project that aims to simulate a “brain in a dish”, is the primary goal of the work described in this thesis.

In this thesis, the strategy used was to develop chambers to house a small network of cultured neurons. The chambers were integrated with existing cell recording and stimulating technologies, so that specific connections between neurons could be both monitored and induced.

Additionally, a fluid-handling system was built in order to replace the continual replenishment of nutrients and soluble gases that are essential to cell survival. The system is intended to deliver molecules that modulate neuronal activity, on a timescale that is consistent with neuromodulator delivery in the body.

The scope of this thesis is to develop a suite of replicable systems and fabrication techniques for achieving these technical goals, as part of a larger collaborative project seeking to decipher neuronal encoding by ensuring complete knowledge of all activity and all environmental cues, and possessing the capacity to adjust the relationship between external input and network response.

The scale of the problem

The mechanism by which an individual neuron receives and relays information is through controlled changes in membrane potential, which induce electrical waveforms known as *action potentials* (APs). At a global level, therefore, the spatiotemporal pattern of action potentials passing through a neuronal network must be the means by which specific computational tasks are achieved by the brain. The association between whole brain regions and particular cognitive functions is also well established, and the intensity and location of neural activity in response to external stimuli has been mapped in the living brain through techniques such as functional magnetic resonance imaging (fMRI).

What is not known is how the patterns of action potentials propagating though a particular set of connected neurons encode information in order to store and retrieve memories. It is also not clear how these same patterns can be mapped to cognitive processes such as learning, in which information is modified, leading to a change in behavioural response. In practical terms, an attempt to map all of the synapses and all of the action potentials in an intact brain is not feasible. A recent study analysing the connectivity of a small region of neocortex highlights the scale of the problem (Kasthuri et al. 2015). Accordingly, simplification is essential if a realistic attempt to identify key mechanisms of patterning and reinforcement is to be mounted.

The Neurophotonics Laboratory (NPL) at the University of Nottingham is developing a system that will permit an artificial environment to interact with a small network of cultured neurons in real time, so that both environment input and network response are fully known, and the correlation between them can be inferred.

We posit that to decipher the neural encoding requires complete knowledge of the inputs into that finite network of connected neurons, and complete knowledge of the response of each neuron in the network. Furthermore, a reinforcement mechanism that encourages some but not all connections is critical, since without this there is no systematic incentive for the network to follow a particular propagation path over all alternatives, and so no learning can occur.

A novel system, consisting of a subset of cultured neural cells interfacing with a fully-controlled and monitored environment in a feedback paradigm, is proposed, to emulate brain activity and interaction with an environment. It is desirable that none of the information in the system is hidden or lost. The more information that is missing, the harder it will be for the neural encoding to be deciphered. This is analogous to attempting to decipher a written code from excerpts with missing words and incomplete sentences.

Thus knowledge of the total culture activity, coupled with the capacity to detect and discriminate individual neuron signalling, is essential. This system will therefore use only a few hundred cultured cells, thereby significantly

reducing the total amount of electrical activity information that must be detected and processed.

This project focuses upon the development of an experimental system for rapid, controlled delivery of neuromodulator to neurons grown in culture, on a confined scale that allows all the neural signals to be captured.

1.2 Neuroscience in the intact brain

1.2.1 The physicochemical environment *in vivo*

To determine the technical requirements of an artificial system that is intended to emulate the healthy brain, it is necessary to understand what physicochemical parameters are critical for long-term neuronal survival, and what their typical ranges are *in vivo*.

In the intact brain, neuronal cells are contained within a flexible, soft matrix of glycoprotein, known as the extracellular matrix (ECM) (Ricks et al. 2014). This matrix protects the cells from any shear forces induced by the circulating Cerebrospinal Fluid (CSF), meaning that molecular transport to and from the cells is dominated by diffusion rather than convection.

The *extracellular* volume is the complete volume of the brain consisting of all the spaces between individual neurons. The *intracellular* volume is the total volume of all neurons, where a single neuron is of the order of 1-10 picolitres (10^{-12} L) (Kuffler, S., Nicholls, J., & Martin 1984) . *In vivo*, these volumes are of the same order of magnitude and the extracellular volume is smaller than the total intracellular volume (Duong et al. 2001) This means cells are tightly packed together, with little unoccupied volume between them. Local and global concentrations of ions, neurotransmitters, and other solutes are tightly regulated both in release and uptake, and the diffusion distances between cells are typically very short: a synaptic cleft is usually no more than 20nm across.

pH is a measure of how acid or alkaline a solution is. Many of the enzymes and proteins essential for homeostatic regulation and metabolic processes are optimised to work within very specific pH ranges, and will denature, losing their biological function, if taken out of that range. The CSF *in vivo* is typically

maintained at a pH of 7.5, and it is noted that increasing pH increases neuronal excitability while lowering pH reduces it (Obara et al. 2008).

Soluble gases in the circulating CSF are typically 5% CO_2 and 5% O_2 (Zhu et al. 2012). The acidic CO_2 balances the alkaline bicarbonate (HCO_3^-) which the cells generate, keeping the *in vivo* pH in the correct range.

Osmolarity, or osmotic concentration, is the concentration of dissolved ions per unit volume. Salts such as Sodium Chloride (NaCl) naturally dissolve into Na^+ and Cl^- ions. If the osmolarity of an extracellular solution differs considerably from that of the cell interior, then water will cross the cell membrane to redress the imbalance. If water is drawn out of the cell by a higher (hypertonic) external concentration, the cell will shrivel up, while if the external concentration is too low (hypotonic), water is drawn into the cell until it bursts. Both conditions are lethal. *In vivo*, the isotonic osmolarity of the CSF is 280-300 milli-Osmoles, and is regulated by daily production of salts and proteins in the CSF.

Pressure: The brain is maintained at a pressure greater than the environment outside the body. *In vivo* CSF pressure is typically 2.1 to 2.3 kPa (21 to 23 mbar) above atmospheric.

Perfusion: In order to recirculate the CSF in the brain, the choroid plexus region continually releases high levels of sodium ions, creating an osmotic imbalance. Chloride ions are drawn into this region, inducing water circulation. CSF circulates at around 0.4µL/s (400nL/s) in the capillaries that branch to individual neurons. However, as noted previously, the shear effect of this flow rate is mitigated by the ECM surrounding each cell.

These general homeostatic features of the healthy brain must be borne in mind when designing an *in vitro* system, and external physicochemical control to regulate these parameters within the physiological range will be necessary.

1.3 **Neurons and action potentials**

Every neuron in a network is linked to several others via *synapses*, which are extremely small inter-cellular gaps between the axon terminal of a presynaptic

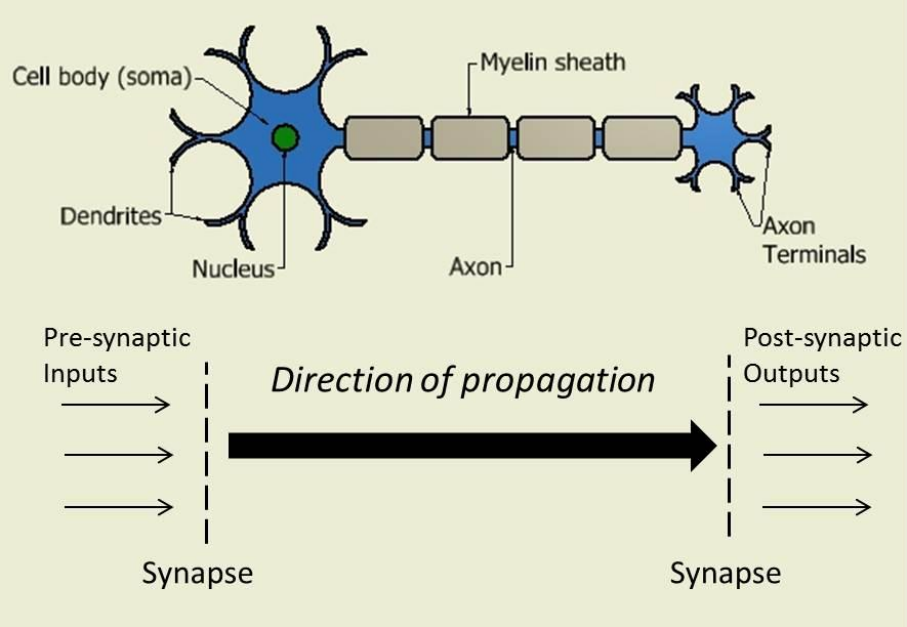

Figure 1 Schematic of a neuron, showing the direction of signal propagation from dendrite to axon

neuron and the dendrite of a postsynaptic neuron (Kuffler, S., Nicholls, J., & Martin 1984).

A neuron is essentially formed of a central body (soma) connected to a transmission element (axon). The axon branches to form presynaptic terminals, each of which abuts across the synapse to a *post*-synaptic neuron. The neuron also has potentially hundreds of reception elements (dendrites) each receiving inputs from presynaptic neurons. These chains of interconnected cells form the neuronal network.

1.3.1 **The resting potential**

The neuronal membrane is a lipid bilayer a few nm thick which is impermeable to ions. The exterior of the cell is characterised by high concentrations of negatively charged chloride (Cl^-) ions and positively charged sodium (Na^+) ions, while the interior of the cell has higher concentrations of positively charged potassium (K^+) ions.

This comes about because the ion exchanger Na^+/K^+-ATPase actively pumps 2 K^+ ions into the cell for every 3 Na^+ ions that are removed. This acts in part

to counter the occasional leakage of ions through the membrane, which is not perfectly impermeable. Because the exterior of the cell membrane is now

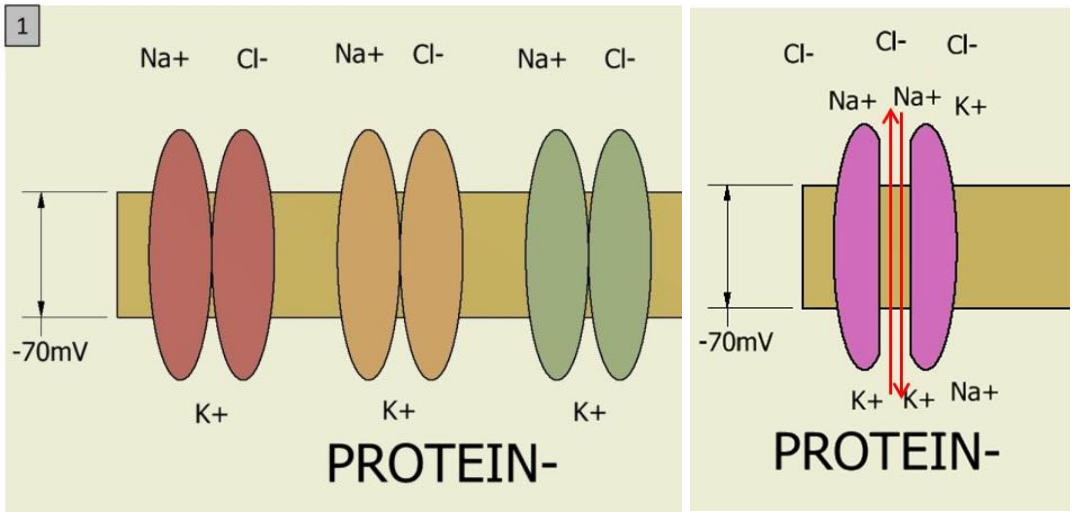

Figure 2 The resting transmembrane potential, with high extracellular sodium and intracellular potassium concentrations, creating a potential difference of 70mV. This is maintained by the ion exchanger (right, magenta),which continually pumps sodium out and potassium in.

more positive than the interior, an electric potential difference is formed (see Figure 2).

The heterogeneity in charge distribution creates an electrochemical gradient, causing a potential difference across the membrane called the *transmembrane potential*, and since the exterior of the membrane is always considered to be ground (0V), the transmembrane potential is denoted negative. At rest, this potential is around -70mV (Kuffler, S., Nicholls, J., & Martin 1984).

1.3.2 Ligand-gated ion channels

The membrane contains embedded proteins which can change their conformation, opening pores in the membrane known as *ion channels*. Unlike the ion pump which exchanges sodium and potassium, the channels are simply gaps in the membrane permitting ions to travel down the concentration gradient and either enter or exit the cell. The stimulus to open these proteins can be ligand-gated. At the synapse, molecules of neurotransmitter, such as glutamate, are released from a presynaptic vesicle, into the synaptic cleft between dendrite and axon (Zhou & Danbolt 2014). In this case (see Figure 3), a neurotransmitter molecule triggers a post-synaptic receptor on a dendrite, and a sodium channel opens. Sodium ions now pass into the cell

interior until the channel closes, adding positive charge and raising the transmembrane potential from -70mV closer to 0V. This is referred to as *depolarisation*.

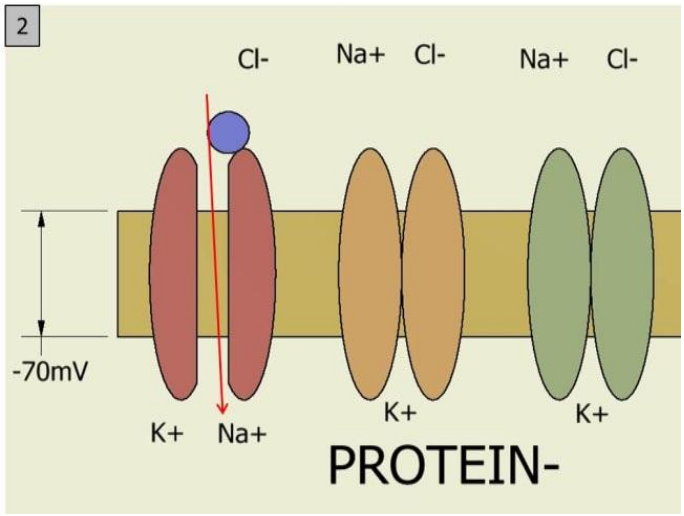

Figure 3 A neurotransmitter (blue) causes a sodium ion channel (red) to open

caused by ligand-gated ion channel from a pre-synaptic axon is known as an Excitatory Post-Synaptic Potential (EPSP).

Alternatively, the neurotransmitter may open a potassium ion channel. In this case, the concentration of potassium ions inside the cell drops, making the internal charge more negative, and the membrane potential drops below -70mV. This is referred to as *hyperpolarisation* and leads to Inhibitory Post-Synaptic Potential (IPSP).

1.3.3 Threshold potential, depolarisation

If only a few ligand-gated sodium ion channels open within a short period of time, then the Na^+/K^+-ATPase pump will remove the additional sodium before the transmembrane potential can significantly increase. If, however, a significant number of ion channels are opened simultaneously, then the transmembrane voltage crosses a threshold (typically -55mV), and other voltage-gated sodium ion channels open (see Figure 4). The EPSP propagates along the dendrite to the cell soma, and if a sufficiently high number of *ligand-gated* sodium ion channels, on one or more dendrites, open within in a short space of time (temporal summation), the membrane potential crosses a certain threshold. This opens many more *voltage-gated* ion

channels in the *soma* (the central body), and rapidly increases the rate of ion movement, causing the membrane potential to rise above 0V. When the membrane potential has crossed the threshold value, the neuron is said to have been *triggered* to *fire*.

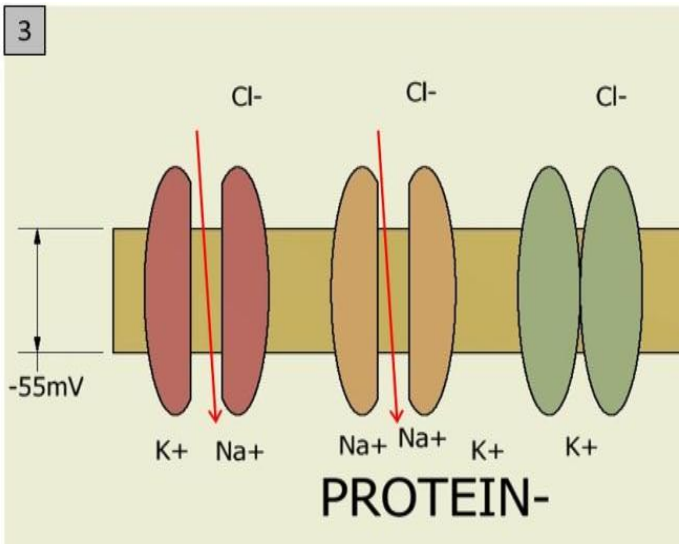

Figure 4 If the transmembrane potential crosses a threshold, other sodium ion channels open

The number of sodium ions entering the cell is now so high that the Na^+/K^+-ATPase pump cannot compensate for it, and so the transmembrane voltage rises until it becomes positive – there are so many positive ions inside the cell that the interior is more positive than the exterior.

1.3.4 Potassium ion channels open, hyperpolarisation

When the membrane potential crosses +40mV, the sodium ion channels begin to close, but potassium (K^+) ion channels begin to open, permitting K^+ transport out of the cell (see Figure 5). The Na^+/K^+-ATPase pump is now able to reduce the high internal concentrations of sodium, but cannot keep pace with the loss of potassium. The net effect is rapid loss of positive charge inside the cell.

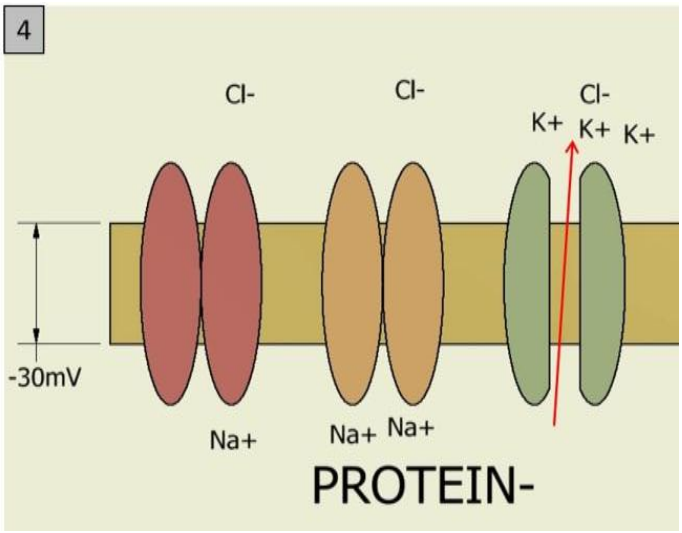

Figure 5 Potassium channels begin to open as the transmembrane potential increases

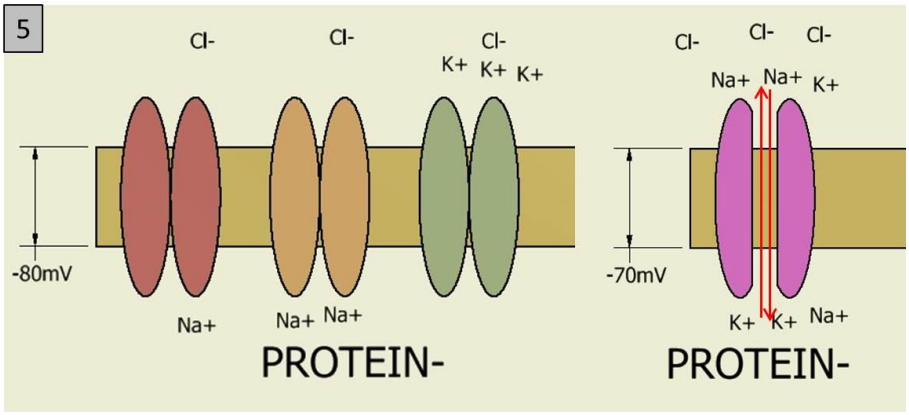

Figure 6 All ion channels are now closed. The ion exchanger acts to restore the concentrations of potassium and sodium that were present in Figure 2

This is the *polarising* phase, during which the transmembrane potential drops rapidly from its maximum of +40mV to a state of *hyperpolarisation*, below the resting potential.

1.3.5 **Refractory period**

As the transmembrane potential drops, the voltage-gated potassium channels also close. There are now no routes for passive ion transport across the membrane, and the Na^+/K^+-ATPase pump can begin restoring the resting concentrations of potassium inside the cell and sodium outside it.

Voltage-gated sodium ion channels which have closed after hyperpolarisation cannot be induced to open again for some time afterwards. During this time, known as the *refractory period*, the neuron therefore cannot fire again.

This sequence of changes in membrane potential, mediated by controlled changes in Na^+ and K^+ flux, is the *action potential* (see Figure 7)

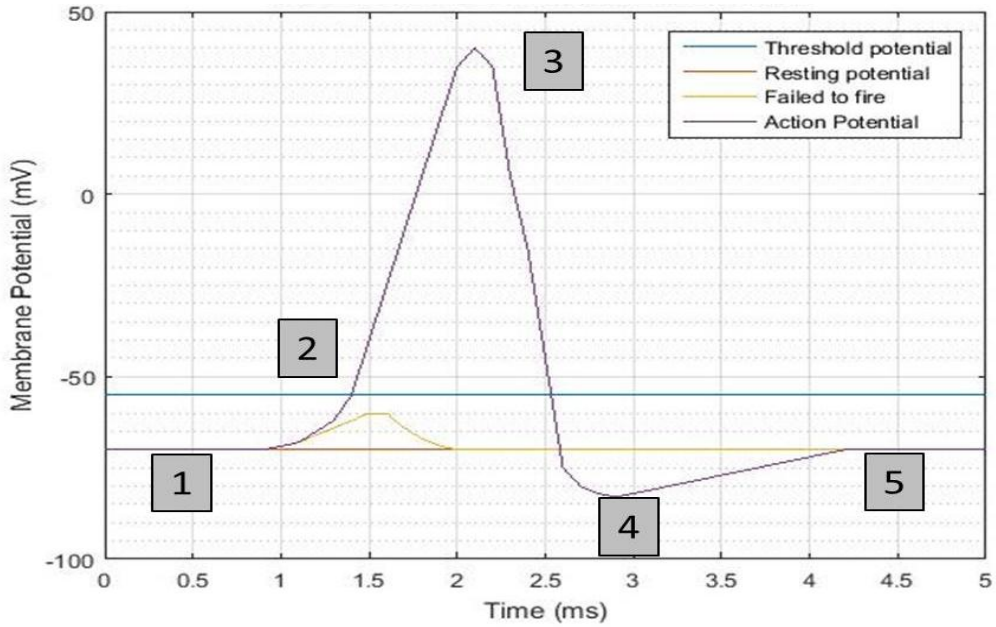

Figure 7 The progress of an Action Potential (see also figures 2 to 6). This characteristic voltage change is also called a *spike*.

Once initiated (often in the axon hillock next to the soma), it propagates along the axon as adjacent regions of the cell membrane depolarise in turn. For rapid propagation over long distances, so called *saltatory conductance* is observed, due to selective myelination of the axon, which forms an insulating layer that limits ion flow to small regions of the axon known as Nodes of Ranvier (Kuffler, S., Nicholls, J., & Martin 1984). This increases conductance velocity, compared to simple passive voltage propagation.

1.3.6 Temporal synchronisation and synaptic plasticity

As the channels are activated by neurotransmitter, this means that a certain number of EPSPs must occur simultaneously, in order to sum to the threshold necessary to induce an excitatory post-synaptic potential. The timescale typically reported for this superimposition of depolarisation events, called *coincidence detection*, is 10-20ms. (Tovee 1994) (Yagishita et al. 2014).

The probability that synaptic transmission will trigger an action potential depends on several factors. The first is the probability of presynaptic neurotransmitter release – if this is high, then every action potential that

reaches the synapse in the presynaptic cell is likely to be effectively transduced into a postsynaptic response. If release probability is low, however, then temporal summation of presynaptic action potentials will be necessary to initiate synaptic transmission. The second determinant is the amount of neurotransmitter released during the synaptic event. The third determinant is the density of receptors in the postsynaptic membrane. If density is high, then many ion channels will be opened and the amplitude of the EPSP will be substantial. All of these parameters will determine how many synaptic events are needed to provoke a postsynaptic response, and how much each individual synapse contributes to the EPSP.

These considerations are particularly important, because many physiological mechanisms have been identified that can change synaptic strength. All of the preceding parameters can be altered by cell signalling pathways that modulate the proteins that mediate synaptic release and transmission. A major mechanism for synaptic plasticity is *coincidence detection* (Bi & Poo 1998; Bi & Poo 2001). This concept depends on postsynaptic depolarisation being closely synchronised with presynaptic release, leading to a reinforcement of synaptic strength (and so an increase in the EPSP generated by such synapses). This is the basis of so-called long-term potentiation (Bliss & Lomo 1973), where a period of coincident stimulation leads to long lasting increase in synaptic strength (Gruart et al. 2015). Such changes are termed “synaptic plasticity” and are believed to be the cellular correlate of learning and memory (Martin et al. 2000).

A different kind of coincidence detection which has also been implicated in synaptic plasticity, involves the extrasynaptic activation of modulatory receptors that do not themselves alter membrane potential, but can couple to signalling pathways that alter synaptic strength. A well-known example is the dopaminergic fibres that run throughout the brain, and periodically release the neuromodulator dopamine across large regions of the brain, including the hippocampus, simultaneously (Björklund & Dunnett 2007). It is hypothesised that if a synapse is active in close temporal proximity to the dopamine surge (which time window is still debated, but it should not be more than a few seconds), then it will be reinforced, while any synapse where this is not the

case will not be reinforced. This means that those specific patterns of synaptic firing will ultimately emerge from a random background of activity.

By adjusting the timing of the dopamine release to coincide with particular patterns of network activity, it may be possible to reinforce particular connections, and at the same time discourage others that are not coincident. The strong connection set could further be altered over time by changing the timing of the dopamine release. Such temporal control over the drug is not feasible *in vivo*, but could theoretically be implemented *in vitro*.

The ability to recreate these kinds of temporal associations between synaptic release from presynaptic cells, responses in postsynaptic cells, and extrasynaptic delivery of neuromodulators such as dopamine, would be essential for testing key concepts about how coincidence detection can be used to entrain neuronal networks to particular patterns of activity. This therefore represents another challenge for our system design to overcome.

1.1.1 **1.3 Methods for measuring neuronal activity**

1.3.1 *In vivo* recording techniques

Experiments involving the entire brain *in vivo* can demonstrably associate certain neural structures with organism behaviour, and with particular environmental inputs. This may be achieved by inhibiting connections with inhibitory agonists, or though surgery which permanently severs the connections. A less invasive approach is through *neuroimaging*, in which the neural activity in a region is indirectly measured by monitoring an associated physiological variable.

In the case of fMRI, this is the oxygen level of blood perfused in the vicinity of the tissue being scanned, which indicates how much glucose is being taken up by the cells. The imaging has a spatial resolution of 2-3mm^3 (Rey et al. 2015). As a neuron is typically 10-20μm across, this equates to several hundred neurons in each direction.

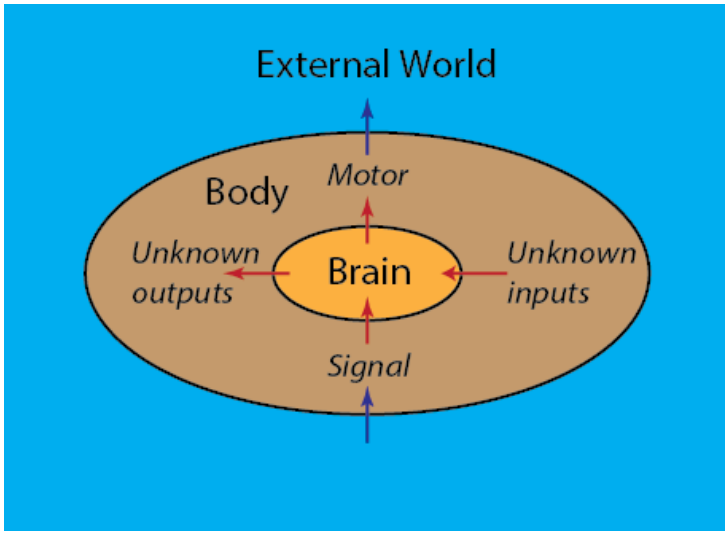

Figure 8 The Entire brain linked to an external environment (which includes the body). The one stimulus-response relationship of interest (represented by the vertical arrows) is masked by the hundreds of other environmental and metabolic processes occurring simultaneously (horizontal arrows) and which cannot be measured, and the total information being acquired and processed at any given moment is simply too large to be easily handled.

Measuring individual action potentials, also known as *spikes* due to their short duration, in the intact living brain (*in vivo*) is possible with microelectrode techniques, but clearly only samples from a tiny fraction of the vast interconnected network of neurons. An experimenter has little direct knowledge of what most of the individual neurons are doing. Such invasive methods also require the subject to anaesthetised and the tissues traumatised, which may have considerable bearing on the activity subsequently recorded.

This approach minimally affects the physicochemical stability of the brain, because the animal is alive and healthy. It can thus be assumed that the physiological responses of the cells are as close as possible to the responses under normal conditions, which is a great advantage of *in vivo* methods.

Essentially, however, any investigation in the intact brain is complicated by the sheer number of simultaneously active connections, and the limited control of the experimenter over what stimuli the neurons receive from other areas of the brain (see Figure 8). Thus the specific input associated with a specific action potential cannot be known with certainty, and certainly not across the entire region of interest. It is extremely difficult for an observer to

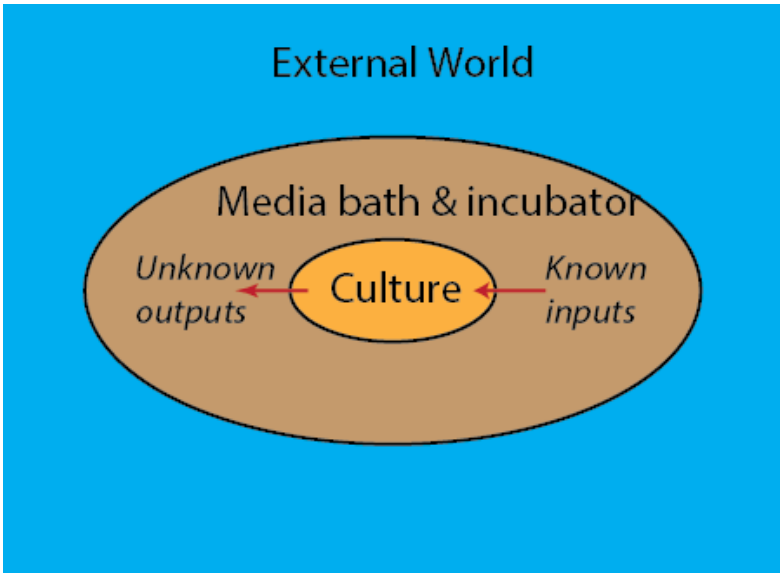

Figure 9 *In vitro* culture with artificial body and no environmental links. Although some or all of the bath culture inputs are known due to the composition of the media and the regulation of the incubator, as well as knowledge of the agonists delivered, the cell response is not readily discernible.

isolate their functionality, or to be certain that the response is not to some other unknown input from the body or external environment.

To effectively understand how the patterns are being processed and encoded, without ambiguity regarding what network responses are associated with certain stimuli, it is desirable to somehow remove the network from a partially known environment and place it in a system in which all inputs and outputs are known and regulated by the experimenter. Such a system cannot exist *in vivo*.

1.4 *In vitro* culture

The alternative approach to *in vivo* is to culture a relatively small number of cells *in vitro* by removing them from the intact brain, disassociating them from the ECM and breaking the existing synapses, and placing a suspension of cells into an environment that meets their physiological requirements (see Figure 9).

By doing this, the functionality of the original tissue section is lost and the cultured cells are no longer representative of intact tissue. However, since we have established that the recording of all network activity down to every single spike cannot be undertaken *in vivo*, this is a rational alternative approach. It makes possible the complete recording of electrical activity in a set of cultured

neurons, but that set should not be considered functionally identical to an *in vivo* network.

1.4.1 Emulating the physicochemical environment

The first obstacle to overcome, is maintaining a population of neurons in an *in vitro* environment. Tissue culture and the sub-discipline of cell culture has been a distinct field for over a hundred years (Harrison 1907). The use of culture media rich in essential salts, proteins and minerals, and in particular the development of completely synthetic supplements that can replace natural serums whose precise formulation is unknown (Brewer et al. 1993), allows the culturing of cells *in vitro* and the observation of cell behaviour independent of the animal.

All mammalian cells cultured *in vitro* require delivery not only of essential chemicals and proteins, but also of oxygen (O_2) and carbon dioxide (CO_2), which *in vivo* would be delivered by the bloodstream. Consequently cells are cultured in an incubator kept at 37°C with high humidity to prevent the drying out of media, and with 5% CO_2 mixed into the air. The O_2 content is generally left at atmospheric levels (20-21%).

Any experimental apparatus on which cells are to be observed and investigated for any length of time must also meet these conditions.

In order to maintain the desired osmolarity and salinity, 50% by volume of the media can be replaced every 2-3 days. This also replenishes the vital proteins and minerals, but imposes an osmotic shock on the cells.

Neuronal cells cannot directly adhere to glass, and so a chemical link (ligand) is needed to prepare a surface for them to adhere to. For example, Poly-L-Lysine (PLL) is pipetted onto a glass surface and left for a minimum of 30 minutes to form a uniform layer on the glass, before washing with distilled water (dH_2O).

In order to optimise the chance of culture survival, robust embryonic cells that are more likely to survive the extraction and disassociation process are used. The neurons used in this project are taken from rat embryos 19 days after

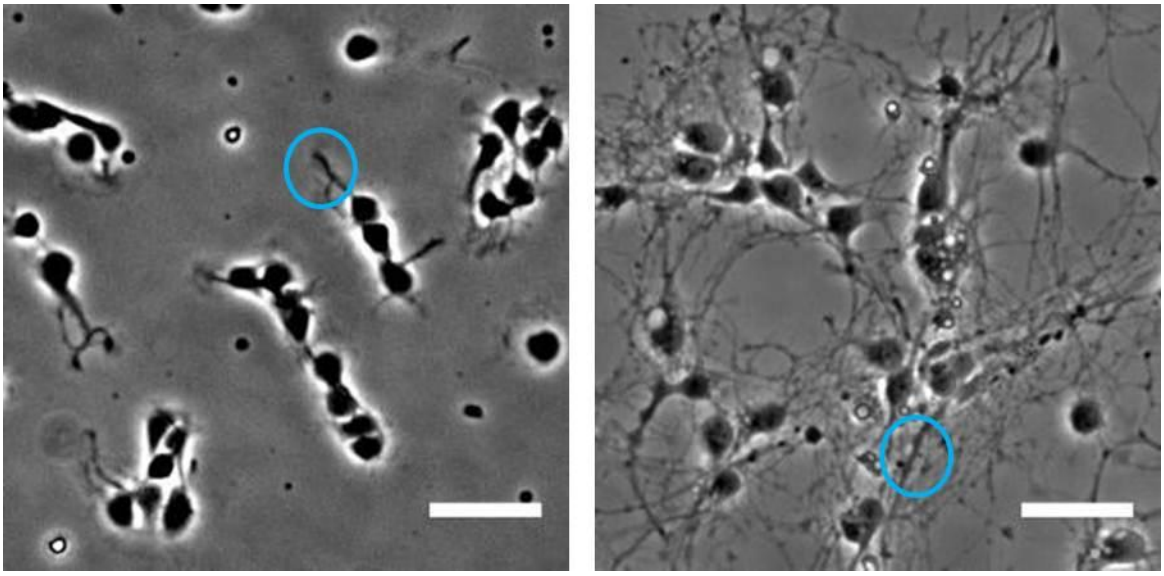

Figure 10 Neurons growing *in vitro* after dissociation from the original brain tissue. After 1 div (left), the cells settle on the glass substrate and begun to extend neural processes (blue). After 7 div (right), they have formed branching connections with several neighbouring cells. Scale bar 50µm.

conception (E19). They typically do not begin evincing electrical activity until 10-14 *days in vitro* (div). The cells selected are rodent hippocampal neurons, due to the strong association of the hippocampi with some types of memory formation. In whole rats where the hippocampus is damaged, the ability to perform tasks involving spatial memory is impaired, and the size of the hippocampus in humans is loosely related to the ability to perform memory tasks. It is therefore inferred that the encoding of information in this brain region is particularly significant to memory, and neurons isolated from this region will have the capacity to exhibit synaptic plasticity.

As the cells drop out of suspension and adhere to the substrate of the new environment, they begin to explore the surface, seeking the chemical cues, known as *neurotrophic factors* that other neurons release into the environment. The gradient of factors will guide the cell growth processes.

After several days *in vitro*, neurons cultured in this way will form a network of synapses - ultimately the cells 'rewire' (see Figure 10). Recording from individual cells shows the appearance of EPSP and action potentials, and many investigators have demonstrated the feasibility of measuring synaptic plasticity in cultures of hippocampal neurons under these conditions (Li et al. 2004).

This network is typically ‘two-dimensional’, meaning it forms a single layer of cells, rather than the ‘three-dimensional’ architecture originally present in the brain. This approach permits greater experimental access to individual cells and their activity, and if the culture extent is sufficiently small then in theory all the activity from all of the cells in the network can be recorded.

Why use embryonic rat neurons?

A downside to the use of cultured neurons is the heterogeneity of cell types present in the culture – as many neuronal types are known to exist in the hippocampus *in vivo* (Breier et al. 2010). An alternative to such ‘primary’ cells is the use of so-called ‘immortal’ stem cells that have been genetically altered to differentiate into a phenotype with many of the features of neural tissue (Wu et al. 2011). These *cell lines* have the advantages of homogeneity and stability, so that experiments performed months or years apart can be directly compared, whereas experiments performed using cells from different animals require more qualified comparison.

Because of the production line culturing of such cells at different stages of development, it is also possible to greatly increase experimental throughput, and the availability of the cells is not tied to an animal house breeding laboratory animals, with the attendant costs and ethical considerations.

However, although many of the protein markers and gene products expressed by the stem cells are consistent with a neural lineage, in many functional respects these differentiated stem cells do not resemble primary neurons. Accordingly, there are significant concerns as to whether the properties of synaptic transmission, synaptic plasticity and response to neuromodulation in stem cells would resemble neurons *in vivo*.

Primary cultures of embryonic neurons are therefore favoured until such time as the functional characterisation of induced stem cells is unequivocal.

1.4.2 *In vitro* recording of action potentials

As for *in vivo* recording methods, microelectrode methods (including patch clamp recording) can be used to record from individual (or small numbers) of neurons. However, our requirement is for recordings from large numbers of

cells – ideally the entire network. We will therefore focus on *in vitro* methods that can potentially meet these needs.

In vitro electrode arrays were first introduced forty years ago (Thomas 1972) with electrodes composed of gold and tin. For microscopy and imaging purposes, the substrate used in most MEAs is optically transparent, typically glass.

Fixed planar arrays were subsequently developed for individual neuronal recordings (Gross 1977) (Rolston et al. 2009). It has been observed (Robinson 1968) that electrode impedance must be minimised in order to improve signal-to-noise ratio (SNR), but the trend has been towards geometrically small electrodes to improve spatial resolution, and a smaller electrode has higher impedance.

Electrode arrays are usually fabricated utilising photolithographic techniques (Levinson 2005) which deposit a layer of metal in specific regions on a rigid insulating substrate (typically silicon or glass). The electrodes act by coupling charge to and from the metal surface into the extracellular medium.

In addition, all metals and insulators used must be both biocompatible and electrochemically stable. A symmetrical and reversible redox reaction is necessary to allow the ionic currents in the salty media to couple onto the metal electrodes for both recording and electrical stimulation purposes(Peck & Martyniuk 1995; Balasubramanian et al. 2006; McAdams et al. 2006). An unstable and irreversible chemical change, however, leads to pH change, bubble formation, and release of metallic elements which may prove cytotoxic and also alter the electrode current-carrying properties (Shleev et al. 2005).

Insulation is essential to ensure the electrode: electrolyte interface only occurs at the circular contacts and not the connecting tracks. Typical insulators include Silicon Nitride and Parylene-C (Delivopoulos et al. 2010); though the photoresist SU-8 has also been found to be an effective insulator at thicknesses of 11µm, and is biocompatible (Zhang et al. 2010). It has been demonstrated that plasma activation of the SU-8 will also permit cell adhesion (Hennemeyer et al. 2008)

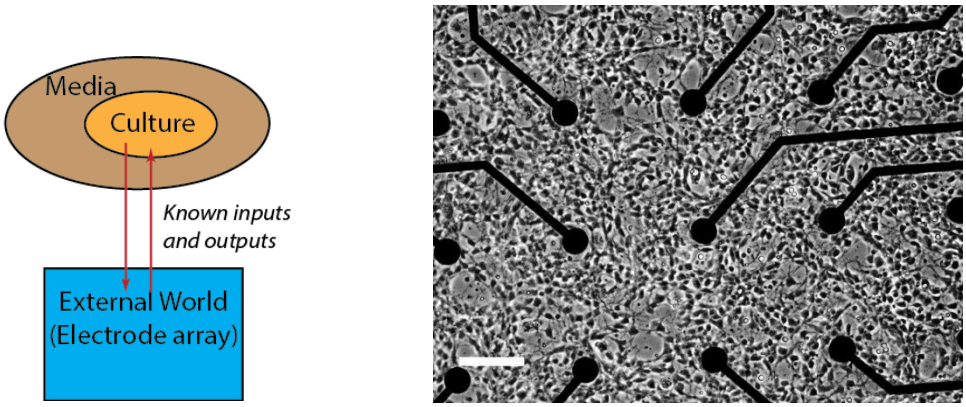

Figure 11 Left: Schematic of simple feedback loop using an electrode array to both record neural activity and stimulate it with injected biphasic current. Although this creates the capacity to provide feedback to the network in response to its activity, there is no means of selecting or promoting specific connections. Right: neurons at 5 div grown on a glass substrate with integrated electrodes (black circles connected to insulated tracks). Note the very low spatial precision of the electrodes with respect to individual neurons. Scale bar 100µm.

This is typically achieved (see Figure 11) using a micro-electrode array (Thomas 1972), developed in order to interface with 2 dimensional cultures by using planar rather than pointed electrodes (Gross 1977). Electrode arrays (see Figure 12) have the drawback that their spatial resolution is usually lower than the inter-neuron separation in a planar culture.

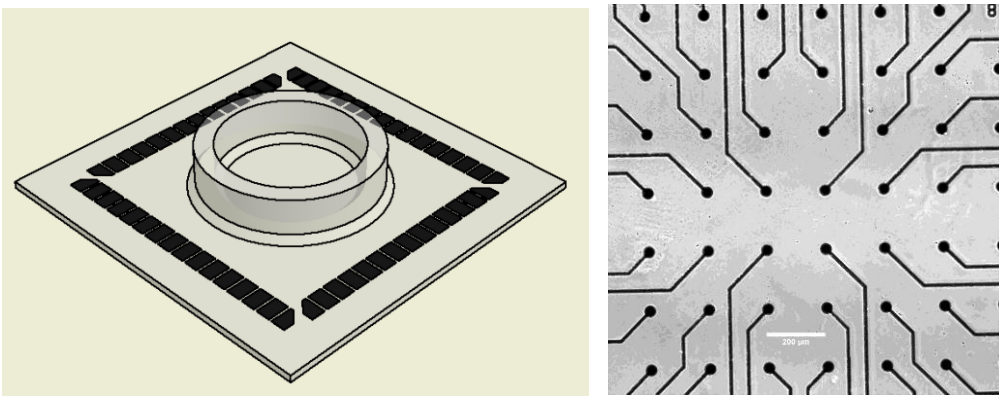

Figure 12 A Multichannel Systems™ Micro-Electrode array with attached glass ring to create a well for culture containment. The pads at the perimeter of the glass plate interface with a spring-contact head stage which amplifies and filters the recorded signals at each electrode. The MEA seen here (right, scale bar 200µm) has 60 Titanium Nitride electrodes, each 30µm in diameter and spaced 200µm apart.

Because of this, two neurons in close spatial proximity may be indistinguishable to a nearby recording electrode. Indeed this is a major problem when using electrodes to detect neuronal signalling, and a variety of

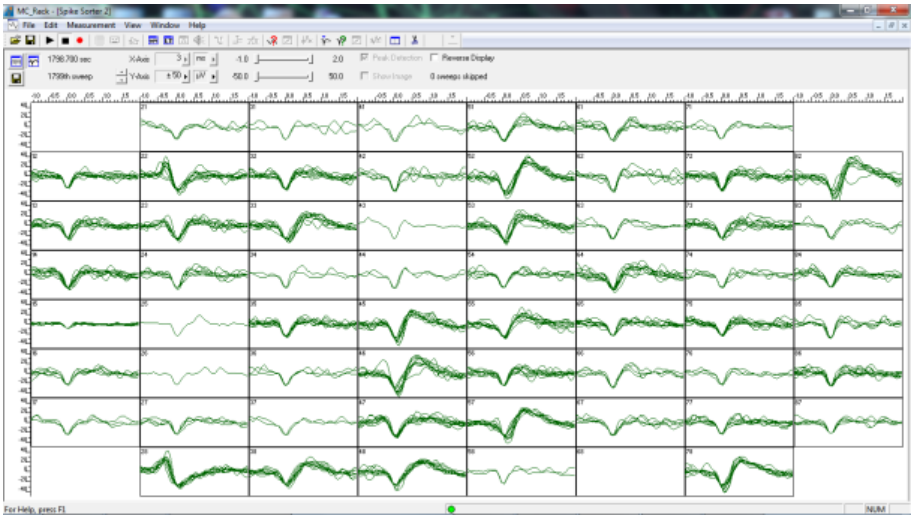

Figure 13 The activity recorded at each electrode is analysed using MultiChannel Systems MCRack™ spike detection software. Each part of the grid represents all activity recorded by that electrode, though it does not discriminate which cell is being recorded.

time-dependent algorithms collectively called 'spike sorting' are utilised in an effort to establish which neurons fired when an action potential is recorded on an electrode. However, these tools can allow recording of multiple cells with good spatiotemporal resolution (see Figure 13). Refinement of this technique may make the ultimate goal of the project possible.

1.4.3 Advantages and disadvantages of *in vitro* methods

Simplifying the entire organism to a finite cell network removes the complex unpredictability of the body and environment, which are continually providing uncontrolled input to the system. In addition, the reduction of the brain from billions of cells to a few hundred or thousand means that the data can be evaluated and processed far more easily.

The disadvantage is that it is extremely difficult to match all of the physiochemical conditions present in the intact brain. This presents challenges for cell survival, or will develop differently and thus any observed behaviour may be due to an abnormal or missing physicochemical factor, rather than the intended stimulus-response.

Nevertheless, the advantages of *in vitro* culturing and recording techniques are such that the basic premise of recording activity in a limited network is feasible.

1.4.4 Implementing time-dependent reinforcement *in vitro*

The previous sections confirm the underlying premise that coordinating the detection of action potentials in a network with the artificially induced release of dopamine with a novel delivery system should be possible with an *in vitro* system (Figure 14).

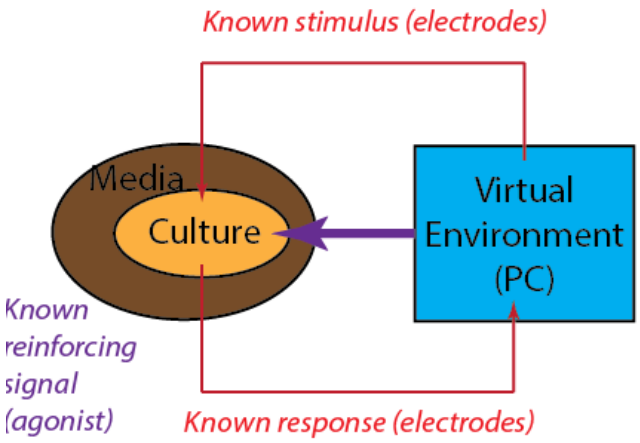

Figure 14 The ultimate aim: a system combining high-frequency (kHz) opto-electrical feedback for monitoring and stimulating neuronal activity on a single cell basis, coupled with a pharmacological dleivery system synchronised to electronic feedback, but with global agonist delivery on a slower timescale (1 Hz).

A feedback loop comprising only the monitoring and stimulating electrodes is feasible. However, such a feedback loop alone is not sufficient for learning and memory formation, since there is no mechanism for promoting the reinforcement of preferred pathways throughout the network by neuromodulatory signalling pathways. Consequently, the electrical feedback would simply take background chatter from the network and repeat it without emphasising or suppressing any signals. No meaningful adaptation can occur in this scenario.

A reinforcement signal is needed to deliver neuromodulator across all neurons in the network at a defined moment, which occurs within a certain time window (see Figure 15) after the activity it is intend to reinforce. This reinforcement should act to increase the synaptic strength, or probability that the post-synaptic neuron will fire the next time the pre-synaptic neuron does so. Based upon *in vivo* studies of neuromodulation, it can be inferred that the

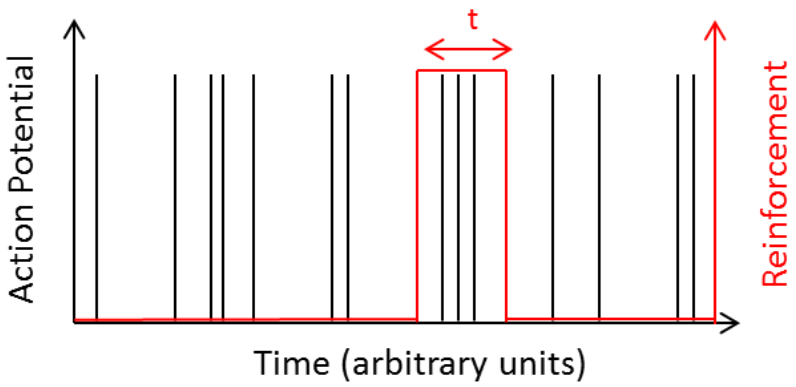

Figure 15 Feedback with reinforcement pathway. The agonist, a neuromodulator such as dopamine or Carbachol, coincides with some but not all network activity, leading to selective reinforcement

reinforcement window is short; within a few seconds at most, and ideally under 1 second (Roberts et al. 2013) (Arbuthnott & Wickens 2007).

It is proposed that in order to develop an understanding of how signals are encoded and memories are formed in neuronal networks, it is necessary to know all inputs and outputs to and from the network, regulating the physicochemical environment so that it does not cause any perturbation to the network, and to have a spatiotemporally controlled neuromodulator signal that can be timed to encourage or discourage (i.e. potentiate or depress) certain synaptic firing patterns.

If we could insure sufficient control of inputs and outputs both spatially and temporally, with deterministic synchronisation of the electrical and pharmacological signals, then it becomes possible to test the hypothesis that a network of connected neurons can be manipulated into demonstrating recognisable 'behaviours'.

1.5 The Technical Capability Gaps

The ability to deterministically integrate chemical reinforcement and electrical recording, on a finite network of primary neurons has not been implemented, due to the considerable technical difficulties such a system imposes.

Cell biology, pharmacology, and surface chemistry must be combined with a range of engineering disciplines including signal processing, automated control of systems in parallel, materials science, computer scientists,

mathematicians, and electrical and mechanical engineering. This requires collaboration between many subject specialists for effective implementation of the concept.

The single most important barrier is the current inability to deliver reinforcement cues on the timescale required, while leaving the physicochemical environment unperturbed. Solving this problem is the central theme of this thesis.

Due to the very interdisciplinary nature of this research question, however, it will be necessary to collaborate with experts in cell biology, *in vitro* culture, computer science, surface chemistry, and mechanical engineers.

1.6 First Requirement: Perfusion without perturbation

In order to deterministically link the chemical signal to electrical network activity, a mechanism for rapid and complete onset and removal of the neuromodulator chemical on the timescales of a few seconds or less is necessary. Furthermore, in order to monitor the network it is necessary to interface with an electrical recording apparatus or microscope, which will require removing the culture from the incubator for extended periods of time. Although the network can be kept at a stable temperature by means of a hotplate under the culture, other physicochemical parameters such as osmolarity will be affected by evaporation of the water content in the culture solution, and the sterility of the solution may be compromised. Replacement of the media to replenish nutrients and remove waste products must also be achieved while the network is *in situ* at the microscope.

1.6.1 Using Microfluidic channels to perfuse nutrients

In order to maintain physicochemical stability and sterility outside an incubator for long periods, it is necessary that the cells be housed within a temperature controlled chamber through which moisture cannot escape. The volume of this chamber can be much reduced from a typical bath culture (a few millilitres or more) to a few microliters, which is more equivalent to *in vivo* extracellular volume.

In order to refresh the nutrients in solution, the fluid in this chamber will need to be replaced, which requires flowing liquid and a chamber which acts as a channel rather than just a reservoir of liquid.

Microfluidics is an established discipline (Whitesides 2006) that offers a suite of methods and technologies suitable for the miniaturisation of fluid handling. Channels are typically fabricated from the elastomer *polydimethylsiloxane* (PDMS), which can be moulded into complex geometries using *soft lithography* (Whitesides et al. 2001; Whitesides 2002). These are then bonded to substrates such as glass.

Amongst its many applications microfluidics is suitable for cell culture (Young & Beebe 2010; Meyvantsson & Beebe 2008) and indeed can be utilised to mimic some aspects of *the in vivo* environment (Ziółkowska et al. 2011). This extends from very robust cell lines such as CaCo-2 (Wang et al. 2010), HEK293 (Xu et al. 2015) and SY-SH5Y (Dinh et al. 2013) to primary mammalian cells (Barbulovic-Nad et al. 2010) (J. N. Lee et al. 2004).

Of particular interest are of course neuronal primary cells. Biffi et al have established long term recordings of neuronal cultures in a channel placed on an MEA (Biffi, Menegon, et al. 2012), while devices permitting culture of different neural cell types (Taylor et al. 2003; Taylor & Jeon 2010) are routinely used for investigation of neurodegeneration (Lovchik, Bianco, et al. 2010) (Millet & Gillette 2012) or the importance of glia (Majumdar et al. 2011).

Thus it is clear that primary neuronal cultures can be grown successfully in microchannels replicating the physicochemical environment. The next logical step is to connect the microchannel to a fluid handling apparatus that can induce flow.

Before doing this, however, it is important to understand what physical effects the flow will have, particularly in small geometry channels, since we do not wish to perturb the physicochemical environment with the circulating liquid.

1.6.2 **Flow rate in a channel**

In an enclosed channel of fixed geometry (see Figure 16) liquid passes through the system at a *volumetric flow rate,* ***Q***. This is derived from the time

taken for a volume V to pass a particular point**.** It can alternatively be expressed as the product of the cross sectional area **A** and the mean velocity **u** of the liquid

$$Q = u.A = V/t \qquad [1]$$

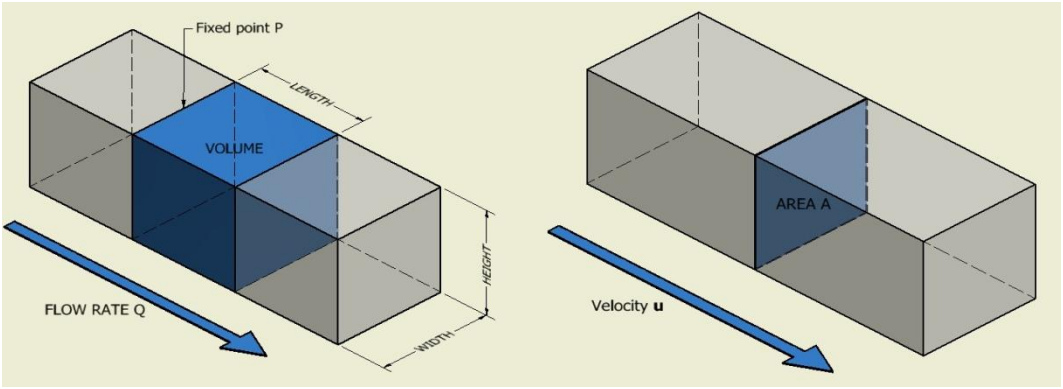

Figure 16 Flow rate Q can be considered as the either a volume per unit time or the product of area and velocity. The latter is often more useful for comparing flow rates in different sized channels

The continuity of momentum and mass (Bernoulli's principle) means that **Q** is constant, so that if the channel cross-section **A** increases then the velocity **u** is reduced, and vice versa.

1.6.3 **Poisseuille flow and shear stress**

The 'plug flow' in Figure 16 indicates that the velocity is constant across the width of the channel. This is not true, because the boundary of the channel is a fixed surface which does not move, and any liquid in direct contact with it is also defined as having zero velocity. This is the *no-slip* condition.

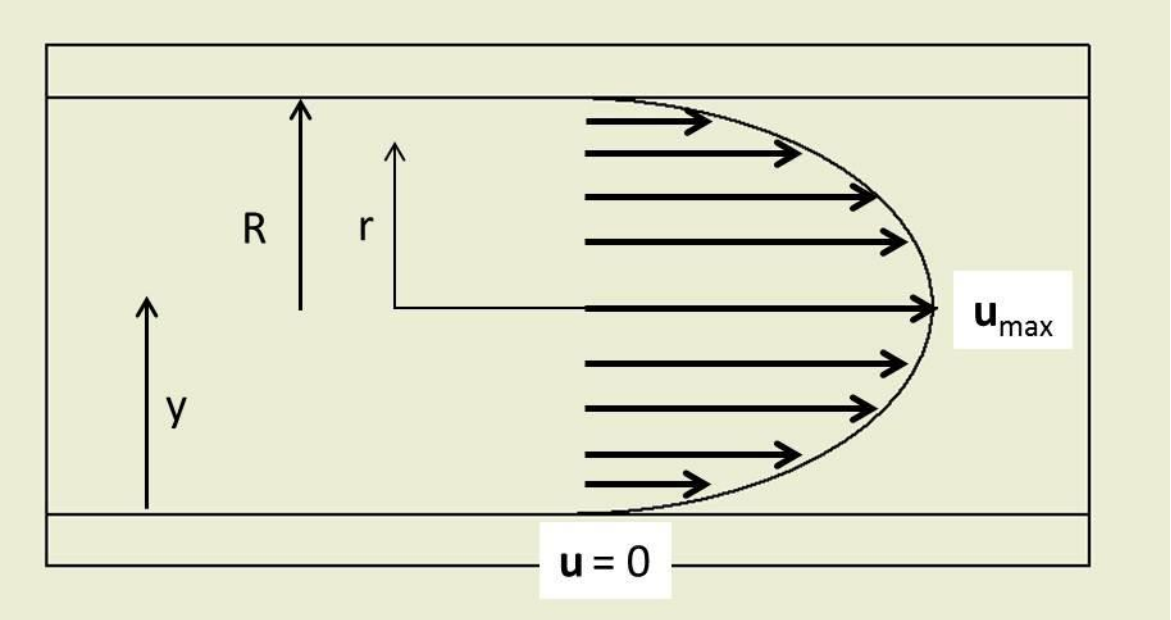

Figure 17 Under the no-slip condition at the channel walls velocity u **at the wall is zero. As the distance y increases away from the wall, the velocity u increases, reaching its maximum at the centre of the channel, where r=0.**

$$\boldsymbol{u}(r) = u_{max}\left[1 - \frac{r^2}{R^2}\right] \qquad [2]$$

From Figure 17, the fluid in the channel travels fastest when r = 0 at the centre line, while when r = R, the velocity is zero. This creates a parabolic profile in which liquid in adjacent regions is moving at different speeds, and so a shearing force is exerted on any object which extends from the wall, which will be the case for an adhering neuron.

This *shear stress σ* takes the form

$$\sigma = \mu\frac{du}{dy} \qquad [3]$$

where μ is the dynamic viscosity of the fluid (units $Pa \cdot s$) and the shear rate is the rate of change of **u** at distance y from the channel wall.

In a channel of square cross-section, shear stress in a square channel may be idealised as

$$\boldsymbol{\sigma} = \frac{\boldsymbol{6\mu Q}}{\boldsymbol{wh^2}} \qquad [4]$$

where w and h are the channel width and height, respectively (Bruus 2008).

This shear stress may be highly inimical to neuronal survival, since *in vitro* planar cultures of the kind already discussed do not have an extracellular matrix which would protect them from the effect. Thus it is important to review under what circumstances neuronal cultures have been grown in microchannels previously, particularly with regard to the velocity of the liquid used to perfuse over them.

1.6.4 **Appropriate velocities for primary neuronal perfusion**

Primary neurons have been successfully cultured in microchannels under low shear velocities. The velocities reported are usually in the range of 10 to 50 microns per second: 7-14µm/s (Millet et al. 2007), 9µm/s (Taylor et al. 2010), 10µm/s (Joanne Wang et al. 2008), 50µm/s (Kumamoto et al. 2015), but can be as high as 3.2mm/s (Biffi, Piraino, et al. 2012).

Notably, the longer term (more than one or two hours) perfusion experiments are associated with lowest flow rates, which will have the least effect on the physicochemical stability.

Thus little work has been done work to date involving high flow rates over primary neuronal cells. Axon growth is affected by flow rate (Kumamoto et al. 2015) (Joanne Wang et al. 2008) or by the pressure differences that can induce flow rate (Nguyen et al. 2013), which may be unacceptable for some applications where growth and cell migration due to chemical cues (*chemotaxis*) is under investigation.

Primary neurons are not typically subjected to high flow rates except where the shear stress is the source of study (Abaci et al. 2012; Li et al. 2004; Chau et al. 2009) (Toh & Voldman 2010), or is used as a traumatic stimulus which can be mitigated by modulating the concentration of a neurotrophic factor such as Galinin (Liu et al. 2013).

From the foregoing, it would appear that an appropriate range of velocities is in the region of 10 to 100µm/s.

1.7 Second requirement: Prompt Neuromodulator Delivery

1.7.1 Bath application

Agonists used for *in vitro* dose-response experiments are typically administered by manual pipette into a bulk buffer solution. This delivery approach is primarily dependent upon passive mixing over a comparatively long distance, meaning a significant delay of many minutes and dilution of the original concentration.

Diffusion is the transport of molecules in a fluid due to heterogeneity in substance distribution, such that molecules move along a gradient from high to low concentration.

Fick's First Law of diffusion (Bruus 2008) states that

$$\boldsymbol{J = -D\frac{\partial ø}{\partial x}} \qquad [5]$$

The diffusion flux *J,* which is the amount of a substance to be found per unit area per unit time, is proportional to the gradient of concentration *ø* with respect to distance *x* from the region of highest concentration. The flux is negative since concentration falls as distance increases.

The proportionality factor *D* is the *diffusion coefficient* which is specific to the pair-wise combination of the liquid solvent and the solute molecule. Neuromodulator molecules such as dopamine are reported to have diffusion coefficients of around 6 x 10^{-10} m^2/s in saline media (Lin et al. 2013).

Fick's first law can be simplified to

$$\boldsymbol{l = 2\sqrt{Dt}} \qquad [6]$$

Where l is the distance a molecule has travelled from its initial location, after elapsed time *t*.

By rearranging, this gives

$$\boldsymbol{t = \frac{\left(l/2\right)^2}{D}} \qquad [7]$$

so that time squares with distance.

Thus the time for dopamine to cross a cell 20µm in diameter by diffusion alone would be 167ms, but to cross a network 10 cells (200µm) across would

take 16.67 seconds. Simultaneous neuromodulator release across large areas is possible *in vivo* because the extra-synaptic dopaminergic fibre has many hundreds of branches throughout the brain tissue, so that the released molecules do not need to travel long distances before encountering a receptor. Such an extra-synaptic delivery system is not present *in vitro*, because the brain tissue is disassociated during the cell plating process.

Subsequently, the drug remains in solution even after several partial replacements of the bath media. This method clearly does not emulate the extremely rapid onset and removal of neurotransmitters *in vivo* (Yagishita et al. 2014; Arbuthnott & Wickens 2007).

1.7.2 **Uncaging of neurotransmitters via photolysis**

In photolysis, a ligand is cleaved by a light source of the correct wavelength and intensity (Monat et al. 2007). If the ligand was a matrix isolating a molecule of neuromodulator from its environment, then the act of photolysis would induce targeted agonist release. The ligand can form part of a surface coating that the cells later grow upon. This method typically requires a laser source in order to precisely target the area of effect at the required intensity level to achieve photolysis.

The temporal precision of the laser (Beta et al. 2007; Lutz et al. 2008) (Baigl 2012) can cause very rapid, spatially precise agonist delivery, as opposed to waiting for the effect to propagate from elsewhere, but require the fluid or surfaces to have certain inherent properties. These may be irreversible or may be incompatible with the biology. There is also a risk of tissue damage associated with high intensity (and typically 405nm, near UV) laser illumination, and indeed lasers are often used to deliberately sever axonal connections (Tong et al. 2015). This means that repetitive photolysis in a single sample on the time scales relevant for synaptic plasticity is rarely feasible.

In addition, this approach does not address the extracellular volume issues or the maintenance of the physicochemical environment.

1.7.3 Using microfluidic channels to deliver the neuromodulator

Since flow is required in order to replace the culture media, an obvious approach is to deliver the neuromodulator in flowing buffer solution. This would involve two regimes of liquid, one in which the concentration of neuromodulator is sufficiently high to reliably couple to extracellular receptors, and one in which the concentration is low enough that the chances of inadvertent coupling are minimal. There should be a clear contrast between the two regimes so that the reinforcement signal is unambiguous, and the transition should occur on timescales suitable for synaptic plasticity.

Given the constraints on acceptable microfluidic velocities determined above, we now check if neuromodulator can be delivered on the necessary timescales.

1.7.4 The distance problem (valve-mediated switching)

Altering the neuromodulator concentration upstream of the culture microchannel, and allowing it to propagate into and through the channel, is not a feasible approach.

To illustrate this, consider that the media and agonist reservoirs will need to be connected to the cell culture channel, typically by High Pressure Liquid Chromatography (HPLC) tubing. Minimising the internal diameter of such a tube is desirable to increase the speed of propagation, and a standard internal diameter is 150µm.

Assuming that the microchannel has a cross section of 100µm height by 1mm width, which are typical geometries for many microfluidic equations, then perfusing at 100µm/s the flow rate Q is 10nL/s (1e-11m^3/s).

Due to continuity of flow, in the HPLC tube attached to the channel the velocity is now 566µm/s. If the neuromodulator enters into a length of tubing even 1cm long, it will take over 17 seconds to enter the channel. This timescale is far too long for useful reinforcement.

1.7.5 **Microchannels and Laminar flow**

One very useful property that emerges from the use of microfluidic channels is the capacity for *laminar flow*. In a laminar regime, viscous forces dominate over inertial forces, and the kinetic energy associated with the liquid movement is damped out by the viscous forces. This means that adjacent regions of flowing liquid remain distinct, as was observed for Poisseuille flow.

The converse condition, *turbulent flow*, is characterised by the dominance of inertial forces. Kinetic energy is not damped out by viscous force, so both pressure and velocity can change rapidly and unpredictably over short distances. Chaotic convective mixing is very common. Such a regime is not appropriate for stable physicochemical environment or for controlled chemical reinforcement, and so it must be avoided.

How can we ensure that the flow regime is laminar and not turbulent? The key metric that determines this is the Reynolds number (Re).

This dimensionless number is defined as the ratio of viscous to inertial forces:

$$\boldsymbol{Re} = \frac{\boldsymbol{QD_H}}{\boldsymbol{\nu A}} \qquad [8]$$

Where Q and A are the volumetric flow rate and cross sectional area of the channel, defined previously. The kinematic viscosity ν of a fluid is the ratio of the properties (ρ/μ) where $\boldsymbol{\rho}$ and μ are respectively the density and dynamic viscosity. Both are temperature-dependent properties intrinsic to the fluid.

D_H is the hydraulic diameter or wetted perimeter of the channel, which for a rectangular channel is

$$D_H = \frac{2wh}{w+h} \qquad [9]$$

The flow regime in an enclosed channel is considered laminar if Re is below 2000, and turbulent if Re is above 2000.

Since Q is defined

$$Q = u.A \qquad [10]$$

Then

$$Re = \frac{u.D_H}{\nu} \qquad [11]$$

As the kinematic viscosity can only be altered by changing the system temperature, which we must not do given the need for physicochemical stability, the only variables that can be changed to reduce Re are the hydraulic diameter and fluid velocity. Thus channel geometry and induced velocity are the design parameters to be adjusted.

1.7.6 Using COMSOL to model phenomena

The finite modelling software COMSOL is used extensively in this thesis to test multiple physical parameters at the same time, and to illustrate concepts, beginning with Figure 18 and Figure 19 below. A range of physical parameters can be simultaneously modelled to assess their interactions, and optimise both the geometry of the object and any controlled variable like flow rate.

COMSOL splits a solid continuous object into a mesh of small regions, called finite elements. Equations governing physical phenomena such as diffusion and fluid mechanics are approximated to give element values at the boundaries of each element, based on the known inputs (such as flow rate and diffusion coefficient) provided by the user. These values are then recombined into a single system of the original equations, which converge to a solution which minimises the residual error.

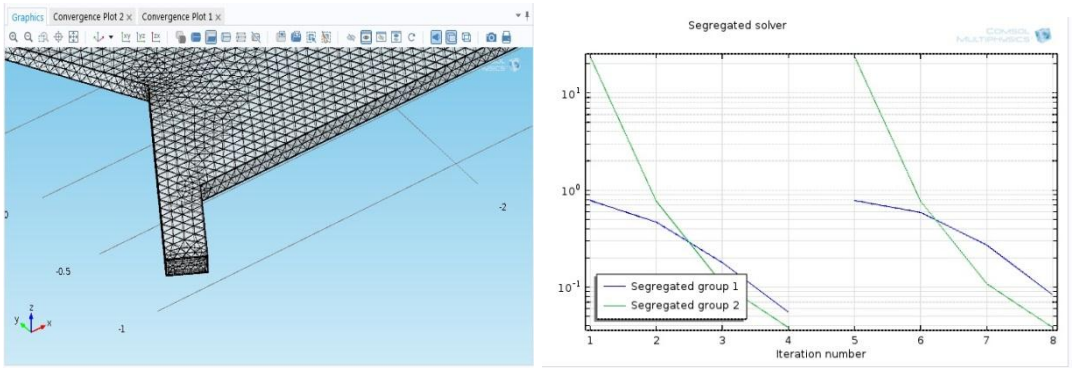

Figure 18 Left: the finite element mesh of a modelled microfluidic channel, and right: solving two systems of equations to within a specified error margin.

This modelling approach allows in theory for a great deal of exploration of the possible physical phenomena and geometries, without having to actually

construct and test every single one, so in theory it saves a lot of time. However caution must be exercised in interpreting the results. If the element mesh is too coarse, or the specified residual error is too lenient, then the fidelity of the finite element model to the physical system it represents may be poor. If the input values are not correct the model will be useless, and it is possible to plug numbers into the COMSOL equations without fully understanding their significance, and thus accepting a mathematically legitimate solution that is physically impossible, such as concentrations that are negative. For this reason any model that seems to be satisfactory should always be tested with a physically built analogue, to ensure the behaviour is as expected. A thorough grounding in the physical equations being used in COMSOL is essential.

1.7.7 **Concentration interface shifting**

The laminar flow regime means that if adjacent streams of liquid with different chemical content flow in parallel, the concentration does not equilibrate, so the high concentration volume is confined to one part of the channel length. The extent of that domain is determined by the ratio of the flow rates (see Figure 19), and the lateral position of the interface is linearly proportional to that ratio.

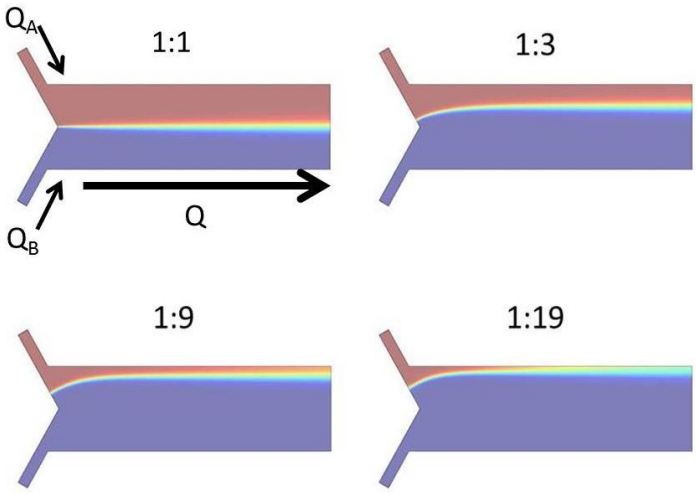

Figure 19 Models of parallel liquid streams entering a channel, and forming a distinct boundary. The total flow rate Q is the same in all cases. Depending on the flow rate ratio of agonist to buffer, denoted Q_A and Q_B respectively, the boundary position moves laterally from the centre to the edge of the channel.

Spatiotemporally varying concentration gradients can be achieved by transiently adjusting the flow rates of the parallel streams, so that the boundary between the agonist and buffer as swept laterally across the channel and back again. This is referred to as the *interface shifting approach*

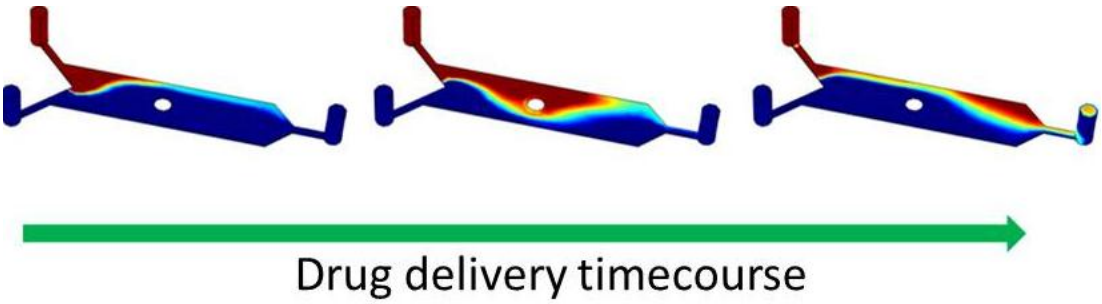

Figure 20: Rapidly switching and then restoring the ratio of inlet flow rates causes the agonist (red) to be transiently swept across the channel, before being replaced again with buffer (blue).

(Bae et al. 2009), and is illustrated in Figure 20**,** where the interface between high (red) and low (blue) concentration sweeps across the channel. The central white region represents a finite area in which the neuronal network may be confined.

Even interface shifting at the point of entry into the channel cannot induce change instantaneously. Groups reporting chemical switching times of a second or less do so by using very high velocities of several mm/s or more (Yamada et al. 2009) (Kuczenski et al. 2007). These high velocities appear necessary for rapid chemical switching on the timescale anticipated for reinforcement learning (Bae et al. 2009). By using either very fast velocities up to 20cm/s (Kuczenski et al. 2007), and narrower channels less than 1mm across (Kuczenski et al. 2009), a switching time of 0.1s is reported.

However, high velocities and rapid switching times are not associated with primary cultured cells, but more robust cells such as fibroblasts. Switching applications involving primary cells are usually observing a response to a slower change in hormone or neurotoxin levels, and occur over tens of

seconds, with the entire experiment not lasting longer than a few minutes (Biffi, Piraino, et al. 2012) It is simpler to use a robust cell line to demonstrate the utility of a microfluidic concept, without struggling to keep primary cells alive. Thus systems capable of rapid switching are not necessarily compatible with stable culture of primary neurons.

The longevity and environmental stability noted previously for perfused neuronal cultures may come at the expense of being able to generate rapid agonist changes that are comparable to those posited to occur *in vivo*.

A key question in the initial design of the microchannels used in this thesis will be to confirm if interface shifting on the timescales required is possible given the preference of keeping linear velocities low. It may be necessary to perfuse faster than 100µm/s, and so the range is extended to 1mm/s.

1.7.8 **The diffusion problem**

In order to reduce the value of Re and ensure laminar flow, and to reduce the shear stress that is induced on cultured cells, it is desirable to keep the flow rate low.

However, if the flow rate drops below a certain threshold, then diffusive transport becomes dominant once more, and the distinction between neuromodulator and buffer will be lost (see Figure 21).

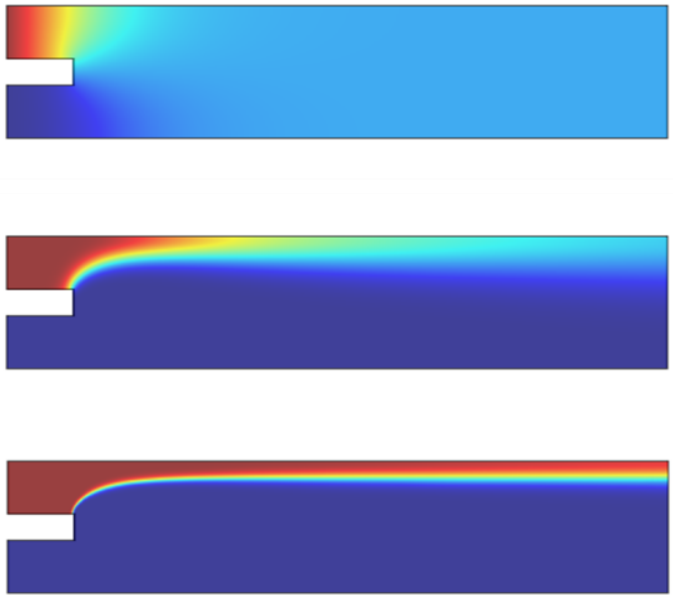

Figure 21 A COMSOL concentration gradient model. Two parallel streams of fluid, agonist (red, high concentration) and buffer (dark blue, zero concentration) are delivered into the microchannel. The flow rate ratio is 1:5. The cross section is 100µm by 1.5mm. The total flow rate changes by an order of magnitude from 1nL/s (top) to 100nL/s (bottom). This equates to velocities between 7 and 700µm/s. Only above 10nL/s (70µm/s) is a region without agonist (dark blue) attained.

Consequently, the flow rates utilised must not be so low that diffusion dominates the spatiotemporal distribution of the neuromodulator. COMSOL modelling, taking the diffusion coefficient of dopamine as 600µm^2/s(Lin et al. 2013), indicates the flow rate would need to be above 70µm/s to be sure of maintaining the distinction between agonist and buffer, and should ideally be faster than this.

From the foregoing discussion, the combination of rapid agonist delivery and primary neurons for the purpose of reinforcement signalling is novel and has not been attempted. However, it certainly appears to be theoretically possible, subject to a method of perfusion compatible with the flow ranges and switching times required.

1.7.9 Perfusion Strategies appropriate to microfluidic culture

We have determined a set of flow rates that are useful for laminar flow and in the range that supports neuronal culture.

Arising from the above, it is necessary to have a fluid handling system that can control at least two flow rates independently, and that is compatible with

the microfluidic devices that will be built and the survival of cells cultured within them.

1.7.9.1 *Gravity driven flow*

The easiest and least complex method is to use a liquid height difference between the media reservoir and the microchannel (see Figure 22), in order to induce hydrostatic pressure and thus velocity u (Millet et al. 2007)

$$u = \sqrt{2gz} \qquad [12]$$

where z is the height above the datum point (in this case the channel).

Thus the velocity induced is proportional to the height. This flow method is generally extremely smooth, as there is no noisy driving mechanism.

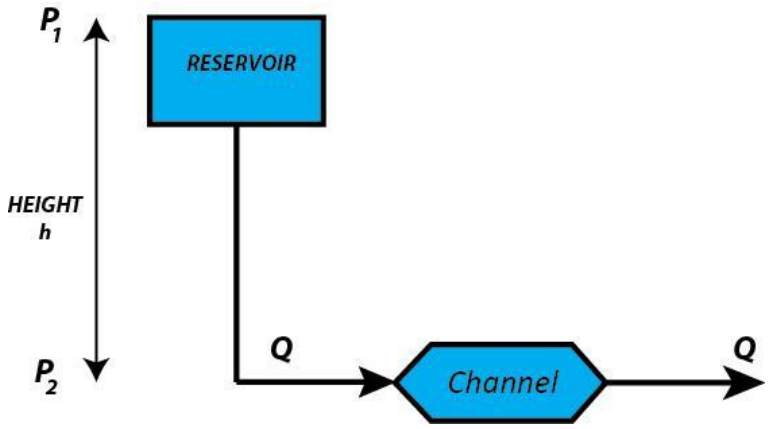

Figure 22 Schematic of gravity driven flow. A height difference h imposes a pressure P difference P1-P2 on the fluid, inducing a flow Q proportional to the pressure difference.

This method does require that the reservoir level be constantly topped up, otherwise the height difference and thus the flow rate will drop off over time. The replenishment may be achieved using an IV drip (Marimuthu & Kim 2013)

If attached to a microfluidic network (Kondo et al. 2014), very low flow rates and shear stress levels are reported (1.5nL/s and 10mPa, respectively).

1.7.9.2 *Syringe Driver*

The syringe pump (see Figure 23) is a readily available pump system, used for infusion of controlled volumes at a range of flow rates. A stepper motor is used to engage the worm drive which compresses a syringe plunger. By adjusting the syringe volume, the same step size will invoke a different flow rate Q because the cross-sectional area A of the syringe has changed.

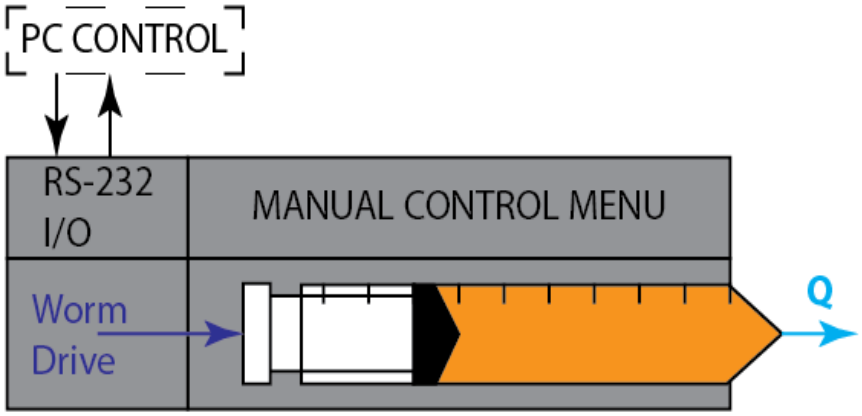

Figure 23 Schematic of syringe driver. A stepper motor rotates a worm drive pushing a block to which the syringe plunger is attached, while the syringe barrel is locked in place. The plunger is thus depressed continually, with step size and advance speed determined by the selected syringe size and nominal flow rate. The syringe driver may be manually set and left to run for a set time, or may be controlled dynamically from a computer.

A potential problem is that the actuation of the worm drive induces a periodic pulsing effect which will cause fluctuations in the flow rate (Li et al. 2014). This variation will be particularly significant at flow rates under 1mL/minute, which is the regime in which we require to operate, and may cause the interface between fluid streams to vary, inducing reinforcement pulses that were not intended.

It remains to be seen if the syringe drivers available will be suitable for stable perfusion that does not induce unwanted variation in flow rate and interface position.

1.7.9.3 *Peristaltic pump*

Peristaltic pumps, as commonly used for dialysis and *in vivo* drug infusion, operate by continually constricting a compressible tube containing a fluid via a set of rollers (see Figure 24) which revolve around a central axis at a certain frequency. As the tube is compressed by the rollers so that the cross sectional area is reduced, a pressure wave is built up, inducing flow through positive displacement of the incompressible fluid. The flow rate induced is proportional to the number of rotations per minute (RPM) about the central axis.

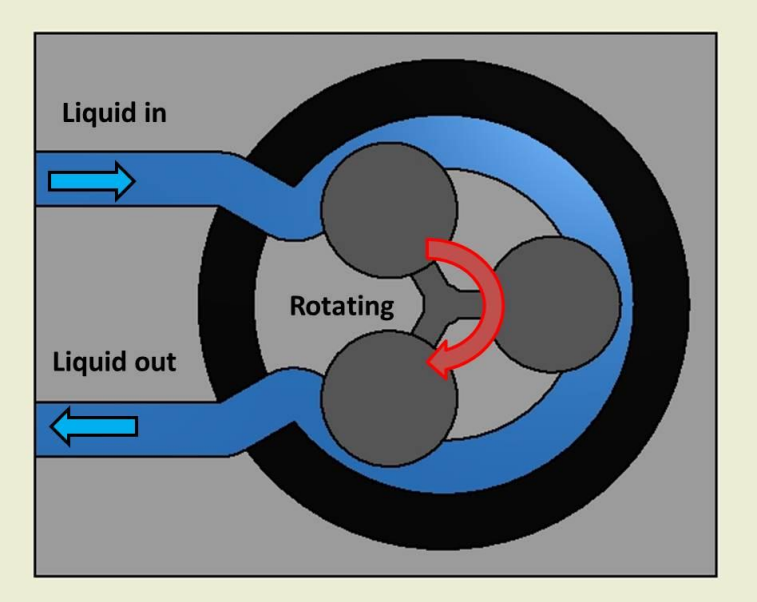

Figure 24 Peristaltic pump operation. The compressible tube is filled with liquid, and passes through a ring (black) within which several cams on a rotating axle (grey). As the cams compress the tube they displace liquid forward, at a rate determined by the frequency ω of the axle rotation.

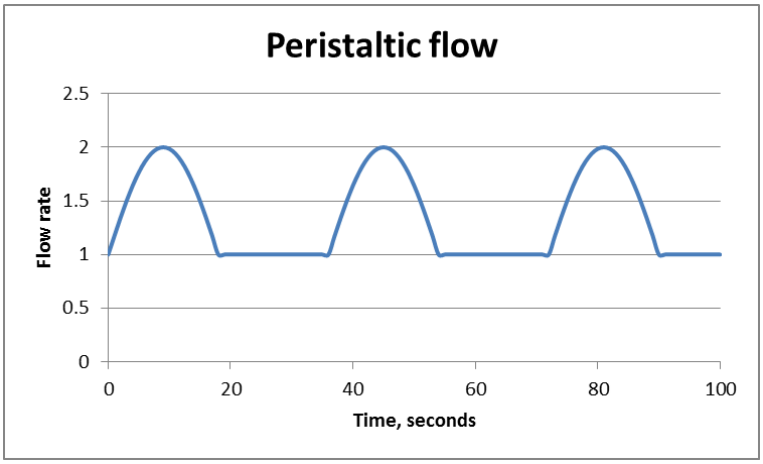

Figure 25 Variation in flow rate cause by the peristaltic pump, on an arbitrary y-axis. The flow induced, especially at low volume rates, is not smooth and has large variation.

These pressure waves (see Figure 25) will be very significant at the low RPM needed for lower flow rates. This renders it unsuitable for precise interface shifting as will be required for the drug delivery concept.

1.7.9.4 *Electro-Osmotic pump*

An applied electric field induces a Coulomb force upon any positively charged particle (anion) held in solution. As the anions move parallel to the channel walls (see Figure 26), the cations (negatively charged ions) are drawn after them, leading to net flow rate. This is analogous to the way in which CSF is

regulated in the brain by altering the sodium concentration, except that no new ions are added to the solution; only their spatial distribution changes.

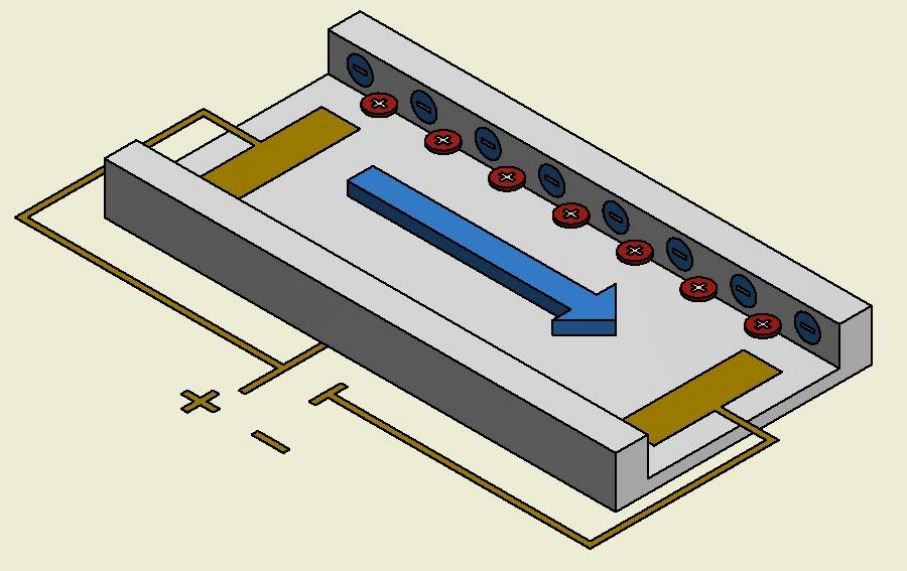

Figure 26 Electro-osmotic principle. A channel of glass or silicon walls has integrated electrodes which can impose a net electric field. A surface layer of negative ions (blue) is strongly attached to the channel walls. Under the applied electric field, positive ions (red) are drawn towards the cathode, creating a Coulomb force, and a net flow (light blue)is generated.

There is no boundary layer of zero flow next to the wall, and so the flow rate profile is planar rather than parabolic. This means that shear stress is constant across the width of the channel. Such a pump can potentially draw liquid through a channel with much higher flow rate range than a syringe pump (Suzuki et al. 2014),

This approach requires an anode and cathode in the channel devoted solely to perfusion rather than electrical recording. The reaction between the electrode and media is known to generate hydrogen peroxide and bubbles of oxygen and hydrogen. This can drastically alter the pH and is would be inimical to cell survival. These electro-osmotic effects may also interfere with the ability to record action potentials in the chamber. Since one of the requirements of the proposed system is that agonist delivery should not interfere with recording, this is not a viable approach.

1.7.9.5 *Acoustic / Acoustofluidic pump*

Piezoelectric transducers can be used to induce a mechanical resonance in the substrate of the microchannel (Bruus 2014), where the intensity of the vibration is proportional to the applied piezoelectric voltage. The resulting

vibrations in the ultrasound range (>20kHz) are used to perturb the fluid in the channel. If precisely angled protrusions jutting into the channel are incorporated (Huang et al. 2014), then the vibration is directed such that a net flow occurs down the length of the channel.

This technique is capable of at inducing flow rates across a large linear range, based solely on the applied voltage. It does not require the design and integration of a perfusion apparatus, since the microchannel is effectively itself the apparatus.

It is not considered for long term perfusion, however, since the induced vibrations could disrupt cell adhesion, and the electro-mechanical noise may interfere with sensing the neuronal network activity.

1.7.9.6 *Gas Pressure-Driven pumps*

Air-over-liquid or *air-driven liquid* pumps are well established. Briefly, a source of air at higher than atmospheric pressure is used as the driving mechanism. The compressed air may be used to induce liquid flow indirectly, such as acting to depress a syringe plunger (Kuczenski et al. 2007).

Alternatively, it may be used to directly forcing the liquid in a gastight vessel into a smaller space. In this instance the liquid in that vessel is ejected through an exit tube. From Poisseuille relationship already noted, the flow rate induced is thus linearly proportional to the pneumatic pressure permitted into the gastight pressure vessel, and inversely proportional to the fluidic resistance of the tube.

Because the gas pressure can itself be very precisely and rapidly modulated through a range of electrically actuated valves, the response of the system is typically very prompt, without lagging. There is no noisy drive system creating a periodic pulsing effect, as for syringe or peristaltic pumps, so in theory the precision of the system is constrained principally by the stability of the electro-pneumatic valves controlling the rate of gas ingress.

Most usefully for the purposes of perfusion, the compressed gas can simultaneously be used to drive soluble oxygen and carbon dioxide into the media reservoir that leads to the cell culture microchannel.

One important consideration is that by directly controlling the pressure without complete knowledge of the fluidics resistance, it cannot be precisely predicted what flow rate will be induced, and so it is advisable to have a sensor element capable of detecting mass flow transfer. This however would be a prudent consideration for all the pump options considered, since the nominal flow rate commanded by the user is not necessarily what will be delivered to the cell culture chamber, due to inconsistencies in the fluidic resistance of the connecting tubing.

As the syringe pump approach has been used without apparent detriment to physicochemical stability (Biffi, Menegon, et al. 2012), it will be considered first. However, looking ahead to reinforcement delivery requirements and long perfusion times, the gas-driven concept will also be considered as a longer-term solution.

1.8 Third Requirement: A Finite Cell Network

As discussed, it is desired that the entire neuronal network be subject to recording and stimulation, so that all the information entering and leaving the network can in theory be known. Furthermore, if the reinforcement signal covers only part of the network during agonist delivery, then the network activity recorded is not a true representation of the response to the stimuli. Finally, it is noted that if given the option, neurons can migrate away from a region (Claverol-Tinturé et al. 2005).

Thus the network needs to be confined to a single finite region within the microchannel. There are several possibilities for attempting this, which are considered below:

1.8.1 Surface Patterning

The substrate on which the cells grow can be functionalised with ligand patterns. These areas proscribe the cell culture boundaries. As there is a range of patterning techniques suitable for creating spatially heterogeneous cultures, this is preferred as the starting point.

1.8.1.1 *Micro contact printing*

Here a precisely formed mould, typically made of PDMS, is ‘inked’ with the ligand in solution and then stamped onto the substrate (Wheeler et al. 2010),

(Kim et al. 2014). This deposits ligand only in specific regions. The method has several drawbacks, chiefly the need to create a master mould for every variation on the desired pattern, as soft lithography is used to make the PDMS mould (Théry 2010). It is simpler to directly pattern the substrate, as described below.

1.8.1.2 *Photolithography*

Photolithography (literally 'writing on stone with light') is a suite of microscale fabrication techniques most commonly associated with the microelectronics industry (Levinson 2005). It involves the use of light-sensitive *photoresist*, a material which is deposited as a liquid onto the substrate and rendered uniformly flat by centripetal force, and then thermally hardened.

The resist contains a *photo-initiator* chemical which is sensitive to ultraviolet wavelengths. Depending on the nature of the resist, the photo-initiator will either cross-link or cleave the surrounding photoresist where it has been exposed. A photomask with some regions opaque to ultraviolet is used to transfer the mask pattern onto the photoresist, so then when exposed to chemical etchant, the *developer*, some photoresist regions are rapidly removed while others remain.

The exposed substrate areas can now have material added or removed while the shielded regions are not affected. Finally the remaining resist is removed with another etchant.

This concept has been used in conjunction with ligand deposition in a variety of ways. Kleinfeld (Kleinfeld 1988) used a resist to shield part of the glass substrate while an alkyl-chlorosilane group, which proteins cannot adhere to, was deposited in the gaps. The resist was then removed and an aminosilane group was deposited in the gaps where the resist had been. Finally, poly-D-lysine (PDL) was uniformly deposited over the pattern, but could only bind to the aminosilane groups. Cultured neurons consequently only grew where the aminosilane groups had been deposited (Kleinfeld 1988). Variations on this process have been carried out by Prucker et al (Prucker & Park 1999; Prucker et al. 1999), Shi et al (Shi et al. 2007) and Kwiat et al (Kwiat et al. 2012).

Photolithography can also be used to deposit a metal layer such as gold on the substrate, which an appropriate ligand (a *thiol* group) can then be attached to. Since the ligand is not a silane, it will not bond to the glass. This is functionally more elegant, since metal patterns in the form of electrodes will need to be present on the substrate. Neurons can also be grown readily upon gold surfaces (K. Lee et al. 2004) (Palyvoda et al. 2007) (Yoon & Mofrad 2011), (Albutt 2013) by using the ligand *11-amino-1-undecanethiol* (AUT).

1.8.2 Combining surface patterning with microfluidics

Combining a patterned substrate with a microfluidic channel is not trivial. There are essentially two ways to achieve surface patterning in a microchannel (Priest 2010):

Post-bonding, in which the substrate and channel are attached, and the pattern is then rendered on the substrate in a sealed device.

Pre-bonding, in which the pattern is rendered onto the substrate before the channel is attached, and the device is then sealed.

Both are problematic, as post- bonding the channel may damage deposited ligands, while conversely solvents used to suspend ligands such as AUT during deposition, may damage the pre-bonds formed during assembly.

Techniques have been developed to overcome these issues. A common technique in post-bonding is to cover the patterned ligand with a temporary shield such as polyvinyl alcohol (PVA) during the bonding step (Wang et al. 2009). The shield can be subsequently removed by flushing with water.

Conversely, the pattern can be heterogeneously deposited in a pre-bonded channel, by making use of the laminar flow regime to lay down parallel regions of different ligands in solution (Millet et al. 2010).

1.8.3 Creating a topographical barrier

Grooves and small pits, called *microwells*, are often added into microchannels to confine cells to particular regions. This is typically harder to achieve than surface chemical deposition, as it requires either the selective ablation of particular regions by etching the substrate (Guenat et al. 2006), (Lovchik, Tonna, et al. 2010), or the addition of a layer of material between the

substrate and the microchannel (Bartholomeusz et al. 2005), (J. Kim et al. 2009).

As for chemical confinement, the modification of the surface can be undertaken before or after (Rhee et al. 2005;) the final sealing the microchannel . It is also possible to culture cells in the wells separately and reversibly attach them to the microchannel for perfusion experiments (Morel et al. 2012).

Typically approaches involving etching or additive processes are logistically more complicated, and require more specialised equipment, than surface deposition techniques, so the latter are preferred as a starting point for neuronal confinement.

1.9 Fourth Requirement: Alternative Electrical Activity Recording

Given the relatively poor spatial resolution (for the intended purpose of capturing all activity in a network)of existing microelectrode arrays discussed previously, alternative means of capturing electrical activity of individual action potentials without this limitation are considered.

1.9.1 Novel electrode arrays

Ultimately it may be necessary to create bespoke high-density electrode arrays with higher spatial resolution, which are compatible with the microfluidic channel and confinement methods. However, as a proof of concept and compatibility with the microchannel this is certainly worth investigating.

1.9.2 Surface Plasmon Resonance Imaging

Surface Plasmon Resonance is a phenomenon observed when incident light causes bound (conducting) electrons on a conducting surface to oscillate, at a resonant frequency determined by the wavelength of the light and the particular metal used.

If a polarised, coherent light source at around 700nm encounters a 50nm thick gold surface (Kuryoz et al. 2013a) at a specific angle, then some of the incident photons are coupled by the surface electrons into a standing wave that travels parallel to the surface. This is the *surface plasmon*. Most of the

light is reflected to a detecting element (a camera) which records the reflected intensity of the entire region of interest.

Gold in contact with a cell will have a baseline reflectivity based on the permittivity of the cell membrane. When a neuron undergoes an action potential, the membrane alters its permittivity since it now permits ions to cross where formerly it did not, and this alteration can be detected as a change in intensity in that region .The spatial sensitivity of the technique is potentially very high (around 1µm, a fraction of the cell). The SPR gold geometry can be a simple circle with a diameter corresponding to the desired culture extent.

1.10 **Thesis Structure**

This thesis now aims to answer the question: *can a microfluidic chamber and perfusion system be developed, capable of monitoring all network activity in a small network of cultured neurons, and providing spatiotemporally precise drug delivery that can selectively reinforce synaptic activity?*

1.10.1 **Chapter 2: Methods**

This chapter covers a suite of commonly used methods applicable to the fabrication of microfluidic devices, modification of substrates, and culture of primary neurons.

1.10.2 **Chapter 3: Culture in a purpose-built micro channel**

Although primary neuronal culture in microfluidic devices is not new, it is essential to demonstrate that viable cultures can develop in the microchannels that will be used. The geometry of a microchannel suitable for rapid drug delivery is modelled and devices are subsequently fabricated. Primary neurons are cultured in the resulting devices, to establish a benchmark for neuronal viability in the absence of perfusion.

1.10.3 **Chapter 4: Designing the perfusion apparatus**

A perfusion apparatus capable of perfusing media at low flow rates and shifting the concentration interface in a microchannel is developed. This apparatus has scope beyond the rapid delivery of neuromodulators, and a separate application involving slowly time varying release over cell lies, underlying the possibility of hormonal delivery to astrocytes, is shown.

1.10.4 Chapter 5: Confining the culture extent

In order to ensure complete coverage, stimulation, and agonist delivery, the cells must be kept confined to one manageable region of the microfluidic culture chamber, and methods for doing this are considered and tested, beginning with chemical patterning.

1.10.5 Chapter 6: Culture under Perfusion in the channel

The work already done is now integrated into one system, incorporating the microchannel with a confined neuronal network, and a perfusion system capable of prompt drug delivery. Where the system does not yet meet the design requirements, design changes are made in order to overcome the issues.

1.10.6 Chapter 7: Integrating recording alternatives

Novel electrode and SPR patterns are fabricated, and demonstrated to be compatible with the microfluidic channel, paving the way for future development of high-resolution electrical recording in a microchannel.

1.10.7 Chapter 8: Discussion.

Finally, the utility of the final system is assessed, and compared to the original technical requirements and research question. Future work and further testing that will be necessary is described, together with an appreciation of where this work sits in the field of microfluidic systems applied to neuroscience.

2 Methods

2.1 Ethics:

All primary neural cells used for experiments were obtained in accordance with guidelines set out in the code of practice for humane killing under Schedule 1 of the UK Home Office Animals (Scientific Procedures) Act 1986, and approved by the University of Nottingham Animal welfare and Ethical Review body.

2.2 Fabrication of basic microfluidic devices

2.2.1 Preparation of basic materials

Basic materials must be prepared before any fabrication can occur. In accordance with the need for Brightfield imaging and microscopy, all materials must be optically transparent to some extent.

PDMS is typically used for formation of channels, while glass is used to seal channels and as a substrate for the deposition of surfaces; both metal and chemical.

2.2.2 Glass cleaning

Coverslips were sonicated in 10% Decon-90™ for 10 minutes, then rinsed in deionised water and sonicated in more deionised water for 5 minutes. The glass was then dried with a nitrogen stream. The glass was sonicated in Acetone for 30 seconds, rinsed in more acetone, then sonicated for 30 seconds in Isopropanol (IPA), rinsed in IPA and then dried again under a nitrogen stream. This rendered the glass suitable for subsequent heat sterilisation at more than 100°C, and cell culture on Poly-L-Lysine (PLL).

For subsequent deposition of silanes, the glass was then plasma cleaned to activate the surface (50W power and 0.28mbar chamber pressure, for 5 minutes).

2.2.3 PDMS mixing

Sylgard 184 pre-polymers were mixed in the ratio 10:1 w/w base monomer to cross-linking catalyst, and de-gassed in a desiccator unit attached to a

vacuum pump. The resulting viscous liquid was poured onto moulds or substrates and de-gassed again if required. The PDMS was cured at 60-80°C for 2 hours.

2.2.4 Thin film spinning

To generate thin films of PMDS, the mixed pre-polymers were poured onto the central third of a 3 inch (76.2mm) Silicon wafer and processed on a spin-coater, with film thickness determined by spin RPM and time (see later chapter). Wafer and pre-polymer film were then transferred to a hotplate at 100°C and baked for at least 15 minutes, to harden the PDMS before reflow could occur.

2.3 Functionalization of the surface

Neuronal cells will not grow directly on untreated glass or gold. Ligands must be deposited in monolayers, for successful cell adhesion.

2.3.1 PLL on glass

Poly-L-Lysine (PLL) is a homopolymer which promotes cell adherence due to its positive charge, which attracts negatively charged proteins and cell membranes.

500µL of PLL at 0.01% in distilled water was pipetted onto cleaned sterile glass (Figure 27). The PLL solution was left on the glass for a minimum of 30 minutes.

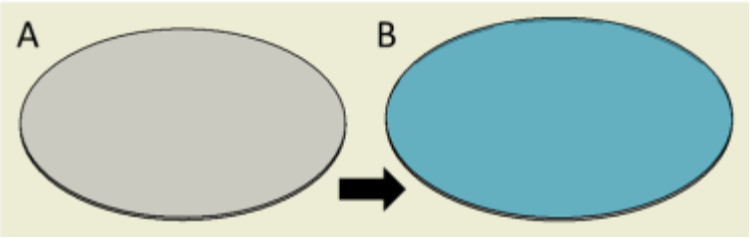

Figure 27 A 19mm coverslip (A) cleaned with Decon 90 and solvent as described is uniformly coated with PLL (B, blue) by pipetting onto the surface and leaving for 30 minutes.

The liquid was then removed with a suction line. Deionised water was then used to flush remaining liquid PLL from the glass, leaving a monolayer of ligand. To keep the ligand wetted, the coverslip was immersed in Neurobasal medium until cell plating.

2.3.2 MPTS on glass

Gold does not form an oxide bond with glass, and would easily detach if not secured by a wetting layer. This is usually a metal such as Titanium, which is capable of forming an oxide with glass and also bonding to gold. For the intended application of Surface Plasmon Resonance (SPR), however, an intermediate metal layer between glass and gold is detrimental to the sensor performance.

Accordingly, the ligand (3-mercaptopropyl) trimethoxysilane (MPTS) was used instead (Figure 28). This consists of a silane group linked to a thiol group, which bind to glass and gold respectively.

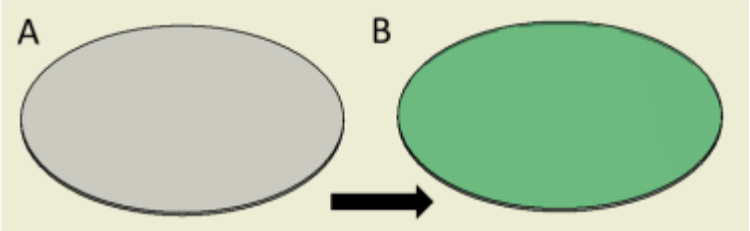

Figure 28 A recently plasma activated coverslip (A) is immersed in MPTS (B, green) in toluene

Concentrated MPTS solution was mixed to 1%v/v (500µL in 50mL) in anhydrous toluene using sonication for 1 minute.

Coverslips that had undergone the solvent cleaning regimen were subsequently exposed to oxygen plasma (Diener Zepto plasma system, 50W, 0.28mbar chamber pressure, for 5 minutes) to activate the surface for subsequent silane attachment.

Freshly plasma cleaned coverslips were immersed first in pure toluene for 1 minute, then in the dilute MPTS solution for a minimum of 30 minutes.

Coverslips were subsequently rinsed in pure toluene, followed by IPA, and dried under a nitrogen stream. To eliminate all remaining solvent, the coverslips were baked on a 100°C hotplate overnight.

2.3.3 Gold atom deposition

Gold was thermally evaporated (Figure 29) onto the MPTS prepared surface in a sample chamber under high vacuum (HV, 10^{-7} mbar). A liquid nitrogen cold trap prevented oil contamination of the samples by the diffusion vacuum

pump. A gold target was placed in a filament injected with high current (30A), causing evaporation of gold ions. The high vacuum allows ballistic ion trajectories, producing a uniform deposition of metal on the targets. The thickness of the deposited gold was measured with a quartz microbalance, located at the same distance from the target as the samples. To ensure Brightfield and fluorescent imaging is not impeded, the metal thickness should not exceed 100nm, and for Surface Plasmon Resonance considerations the gold thickness should be 50nm (Kuryoz et al. 2013b).

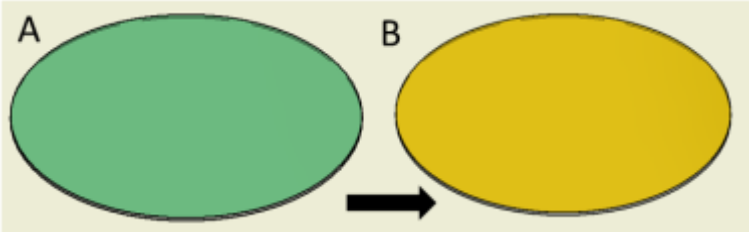

Figure 29 A previously prepared MPTS coverslip (A, green) is coated with a layer of evaporated gold (B, yellow).

2.3.4 AUT on gold

Epithelial cells such as neurons will not adhere to gold without a suitable ligand. An aminothiol (AUT) which binds proteins to gold was used (Figure 30).

AUT was mixed at 1mM in pure ethanol, based on previous work by Dr Darren Albutt (Albutt 2013). This typically used quantities of 4.8mg AUT solute in 20mL ethanol.

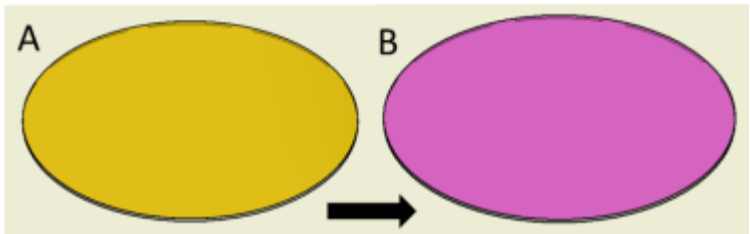

Figure 30 Gold coated coverslip (A) is plasma activated as for the MPTS protocol, and functionalised with AUT (B, magenta) by immersion for 18 hours. One hour immersion will deposit most of the layer but uniformity requires much longer.

Gold surfaces were plasma cleaned and immediately rinsed in pure ethanol, then immersed in the 1mM AUT solution for 18 hours.

Surfaces were then removed from the AUT solution, rinsed in pure ethanol to leave behind the monolayer, then deionised water, and dried under a nitrogen stream.

2.4 Substrate patterning and soft lithography

In order to mould the PDMS into repeatable microchannels, it was cast onto a master mould composed of embossed features on a flat substrate.

2.4.1 SU-8 100/50 and SU-8 5

To create microchannel moulds according to the intended feature height (see chapter 1 rationale for dimensions) a thick film photoresist was required. SU-8 is known to produce features of high aspect ratio and vertical sidewall, both essential for microchannel fabrication.

SU-8 film thickness is primarily determined by spin-coater speed and time, and by the ratio of solvent to epoxy in the photoresist. The higher the epoxy content, the more viscous it will be and more resist will remain after the spin-coating and heating steps described below.

A 3 inch (76.2mm) Silicon wafer of orientation [100] was sonicated for 5 minutes in Ethyl Lactate and then rinsed in more of the same solvent. This process was repeated for acetone, methanol, and IPA. The wafer was dried under a nitrogen stream and dehydrated at 150°C for at least 30 minutes.

SU-8 2050 was deposited onto the centre of the wafer and spun at 500rpm for 10 seconds to coat uniformly, followed by 30 seconds at 2000rpm to thin the photoresist to the intended height (Figure 31). The wafer was baked on a 65°C hotplate for 5 minutes followed by 95°C for 10 minutes, to remove all solvent from the photoresist.

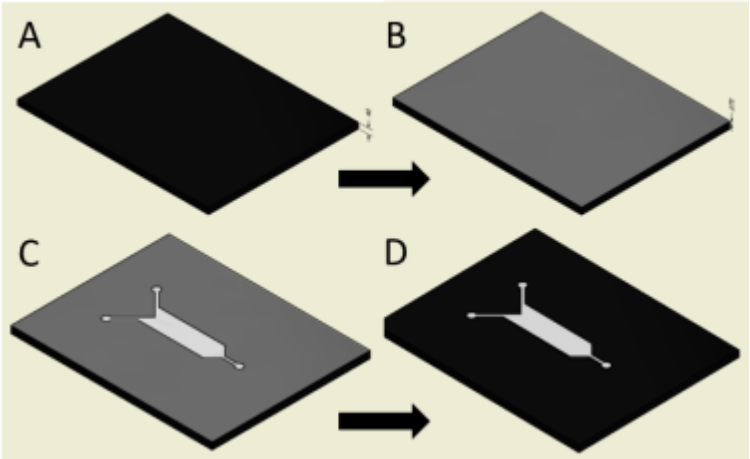

Figure 31 A) A silicon Wafer is solvent cleaned, B) coated with SU-8 photoresist, C) exposed to UV light through a mask to cross-link the epoxy where exposed, and D) developed in Ethyl Lactate to remove unwanted resist.

Photomasks of chrome on soda glass were designed using Inventor Professional (Autodesk, see Appendices) and fabricated by JD Photo-tools Inc. After aligning the mask, the baked wafer was exposed to i-line ultraviolet (UV, 365nm) light at 9mW/cm^2 for 30 seconds. The pattern dimensions are given in appendix 10.4.1.

The exposed wafer was heated again for 5 minutes at 65°C and 10 minutes at 95°C, to cross-link the exposed regions of the SU-8. The wafer was immersed in Ethyl Lactate with mild agitation for 15 minutes, to strip off the unexposed SU-8 from the wafer. After rinsing with more ethyl lactate, the wafer and SU-8 features were heated to 150°C for 30 minutes and allowed to cool, in order to render the photoresist mechanically robust (*hard bake*). Measurement of the SU-8 features with a contact profilometer confirmed the height to be between 70 and 100µm.

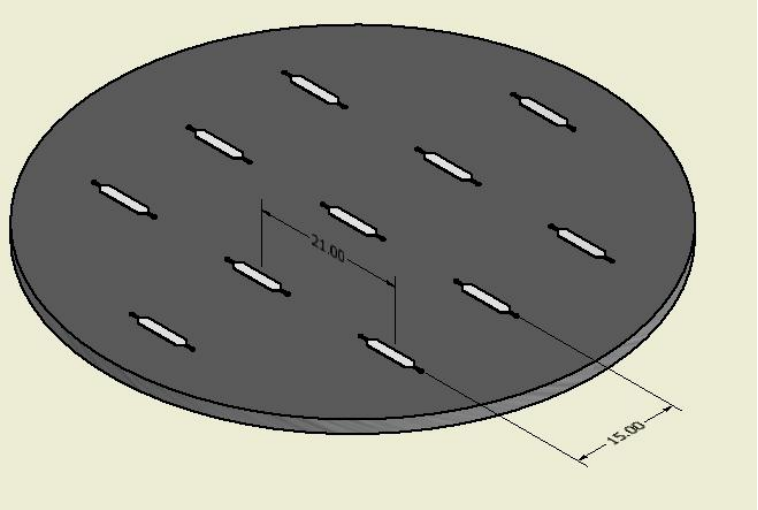

Figure 32 3inch (76.2mm) SU-8 patterned silicon wafer with 11 identical features. The features are separated by several millimetres to facilitate cutting out of PDMS blocks after casting.

To make complete use of the 76.2mm wafer, a photomask of 11 identical features was used (Figure 32).

After the 150°C hard bake, the wafer was thermally glued (Epo-Tek) to a machined disk of aluminium 76.2mm in diameter and 2mm thick. This provided rigidity to the wafer, greatly reducing the possibility of it shattering if exposed to a flexing force during subsequent PDMS degassing and excising steps.

The gluing process took 20 minutes on a 115°C hotplate. This temperature was chosen to ensure the SU-8 features were not reheated close to their glass transition point.

2.4.2 BPRS100 and AZ6612 / AZ 5214E resists

Where Surface Plasmon Resonance (SPR) applications are intended, the gold may not be deposited on a standard wetting layer such as Titanium due to interference effects (Aouani et al. 2009). Instead, a coverslip functionalised with MPTS is brought to the cleanroom and processed (Figure 33) as follows:

2.4.3 BPRS100 positive photoresist

Glass functionalised with MPTS was coated with BPRS100, by depositing 300µL of photoresist on the coverslip and spinning at 4000rpm for 30 seconds to produce a 1µm thick layer. The resist was hardened by baking on a 90°C hotplate for 3 minutes. The resist was exposed though a photomask (JD

Phototools) to i-line UV at 9mW/cm^2 for 6.2 seconds. Where it had been exposed, the BPRS100 was subsequently removed by 30 seconds immersion in AZ 400K, diluted 1 part in 10 in deionised water. To halt the resist removal, the coverslip was then immersed in pure deionised water, and N_2 dried. 50nm gold was evaporated onto the coverslip as previously described. Acetone was used to remove the remaining BPRS100 and the gold coating it, leaving gold on MPTS only where the resist had been exposed to UV.

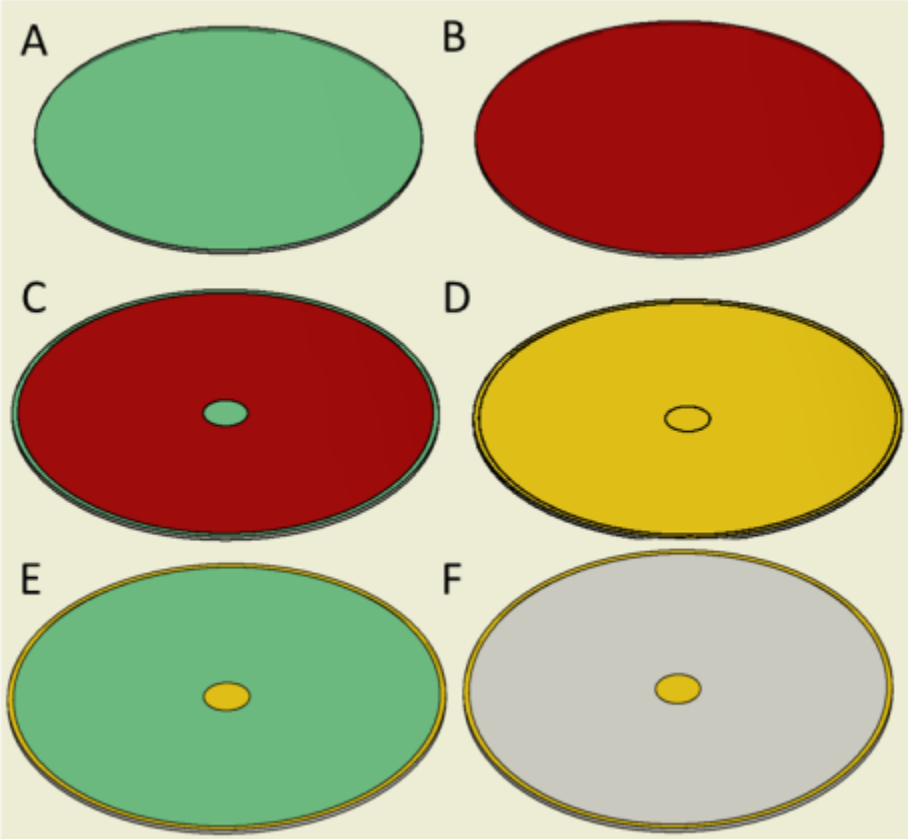

Figure 33 A) MPTS is coated with photoresist, B). After exposure and development part of the resist is removed, leaving MPTS, C). 50nm gold is evaporated over the entire coverslip, and removed with solvent E) except where it has bonded to MPTS. The uncoated MPTS is later removed with oxygen plasma F).

2.4.4 AZ5214E positive image reversal photoresist

300µL of AZ5214E was deposited on the MPTS coverslip and spun for 5 seconds at 500rpm followed by 30 seconds at 4000rpm.

The coverslip was baked at 90°C for 3 minutes, before UV exposure for 2 seconds at 9mW/cm^2 through a photomask. The pattern was reversed by subsequently baking the coverslip at 120C and 30 seconds UV exposure with

no photomask. Development was done in AZ726 developer for 19 seconds. This removed all resist that had not been exposed. 50nm gold evaporation was as previously described. Lift-off was done in dimethyl sulphoxide (DMSO) for 1-2 days.

2.5 Channel fabrication

Purpose: This process produces a microchannel which can subsequently be fused to a substrate.

2.5.1 PDMS soft lithography

Sylgard 184 pre-polymers (Dow Corning) were mixed, and degassed as described previously, and poured into a polystyrene petri dish or onto a Si wafer patterned with SU-8 (Figure 34). The ratio of monomer to crosslinking agent was 10:1 by weight.

The PDMS was polymerised at 60°C for at least 2 hours. After this time the PDMS was peeled off the mould and individual dies were separated with a scalpel.

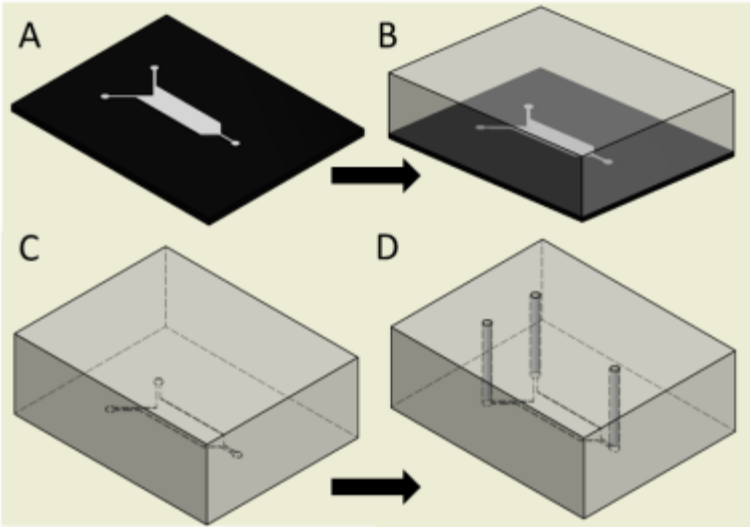

Figure 34 A) The SU-8 master mould is covered with liquid PDMS B). After curing at 60-80C forv2 hours, the PDMS is excised with a scalpel and peeled from the mould C), and access ports are cut with a biopsy punch D).

Fluid access ports were created with a 0.5mm biopsy punch (0.5mm Harris Uni-Core), flushed with deionised water to remove debris, and nitrogen dried.

The moulded face of the PDMS was cleaned 3X with scotch tape to remove debris.

2.5.1.1 *Channel bonding*

These protocols form irreversible bonds between surfaces, to create microchannels capable of withstanding pressurised fluid transport.

2.5.2 Plasma bonding

Oxygen plasma activation creates hydroxyl (OH^-) groups on surfaces. Where silicon (Si) atoms are present as in glass and PDMS, the OH^- groups will covalently bind to them.

PDMS surfaces were pre-cleaned 3X with scotch tape. Glass surfaces were pre-treated as described previously.

The parts were placed in a plasma oven with the active surfaces facing up. The parts were oxygen (N_2 free) plasma-activated at 50W and 200 mTorr for 30 seconds (Figure 35).

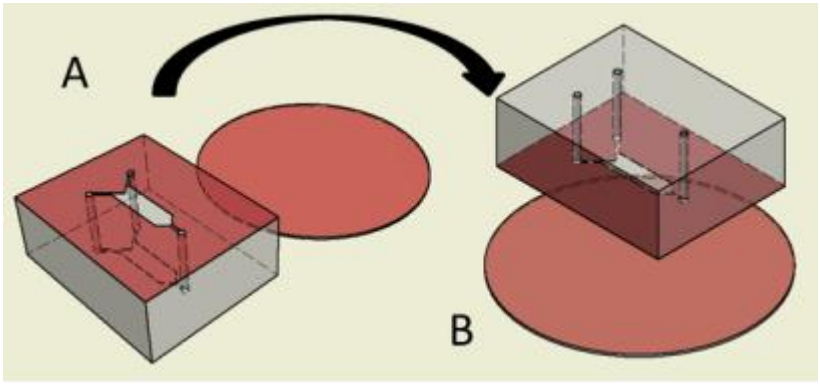

Figure 35 A) Surfaces are activated with oxygen plasma (50W, 0.28mbar chamber pressure, for 30 seconds) and B) brought into contact within 2 minutes.

Activated parts were removed from the oven and bonded within 2 minutes, before the OH^- groups could be passivated by moisture content in the air. Where careful alignment between surfaces was needed, a droplet of methanol was pipetted onto the glass surface to delay the contact of the surfaces. Once the solvent evaporated, the surfaces bonded *in situ*. Bonding was typically done at 60-80°C in order to accelerate the process.

2.5.3 **Pre-polymer bonding ('Stamp and stick')**

This method, adapted from Samel et al (Samel et al. 2007), does not require plasma activation of the glass surface, which has implications for deposited monolayers and cell culture as discussed later.

The 19mm coverslip and PDMS channel were prepared as before. A 22mm diameter coverslip was placed on the spin-coater. A few drops of PDMS curing pre-polymer were pipetted onto the glass (Figure 36), and the coverslip was then spun at 2000rpm for 30 seconds, leaving a 20µm layer of pre-polymer.

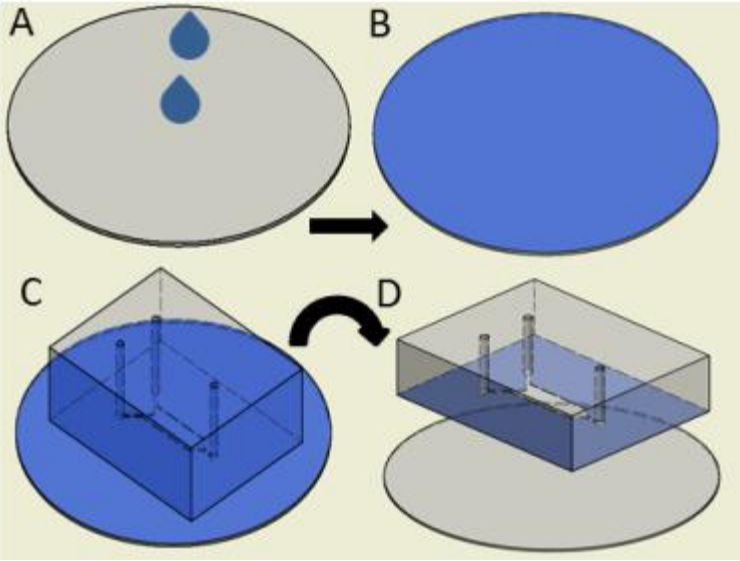

Figure 36 A) Catalyst is pipetted onto a 22mm coverslip and B) spun to a uniform thickness. PDMS channel is stamped on the catalyst C) and transferred to a 19mm coverslip D) before thermal curing of the catalyst.

With the 22mm coverslip vacuum clamped in place, the PDMS channel was brought into contact with the pre-polymer layer for a few seconds *(stamping)*, and then lifted off. This coated the base surface of the PDMS with catalyst while leaving the channel unaffected.

The PDMS was then placed in contact with the 19mm glass coverslip *(sticking).* The catalyst was cured on a hotplate at 60°C for 4 hours, with the glass in direct contact with the hotplate. Once cured, the catalyst pre-polymer formed a strong bond with both PDMS and glass.

2.5.4 Silane bonding for non-silica surfaces

Where one surface is not silicon based, neither the plasma activation nor pre-polymer catalyst methods are directly applicable. Several methods exist in which a silane may be functionalised on a plasma-activated surface, and subsequently linked to a different silane deposited on glass or PDMS. Two such methods were considered:

2.5.5 Aminosilane (APTMS) bonded to Epoxysilane (GPTMS)

Based on the method of Tang at el (Tang & Lee 2010), PDMS channels were prepared and plasma activated as described previously (2.5.2), then immersed in 1% (by volume) APTMS in deionised water for 30 minutes. Channels were then sonicated and rinsed in deionised water before drying under a nitrogen (N_2) stream.

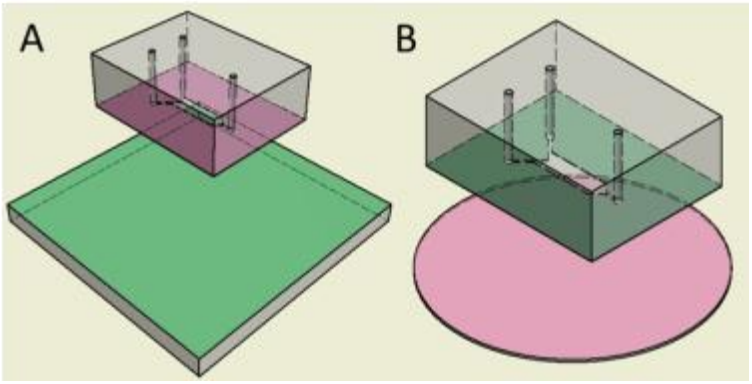

Figure 37 A) APTMS (pink) functionalised PDMS is brought into contact with GPTMS (green) functionalised polycarbonate. B) Theoretical bonding of APTMS on glass to GPTMS on PDMS, which is feasible but was not done here

Test pieces of 2mm thick polycarbonate (PCTE) were cleaned by sonication in IPA and deionised water, and dried with N_2. The pieces were plasma activated (50W, 0.27mbar, 30 seconds) and immersed in 1% (by volume) GPTMS in Hexane for 30 minutes (Figure 37). Pieces were sonicated and rinsed in Hexane, and dried with N_2. PCTE and PDMS pieces were brought together and cured at 80°C (oven) overnight (see chapter 6.6.1). A weight (1kg) was used to apply pressure during the cure and improve the bond.

2.5.6 **Silicone Tape excision and adhesion**

Assembling microfluidic devices from pre-cut layers of adhesive tape is an emerging technique coined Xurography (lit. *'razor-writing'*, (Bartholomeusz et al. 2005)).

Silicone-based adhesive transfer tapes of thickness 50µm and 125µm (3M™, USA) were used. The tapes are provided with a white Polyethylene terephthalate (PET) primary release liner (Figure 38), and were backed onto an optically clear Polyester (PE) secondary release liner (also 3M™).

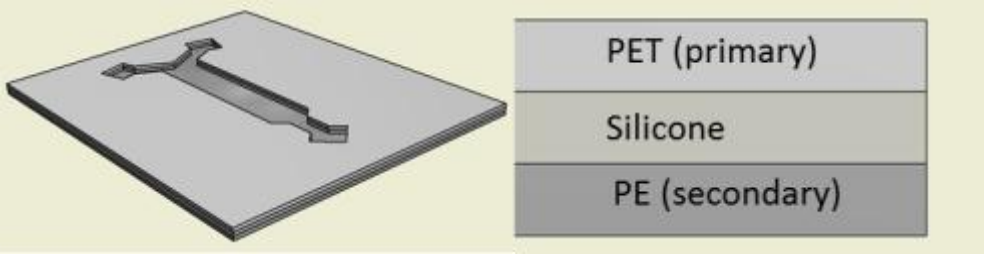

Figure 38 A representative microfluidic channel geometry was cut into primary liner and silicone tape but not into the secondary liner (left), Schematic of the silicone tape between the liners (right)

Geometries were designed in Autodesk Inventor Professional™ and exported in *.dxf* format to the plotter cutter (Silhouette Cameo, Graphtec™), which excised them from the liner-tape-liner stack. Devices were assembled starting with a bulk PDMS layer. PDMS was mixed, cast and cured as described previously, in a petri dish with no feature mould, so that a smooth flat surface was formed for the tape to adhere to.

The secondary release layer was removed from the tape and the exposed silicon adhesive brought into contact with the PDMS. Flow connections were cut and cleaned as previously described (Figure 39).

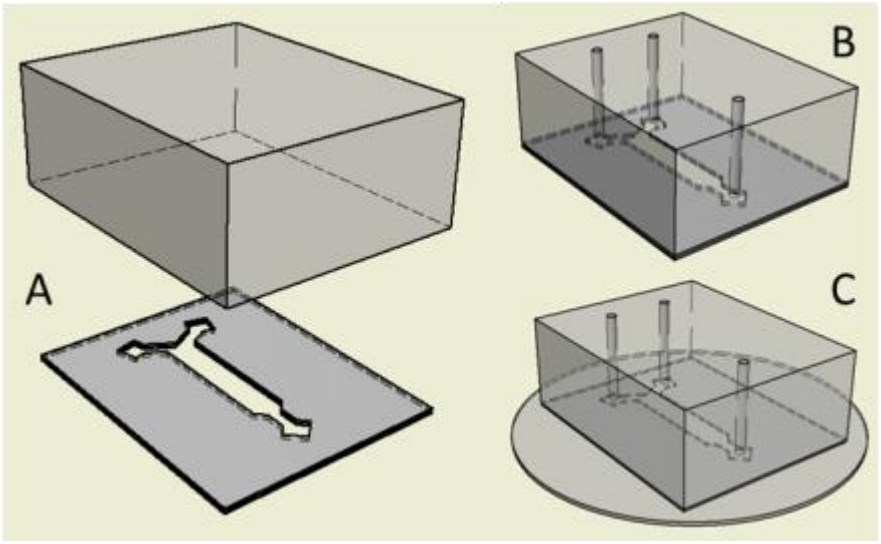

Figure 39 A) The secondary liner is removed and the tape flipped over to adhere to the PDMS. Once adhered, access ports are cut with a biopsy punch B), before the primary liner is removed and the device attached to glass C).

The primary release liner was then removed and the second adhesive surface brought into contact with the glass. Initial contact was performed at room temperature. Curing to improve the bond strength was done on a 45°C hotplate under moderate compression (a 1kg weight placed on the device) overnight. Typical dimensions are in appendix 10.4.2.

2.6 Cell culture

2.6.1 Sterilisation

All devices and materials for cell culture were sterilised at >100°C for at least 1 hour. Cell and reagent handling was performed in a laminar flow hood with aseptic technique. Solvent sterilisation was avoided as it can have deleterious effects on bonds between layers, and could remain in the porous PDMS with later cytotoxic impact (see later results).

The sterilised surfaces were then coated with ligands and covered in culture media overnight, before cell harvesting and plating

2.6.2 Harvesting

This protocol was carried out by technicians Mr Tim Smith and Mrs Dhruma Thakker.

Hippocampi were dissected from the embryos of Wistar E18/19 neonatal rats, and the neural cells were dissociated using enzyme (Trypsin-EDTA, Sigma). Cells were suspended in Neurobasal buffer with B27 supplement and Pen/Strep antibiotic.

The cell suspension was centrifuged and re-suspended in more media, in order to dilute it to volume densities appropriate for either coverslip or microfluidic channel culture.

2.6.3 **Plating**

For culture on coverslips cells were plated at $1.5x10^5$ cells per mL (150 per µL or mm^3). 500µL droplets of suspension were plated onto 19mm diameter ($284mm^2$) coverslips, giving a plating density of 264 per mm^2.

The suspension media was drawn off after 30 minutes cell settling time, and replaced with fresh Neurobasal buffer.

2.6.4 **Feeding**

Culture media was replaced at 1 day in vitro (div), 2 div, and 5 div by removing 0.8mL of buffer from the well and replacing with 1mL of fresh buffer. The additional volume compensates for any evaporation that might have increased osmolarity in the buffer. Additional media replacement was not done after the 5 div time point.

2.7 **Summary**

A range of materials and ligands are available, but not all can be utilised in the same device, and many require separate/conflicting protocols for their use.

The fabrication processes must meet a number of conflicting requirements, as discussed in chapter 1, balancing the need for a robust bond between channel and substrate, homogeneous ligand deposition, sterility, incorporation of sensing and recording elements, facility of cell suspension injection, and time required.

Initially the emphasis is on the survival of cells so that they are as likely to survive and grow healthily in a confined channel as on an entire coverslip. Cells must be able to survive in the device. This requires a viable ligand at the end of fabrication, so any process which invalidates this cannot be used after

the ligand deposition. As a precursor step, ligands and other bonds cannot be reliably placed on a contaminated surface, so the substrates must be cleaned beforehand.

To seal the PDMS channel to the substrate it is possible to use plasma bonding, PDMS pre-polymers, silane immersion, and ultimately silicone tape. These represent a method evolution covered in subsequent chapters, from the most common and available method (oxygen plasma) to a more flexible process compatible with all other device elements (silicone tape).

Metal features of different geometries can be deposited using photolithography and evaporation. These are entirely compatible with subsequent fabrication steps, but forethought is needed to correctly align them with other device features, and access them off-chip.

Where it is anticipated that the sensor may be optical rather than electrical (as in the case of SPR) the attachment of metal to substrate requires a ligand instead of wetting metal.

In all cases the device must be rendered sterile before functionalization and cell seeding. This precludes some pre-bonding methods as the bond requires heat to cure.

The reagents and other consumables used in this thesis are listed in appendix 10.1.

3 Primary cell culture in microchannels

Although it is commonplace in literature to grow dissociated neural cultures in microfluidic devices (Kim et al. 2007a), such devices are not typically intended for rapid drug delivery. Consequently the attachment of channel to substrate may not be particularly strong and could fail under pressurised liquid flow. To ensure a very robust bond between the channel and substrate, it may be necessary to use materials and bonding techniques that could prove inimical to cell survival.

A baseline of cell growth under static control conditions needed to be established in such devices before adding the complexities of perfusion. This baseline includes morphology longevity of the culture, with regard to surface, channel volume, cell plating density, and bonding strategy.

3.1 Design and fabrication of channels

A drug delivery system that can wash agonist on and off a cell culture within a few seconds is required. Ideally the switching time would be under 1 second, though this may not be achievable. An in-line delivery method would be far too slow, and so an arrangement of two parallel fluid streams, one containing agonist and the other purely buffer, is preferred. By altering the relative flow rates of the streams while keeping the total fixed, the interface between the agonist and buffer can be swept over the culture region.

The system must ensure a clear distinction between drug and buffer regimes, to ensure no inadvertent pharmacological stimulation when in theory only buffer should be over the cell region. This requires a very sharp concentration gradient. The typical dose-response curve for neuromodulators such as dopamine is logarithmic rather than linear. Doses of 4µM or even 0.3µM are reportedly sufficient to induce a receptor response (Kebabian et al. 1972), and so a contrast of at least 100:1 between the agonist and buffer is desired.

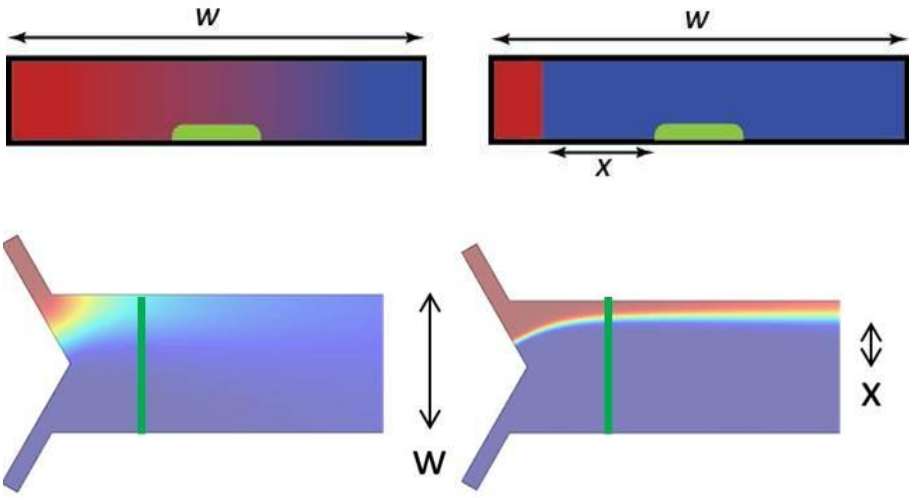

Figure 40 A COMSOL modelled channel in cross section (green lines). On the left, a regime dominated by diffusive transport is shown. There is no clear distinction between agonist (red at 100% concentration) and buffer (blue at 0% concentration). On the right, a regime dominated by inertial transport has a much sharper transition region. However, in order to ensure that the cells (green) only experience drug exposure when it is intended, a distance x between cell region and concentration boundary is necessary. This presupposes that cells grow only in one region of the channel, which is addressed in later chapters.

Although advection must therefore dominate in the culture chamber, it is important to mitigate the viscous forces exerted on the neural cells. Studies indicate that neurons are very sensitive to high shear stress, though there is no clear-cut consensus on the optimum range, with some reporting 0.5mPa (Kolnik et al. 2012a), and 7.2 mPa (Joanne Wang et al. 2008) while other groups report brief flushing regimes of 900mPa (Biffi, Piraino, et al. 2012) without cell adhesion failure.

In addition, it is preferable to reduce the turnover of nutrients and reagents in the flowing liquid, and thus the volume of liquid used, particularly for long-term experiments that may progress for several days or even weeks (as discussed in chapter 1), should be as low as practical.

These requirements will necessarily conflict, as a flow regime that allows rapid, unambiguous agonist delivery will unavoidably perturb the microenvironment around the cells. Conversely, minimising this perturbation effectively precludes drug delivery on biologically relevant timescales.

3.1.1 **Methods – channel design**

There are two independent parameters that can be altered to influence the flow regime: i) channel geometry, and ii) externally applied mass flow rate. The latter is determined by the perfusion apparatus, and is covered in greater depth later. The former is investigated with finite element model (FEM) analysis, specifically the multiphysics package COMSOL, to estimate the optimal solution before the channel and system are designed.

3D geometries were designed in Autodesk Inventor and exported into COMSOL, with typical parameter values in appendix 10.2. COMSOL modelling is used to investigate the interaction between diffusion and advection in this chapter, in this case by solving sets of equations for laminar flow and for chemical species transport. As described in chapter 1.7.6, caution should be exercised in using such software, as an incorrect input will give a misleading or even impossible answer, as will too much leniency in the size of the element or acceptable residual error.

For all models, parameters relating to inertial and diffusive phenomena on cells were analysed 6µm off the channel floor (as in Figure 41), as this is the typical height of a settled neuronal soma (Kuffler, S., Nicholls, J., & Martin 1984). As the latency (delay of onset relative to the change at the channel inlets) of a flow pulse will increase away from the channel inlets, it is assumed the culture will be placed around 1mm from the inlets. The culture region (Figure 42) is not directly modelled in COMSOL, but the concentration gradient across that region is crucial.

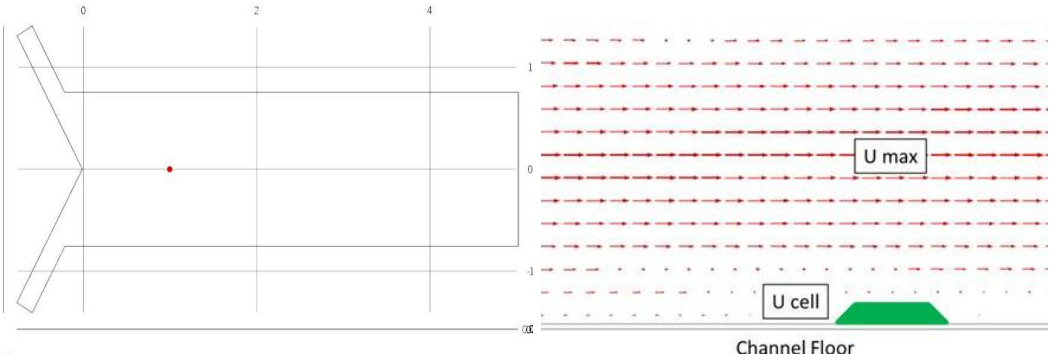

Figure 41 In a typical COMSOL model, a point of interest (left, red spot) is selected and several physical parameters can be observed pertinent to that point. In the case of velocity (right, vector field shown), it can be seen that a cell 4-6μm in height experiences comparatively little velocity due to the no-slip condition, though shear stress will be higher, due to Poisseuille flow.

i) Typically microfluidic channel heights are in the region of 100μm or below. This is partially due to the relative ease of fabricating moulds for soft lithography at such heights, while a channel of such height is also unlikely to block or impede transport of particles or cells in solution. For some purposes, such as the separation of co-cultures such that only their axons and dendrites can make contact (Taylor et al. 2003), the channel heights may be as low as 2μm, but this is not required here

100μm is thus taken as the initial height value.

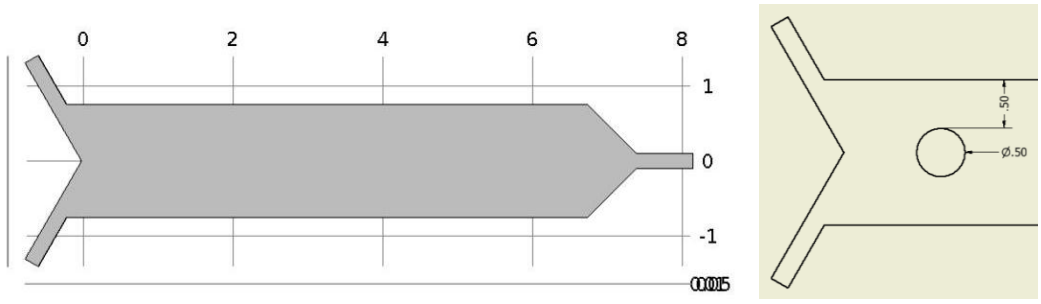

Figure 42 Rendered geometry (x and y) of the channel to be modelled. A region (not modelled) 0.5mm across is where the cells would be confined. The region is located within 1mm of the inlets to minimise latency.

3.1.2 2.1 Shear and concentration profile change with flow rate

A fixed geometry with aspect ratio 1:15 was used initially, and inlet flow rates were altered across several orders of magnitude. Subsequently the effect of altering the height was explored. From this, the channel velocities needed to give a steep concentration gradient became clear, and those velocities giving

a shallow concentration gradient, or inducing too much shear stress, were discarded as drug delivery options for delivery of neuromodulators onto primary cells. Note however that we would in theory also like to run at lower flow rates and slower drug pulses, and for such ranges the ability to control at 1nL/s becomes important.

3.1.3 2.2 Drug latency

The parallel flow inputs were time-varied, in order to determine the latency of boundary shifting in response to altering flow rates. A model of this occurring is shown in Figure 43.

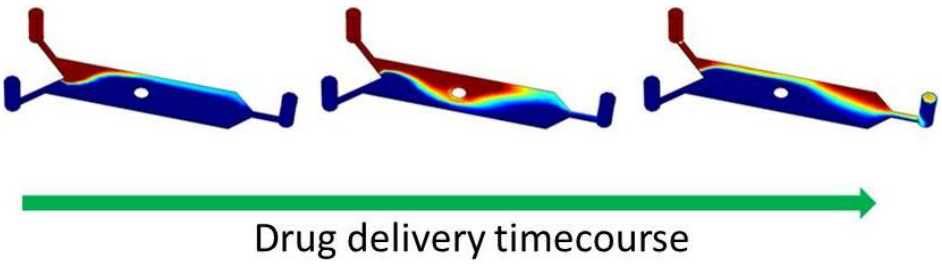

Figure 43: Transiently switching and then restoring the ratio of inlet flow rates

In the figure, altering the ratio of agonist (red) to buffer (dark blue) changes the position of the interface so that is briefly swept back and forth across the channel. As time increases (green arrow) the white circle representing the culture region is temporarily exposed to the agonist. This timescale should ideally be under 1 second. Note that although the circle here is in the centre of the channel, in reality it would need to be closer to the inlets in order to reduce the latency.

3.1.4 Results of channel design

3.1.5 Effect of flow rate on shear and concentration gradient

3.1.5.1 *Shear stress*

It is expected, given that the operating regime is laminar flow in a Newtonian fluid of constant viscosity and density, that shear experienced by the cells will increase linearly with flow rate, as both flow rate Q and shear τ are functions of velocity u.

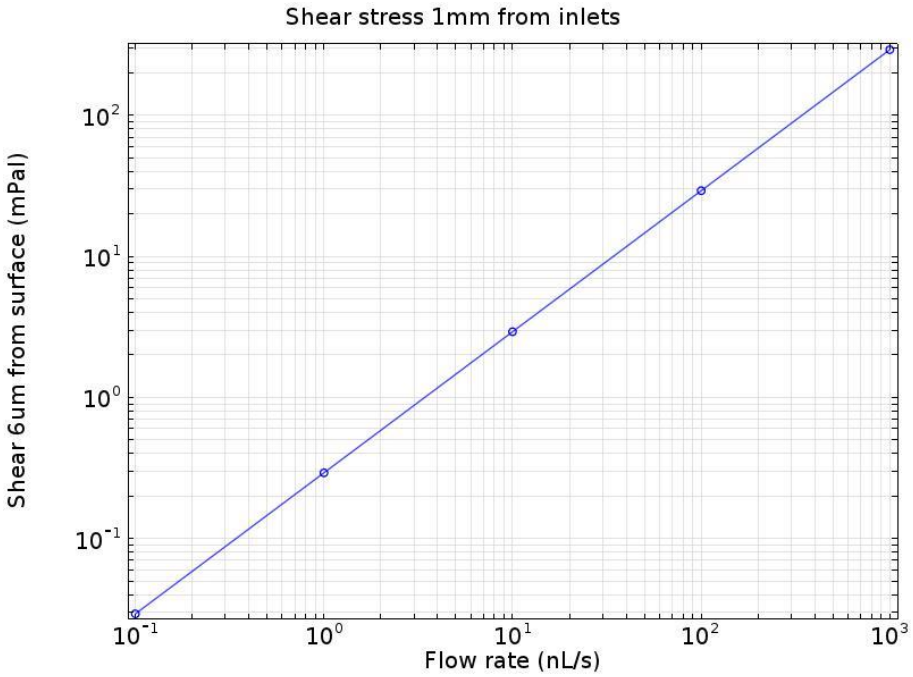

Figure 44 Shear stress (mPa) and velocity (mm/s) increasing linearly with flow rate. These values are taken at a single point 1mm from the channel inlet, 0.75mm from the wall and 6µm from the floor. The channel cross section is 100µm x 1.5mm, an aspect ratio of 1:15.

From the model (Figure 44), flow rates exceeding 100nL/s induce a shear stress in excess of 20-30mPa, which is the higher end of typically reported cell survival regimes. This equates to a velocity (at the cell) of around 0.3mm/s.

This marks the higher end of the usable range. Shear regimes reported for long-term culture of neural cells are typically under 10mPa (Lee et al. 2005), though 500mPa has been reported (Liu et al. 2013), indicating that shear alone is not necessarily the best metric for determining longevity. This is considered further in later chapters.

3.1.5.2 *Concentration gradient*

As for the shear model, the same analysis point and channel geometry are used with a range of total flow inputs (Figure 45). Here the concentration differs between the inlets to the channel. One is held at a finite concentration of 100µM while the other is zero. The diffusion coefficient of the drug is taken to be that estimated for dopamine in free media (Lin et al. 2013) at 37°C, around 600µm^2/second. The flow rate inputs do not alter value and are kept at a fixed ratio of 1 (agonist) to 9 (buffer).

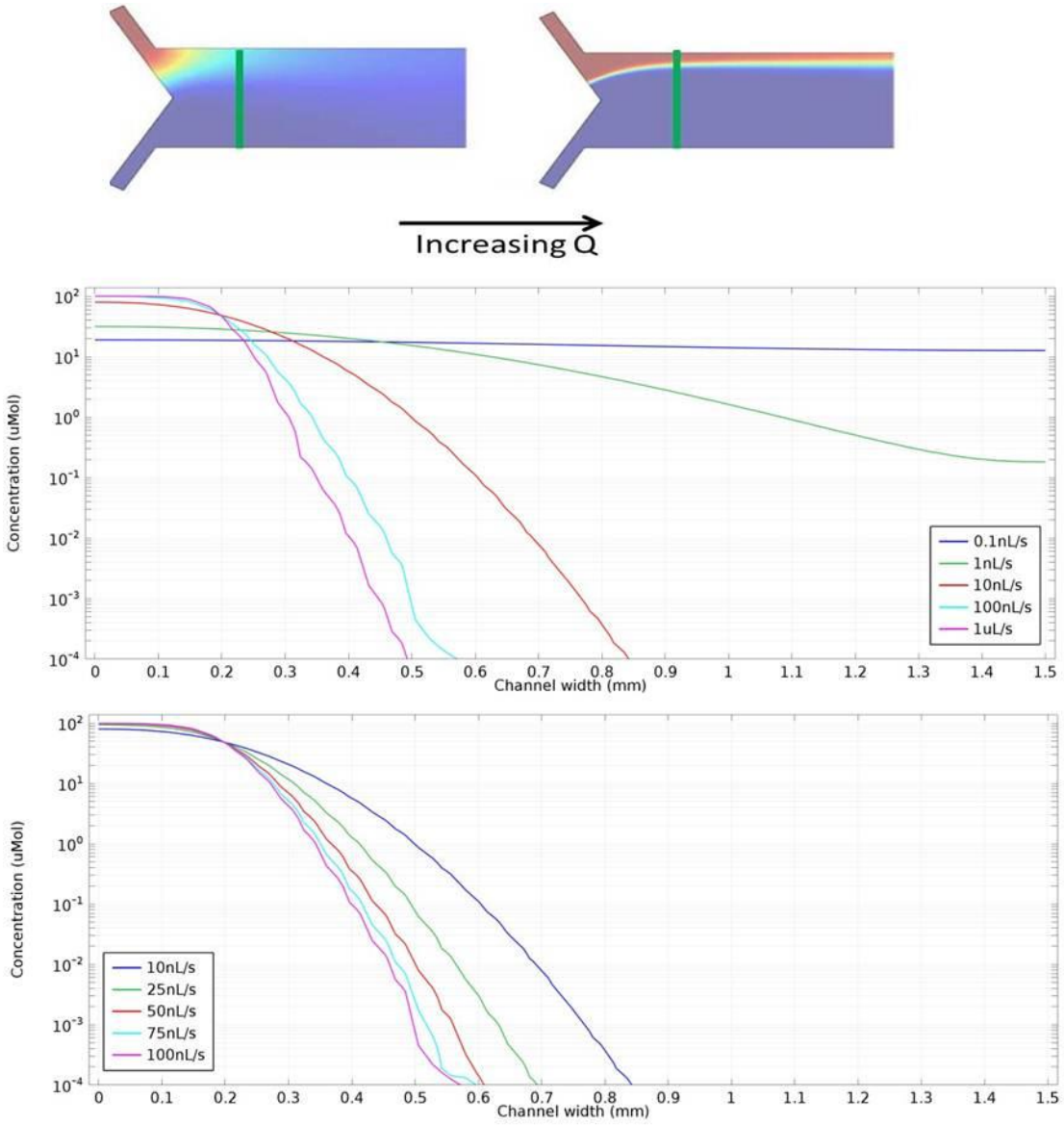

Figure 45 Top: The channel width is shown with the agonist concentration drug inlet (100µM) on the left and the buffer (0M) on the right. Resulting concentration gradients 1mm from the inlets across several orders of magnitude, and within a sub-range (bottom) are shown. The ratio of inlet flow rates drug: buffer is 1:9 here, with the total of Q_{drug} + Q_{buffer} shown in the legend.

When reviewing the concentration gradient, it becomes apparent that anything under 10nL/s does not effect a guaranteed 1:100 change in concentration, such that the concentration over the central 0.5mm of the channel is under 1µM in steady state co-flow.

In fact, the useful ranges appear to between 25 and 100nL/s, for an unambiguous transition.

3.1.6 **Péclet number analysis**

The Péclet number (Pe) is defined as the ratio of molecular transport due to advection to molecular transport due to diffusion. If Pe is greater than 1, advection is said to dominate, while if it is less than 1 diffusion dominates.

It can be calculated as the product of the Reynolds number Re (see equation 8) and the Schmidt number Sc, where

$$Sc = \frac{\nu}{D} \qquad [13]$$

such for a given particular liquid $\boldsymbol{\nu}$ is the dynamic viscosity, and **D** is the diffusion coefficient of a particular solute.

Many of these parameters are also expressed in the Reynolds number, so that

$$\boldsymbol{Pe = Re \cdot Sc = \frac{u.D_H}{\nu} \cdot \frac{\nu}{D} = \frac{u.D_H}{D}} \qquad [14]$$

So Pe is the ratio of velocity $\boldsymbol{u}$ to diffusion coefficient D, with a scale factor of the hydraulic diameter D_H.

Remember from equation 9 that D_H is given by $\frac{2wh}{w+h}$ and thus for a channel of width 1.5mm and height 100µm, the hydraulic diameter is 1.875×10^{-4} m. The diffusion coefficient of dopamine is estimated as before as 600µm^2/s (Lin et al. 2013).

Thus

$$\boldsymbol{Pe = 312500 \cdot u} \qquad [15]$$

For advection to dominate, Pe must exceed 1 and so the minimum $\boldsymbol{u}$ can be is 3.2µm/s.

In the channel of cross-sectional area 1.5mm x 100µm this velocity equates to a flow rate of 4.8×10^{-13}m^3/s, or 0.48nL/s.

To have advection strongly dominate, Pe must be much larger than 1 (see Table 1).

Q (nL/s)	U (µm/s)	Pe
0.48	3.2	1
25	166.67	52.08
100	666.67	208.3

Table 1 Comparison of flow rate, velocity and Péclet number for a specific geometry and diffusion coefficient

Thus for the range of flow rates modelled as useful in COMSOL, a Péclet regime of between 52 and 208 is described.

3.1.7 **Drug delivery latency**

Again the flow rate is tested across several Q values with a co-flow of drug and buffer. A data point located 1mm from the inlets and 6µm from the channel surface is selected, as before. Here however a change in Q_{drug} and Q_{buffer} is modelled such that in 1 second the ratios are flipped and reversed (see Figure 46 below).

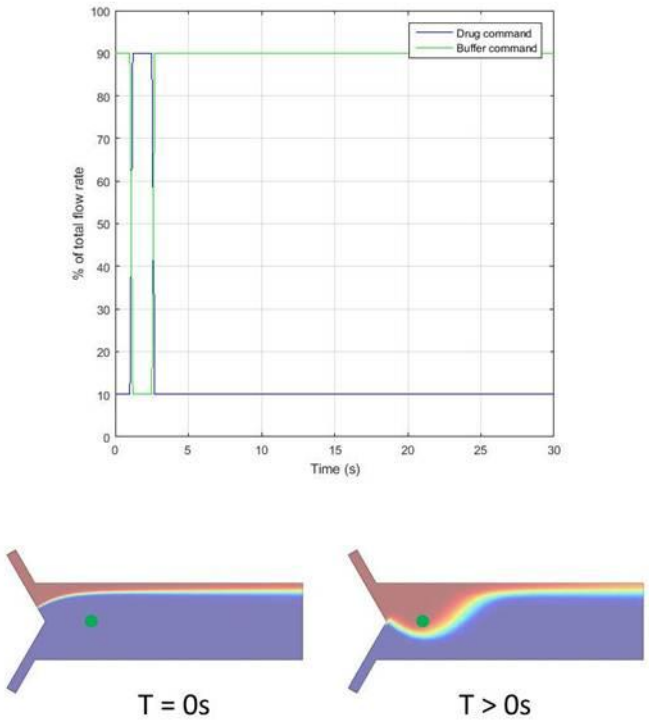

Figure 46 From a steady state 1:9 co-flow, the ratio of inlet flow rates Drug: Buffer is flipped 9:1 and then back to 1:9 in 1 second. The total flow rate Q never changes. As a result, a pulse of agonist (red) crosses the channel and then recedes. At the point of interest (green), the concentration change is modelled.

Based on the range of useful values carried over from the previous section, only the values 10-100nL/s are considered here for total inlet flow rate. The model runs for 30 seconds to evaluate the concentration change over the cells.

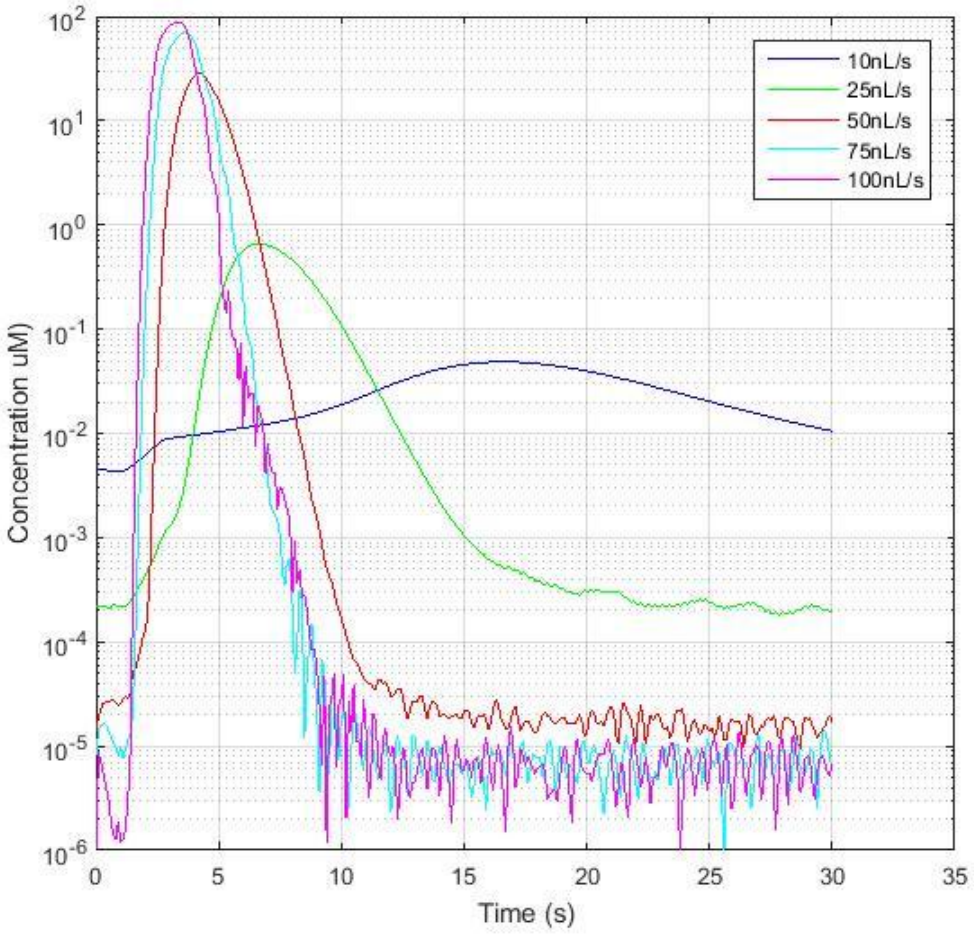

Figure 47 For 5 different total values of Q (total of drug + buffer), labelled in the figure, the concentration change occurring over the green region in Figure 46 is profiled.

It can be seen (Figure 47) for a value of total Q less than 25nL/s the concentration change lags the command by up to 20 seconds and changes by only a few nM, while at higher total flow rates, the concentration almost 100% of the total possible (100µM) and occurs within 1-2 seconds.

Thus the flow rate range 30 to 100nL/s is most useful for prompt drug delivery, and the high end of this range is most useful for very prompt delivery. In theory (see chapter 1) 100nL/s is acceptable to neuronal growth.

3.1.8 Fabricating the channels

Due to the intended feature height, which would be difficult to machine, the channels were fabricated using the soft lithography technique of PDMS on photo-patterned SU-8 100 (see Figure 48 and Chapter 2.5). The SU-8 100

was spun to a nominal height of 100 µm, though when measured with a contact profilometer this value could be as low as 65µm.

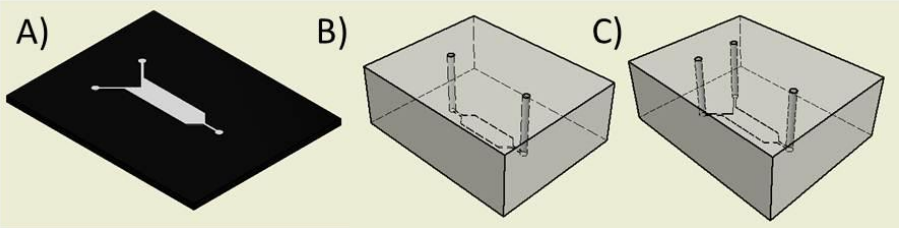

Figure 48 Channels were fabricated in PDMS on SU-8 (A), then the connection lines bored. The first configuration (B) of a single inlet is used initially, as it is simpler to load with fluid and suspension, and co-flows are not considered at this stage.

Once cast and cut out, the PDMS channels were bonded with oxygen plasma to glass (see methods 2.5.2). The plasma bond is irreversible and should not give way when liquid is injected through the channel.

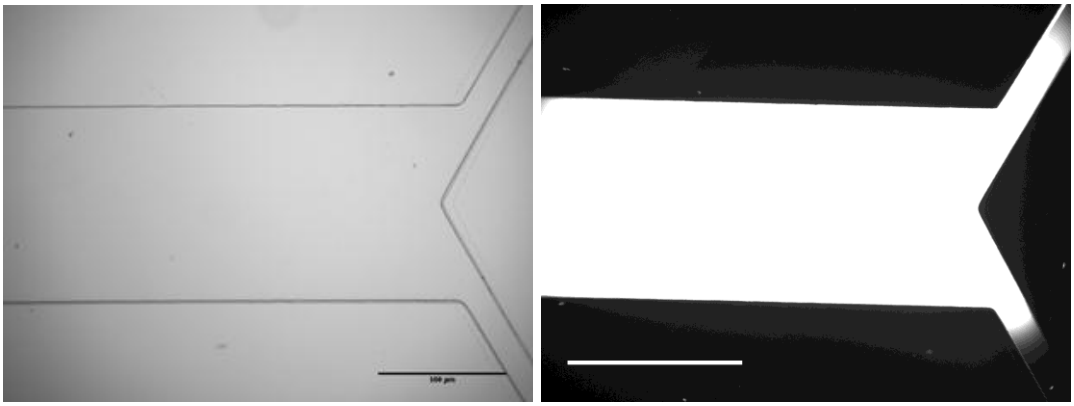

Figure 49 A fabricated channel is imaged in brightfield (left, scale bar 500µm) and fluorescence when flooded with fluorescein in PBS (right, scale bar 1mm).

The channels were tested by injecting co-flows of water and fluorescein (0.1% concentration w/v in Phosphate Buffered Solution, PBS) at syringe flow rates up to 1mL/minute, without the plasma bond delaminating or leakage from the channel (Figure 49).

Although ultimately a 2 inlet channel will be necessary for parallel laminar flows, initially a simpler geometry of 1 inlet is used. This has no effect on the shear experienced 1mm inside the channel.

An alternative approach of *xurography* (Figure 50 chapter 2.5.5) was employed such that a silicon adhesive no more than 125µm high could be

used to form not only the bond but the wall of the channel, as the adhesive was double sided and could bond effectively to both glass and PDMS without the need for surface activation.

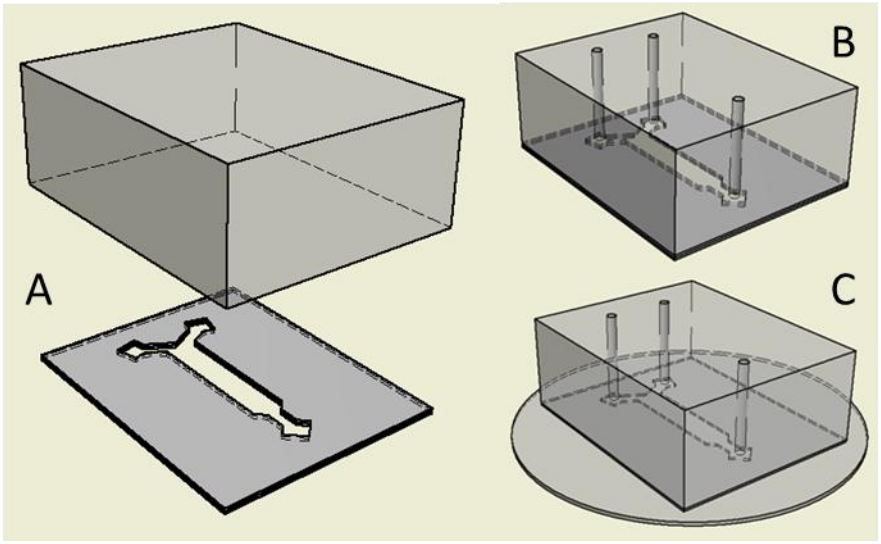

Figure 50 Assembly sequence for a silicone tape microfluidic channel

3.1.8.1 *Interfacing with an MEA*

Ultimately it is intended that the neurons should be interrogated with Surface Plasmon Resonance (SPR) rather than spike sorting. It is intended to confine cells to a tight <1mm region within a channel of the dimensions arrived at above.

The MEA currently represents the most effective method for detecting electrical activity of cells, however, and so cultures and channels will need to interface with it as an interim solution.

In order to fully utilise the 60 electrode array it is necessary to increase the width of the channel beyond the array width of 1.4mm. The channel should be long enough to cover the entire MEA array and the reference electrode. Therefore it should be at least 2-3mm wide and at least 6-7mm long (Figure 51). The microfluidic channel geometries considered so far would not be compatible with this.

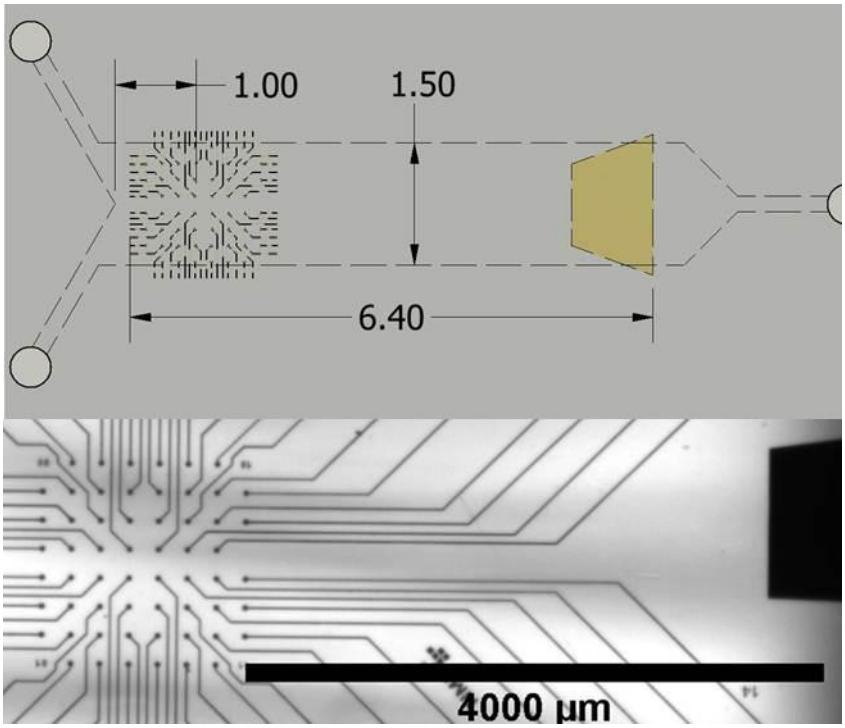

Figure 51 Image of the MEA showing the distance to the ground electrode, and thus what minimum dimensions a channel will need to have. For co-flow experiments involving an array of this size with a reference electrode so distant, the channel will need to be wider, or the cells confined to only a sub-region of the full array, in order that some cells are not continually exposed to the agonist.

The plasma bond cannot necessarily be used to affix a channel to the MEA surface. As the MEA is not a disposable substrate, an irreversible bond is a hindrance, since the MEA will be re-used and any cell or ligand residue will need to be cleaned back before re-applying ligand.

Accordingly, an alternative method of affixing the channel to the MEA was devised. A cruder millimetric mould was machined to provide a much larger cross section.

It was anticipated that the channel might need to be pressed down on to an existing neural culture on the MEA in order to obtain the high density cultures usually grown on such arrays; in such a case air bubbles might be trapped which would kill cells.

To prevent this, the channel height is increased to 1mm. This requires a machined metal mould rather than photolithography (see Figure 52).The channel length remained 10mm so that the reference electrode is included.

Because drug delivery is of the culture is not considered at this stage, there is no need for more than one inlet to the channel this device is used as a test-bed for static culture at different cell plating densities, and can also be used a potential test-bed for continuous perfusion, while evaluating the electrical response via the MEA.

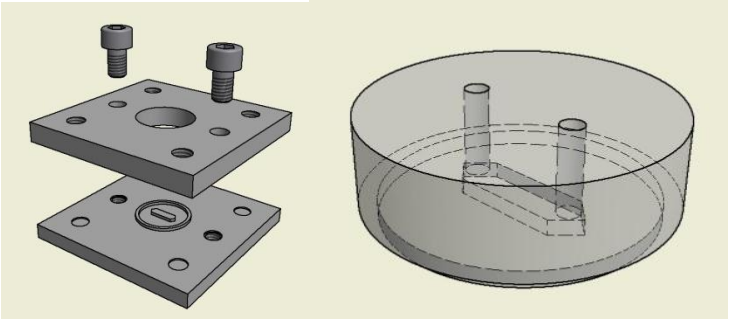

Figure 52 The machined millimetric mould (left) and a cast PDMS disk (right) with access ports punched. Note the rim at the base, which permits the PDMS to form a complete seal with the glass surface without clashing with the glue used to bond the glass ring to the glass plate. See appendix 10.4.3 for dimensions.

The moulds were made before it was discovered the standard glass ring affixed to an MEA plate is not necessarily placed completely centrally, being offset from the centre of the array pattern by several hundred microns in some cases; and thus a 1.5mm wide channel pressed down into the ring might not cover all of the electrodes. A 3mm wide channel was sufficiently wide to ensure all electrodes were covered (Figure 53).

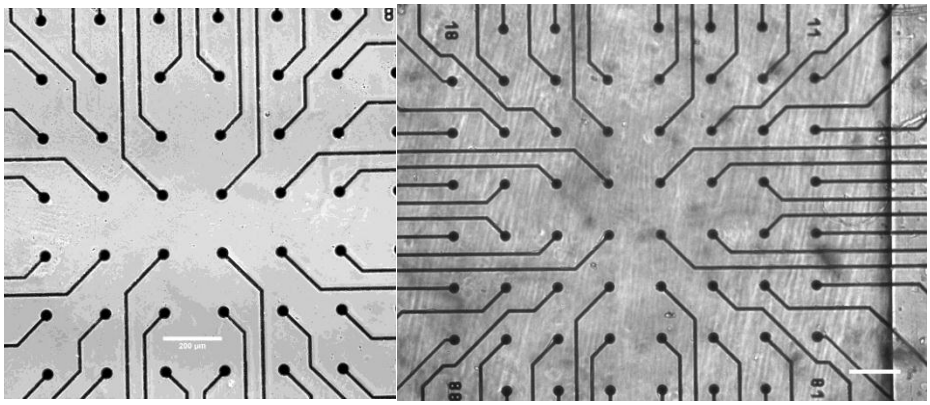

Figure 53 MEA (left) with a PDMS channel attached (right). The channel edge is a vertical line to the right of the array. Scale bar 200µm.

3.1.9 **Design Conclusions**

A channel geometry intended for a particular flow rate range has been designed and built according to the drug delivery requirements. A separate

channel geometry intended for test bed culture analysis on MEAs was also fabricated.

3.2 Biocompatibility of surfaces, and plating density

Before undertaking *in vitro* culture in enclosed microchannels, it is first necessary to get a benchmark of how primary neural cells grow *in vitro* on open surfaces under large, unperturbed media volumes. Without a measure of healthy, typical development on the chosen ligands, it is not possible to isolate the effect of the microchannel and later perfusion. Initially, entire coverslips and MEA wells, uniformly coated, were plated and cell development noted. Simple gold patterns were then generated on glass to establish that there would be no toxicity arising from photolithographic processes.

3.3 Open surfaces (coverslips without channels)

3.3.1 Positive control (healthy cultures)

19mm glass coverslips as received were heat sterilised, and functionalised with Poly-L-Lysine. 500µL of primary neural cell suspension at density 150 cells per µL were pipetted onto the surface. This quantity on a 19mm diameter coverslip equates to 265 cells per mm^2. 2mL of fresh Neurobasal media covered the coverslip in a well plate. The cells were Brightfield imaged at time points up to 14 div.

3.3.2 Negative control (unhealthy cultures)

Cells were plated as before onto sterile glass with no functionalization. As there is no pre-existing extracellular ligand, it is expected that most or all cells will die within 24 hours of plating.

3.3.3 Plasma treated glass

Before PLL functionalization, the coverslip was exposed to oxygen plasma, as this will be necessary for plasma bonding of the glass to a PDMS microchannel. The effect of this exposure, as well as subsequent immersion in Neurobasal media prior to functionalization, was investigated. Cells were plated as before.

3.3.4 Gold control surface

Ultimately the cells will need to grow on gold surfaces for electrode or SPR analysis. Gold coated coverslips were functionalised with AUT, and plated as for the glass: PLL surfaces with equivalent cell suspension densities.

3.3.5 MEAs as surface

Silicon nitride/titanium nitride micro-electrode arrays (Multi Channel systems), were functionalised with PLL and plated with a higher density cell suspension (>300 cells per µL). This is deemed necessary to ensure enough cells will be close to the electrodes for electrical recording.

3.4 Results of Surface compatibility

3.4.1 Positive Control: PLL on glass

The simplest culture is PLL on cleaned glass, at a density comparable to literature (250 cells per mm^2) in Neurobasal kept undisturbed in an incubator. There are no complications due to processing of the glass for bonding or metal evaporation, or due to reduced culture size or plating density.

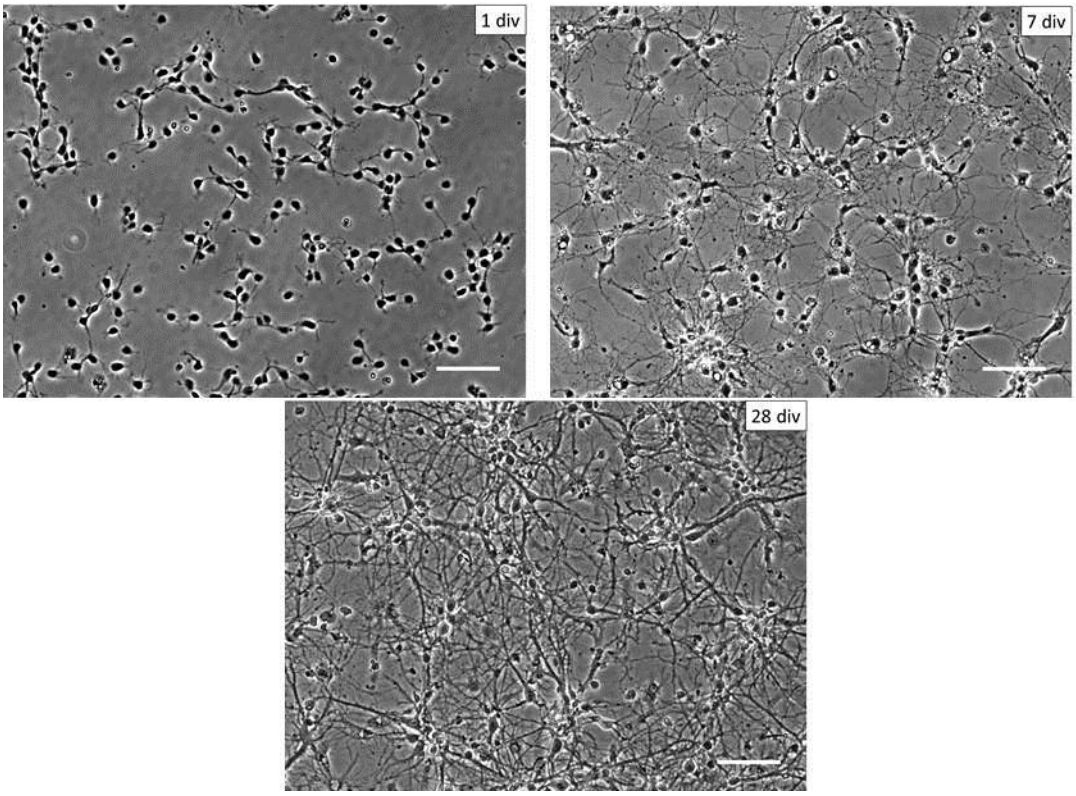

Figure 54 Positive culture control: Primary hippocampal cells grown on PLL treated coverslips at 150 cells per µL, which here becomes 330 cells per mm^2 (counted with ImageJ). Time points shown at 1 div (24 hours after plating, 7 div, and 28 div. Scale bar 100µm.

On the positive control surface (Figure 54), cells settle and form dense networks with very few dells dying. Although there is some fasciculation with age, there are no regions which the cells actively avoid. The ability to visually discriminate an individual neuron in a planar culture in bright-field is lost around 7 div. Cultures can carry on indefinitely.

3.4.2 Negative Control: no ligand

Conversely, it is useful to establish what a surface incompatibility issue looks like. Cleaned glass coverslips were plated directly with the same suspension density and no ligand.

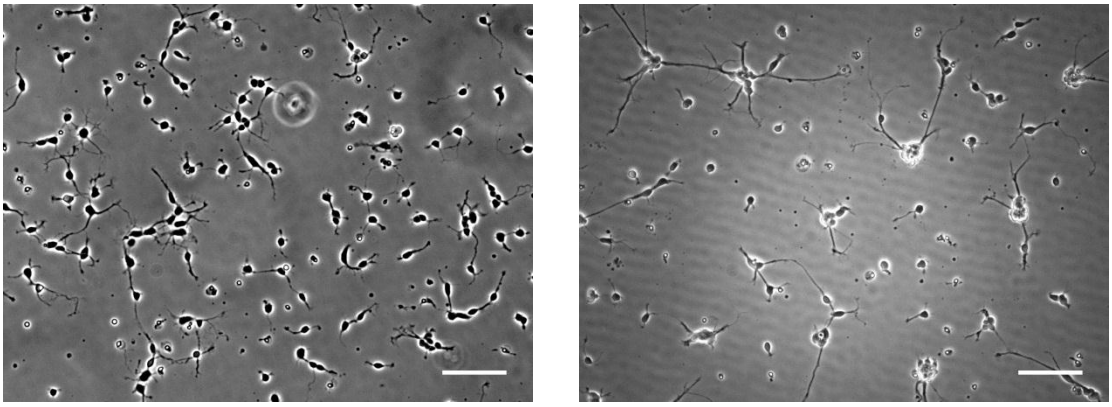

Figure 55 Cells plated on surface with no ligand (1 div and 2 div, scale bar 100μm). Note that cells very quickly begin to cluster and individual soma are not as spread out as for the positive PLL control.

Where no ligand is provided for cell adhesion, the cells cannot settle and remain in a globular form instead of flattening out (Figure 55). Although some axonal connections are formed, these are very sparse and often and do not survive long. Within 48 hours the culture is mostly dead. Where this behaviour is seen in further experiments, it indicates ligands have not been laid down correctly.

3.4.3 Plasma treatment and its effect on PLL deposition

The oxygen plasma treatment was observed to have a significant effect on subsequent deposition of the PLL ligand.

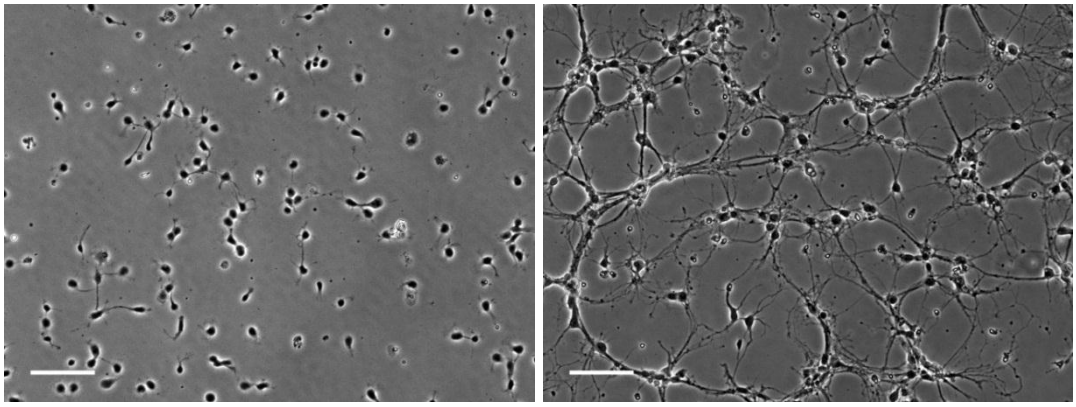

Figure 56 PLL was deposited on recently plasma treated glass, before plating at the usual density. Scale bar 100µm. Images taken at 1 div (left) and 7 div (right).

Clearly evident (Figure 56) is the tendency of the cells to join their axons into thick cables, while avoiding some areas of the glass. This *fasciculation* behaviour is indicative of heterogeneity in the ligand coverage, which is assumed an effect of the plasma treatment interfering with subsequent PLL deposition.

3.4.4 **Plasma recovery and PLL**

To overcome the effect of the plasma treatment, an intermediate step was tested where the channel is flooded with Neurobasal media for several days before flushing out with distilled water and deposition of the PLL.

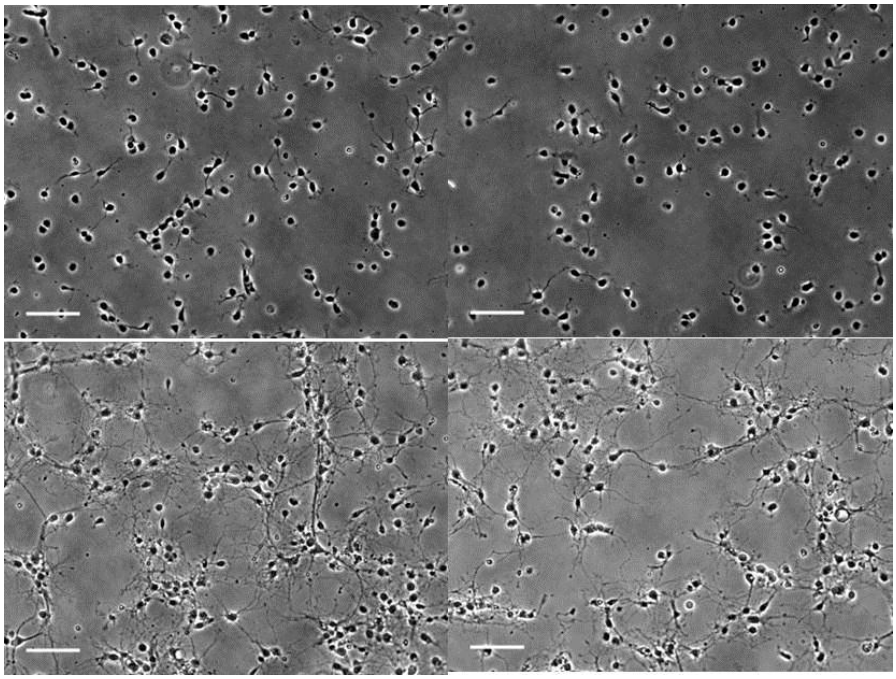

Figure 57 After plasma exposure, the glass was immersed in Neurobasal media for 1 week, before being rinsed and dried. PLL was then deposited as usual. Top left: control at 1 div, top right: recovered surface at 1div. Bottom images both at 7 div. scale bar 100µm.

The effect of the plasma treatment was negated by immersion 'recovery' in the Neurobasal culture media (Figure 57). This rendered the surface suitable for subsequent PLL deposition, with no significant increase in fasciculation.

3.4.5 **Control: Gold and AUT**

As described in chapter 2, gold surfaces were functionalised with AUT and cells grown on the surfaces (Figure 58). Their morphology is compared with similar glass: PLL cultures.

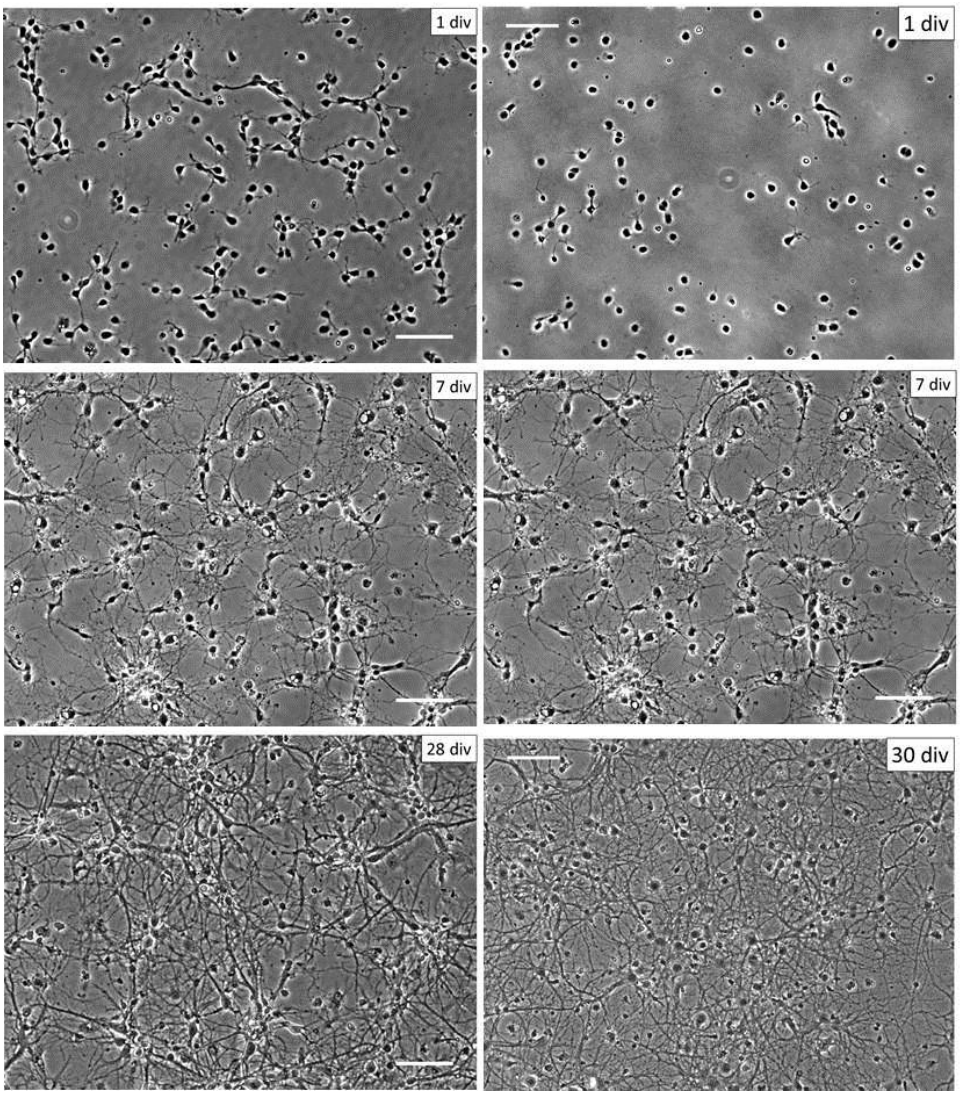

Figure 58 Comparison of gold and glass control surfaces. Although plated at the same nominal density, the glass cultures (left figure at each time-point) fasciculate more over time, while the gold cultures (right figure) appear more homogeneous. Scale bar is 100µm.

From the figures cells plated at similar densities (150-300/µL) on a large gold: AUT region are no worse than cells grown on glass: PLL (see previous), and are arguably better in terms of homogeneity. Cells were plated onto the AUT ligand within 12 hours of removal from the AUT solution.

3.4.6 **Cells on MEAS (no channel)**

Cells were plated on to MEA surfaces coated with PLL (Figure 59). As these substrates are re-used after each culture, the cells, ECM and ligands must be removed to leave a clean surface for the next culture. Detergent (Decon 90) is used to remove the biological debris, before processing in an autoclave (121°C) which sterilises the MEA but does not necessarily remove adhered material.

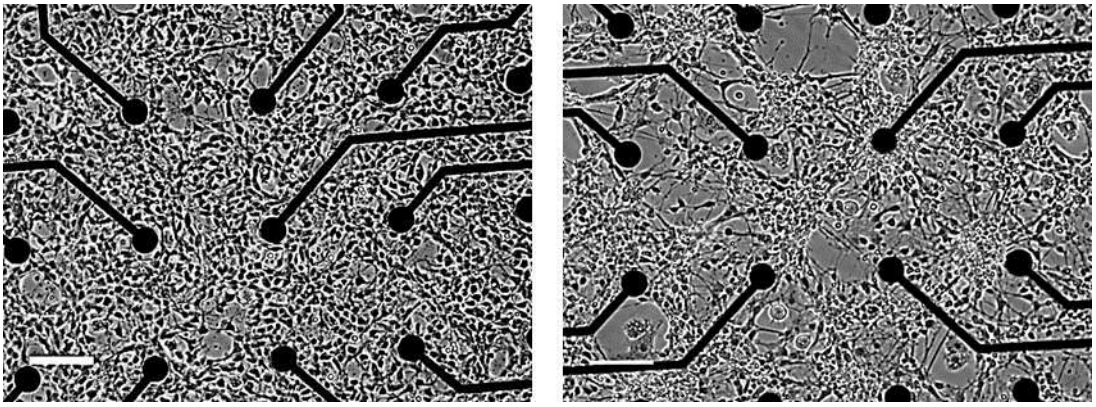

Figure 59 Neural culture growing on PLL in a MEA well. The plating density is double previous (500 cells/mm^2). At 1 div (left), the culture appears healthy and homogeneous, while at 7 div (right) fasciculation is clear. Scale bar 100µm.

Consequently it is possible for the next PLL layer to be heterogeneous, and this may be the cause of the observed fasciculation at 7 div. Cells are typically plated at higher density on MEAs to increase the number of connections and cells near an electrode, improving the chances of recording network activity. This is considered more important than clear imaging.

Large gold area extent

Two simple gold patterns were used in order to determine the effect of gold/ glass boundaries on neural culture growth. The first pattern is a by-product of the gold evaporation protocol (Figure 60): during the process the coverslips must be secured to the ceiling of the thermal evaporation chamber. Rare earth magnets are used to secure the glass to the underlying metal ceiling at the coverslip edge, and occlude the glass there. Consequently there are regions of uncoated MPTS after evaporation, which are stripped back to the glass during the plasma step that precedes AUT deposition.

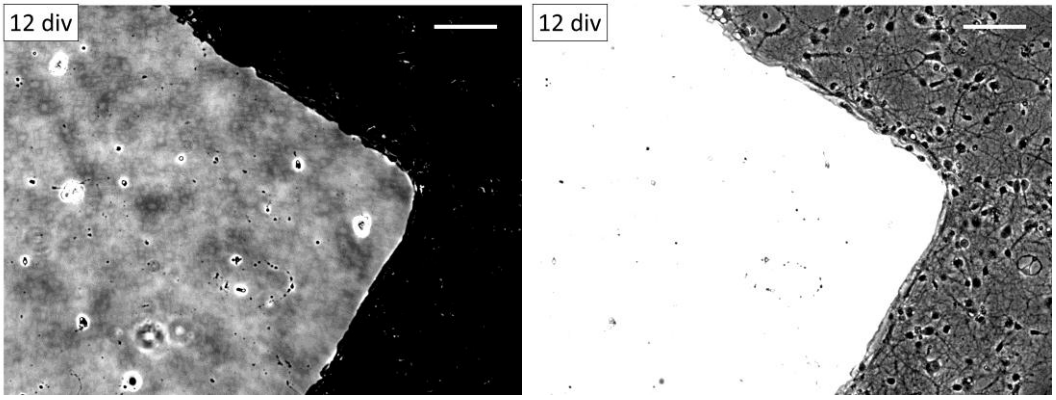

Figure 60 Region of glass on which gold was never evaporated, due to the rare earth magnets that covered that part of the glass. At 12 div, it is possible to see both the glass region (left) and the much larger gold region (right). Image contrast was altered from the original to emphasise each region. The difference in cell adhesion is obvious. Scale bar is 100µm.

The uncoated regions represent only a small peripheral percentage of the coverslip area, so the majority of plated cells will either migrate to the much larger biocompatible AUT region, or die in situ. At 12 div, there is nothing living left on the glass, while the gold region is indistinguishable from a gold region elsewhere on the coverslip.

3.4.7 Surface compatibility Conclusions

On PLL and AUT, cells grow as expected with no evident pathological growth. The surfaces and processes used do not in themselves cause cell death, provided that the functional surfaces (PLL and AUT) are correctly laid down. The culture will die or fasciculate when the surface is not favourable.

3.5 Growth and activity in channels

Having independently checked the effect of materials and fabrication processes, neural cells were then cultured in microchannels, fabricated as described previously.

3.5.1 Methods

3.5.1.1 *In millimetric channels (MEA and glass substrates)*

Millimetric channels were cast and prepared as outlined previously, then heat sterilised (160°C oven for 1 hour). The channels were then integrated with standard MEA arrays in one of two ways, to determine how different the culture plating density and development would be.

i) Pressed down onto wetted cultures.

A press-fit mechanism is used to push the PDMS plug (19.2mm diameter, see appendix 10.4.3) into the MEA well, which is provided with the MEA as an attached glass ring of 19mm internal diameter and 6mm high. Here the plating is prepared as for an open MEA culture, then after 1 div the channel is pressed down on top of the wetted, partially formed cell network (Figure 61).

An anticipated issue here is that the cells caught under the PDMS (over 90% of the culture area) may do one of two undesirable things: a) die en masse and release metabolites associated with traumatic death, which would have an influence on the otherwise healthy cells growing in the channel

b) The cells under the PDMS will continue to survive, if not optimally, and exert an influence on the cells in the channel which cannot be quantified.

In addition, the wetted area under PDMS can be source of leakage during liquid replacement, and would be inadvisable for perfusion.

However, this approach is functionally identical to how cells are normally plated done on MEAs *sans* microchannels as in the previous section, and implied the overall plating density should be comparable. It was not known at the time if a higher suspension density infused into a channel in situ would be equally effective.

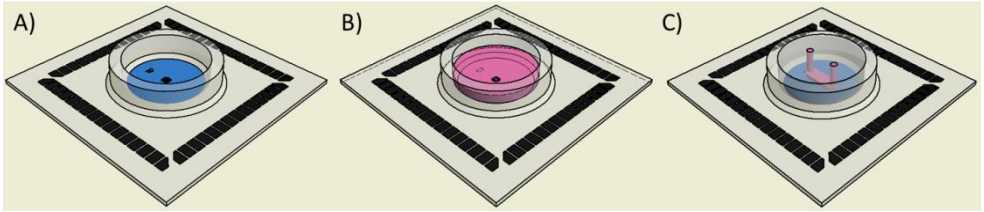

Figure 61 PLL or Laminin is deposited (A) in the MEA well, as for a coverslip. After 1 hour it is washed off. The cells are plated at so-called 'double' suspension density (500uL of 300/µL), which results in a plating density of >500 cells per mm^2 and 2mL of Neurobasal is added (B). After 1 hour for cells to settle on the ligand, the millimetric PDMS channel is pressed down onto the culture.

ii) Pressed down onto PLL functionalised MEA surfaces

Here the PLL ligand is laid down as for an open culture, then the PDMS channel is pressed into the well, and then cell suspension is added at 1000cells/µL to improve the chances of an electrically excitable cell being

present near an electrode (Figure 62). With this method there are definitely no cells outside the channel.

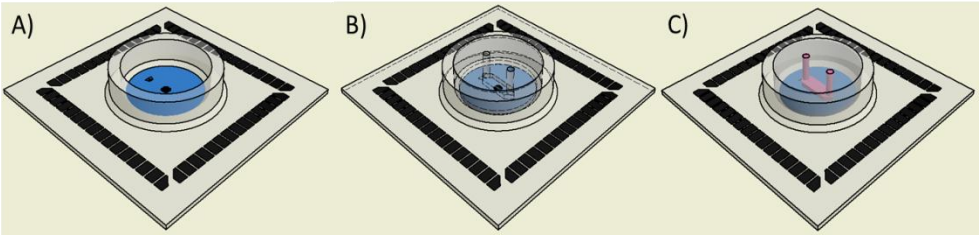

Figure 62 (A) PLL is deposited as before, but the channel is pressed onto the glass (B) before cells are plated. A different suspension density is needed when plating (C) in order to attain the desired plating density of 500/mm^2.

iii) Millimetric channels were also plasma bonded to glass coverslips. Here after the bonding step, media was flooded into the chamber to recover the surface described in section 3.4.4. PLL was loaded and left for 1 hour to functionalise the glass before it was flushed out, and then the cell suspension was added. This protocol is identical to that used for a microchannel (see Chapter 2.6). This method of bonding was used to determine if the bonding process employed had more influence on subsequent cell growth than the substrate used or the channel dimensions. The suspension density used was the same as for the MEA method ii) above.

3.5.1.2 *In microfluidic channels, MEA and glass substrate*

The effect of reducing the culture size by using the microchannel dimensions (1.5mm x 100µm) was investigated. The channel was bonded to a so-called 'flat' MEA without the 19mm ring, then flooded with media and PLL functionalised as before (Figure 63).

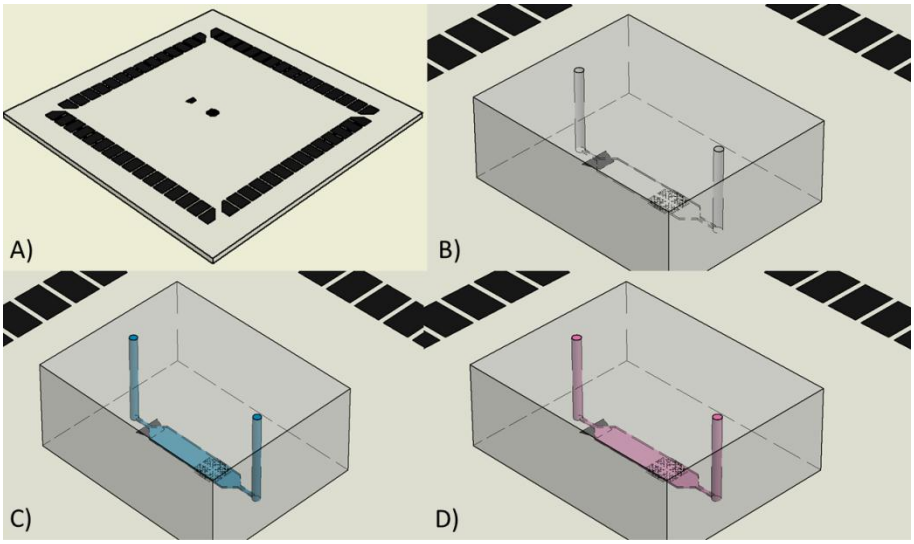

Figure 63 A) A standard MEA has a microchannel bonded over it B) using oxygen plasma. Media is flushed into the formed channel and incubated for several days to recover the surface. PLL (blue) is drawn through the channel C) with a syringe and incubated for at least 30 minutes. B) After thorough flushing of the channel with deionised water, buffer solution (pink, D) is added. Cell suspension is drawn through similarly, and settled for 30 minutes before flushing to remove non adhering cells.

The same procedure was also routinely carried out on disposable glass coverslips (Figure 64).

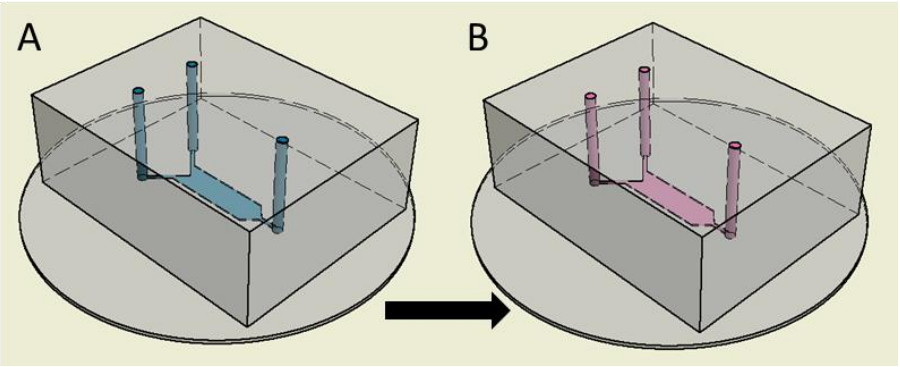

Figure 64 As for plasma bonding to MEA, but on a glass coverslip. Again the device is recovered in media for some days before PLL coating.

Thus a set of channel conditions (channel size, and method of attachment) are possible for glass and MEA substrates.

3.5.1.3 *On gold region (whole channel)*

Since gold cannot bond to PDMS directly using oxygen plasma, a limited region (stripe) of gold is patterned, with sufficient PDMS contact with glass to ensure a bond. This stripe (2mm x 10mm) is formed using the BPRS gold methods described.

Attachment of the channel over the gold with plasma was done 2 ways:

i) Bond the channel and then flush through AUT solution (Figure 65), and immerse for 18 hours. The channel is rendered sterile during the AUT solution immersion.

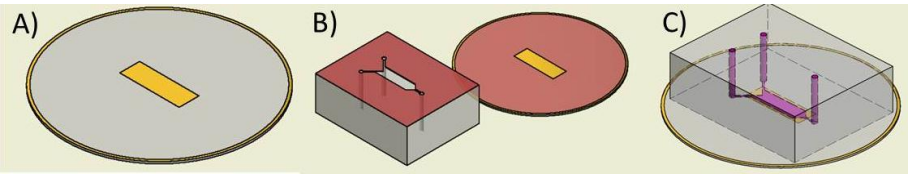

Figure 65 Gold (A) and AUT in channel, formed by creating the channel with plasma bond (B) and functionalising the channel afterwards (C).

ii) Coat the gold with AUT, then protect the gold region with a block of PDMS (Figure 66) during plasma activation of the glass and PDMS.

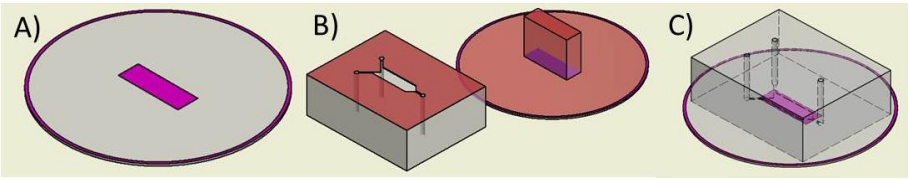

Figure 66 Gold and AUT (A) are plasma bonded (B) with the gold region protected by additonal PDMS. The resulting channel (C) is ready for media and cell suspension.

In the latter case, the PDMS is assumed sterile due to the plasma exposure, and the glass assumed sterile due to the ethanol treatment.

3.5.1.4 *Using a stamp and stick approach*

This is based on the method reported by (Samel et al. 2007), and described in methods 2.5.3. The pre-polymer is used to attach bulk cured PDMS to a glass surface, without plasma activation. This means the process of plasma recovery is no longer necessary.

3.5.1.5 *Using the tape bond method*

It is preferable that ligands should be deposited before the channel is assembled, and this priority conflicts with plasma bonding. Consequently, an alternative approach of *xurography* was employed (see previous Figure 50), such that a silicone pressure sensitive tape no more than 125µm high could be used to form not only the bond but the wall of the channel. The adhesive tape was double sided and could bond effectively to both glass and PDMS without the need for surface activation.

3.5.2 **Results**

3.5.2.1 ***Millimetric channels***

i) Wetted culture: Cells are plated at a density of 1000/µL and incubated for 1 day. The channel is then pressed down into the MEA well (as for Figure 61 . Cells in the channel grew normally up to 7 div (Figure 67), indicating the channel does not impose a drastic change in environment.

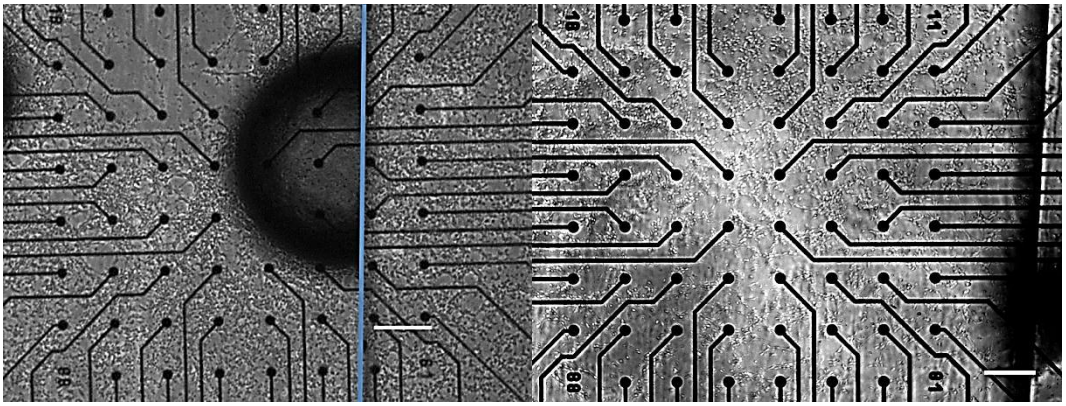

Figure 67 A millimetric channel was pressed down onto a uniformly plated culture; the vertical line (blue) is the channel edge. Note the cells visible under the PDMS, some of which appear unaffected and still alive after 2 div. Scale bar is 200µm in both images.

Air bubbles were often trapped in this process but because of the channel height were not brought into contact with the cells. After several days the bubble diffused out through the porous PDMS.

Cells under the PDMS outside the channel region evidently did not die off, implying the seal between PDMS and glass is not watertight. This means that there is now a considerable network of surviving cells that are not only inaccessible to the electrodes but also experiencing a different microenvironment, and these cells are influencing the cells that can observed on the electrodes. It also means that a watertight means of securing the channel to the MEA is needed.

iii) Aspirated culture on coverslip

Plasma bonding was used to seal a millimetric channel to a disposable glass coverslip (as for method used in Figure 63, but with a larger channel). The

channel was flooded with media for 1 week to recover the surface, then PLL was flushed through before plating at a high volume density (1000 per µL)

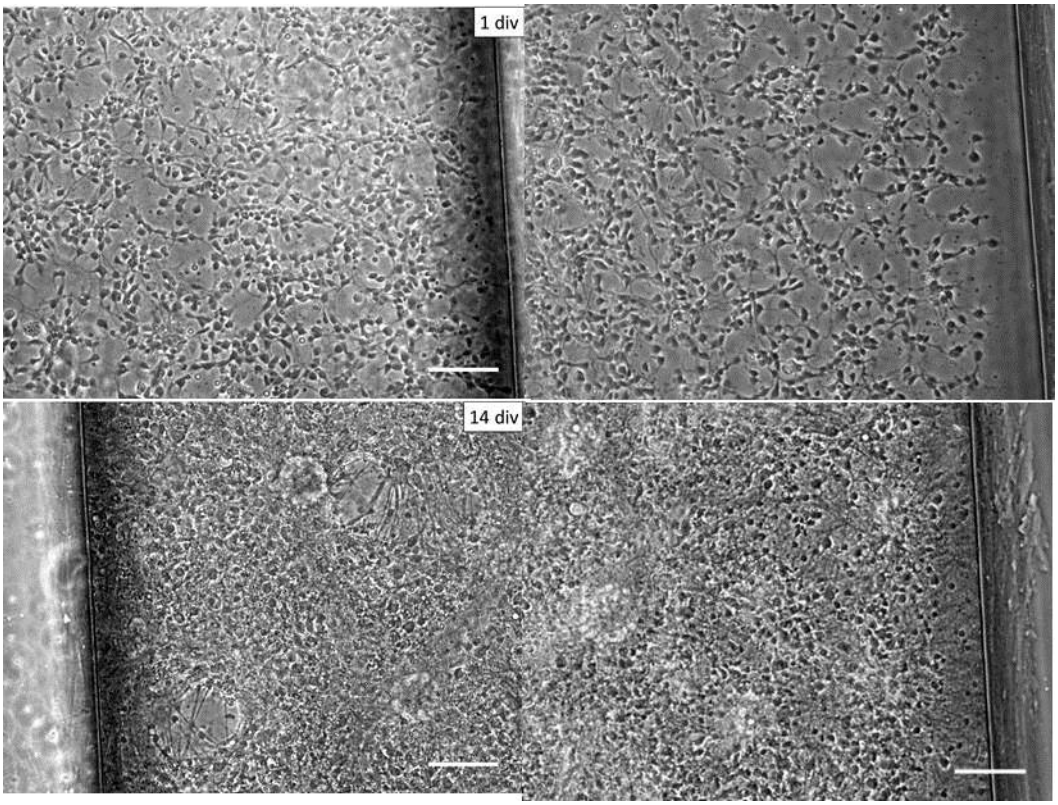

Figure 68 Cultures growing in 2 different channels formed of a millimetric device plasma bonded to a coverslip, plated at (10^6 cells /mL). At 1 div, the plating density is around 300 per mm^2. Scale bar is 100µm.

As seen in Figure 68 this creates networks of comparable plating density to control coverslips, so that a plasma bonded channel of this size has no reduction in cell survival performance.

3.5.2.2 *Micrometric plasma bonded PLL on coverslips and MEAs*

Having established that the cells could grow successfully in a larger channel using plasma bonding, it is preferable to reduce the channel volume in anticipation of the geometries that will be necessary for rapid drug delivery.

Channels of 100µm x 1.5mm were plasma bonded to both glass (Figure 69) and an MEA (Figure 70), recovered in Neurobasal, and flushed with PLL as described in section 3.5.1.2, before plating with the same order of magnitude volume density used in the previous section, (less than 1000 per µL).

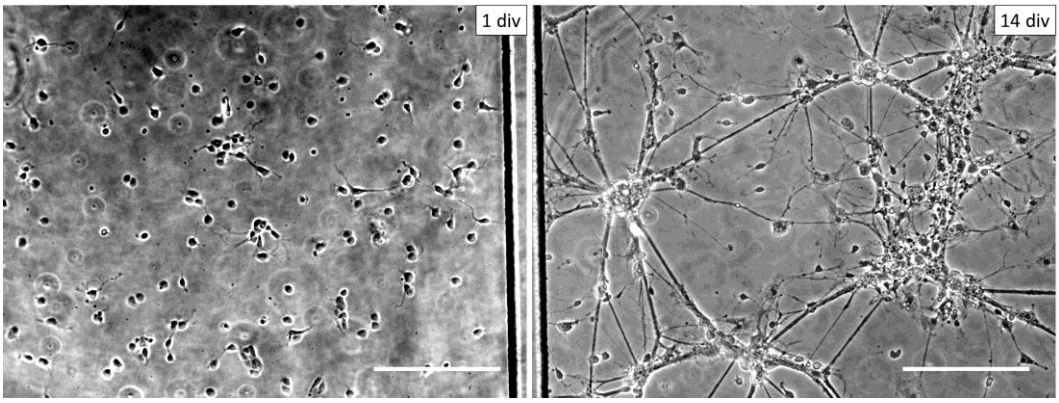

Figure 69 Images of cultures grown at low density (150/µL) in a channel bonded to a coverslip. At 1 div the plating density is clearly sparse (<150/mm^2) and by 14 div the fasciculation is extreme. Scale bar 200µm.

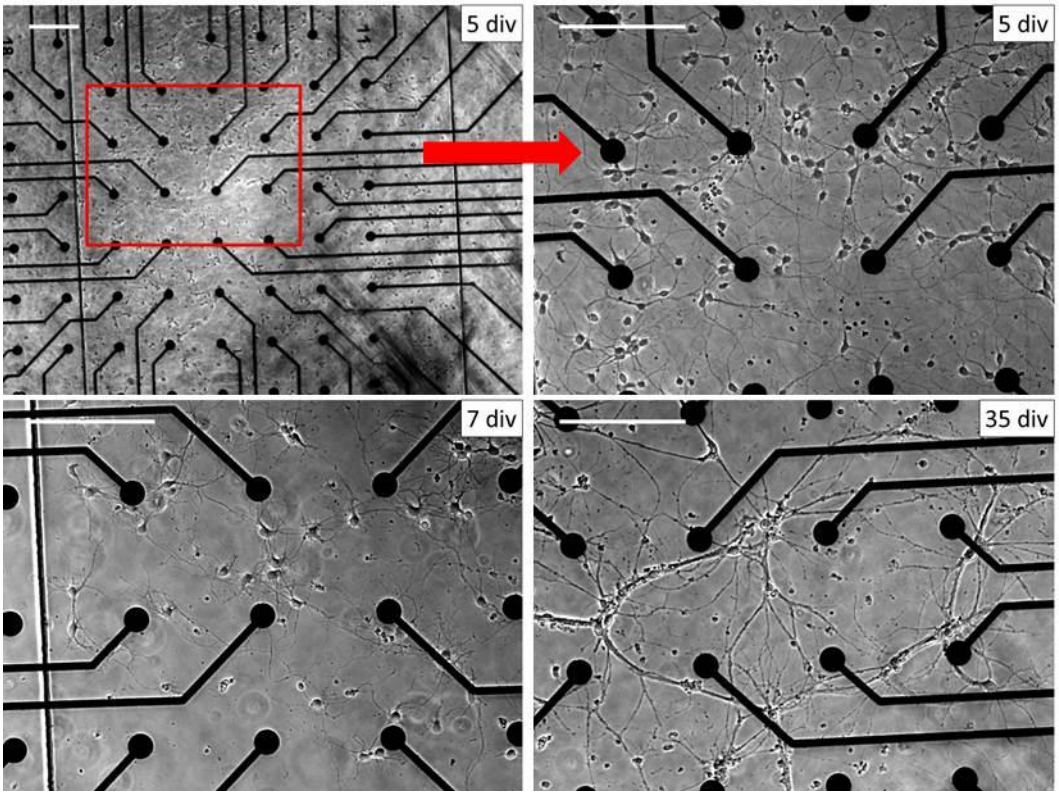

Figure 70 The channel (0.1mm x 1.5mm x 6mm) was plasma bonded to an MEA with no glass ring. The MEA surface was reversed with media immersion before PLL deposition. Cells were plated into the channel at density 150/µL, which become 144/mm^2. Although the plating density is sparse, at 5 div there is no noticeable fasciculation, as all areas of the glass have neural processes growing upon them. However, by day 35 considerable fasciculation is evident. Scale bar is 200µm.

The plating density observed was considerably lower than before. This is believed to be due to the reduced height, so that fewer cells are present in the volume above the same area when dropping out of suspension. The development of such cultures is clearly less optimal, with strong fasciculation. As the cells do not die outright, and the ligand deposition process was

identical to that of successful cultures in larger channels, it is inferred that the density of cells per mm^2 must exceed a certain threshold for optimal culture.

3.5.2.3 *The effect of increased suspension density*

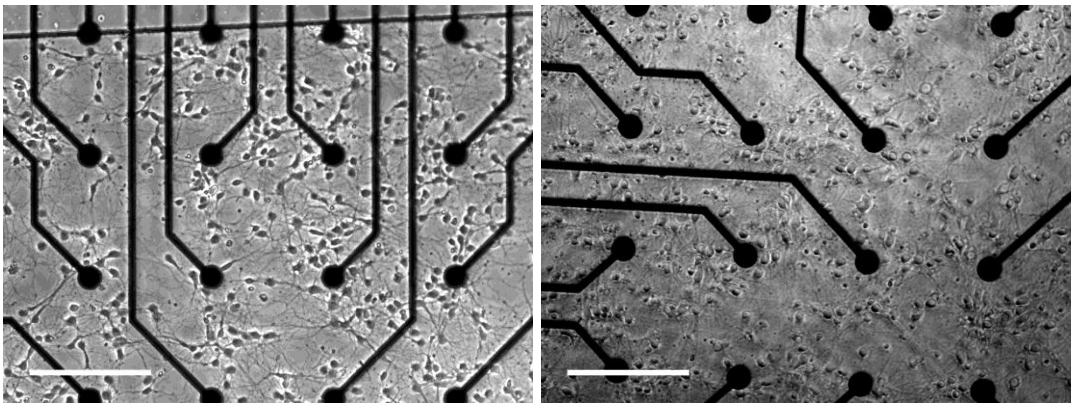

Figure 71 A microchannel plated with volume density 4k/µL on an MEA, leaving a plating density of around 600/mm^2. Left 5 div, right 10div. Scale bar 200µm.

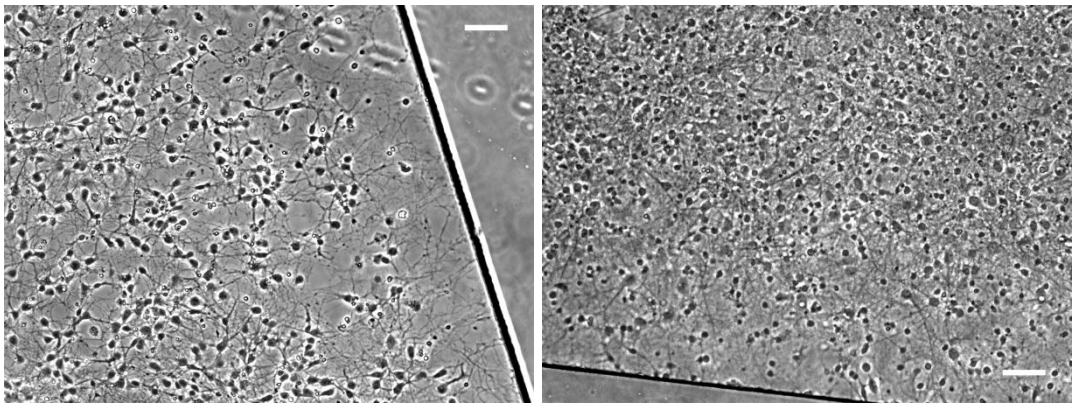

Figure 72 At 2 div, Plasma bonded microchannels on coverslip with volume density 8k/µL. This results in a plating density of around 400 cells/mm^2. Scale bar 100µm.

By greatly increasing the volume density to above 8000 per µL, it is possible to recreate the necessary plating density. The cells now grow normally on both MEAs (Figure 71) and glass (Figure 72).

3.5.2.4 *Using the stamp and stick method*

High density plated (600 per mm^2) cultures were grown in channels formed by pre-polymer bonding. PLL had been flushed through the channel following the bonding treatment (100°C hotplate for 2 hours). Although the plating density was sufficiently high, the neurons rapidly fasciculated (Figure 73). This may have been caused by unbounded oligomers in the pre-polymer, which are known to be toxic to neurons (Lovchik et al. 2011).

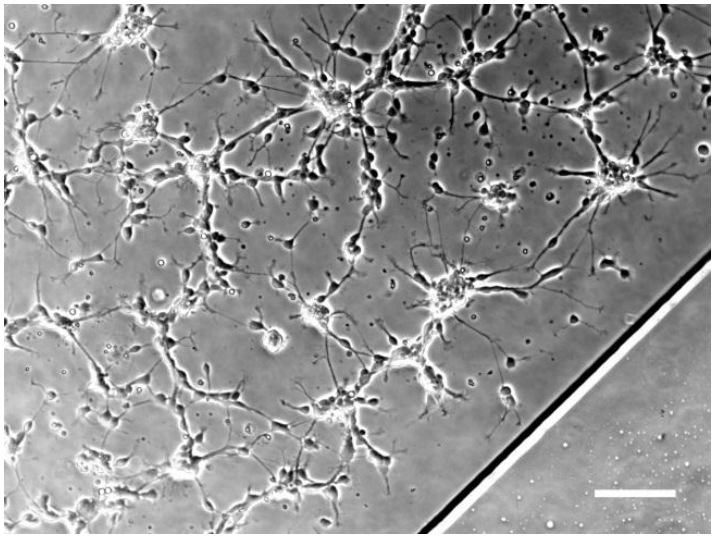

Figure 73 Primary neural cells grown in a polymer bonded microchannel at 5k/µL, giving a plating density of 625/mm^2. At 7 div, severe fasciculation has occurred and many cells are dead. Scale bar 100µm.

Thus although this method does not require recovery from plasma and might have been useful for post-bonding with patterned surfaces, it appears to be cytotoxic when used with primary neurons and thus cannot be taken further.

3.5.3 **Tape bonded channels**

The xurographic approach (Bartholomeusz et al. 2005) was tested with silicone tape as an alternative bonding method. Cut geometries 125µm high and 2mm (Figure 74) across were incorporated into devices as previously described.

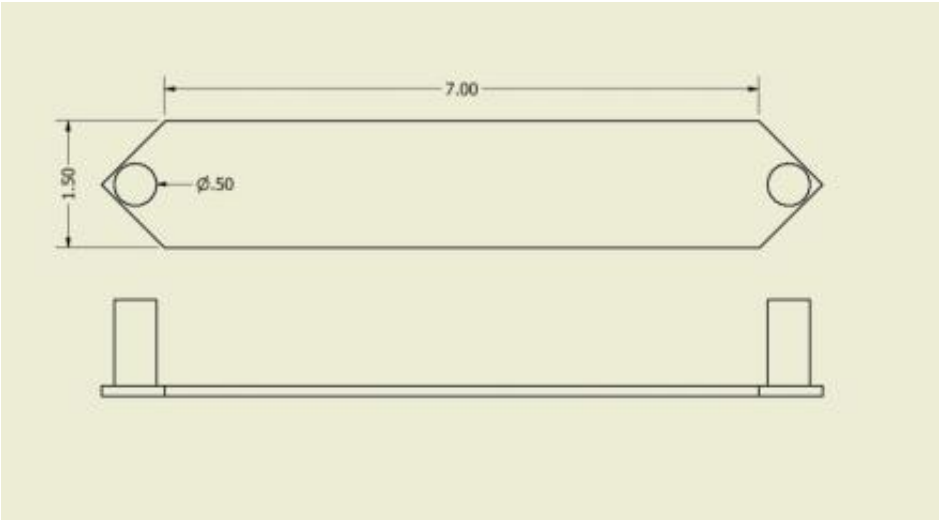

Figure 74 A xerographic channel geometry as used for cell culture.

Cells grew well in the channels at high densities (Figure 75) with no ill effects such as seen for the pre-polymer, indicating there is no toxicity issue with the tape.

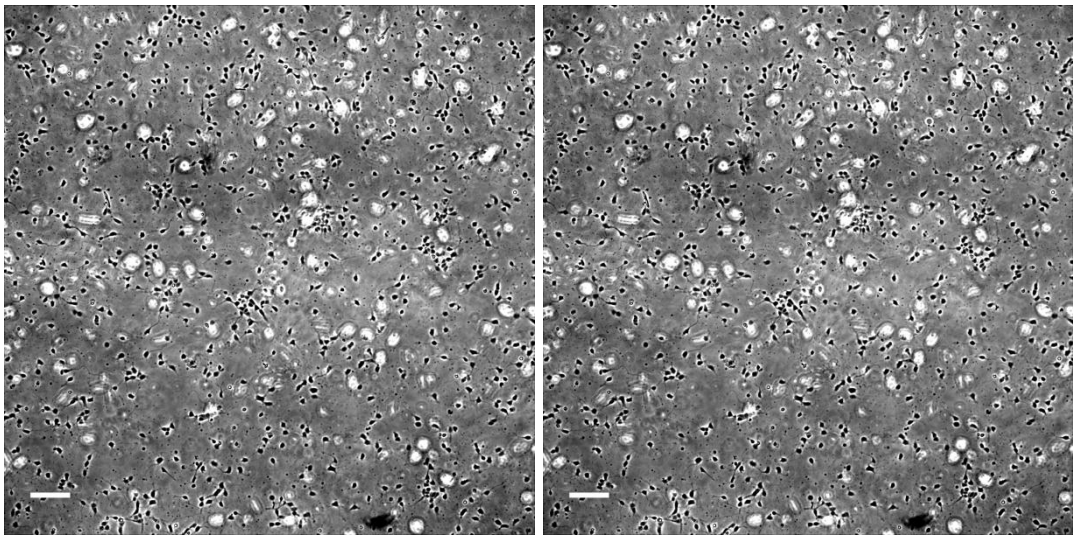

Figure 75 Cells plated onto a PLL surface in a channel formed using the tape bond method. Scale bar 100µm. Left of each image; 4000/µL and right of each image, 8000/µL.

One of the key advantages of this approach is that the PLL can be laid down uniformly on the substrate followed by post-bonding (Figure 76), since the silicone tape is self-adhering and does not require a plasma or heat process which would destroy the ligand.

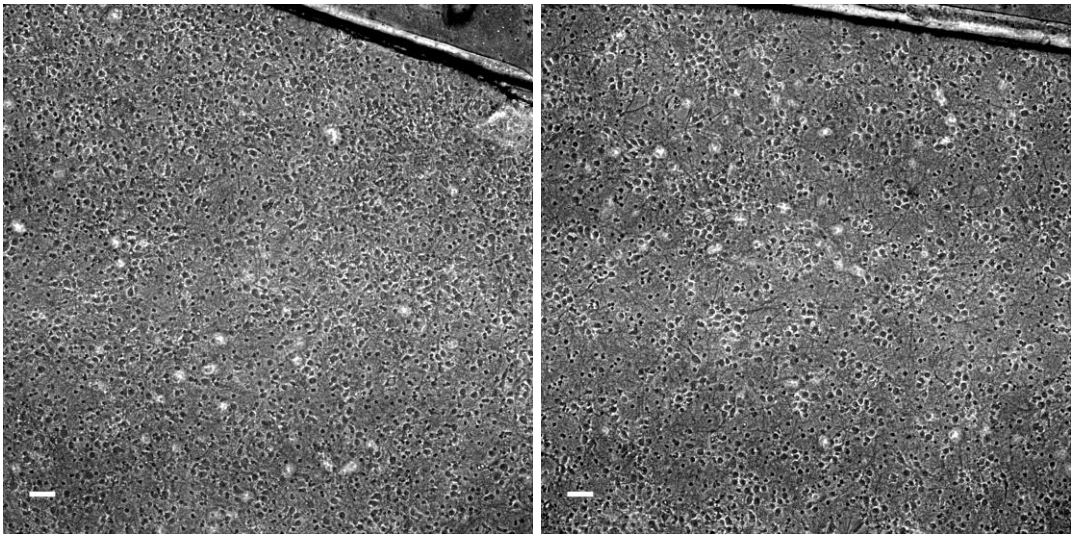

Figure 76 Images 8 div high-density (12k/µL) cultures of the bond before PLL method (left), and culture of the PLL before bond method (right). Scale bar 50µm.

Cells were grown at channels with both pre-bonding and post-bonding techniques, and the resulting cultures are indistinguishable.

3.5.3.1 *Plating density in a planar channel*

To match the coverslip plating density in a microfluidic channel of typically 1µL volume, and plating area of <15mm^2, the volumetric density was required to be no less than 4000 cells in 1µL (4x10^6 cells/mL). Table 1 summarises the expected volume density needed to achieve equiavalent plating densities in different geometries, while Table 3 shows the actual counted plating densities in some tape devices.

Culture type	Plating density/mm^2	Plating area, mm^2	Cells required	Volume available (µL)	Volume density/µL
Single c/s	250	284	75,000	500	150
Double c/s	500	284	150,000	500	300
Double MEA	500	284	150,000	500	300
Single milli	250	25.5	6375	25.5	250
Double milli	500	25.5	12750	25.5	500
Single micro	250	9	2250	0.9	2500
Double micro	500	9	2250	0.9	5000

Table 2 An estimate of the volumetric suspension density needed to obtain equivalent plating densities in all culture type, based solely on area and volume considerations.

GLASS PLL	Suspension density	Plating expected	Plating true mean, Counted in 0.65x0.65 mm^2	Actual fmean / mm^2
Double	300/µL	560/mm^2	315	745 (1)
Single	150/µL	280/mm^2	76, 104, 141	253 (3)
Channel	8k/µL	<280	169	400 (1)
Channel	12k/µL	280<x<560	219	518 (1)
Channel	16k/µL	>560	375	887 (1)

Table 3 Comparison of predicted and actual plating density in high density tape channels

The actual density is usually equal to or more than was anticipated per mm^2.

3.5.4 **Gold surface channels**

In parallel with the glass cultures, the combination of a gold surface and ligand, and a microchannel was investigated. Initially the bond used was

oxygen plasma. As the AUT is dissolved in ethanol for surface deposition, this had implications for the formed plasma bond.

3.5.4.1 *Pre-bonding: plasma bond then AUT*

This approach is that described in Figure 65, where the surface is functionalised after bonding.

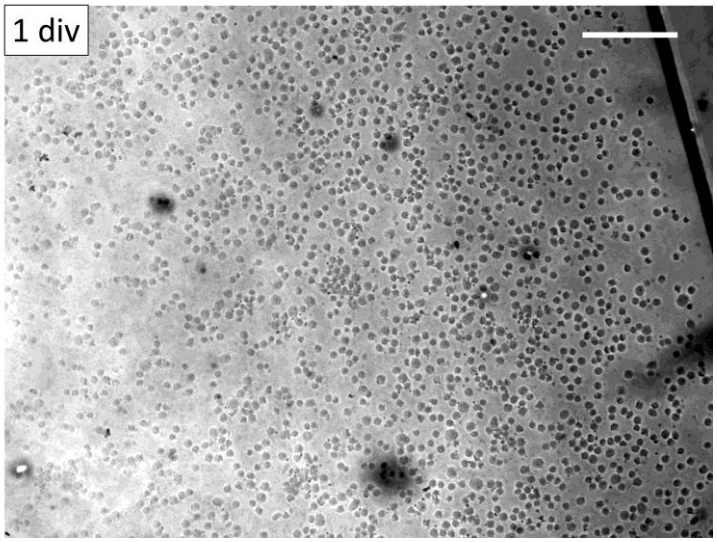

Figure 77 The PDMS channel was plasma bonded over the gold untreated surface. AUT was then deposited by injecting solution (300**/µL) into the channel (boundary visible on the right). Scale bar 200µm**

Delamination issue

This approach was fraught with technical difficulties. The ethanol immersion appears to severely the plasma bond, as 7 of the 8 devices tested delaminated and fell apart in subsequent flushing steps. They could not be used for cell culture. The remaining culture (Figure 77) proved highly cytotoxic as all cells died immediately, and this may have been due to ethanol lingering in the PDMS.

Ligand deposition and cell survival

The use of oxygen plasma permits the gold to be activated, but the plasma exposure time is reduced (since the principal objective is to bond), and a finite time (1 hour at 60°C) elapses before flushing the AUT solution into the channel. This is likely to have a pronounced effect on the gold: AUT bond, in comparison with the deposit then bond approach.

3.5.4.2 *Post-bonding AUT then Plasma Bond*

For both logistical and biological reasons it is therefore preferred to adopt the alternative approach (Figure 66) where all functionalization in ethanol is done before bonding the channel

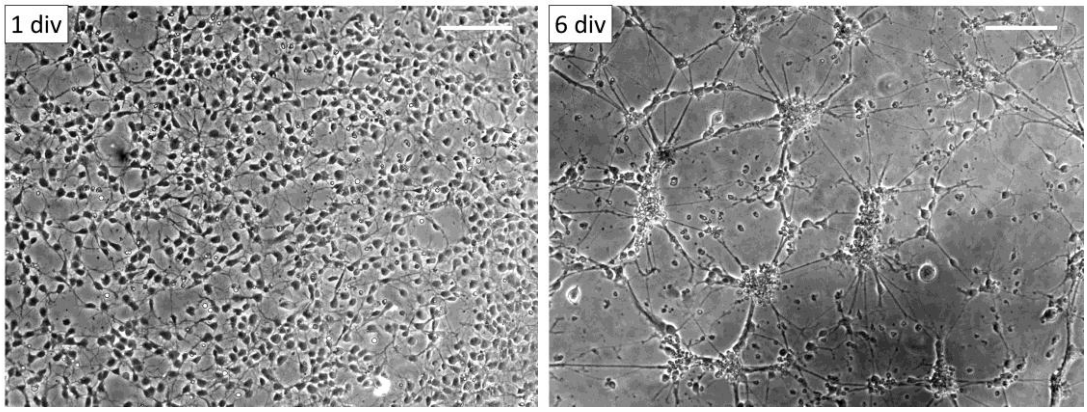

Figure 78 The AUT ligand was deposited and then protected during subsequent channel bonding to the substrate. Neurons were plated at 4k/µL and images taken (scale bar 200µm)

Four such channels were fabricated, and 4 channels bonded correctly with no delamination following the media and cell suspension flush. The cells survived initially (Figure 78) but fasciculate and died off over time (< 7 div).

3.5.4.3 *Tape bonding after AUT*

The tape geometry used for glass and PLL was also used here (Figure 79), with an appropriately high plating density (8k/µL).

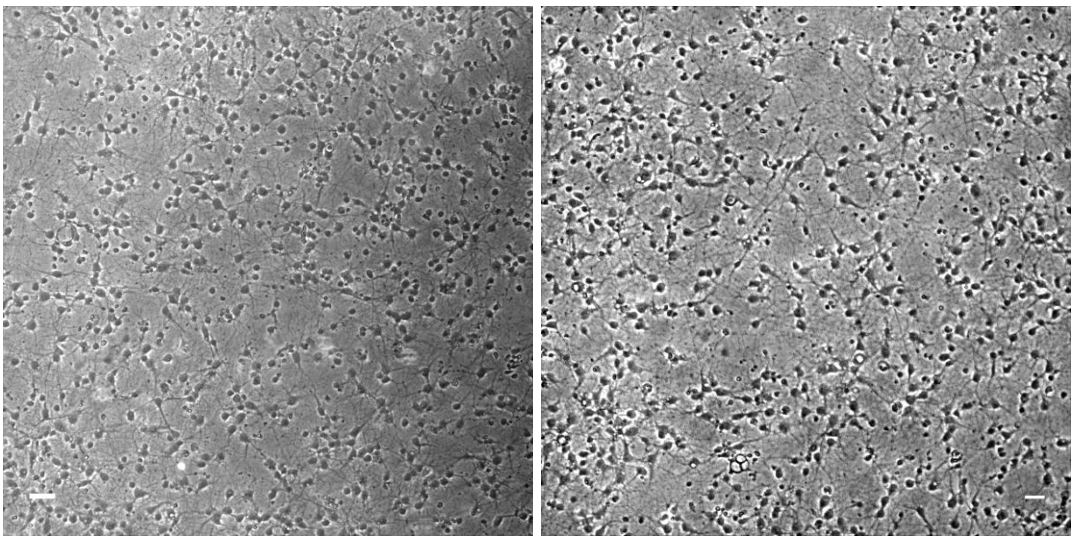

Figure 79 Cells grown on AUT in a silicone tape channel. Cells were plated at 8k/µL. Left 1 div, and right, 7 div. Scale bar 50µm.

The cells now grow optimally on a gold surface in a microchannel, so that all surface and channel conditions that will be used going forward are established as compatible.

3.6 Chapter conclusion

Microchannels were designed to meet the requirement of rapid drug delivery through interface shifting, which will permit timely reinforcement without requiring the total net flow rate to exceed a range compatible with reported neuronal culture survival. These channels have been fabricated from PDMS and silicone tape and are readily integrated with the existing electrode recording systems available.

This approach was selected from many possibilities, as summarised in Table 4 below:

Parameter	Options	Comments
Substrate	**Glass**	Simplest substrate to use
	MEA	Best for electrical recording, but incompatible with some bonding techniques due to its expense
	Gold	Requires additional cleanroom steps
Ligand	**PLL**	Quick to apply, no solvent needed
	AUT	Long application time, requires ethanol Also often incompatible with bonding
Plating density	<500/mm^2	Cultures generally unhealthy
	>500/mm^2	Cultures generally healthy
Bond strategy	Oxygen plasma	Not compatible with post-bonding
	Pre-polymer	Quick and simple, but issues with toxicity
	Silicone tape	Very simple and compatible with all other steps
Ligand Deposition	**Before bonding**	Results generally good , even with AUT
	After bonding	Results sometimes poor, especially AUT

Table 4 Comparison of different culture and fabrication parameters used

In summary, any approach which ensures good ligand deposition and high cell plating density will work, but for logistical ease it is better to use glass and

PLL rather than gold and AUT, and to use silicone tape for channel fabrication.

Cultured neuronal cells can be grown indefinitely in healthy networks on both glass and gold surfaces, even when they have been chemically treated as part of a patterning process, provided the plating density is sufficiently high. In order to be comparable with literature and the control coverslip surfaces, this needed to be above 500/mm^2. Cell volume suspension density must be much higher than would be necessary on an open surface, to get the comparable plating density in a microchannel. The necessary suspension density is inversely proportional to height, as the greater the vole of suspension over unit surface area, the more cells will drop out of suspension onto the same surface area.

The limited spatial resolution of the MEA, indicates a need for our own disposable monitoring surfaces, and the thickness of the glass precludes high-magnification imaging. A different method of spike detection is preferred, ideally SPR imaging, and the channel will need to incorporate this. Ultimately a smaller monitored area (0.5mm across or less) is preferred, since the interface switching time is heavily dependent on the distance that must be traversed, and the network must be confined to this region.

4 Perfusion system development

4.1 Perfusion system specifications

Having demonstrated that cells can be successfully cultured in the microchannels for many days, it is now necessary to consider the perfusion strategy that will induce controlled liquid flow through the channel, and maintain the physicochemical environment (Figure 80) indefinitely, while outside an incubator. No precise or rapid agonist delivery can occur without an appropriate fluid handling system.

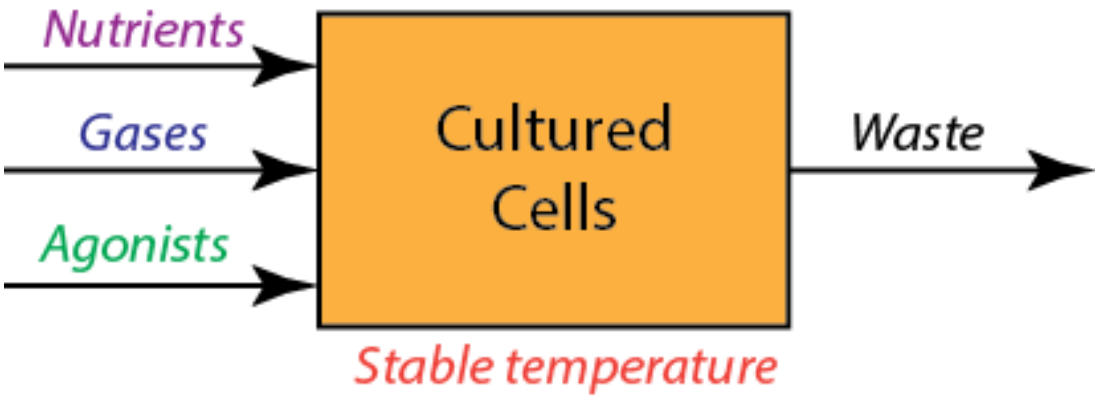

Figure 80 Concept of the physicochemical properties that must be finely controlled over long timescales, in order to successfully emulate in vivo perfusion. Most inputs (nutrients, gases, salts and proteins) are delivered continuously in vivo, while waste products are removed before they build up to pathological levels. The pH and temperature must be held constant.

Whatever the aim of the experiment, the cells must not die during the process due to environmental stress that was not intended. Cultured cells have many requirements, many of which are automatically provided in the culture media formulated for them. Thus, for example, essential nutrient replenishment is inherent in Neurobasal media (Brewer et al. 1993)(Brewer 1997).

When connected to a large supporting media volume with large quantities of vital proteins and salts, as in a well plate, the culture can grow for hours or days without needing an exchange of fresh media. In a device of total volume 1uL, however, significant concentration shifts can occur quickly. Thus it is important to continually replenish necessary factors and remove build-up of waste factors.

Gas levels

In an incubator the necessary gas concentrations (5% CO_2, ideally 5% O_2 (Zhu et al. 2012)) are present in the air above the media and enter through diffusion. The vital gases not only provide oxygen essential for cell metabolic processes, but also act to balance pH and osmolarity.

Cells excrete metabolic certain factors essential to regulate the cell environment, and in doing so render their local environment alkaline.

Under flow in a microchannel outside the incubator, the media cannot come into direct contact with unfiltered room air, as it would invalidate sterility and cause rapid shifts in osmolarity and pH due to the different gas concentrations (<0.1% CO_2). Thus the media supplied to the cells must contain dissolved levels of the gases. This can be done by placing media in the incubator in a syringe, and then connecting the syringe to a syringe driver.

Alternatively the media can be continually gassed to appropriate levels, by flowing a compressed gas mix of 5% CO_2 / 95% room air (21% O_2 and 78% N_2) over a volume of media to be perfused. The pressure of the gas dissolves air/CO_2 mix into the media.

This has the advantage of potentially allowing gas levels to be adjusted or deliberately altered.

Temperature

In vivo temperatures are around 37°C, and most cell metabolic processes are optimised to occur in this range. Although some shorter term experiments can be carried out at room temperature without problems, it is necessary for longer term experiments that the channel be held at a constant 37°C temperature, by using a temperature regulator in contact with the microchannel PDMS. This regulator may take the form of a sealed unit containing a culture in a static media volume, but must be accessible by all the fluid delivery and electrical connections, and be compatible with light microscopy.

Constant stable low flow rates (Perfusion at a set rate)

Physicochemical stability, including minimal change in net shear rate, is important to optimise cell viability and ensure unintended, unknowable culture perturbation does not occur.

Typical ranges for perfusion *in vivo* and reported *in vitro*: as low as 5µL/hour (Kolnik et al. 2012a) but typically µL/min (Kim et al. 2007b)(Cooksey et al. 2009) (under 0.3nL/s), translating in most cases to a linear velocity of under 10µm/s.

In the channel geometries designed, this would equate to sub nL/s flow rates, but it is already established that this would render the system dominated by diffusive transport, and the range of interest is 1-100nL/s (10µm/s or higher).

For higher level behaviour to emerge from a neuronal network under training, the microfluidic subsystem must be capable of keeping the cells alive for days or weeks. Thus the cell environment must be extremely stable for the majority of the time, without any unintentional change in conditions which could induce a network reaction or pathological response.

Arbitrary rapid switching or precise level shifting (Drug delivery)

The agonist may need to be delivered and removed in a few seconds or less, for deterministic reinforcement delivery, emphasising low latency of response. Alternatively, it may need to be incrementally graduated with high precision, emphasising stability over latency. An example application would be to gradually shift the concentration gradient spatiotemporally (Figure 81), with very high precision/stability between levels, in order to investigate cell response to a periodic agonist wave. This is explored in section 4.4.6.

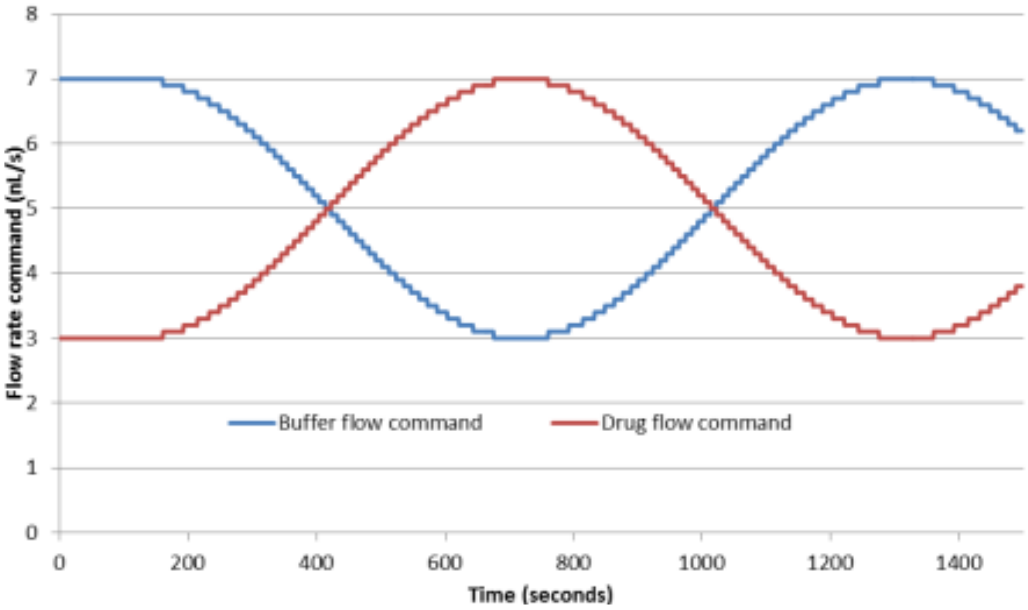

Figure 81 Example of a graduated flow rate command, allowing for slower oscillating exposure doses with periods of many minutes but flow increments of 0.1nL/s.

However, when a genuinely intended flow rate change is commanded via the controlling computer, the perfusion apparatus must react very quickly (less than 5 seconds) so that drug delivery is correlated properly with electro-optical stimulation and recording, and can be unambiguously correlated in subsequent analysis.

Integration with other system elements

As the perfusion system does not work in isolation, it must be capable of physical and signalling compatibility with other elements of the system.

The apparatus should not interfere with opto-electrical stimulation and monitoring. It must be compatible with long term monitoring on a microscope, so the interface with the microchannel cannot be too tall (or it will prevent focussing at higher magnifications), or block the light path.

It must be integrated with the temperature control elements, but since media must be directed in to and out of the microchannel the temperature control cannot occur in a sealed unit without difficulty, as many airtight bulkheads would need to be formed. As a first iteration, a clamp which grips the microchannel and directly heats via conduction is explored.

4.1.1 Stability and precision requirements – quantification

For any application where it is deemed important to exert spatiotemporal control over agonist concentration, the precision and stability of the flow rate is critical. Flow stability where a change is not intended, is crucial to prevent asynchronous/non-deterministic cell stimulation. It is set as a goal, given the range and resolution of the flow ranges of interest, that the steady state flow rate of a pump should not deviate at any point from its target by more than 3 or 4nL/s and ideally rather less than this, especially at low targets, and that the average deviation should be less than 1-2nL/s. Precision of control should also be 1-2nL/s, so the ability to sense must be at least this precise.

The metric of standard deviation from the target command over a given time frame is used, as well as the offset of average data from the target. This indicates stability and long term drift.

4.1.2 Latency requirements – quantification

For biologically relevant agonist delivery as part of a deterministic reinforcement paradigm, it is necessary to temporally co-locate cell activity with the agonist to within a few seconds, and ideally less than 1 second. This implies the system should begin responding within 1 second of the command being given, and complete the transition within 2-3 seconds. Any longer than this and the system can no longer be considered deterministic.

For other applications where an incremental boundary shift occurs and is not intended to occur in response to culture activity, then the need for tight temporal correlation is less stringent, but when shifting flow rates the response time should obviously not exceed the step duration.

A metric for latency estimation is the time taken to shift the flow rate 90% of the required transition, or alternatively how rapidly it then settles to within the precision previously described.

4.1.3 Backpressure and bubble prevention

A common issue in microfluidic perfusion is the generation of bubbles in the fluid stream. These cause nonlinearities in flow response, and can kill cultured cells on contact. Often bubble traps which consist of a dead space above in

the flow line which the liquid will not fill but which the less dense air will naturally migrate into, and out of the flow stream.

The alternative, which makes use of the flow actuators, is to use a pressure source to increase the overall hydrostatic pressure above that at which the gas can remain undissolved. Thus spontaneous bubble nucleation is avoided, and existing bubbles are quickly eliminated. The backpressure can be raised or lowered to modulate net forward flow rate in the microchannel.

4.2 Methods and techniques

4.2.1 Physical and software equipment

A single perfusion pump may be broken down into 4 interconnected elements (Figure 82):

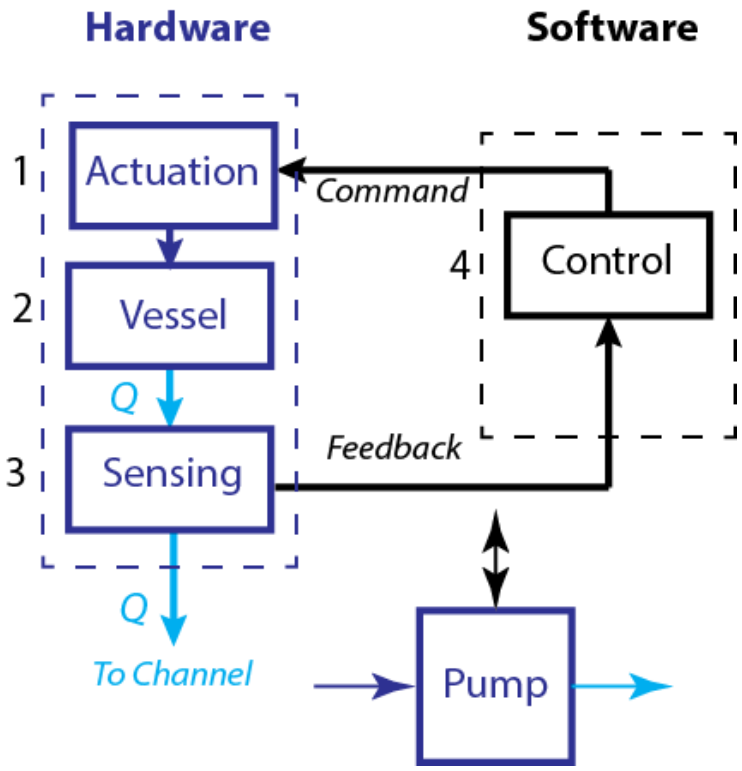

Figure 82 Generalised concept of a feedback flow regulation pump. An actuation element induces pressure in the source vessel containing media; and the resulting flow rate Q is detected by a downstream sensing element. The flow rate is converted to a feedback signal that informs a flow regulation program, resulting in an adjustment to the command signal operating the actuation element. Bottom right: the symbol representing the main schematic.

1 An electronically operated actuator that imposes a force on a liquid to induce flow. This may be direct (syringe driver) or indirect (via an air-over-liquid concept).

2 A sealed fluid reservoir containing a volume of culture media to be perfused.

3 A flow line to carry the media from the reservoir, exiting via a watertight bulkhead, passing through an in-line flow sensor which detects the rate of mass transport, and on into the microchannel.

4 Computer control of the actuator and readout of the sensor in real-time, which should ideally be closed-loop.

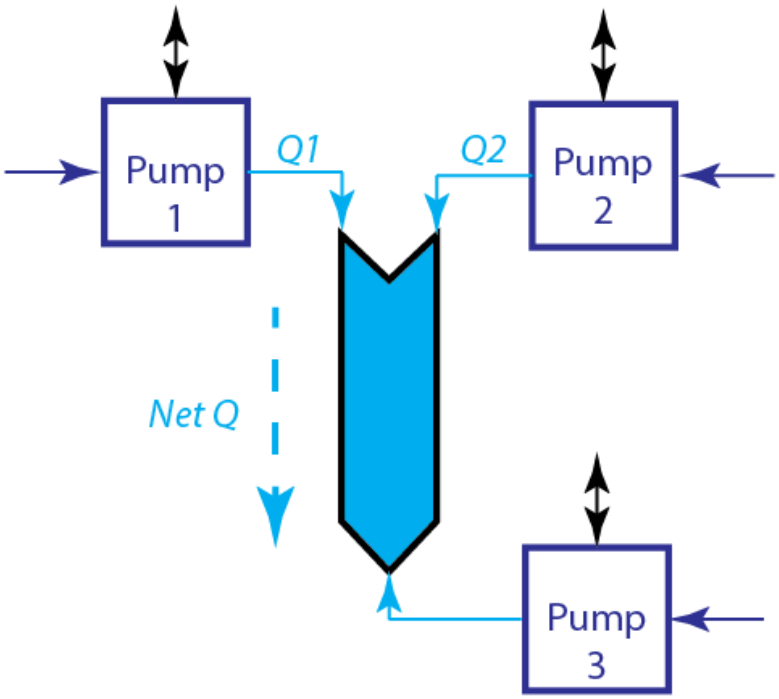

Figure 83 Three of the pumps described above are necessary to induce a co-flow control system. Note that only pumps 1 and 2 are strictly necessary to control the ratio of flow rates 1 and 2. Pump 3 need not be monitored as long as the pressure inducing the back flow is known to be constant. The flow Q3 induced by pump 3 is not shown.

From Figure 83 above, the 'water circuit' analogy between hydraulic and electrical transfer is clear. As with Ohm's Law

$$\boldsymbol{V = I.R} \qquad [16]$$

such that potential difference V is needed to induce electrical current I through electrical resistance R, then in fluid dynamics

$$\boldsymbol{P = Q.R_H} \qquad [17]$$

such that a pressure P is needed to induce volumetric flow rate Q through fluidic resistance $R_{H.}$ The fluidic resistance is determined principally by the cross-sectional area of the channel in which the fluid travels.

When three pumps are operating in opposition as in Figure 83, then Kirchoff's First Law (that the sum of currents entering a node is equal to the sum of currents exiting it) can be applied to infer that the net flow rate Q in the channel is the sum of Q1 and Q2, minus the opposing Q3 induced by Pump 3.

The flow rate sensing technology is always a mass flow sensor, which operates by comparing fractional changes in temperature both upstream and downstream of a heating element. Both temperature sensors and the heating element are housed in a short 0.15mm diameter *polyethylethylketone* (PEEK) tube through which the liquid flows. These flow rate sensors were initially from Sensirion (SLG1430 series), but proved difficult to control in LabVIEW, and so Elveflow Mass Flow sensors (MFS2) were used instead.

The sensitivity and range in each case was around 20nL/minute (0.3nL/s) with a full range of 7µL/minute (116nL/s).

The control element was always a LabVIEW 2012 custom-written program coordinating the command and feedback of data in real time, connected to the physical apparatus by a Data Acquisition (DAQ) card from National Instruments (either USB-6008 or USB-6259).

Connections between pressure vessel and microchannel, and to and from the flow rate sensor, were in PEEK High Pressure Liquid Chromatography (HPLC) tubing of small internal diameter. PEEK is in theory inert to all the reagents likely to pass through the tube, though it is capable of adsorbing some molecules. The alternative, *fluorinated ethylene propylene* (FEP), is gas-permeable and could lose gas pressure and vital gas concentrations.

A high specification power supply (TTi PL303QMD-P) was used where precise control of current drawn by the electro-pneumatic actuators was necessary.

4.2.2 Typical experiments and data analysis

A sequence of target flow rates was commanded and the system response detected. Dynamic stability was determined by level shifting and holding the target for 10 minutes, while static stability was determined by maintaining a target for at least 1 hour. Where there was concern over long term instability the experiments were run for at least 10 hours.

4.2.3 Flow rate and other feedback data

The data returned by the flow rate sensors and other feedback elements was used not only to control the system but was also logged permanently. Data was analysed in MATLAB to assess statistical measures where applicable (variance, average, and time delay).

4.2.4 Imaging data

Where initial testing indicates the system could provide adequate stability, precision, and latency, it was connected to a microfluidic channel. To limit the possibility of bubble ingress, all flow lines were primed with media for several minutes by flowing at high flow rates (100nL/s) into a waste vessel, to remove air and nucleation points for bubbles.

Lines were connected to the channel (pre-filled with media) with a reservoir of liquid on top, and with lines under low flow rate (under 10nl/s) to ensure no air gap was present when pushing the HPLC line into the PDMS port.

For imaging of co-flow boundaries streams of distilled water and fluorescein (0.01%w/v) were imaged with FITC filter on the microscope.

The intensity and extent of the fluorescent stream was used to determine the general position and stability of the boundary, and confirm the flow rates monitored corresponded to the expected spatiotemporal distribution of the fluid streams.

It was not used as a direct measure of concentration (as in Beer-Lambert law) as the optical setup was reflection rather than transmission, precluding spectroscopy. For rapid switching the extinction ratio of agonist to buffer would be high, and so measuring greyscale levels would be unnecessary. For slow gradient switching, however this becomes an important issue as cell

response typically take place on logarithmic scale much lower than the perceivable levels of a CCD camera, and so post-processing COMSOL simulation of the data based on logged flow rates and estimation of diffusion coefficient was carried out.

4.3 Results and experimental progression

4.4 Assessing available perfusion methods

4.4.1 Syringe driver

This utilises a motor-driven gear drive ('worm drive') to incrementally advance (step) the plunger of a syringe at a rate commanded by the user (Figure 84). Depending on the syringe diameter, this stepping rate can be lower than 0.01uL/hour or higher than 1mL/minute.

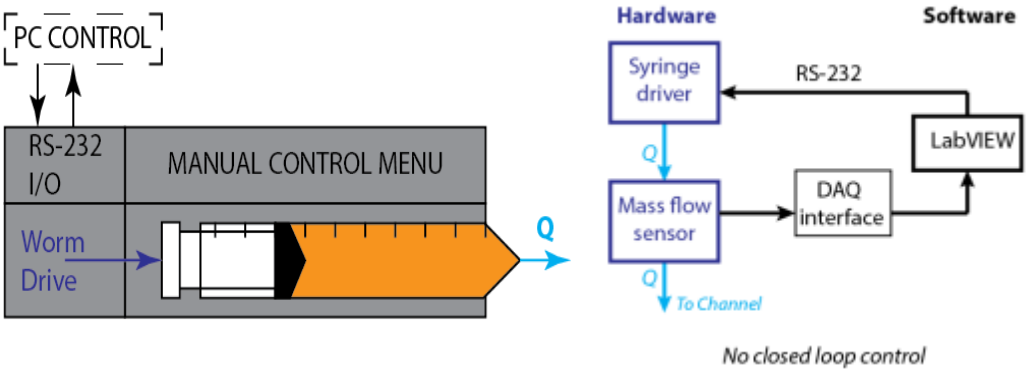

Figure 84 Concept of the syringe driver. This commercial system can be manually controlled or run from a LabVIEW program. The program was not run in feedback mode initially, as the open loop response was characterised.

Here the actuator and pressure vessel are a stepper motor/worm drive, and the syringe itself. The flow sensor is completely separate and usually syringe pumps are not logged, as it is expected they will provide the average flow rate commanded. This is not strictly true, as will be seen.

Mass flow sensor data is logged, but not used to inform or update the syringe driver target flow rate. This cannot be altered externally; the commands are hardwired in the motor mechanism. A Cole-Palmer 789210C was used with 10mL and 1mL disposable syringes connected to Luer tubing adaptors. The syringe driver was commanded from a LabVIEW program written by Mr Solomon Idinyang, via a Data Acquisition card (NI USB-6259). The flow rate sensor downstream of the syringe driver logged the flow rate at 50 Hz.

No backpressure component was used at this point, as the syringe driver has a tendency to stall and stop operating when opposing sufficiently high resistance.

4.4.1.1 *Syringe driver range and stability.*

Most applications where a syringe driver is employed, even for low flow rates, are open loop (Biffi, Menegon, et al. 2012; T. Kim et al. 2009), in that the pump is set to a target flow rate value and assumed to accurately stay at that level. For many applications, such as flushing or flow in a larger volume where flow perturbations can be readily damped out, this variation may not be critical, as long as the true average of the flow rate is approximately what was commanded.

For precise spatiotemporal gradient and switching control, however, such perturbations are not acceptable, and so it is necessary to establish if the syringe driver available could meet the stability / precision criterion.

Flow rates were commanded at 0, 1, 5, 10, 50, and 100nL/s, with step changes to assess the latency (Figure 85).

4.4.1.2 *Stepping 10 minute intervals (short term stability)*

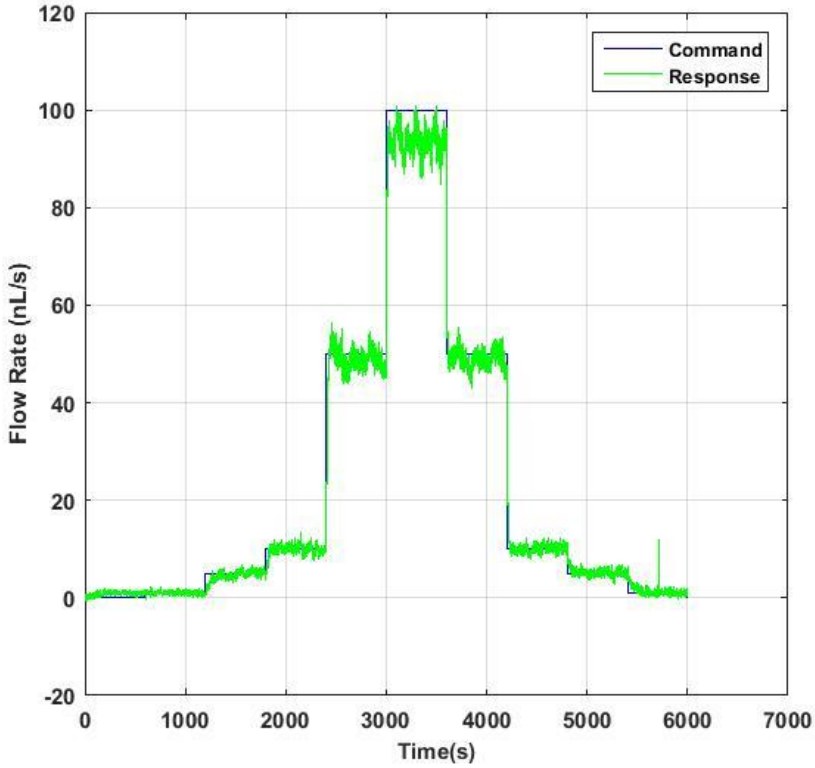

Figure 85 The logged response to both incrementing and decrementing the commanded flow rate. After each step the command value is fixed for 10 minutes, in order to permit the flow rate to settle as far as is possible.

Firstly it is clear that as expected the syringe driver is quite capable of flow rates at any value within the range of 1-100nL/s deemed necessary. At this scale, however, it can be recognised that the instantaneous value of flow may be very different to the commanded value, and the average value differs considerably from the commanded target, particularly at the higher ranges.

A closer look at the logged data at selected flow rates follows (Figure 86). For each 10minute period, the average and standard deviation of the logged values are noted.

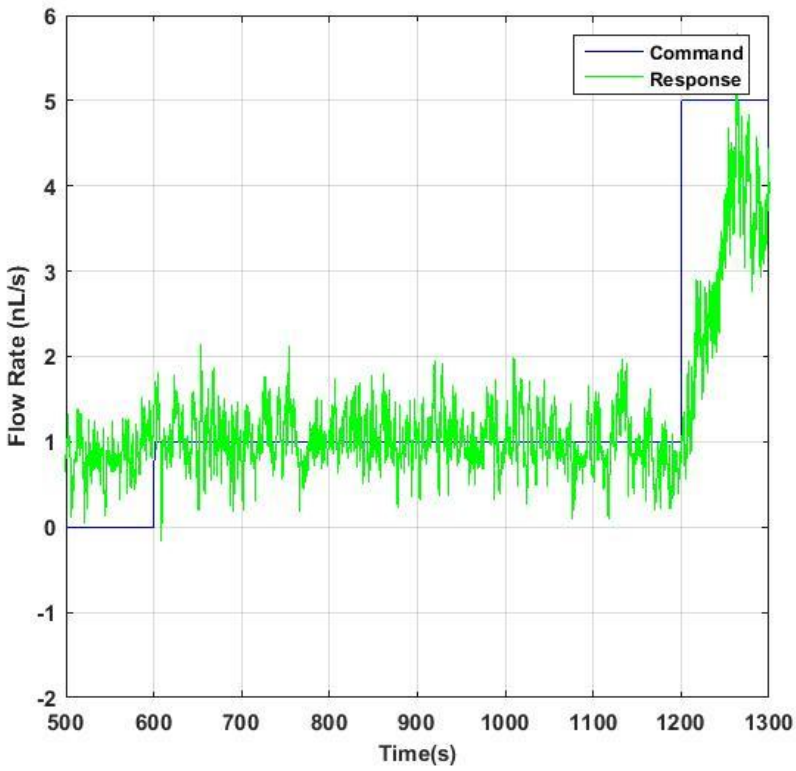
Command
Response
Flow Rate (nL/s)
Time(s)
6
5
4
3
2
1
0
-1
-2
500
600
700
800
900
1000
1100
1200
1300

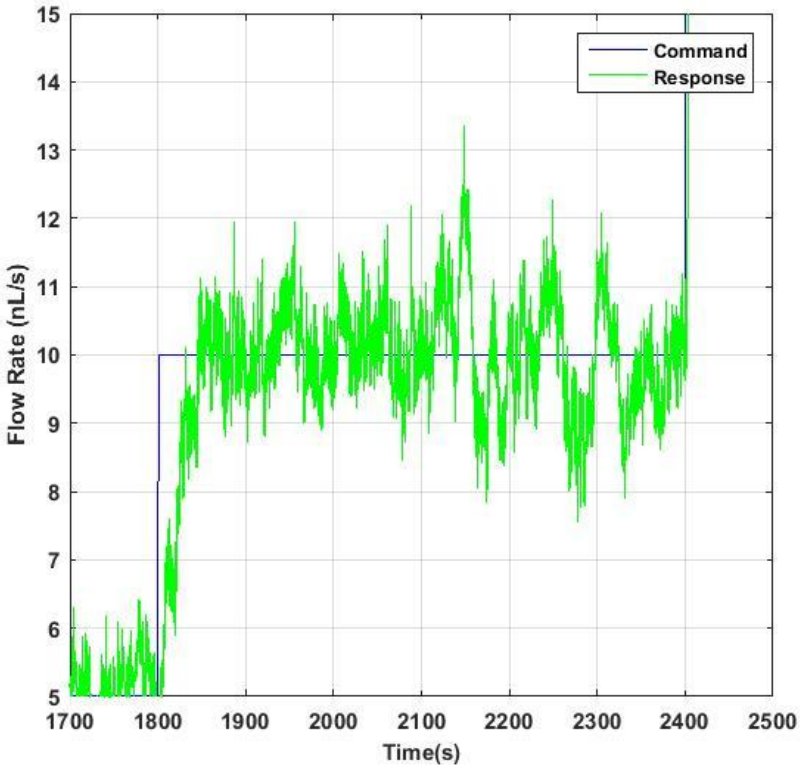
Command
Response
Flow Rate (nL/s)
Time(s)
15
14
13
12
11
10
9
8
7
6
5
1700
1800
1900
2000
2100
2200
2300
2400
2500

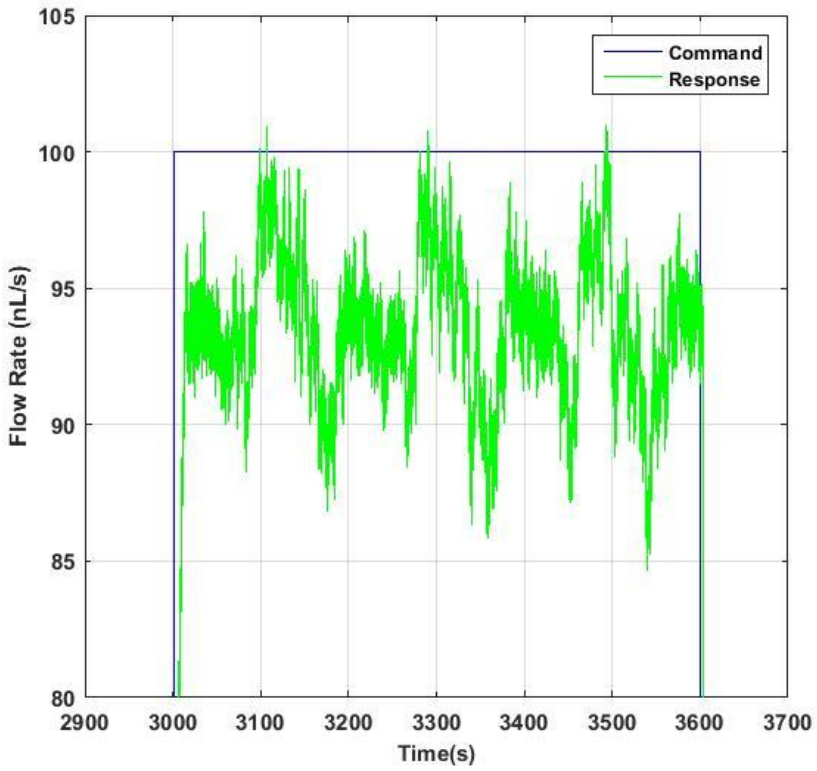

Figure 86 Syringe driver response to commands of flow rate across 3 orders of magnitude: top 1nL/s, middle 10nL/s, bottom 100nL/s.

It is evident from the response that a periodic oscillation occurs around the target value at all flow rates, which is expected due to the periodic nature of the stepper motor.

Furthermore (Table 5), the variance from both the target value and the mean of the logging period is considerable, and is proportionately more significant at lower flow rates (1nL/s) but absolutely larger at higher flow rates (100nL/s).

Flow Target	STD from target	Mean logged	STD from mean
1nL/s	0.1944	1.0146	0.1924
10nL/s	0.784	9.8308	0.7624
100nL/s	3.2023	93.0917	3.9357

Table 5 Summary of offset and variance about the flow command, across 3 orders of magnitude.

From this it is clear that the stability and precision of the syringe pump are not ideal. There is a constant oscillation due to the worm drive, though it remains on average around the target and does not drift consistently away from it, and the imprecision appears proportional to the absolute flow level.

There is clear hysteresis at the higher flow rates, as the actual logged values do not reach the target but settle at an average value up to 7nL/s lower (from Table 5). A long-term (several hours) stability test was not performed, as the system already demonstrates poor stability over short periods.

4.4.1.3 *Syringe driver latency and hysteresis*

In this experiment, the short term response to a sharp command change was noted. The command sequence was again delivered in LabVIEW without closed loop control, using the values 10, 11, 10, 15, 50, 10, 100, 10 nL/s (Figure 87).

This allowed the response of both negative and positive changes at small (±1nL/s) and large (±100nL/s) to be observed. The time held at each value was 60 seconds.

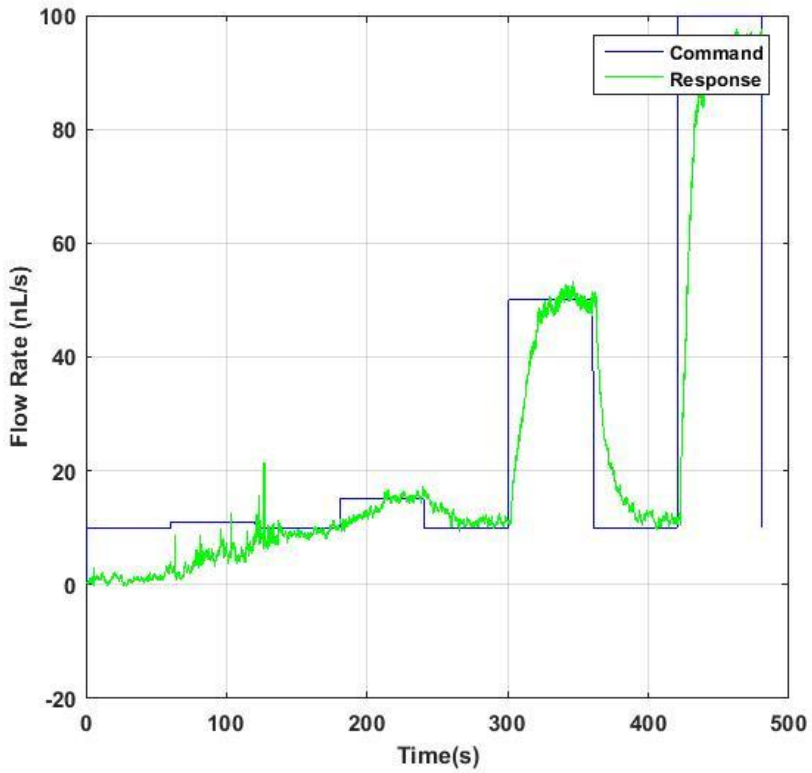

Figure 87 The latency test command sequence, and the response of the syringe driver, with the syringe flow rate initially zero.

This demonstrates the considerable latency of the response, which was not immediately evident when allowing 10 minutes for each command value. Note

particularly that the syringe driver does not overcome the fluidic resistance of the tubing for several minutes, when starting from a state of no flow.

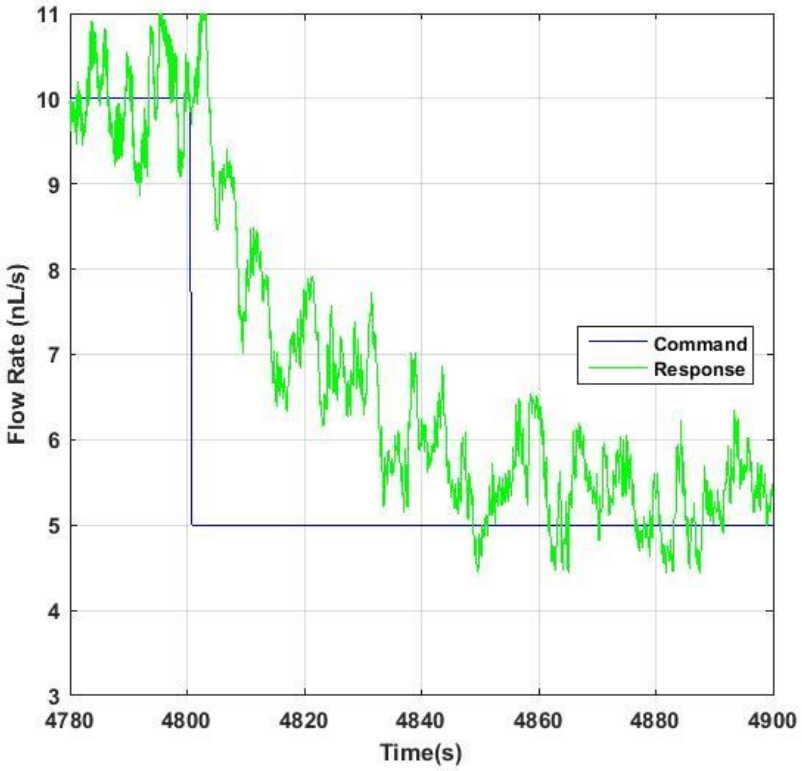

Figure 88 The transient response from 10 to 5 nL/s (sub section of Figure 85)

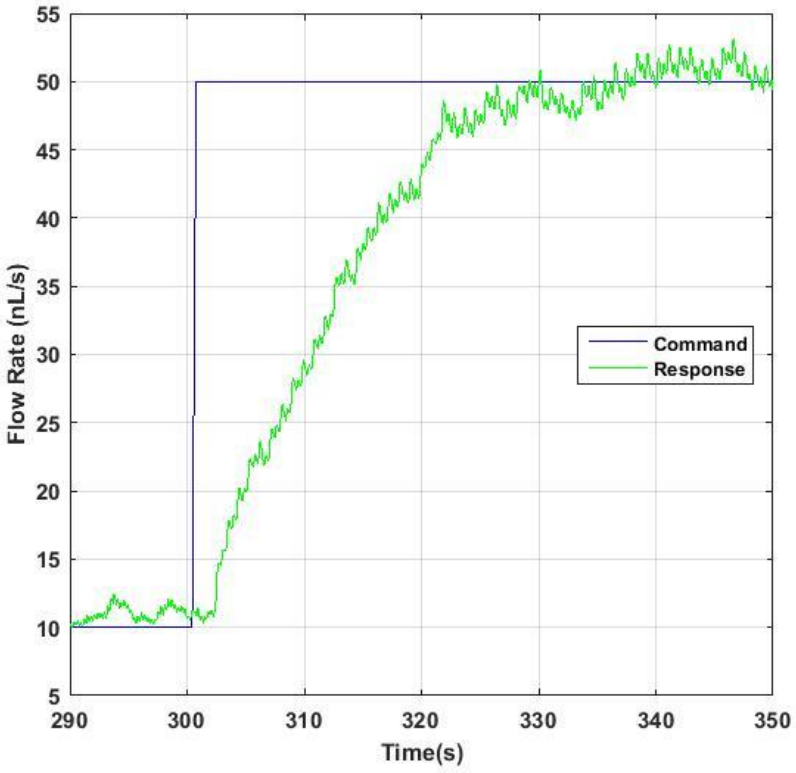

Figure 89 The transient response rising from 10 50nL/s (close up of Figure 87)

The step change of the syringe driver to moderate (∆5nL/s in 1 second, Figure 88) and high switching vales (∆40nL/s in 1 second, Figure 89) is quantified by reading off the time take to travel 90% of the distance, and the time taken to settle to final state (inasmuch as that can be established, given the imprecision already demonstrated).

Level shift (∆Q)	Time to switch 90%	Time to settle
1nl/s	n/a	n/a
5nl/s	45 seconds	>70 seconds
40nl/s	25 seconds	35 seconds

Table 6 The syringe driver latency response across 3 orders of command change magnitude

Intuitively, the response to a rapid change should be implemented more quickly as the change in stepper commands higher, and this is borne out in Table 6. Under no circumstances is the latency under 1 or even 10 seconds.

It is noted that using a more airtight glass: Teflon syringe would mitigate this latency. The syringe approach would still however have issues with rapid volume replacement, gassing media, and flexible control of different flow rates

4.4.1.4 *Syringe Driver Conclusion*

The syringe pump does not drift (or at least not on average), but has large variance about the target, proportional to the target rate, and has poor latency irrespective of target shift. This latency cannot be altered as there is no direct software control of the command. Thus it will never be better than 10s of seconds. The control of multiple syringe drives is achieved by daisy-chaining them from the PC, so synchronisation will be serial rather than parallel.

4.4.2 Gas-driven system: prototype

4.4.2.1 *Concept and preceding work*

The concept of air-over-liquid pumps is well established, though typically they employ an air driven plunger to compress liquid into a high pressure jet. Here it is not considered desirable to decouple the gas and liquid phases with an intervening barrier, as one of the advantages of using air pressure to effect liquid transport is that some of the high pressure gas can be absorbed by the liquid. In addition, it is not desirable to induce very high pressures in the liquid; only enough to overcome fluidic resistance and cause low flow rates proportional to the air pressure.

Bubbles can often form in microfluidic channels, and are lethal to cells as they cause cell rupturing due to surface tension change at the air-liquid interface. Accordingly, several methods have been developed to prevent or mitigate their presence, typically making use of an upstream trap (Zheng et al. 2010; Zhang et al. 2014; Lochovsky et al. 2012) to prevent the bubble entering the channel proper, or a gas-permeable layer through which the bubble can diffuse while the liquid is retained in the flow line. This is undesirable since the soluble gas is necessary for culture survival

Having an opposing *back pressure* ensures that the pressure in the microchannel is always sufficiently high that compressed gas cannot spontaneously nucleate out of solution.

A prototype system had been designed by Dr Oliver Miller, and its performance is evaluated below. Where it was felt the system did not meet the criteria described (particularly regarding stability), iterative improvements were made to the system.

4.4.2.2 *Pressure vessel*

The first requirement for the system is a mechanism for converting the available gas pressure to fluid flow. This means using the media vessel itself (which forms element 2 of Figure 82). Here an airtight Duran bottle is used (Figure 90) with an inlet allowing compressed gas to enter, and an outlet permitting liquid egress via an HPLC (High Pressure Liquid Chromatography) tube composed of PEEK (*polyethylethylketone*).

Compressed air was delivered via a push-fit connector sealed with an O-ring, while liquid passed through a bulkhead connecting the tubing within the bottle to tubing downstream, leading to the flow rate sensor and microfluidic channel. All fittings are sealed with O-rings.

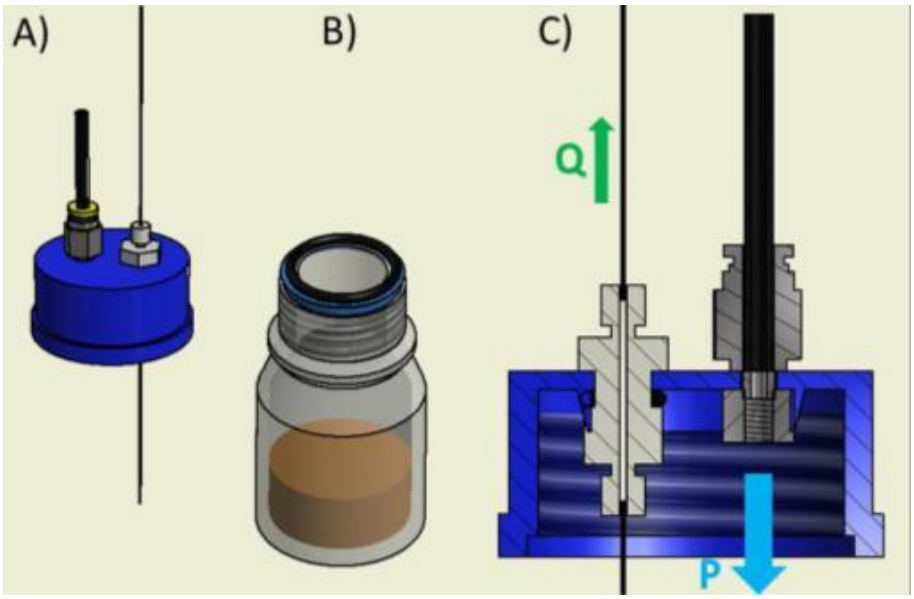

Figure 90 The modified cap (A) and Duran bottle (B) used to convert input gas pressure P to outgoing flow rate Q (C).

4.4.2.3 *Proportional valves in manifold*

The input air pressure is regulated by 2 electrically actuated pneumatic valves seated in a customised manifold (Figure 91, and also element 1 of Figure 82). An electro-pneumatic valve operates by using a solenoid to move the *valve seat*, an element which engages a gasket within the valve. When no current is drawn the seat is clamped against the O-ring by a spring and prevents gas passing, while drawing current actuates the solenoid and opens the orifice. Two such valves in a manifold can regulate both pressure increase and reduction.

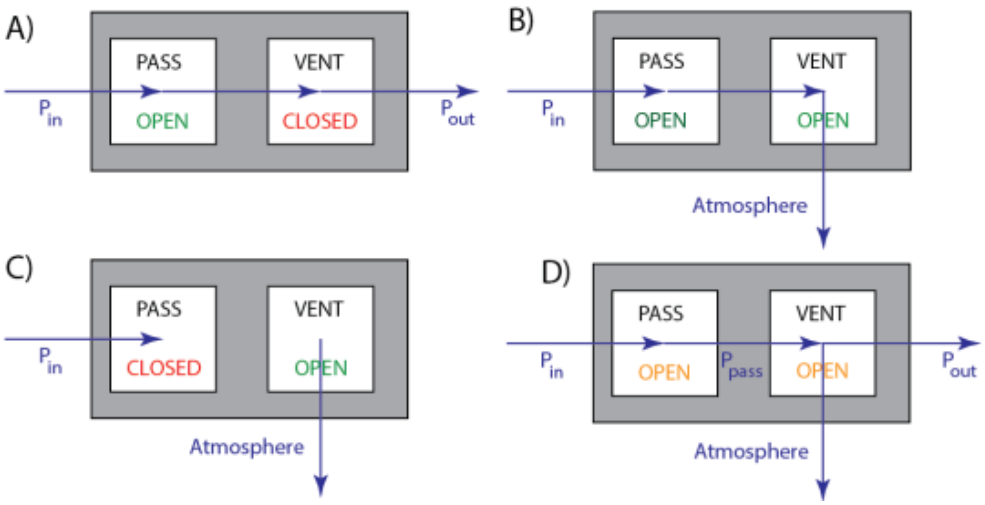

Figure 91 Two proportional valves in a manifold. A) Gas passes freely though the manifold to the vessel, $P_{in} \approx P_{out.}$ B) Gas passes out of the vent valve, and P_{out} becomes atmospheric pressure. No pressure passes to the vessel. C) No pressure enters and the vessel pressure eventually becomes atmosphere. D) In practice, both valves are partially open (proportionally controlled) and $P_{out,}$ the vessel pressure, has a value between P_{in} and atmosphere.

Proportional valves, unlike binary on-off valves, can be incrementally opened by fractionally increasing the current drawn by the solenoid governing the orifice seat. When there is no current drawn by the valve, in theory the valve is airtight. Conversely when the full current is drawn, in theory the entire inlet pressure is passed to the valve outlet.

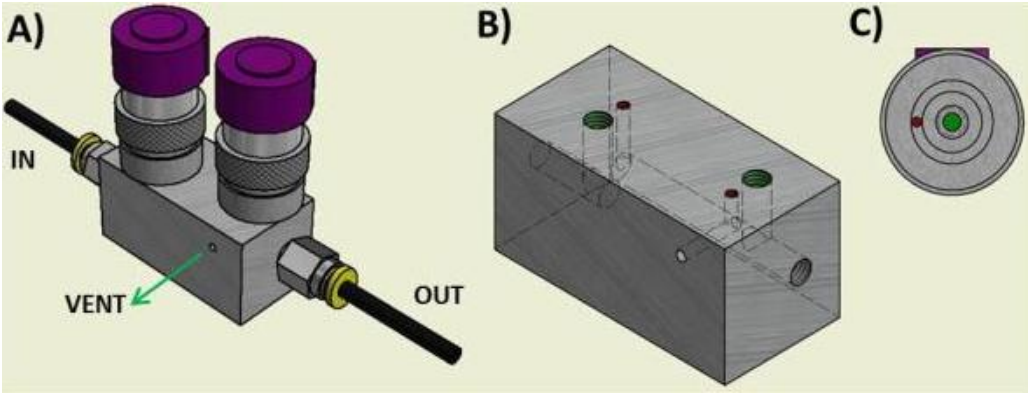

Figure 92 Clippard manifold design, showing 2 valves and the inlet / outlet paths (A). The manifold is machined (B) such that the central inlet and radial outlet of each valve(C) line up with corresponding holes in the metal block.

For pumps 1 and 2, delivering buffer and agonist co-flows which must be switched arbitrarily and swiftly, customised manifolds were built. The valves originally used were Clippard EV-PM-05-6025, which each required a 5V, 500mA power supply in order to run, and were seated (Figure 92) in a custom

built manifold (appendix 10.4.8). As the DAQ card originally used (NI USB-6008) cannot deliver an analogue output of more than 5mA, a current boosting circuit was required (Figure 93).

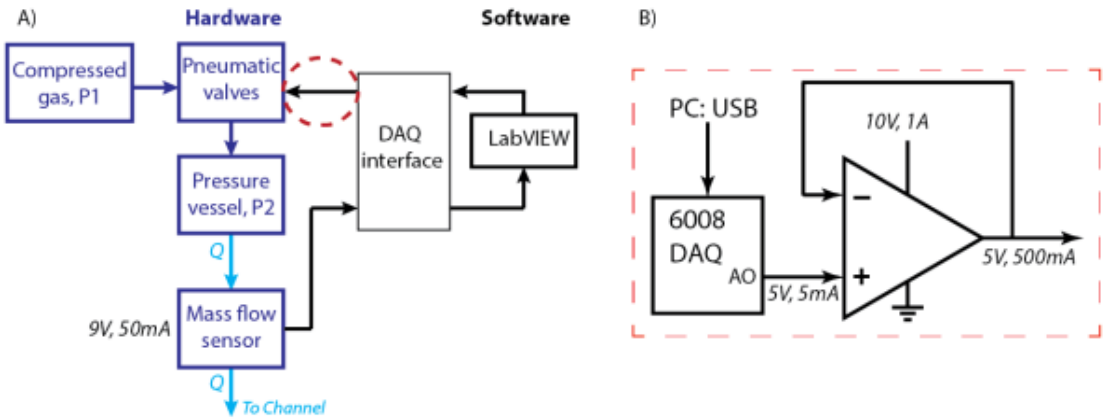

Figure 93 A) Schematic of the pump concept: The actuators tap pressure P1 and pass a pressure P2 to the media vessel. Flow rate Q is fed back to the command program and the voltages controlling the actuators are adjusted accordingly. B) As the DAQ cannot provide the current necessary to actuate the valve solenoids, a voltage follower circuit was constructed to increase the current available by a factor of 100.

For pump 3, which provides back pressure, the most important criteria is stability, and a commercial regulator, the Proportion-Air QVP1TFEE015 was selected based on its advertised performance. It was considered that the QVP regulator might not switch very rapidly since it is pre-set for stability, and that the PID control settings are fixed in hardware and not easily adjusted.

4.4.3 Proportional-Integral-Derivative Control

In order to utilise the sensors, the feedback signal, an analogue voltage representing pressure or flow rate is compared to a target reference determined by the user. The instantaneous difference between feedback and reference is denoted the *error e(t)*, which it is desirable to keep as small as possible. By adjusting the voltage sent to the valves, the pressure and hence flow can be adjusted to reduce the error (Figure 94).

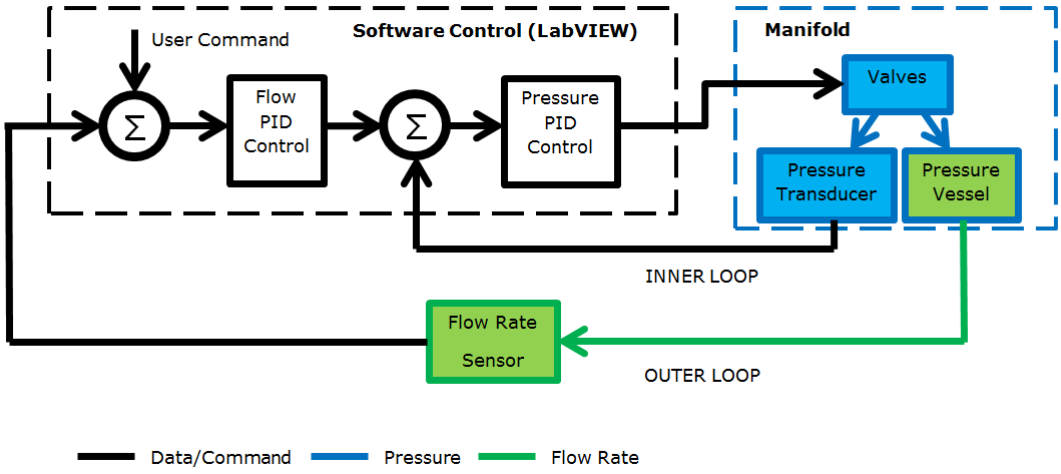

Figure 94 PID control loops, demonstrating the potential for direct pressure regulation (inner loop) or indirect pressure control imposed by direct flow rate control (outer loop).

The adjustment should be *proportional* to the error, so that large errors are compensated for as effectively as small errors. However, very prompt responses may overcompensate (overshoot), leading to another error and a cycle of instability as the pressure oscillates about the target. Conversely slow responses are also undesirable since they do not adjust to meet the target on the necessary timescale.

An *integral* term is used to stabilise the rate of adjustment. This takes account of the sum of the error over a period τ, and accounts for error that has already been compensated for. Thus it accelerates the adjustment while the error is large but reduces it as the target is closer. This can make the control adjustment slower.

$$\boldsymbol{Output}\,(\boldsymbol{t}) = \boldsymbol{K_p e(t)} + \boldsymbol{K_i}\int_o^t \boldsymbol{e(\tau)}\,\boldsymbol{d\tau} + \boldsymbol{k_d}\frac{\boldsymbol{d}}{\boldsymbol{dt}}\boldsymbol{e(t)} \qquad [18]$$

where K_p, K_i and K_d are the gains of the proportional, integral and derivative terms.

A predictive control element is useful to improve response time, and so the slope of the error over time is assessed to determine where it may shift in future. This can be inappropriately sensitive to noise fluctuations, however, and often this term is not used.

The pump system designed by Dr Oliver Miller can be schematically represented by Figure 95 below, where each of the three pumps is composed of a manifold and pressure vessel combination:

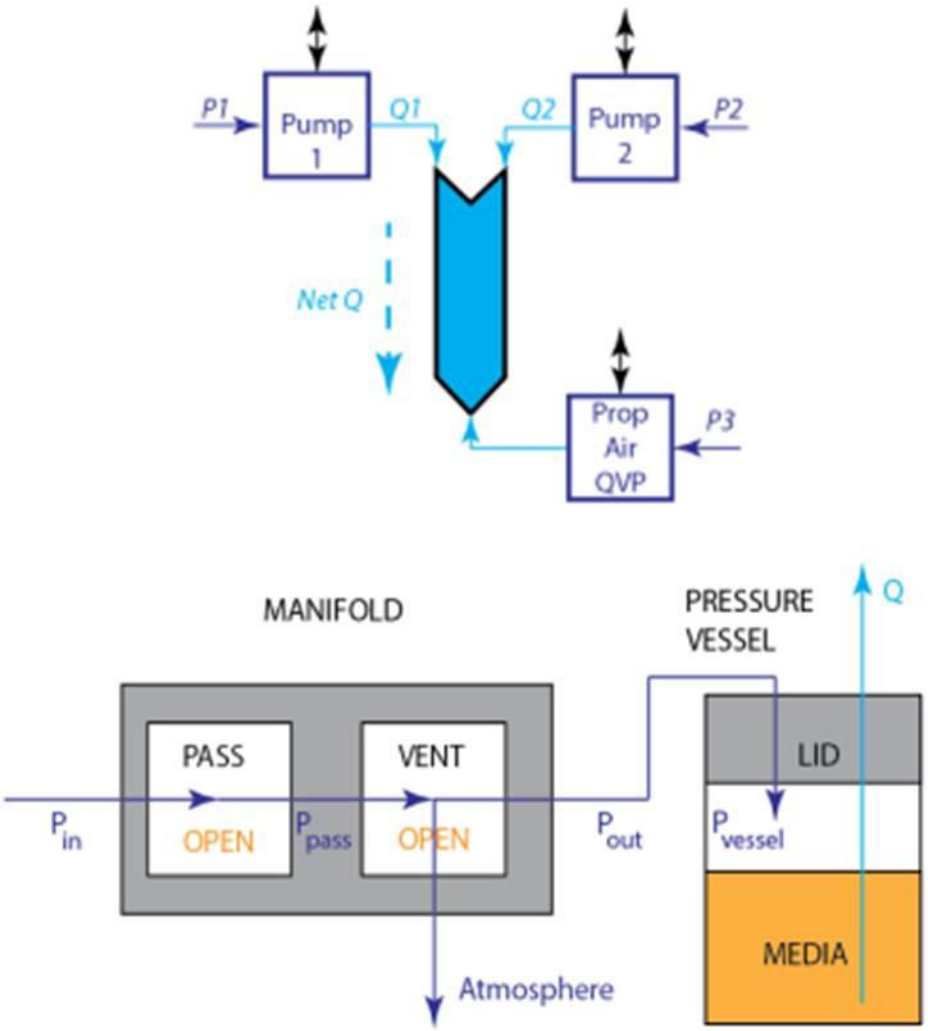

Figure 95 The 3-pump system as developed by Dr Oliver Miller. Note (right) that the pressure at the actuator outlet may differ from the pressure in the pressure vessel, since the two are not integrated as they were in the syringe.

Note that in this configuration we have no direct knowledge of P_{pass}, P_{vent}, or P_{vessel}. The Proportion-Air QVP operates on the same principle as the custom manifolds but uses a built-in pressure transducer and contains its own current boosting PCB.

The QVP1 is also controlled via a DAQ and returns an analogue voltage to the PC which is directly converted to Pressure in barg (1V = 100mbar).

Because the proportion-air is self-regulating, it was assumed that it provided a stable back pressure, with standard deviation within the 1mbar criteria determined earlier.

4.4.3.1 *Gas system Stability*

The long term stability of the system was tested. Only pumps 1 and 3 are used for this test, and a single inlet microchannel connected between the flow rate sensor and the backpressure regulator.

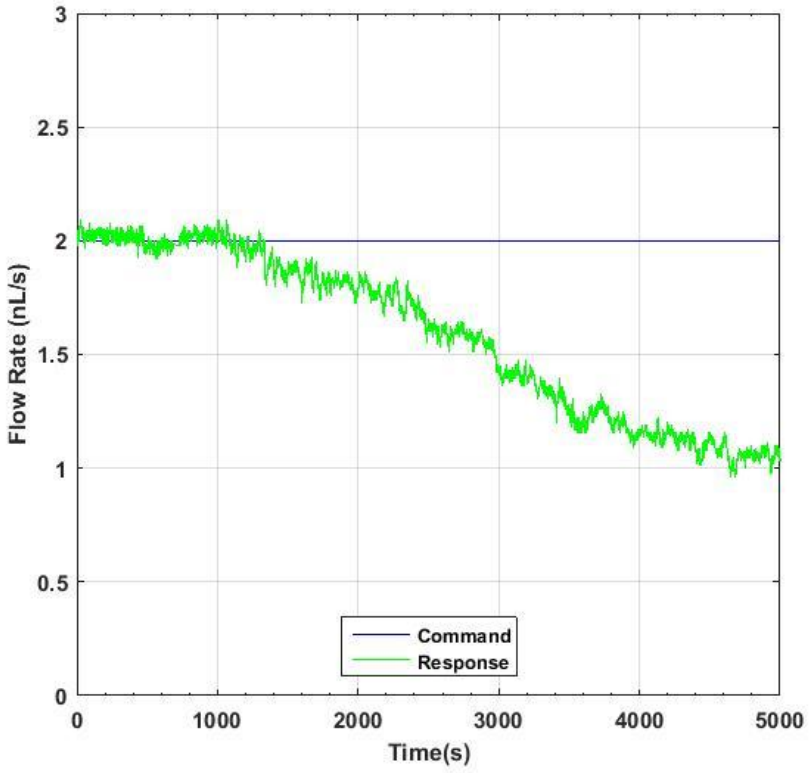

Figure 96 Response of the system over the course of 5000 seconds (>80 minutes). The logged values remain very close to the command; in comparison to the syringe driver for a similar command value (see Figure 86)

From Figure 96 it can be seen even over short periods the flow rate begins to fall away from the command value, though the rate of drift is much slower and therefore superior to the syringe driver.

When using both forward pumps it can be seen (Figure 97) that the interface between the two co-flows (The total flow rate is 100nL/s in both cases) is tightly constrained, in accordance with the models from chapter 3.

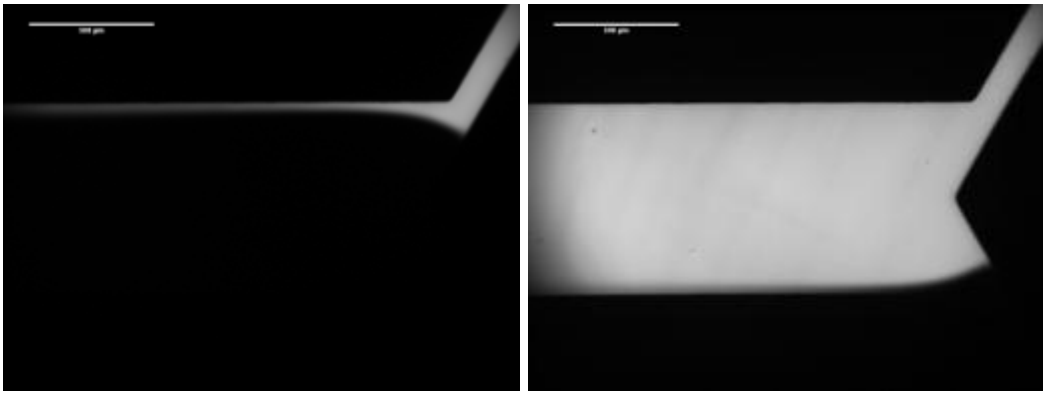

Figure 97 Co-flows of water and fluorescein imaged with FITC filter, representing both 2% (left) and 98% (right) agonist fraction of total net flow rate 100nL/s opposing 70mbar backpressure. Scale bar is 500µm.

This system is clearly on average far more stable than the syringe driver, and remains close to the command value for much longer. However, there is an obvious tendency for the flow rate to drop over time away from the target, which implies a systematic leak. Since no liquid is lost between source and waste vessels, the loss must be a pressure drop. The effect of this is catastrophic (see Figure 98).

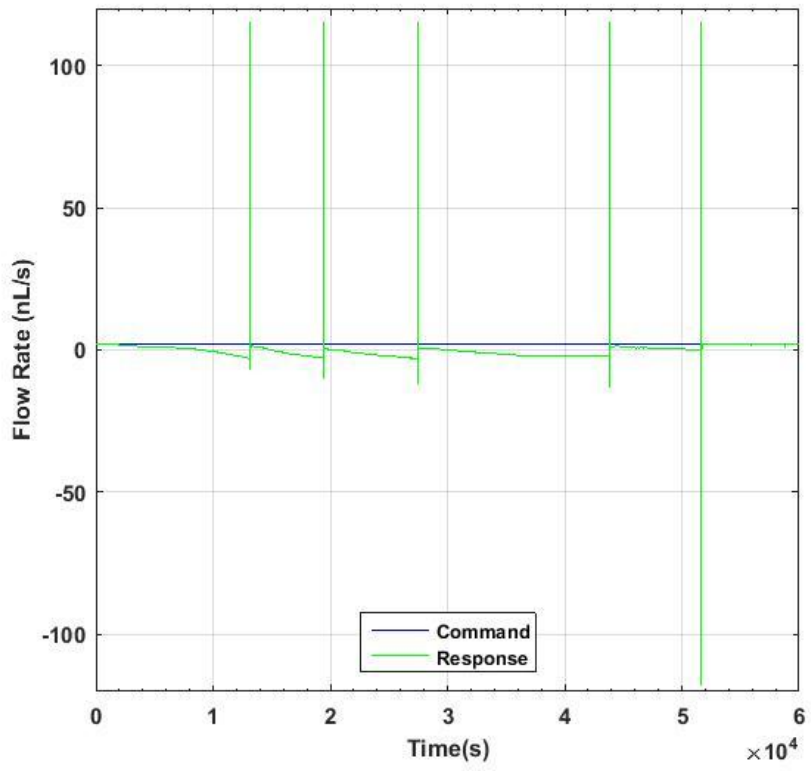

Figure 98 Over the course of several hours the drift observed in Figure 96 increases until the difference between reference (2nL/s) and actual flow is around 5nL/s. At this point, the controlling algorithm institutes a sharp pressure correction.

When the offset between command and actual values exceeds 5nL/s, the LabVIEW program controlling the pressure regulation in Pump 1 institutes a rapid switch. Due to the PID settings used, this leads to a series of high-magnitude pressure ‘spikes’ which are so large they saturate the range of the flow sensor in both directions. The logged flow rate has a mean of 0.0739nL/s and standard deviation 3.6118, a long way from what is required of it.

This is more pronounced (see Figure 99) at higher flow rates (above 10 nL/s net flow rate), which is where the system would typically be operating, based on the useful flow ranges noted in the previous chapter.

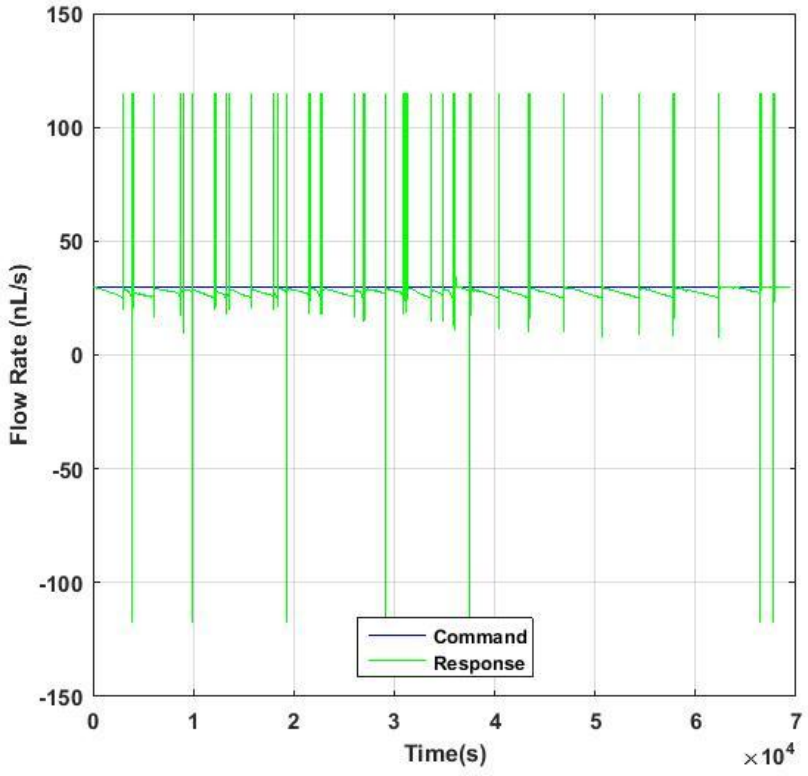

Figure 99 The prototype system with a reference flow rate of 30nL/s. The frequency of the flow spikes is greater.

Thus in the short term the precision and stability of the system appears acceptable, but over the longer term the flow rate clearly drops below the target, culminating in a sharp response when it reaches a deficit of 5nL/s. The prototype perfusion system has relatively good precision in the short term but tends to drift into an unstable configuration over time (see Table 7), so the most important issue to be solved is the instability, and investigate what has

caused it. Unlike the syringe driver, it is possible to alter the hardware and control algorithms for this purpose.

Flow Target	Number of spikes (distinct events)	Mean time between
2nL/s	5	40 minutes
30nL/s	32	< 20 minutes

Table 7 Comparison of spiking behaviour at different operating points using the original gas driven pump.

Bubble removal

The backpressure pump demonstrates the capacity to remove even very large bubbles from the microfluidic channel (Figure 100). Over the course of 15 minutes, a bubble can be removed by keeping the backpressure 70mbar and the net forward pressure higher than this.

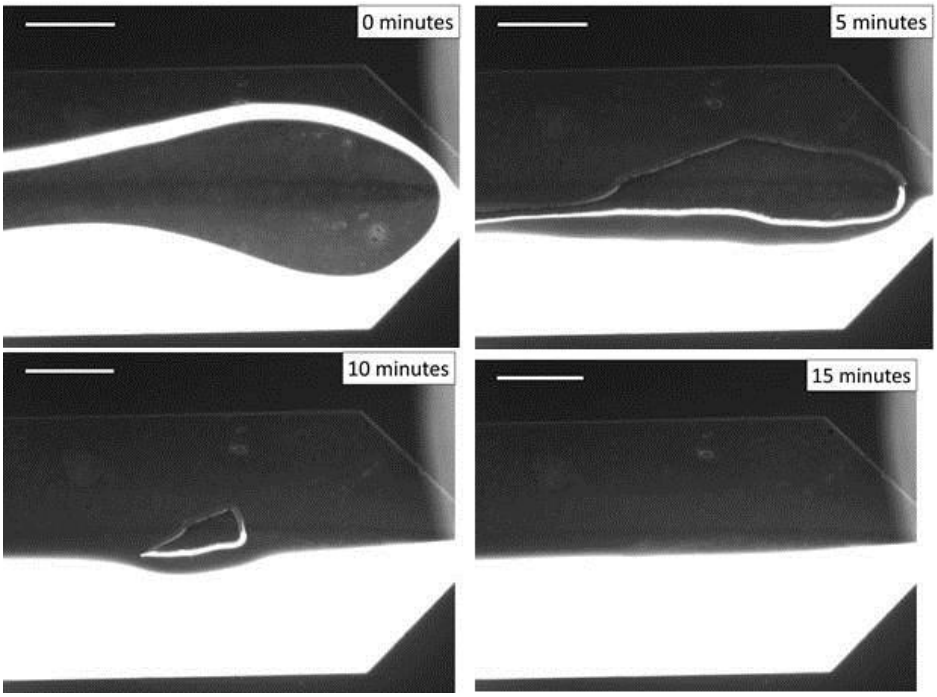

Figure 100The bubble (large irregular dark shape) distorts the boundary of the water and fluorescein co-flows, imaged in FITC filter cube. After 15 minutes, the bubble has been compressed back into to the liquid (or out through the PDMS). Scale bar 500µm.

4.4.3.2 *Latency of gas-driven system*

The latency response of the gas-driven system in comparison to the syringe driver was evaluated, by using a 60 second command sequence programmed in LabVIEW by Mr Solomon Idinyang (Figure 101).

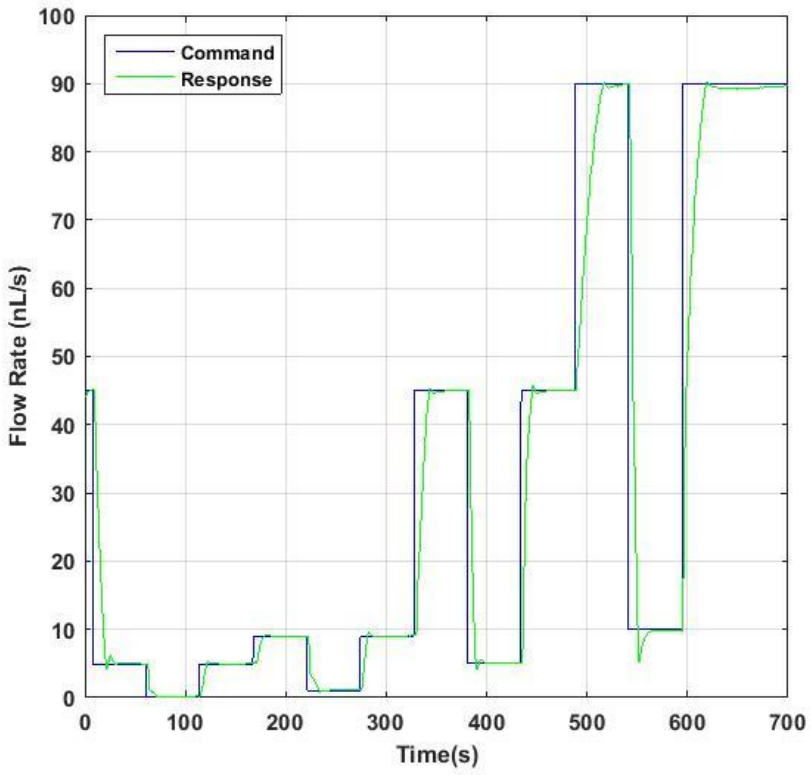

Figure 101 Response of the gas-driven system to changes in command flow rate, over 60s intervals. Compare to Figure 87

The delay in reaching the target is now proportional to the ΔQ command. Given that the command algorithm is now explicitly PID this is to be expected. This is thus an improvement on the syringe driver which took longer than this regardless of level switch.

Latency for a large Q shift

Here the latency is still on the order of 10-20 of seconds, but is much more stable and does not oscillate once it has reached the target.

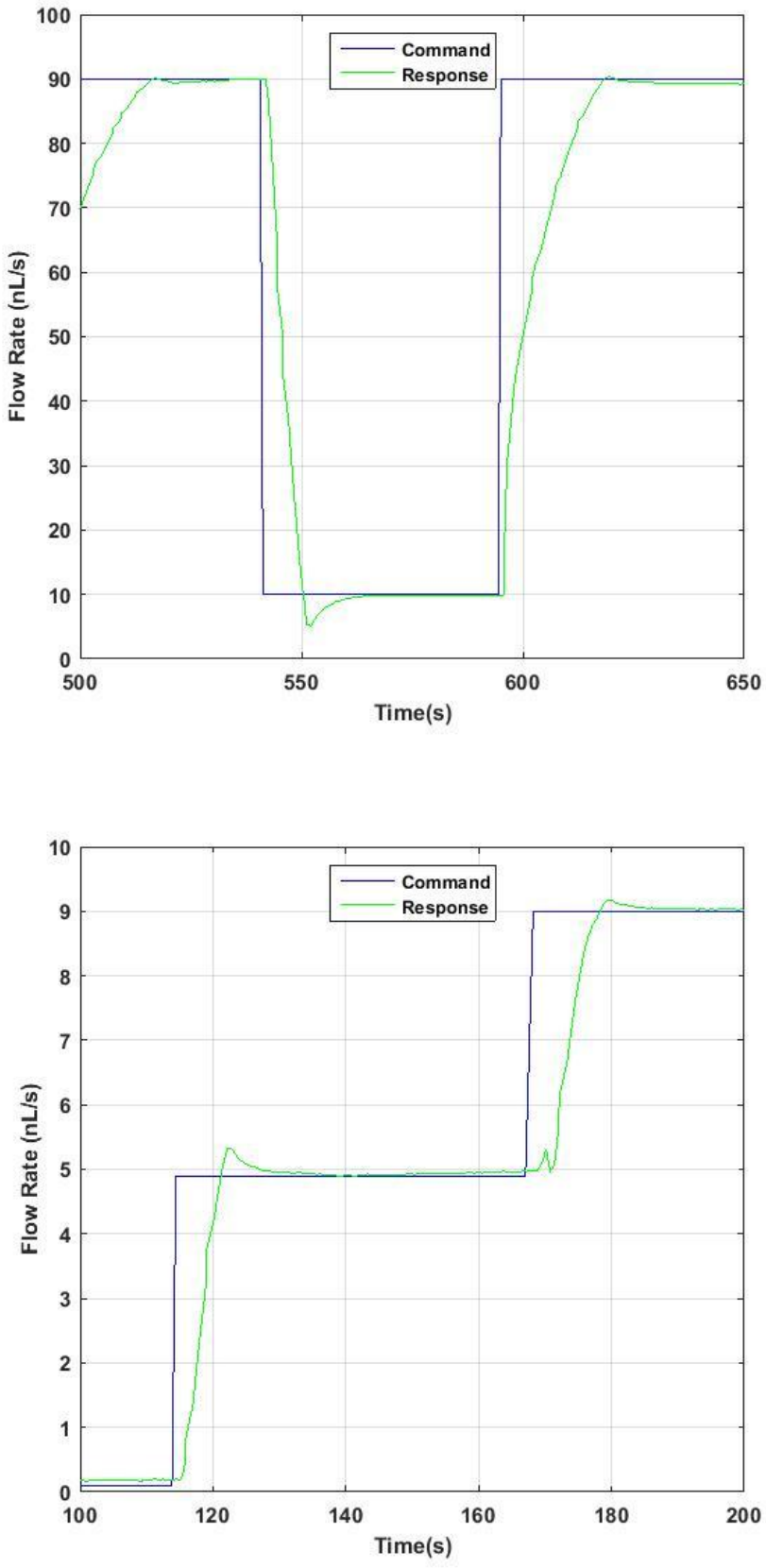

Figure 102 Latency response for both a large (80nL/s) and small (4-5nL/s) ΔQ. Plots derived from data acquired by Dr Oliver Miller

In summary, the latency of the gas-driven system (Table 8) is much superior to that of the syringe driver (Table 6).

Level shift (ΔQ)	Time to switch 90%	Time to settle
5nl/s	5 seconds	15 seconds
80nl/s	<10 seconds	20 seconds

Table 8 The gas-driven pump latency response across 3 orders of command change magnitude

This is still not as fast as would be preferred in order to effect <1s agonist delivery, and so a redesign of some system elements (including the software) is necessary to improve the system.

4.4.3.3 *Co-Flow for slower switching*

Acknowledging the instability of the system long-term, the co-flow application was tested by using a 2-inlet microchannel and including Pump 2. A slow sinusoidal command was implemented with the total flow rate peaking to 25 nL/s (Figure 103).

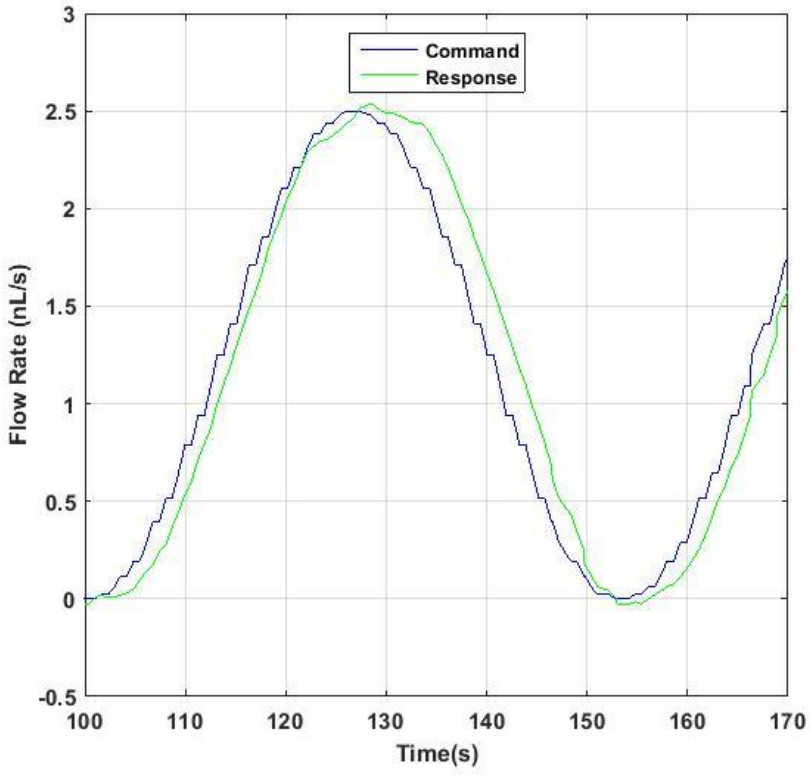

Figure 103 Latency response for a sine wave command where Q (agonist) is 1:9 of the total net flow rate.

This latency, of around 5 seconds, is adequate for slow gradient switching applications, and will be explored further in section 4.4.6.

4.4.3.4 *Investigating instability*

The latency of the system is an improvement over the syringe driver, and is readily improved by altering the PID settings. Currently the instability is the greatest concern, and so the cause is investigated.

4.4.3.5 *Backpressure precision and inaccuracy*

Any significant variation in the backpressure provide by the Proportion-Air QVP1 will have an impact on the net flow rates, as the two forward pressure regulators will attempt to compensate for the change in back pressure.

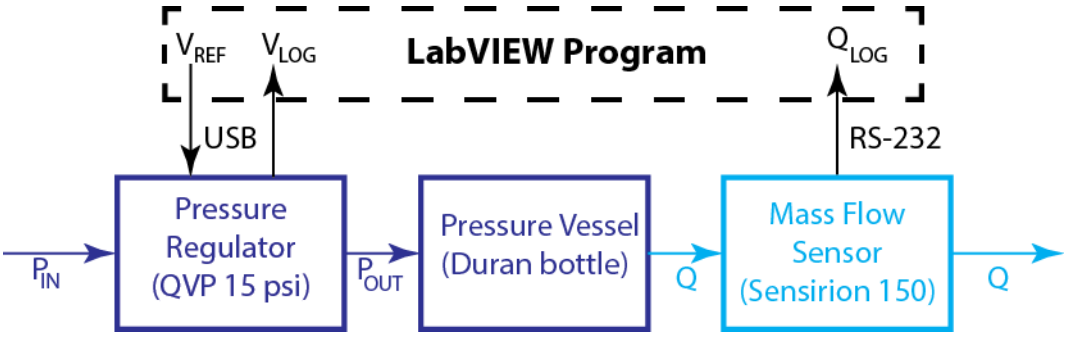

Figure 104 Schematic of testing the flow rate induced by the proportion-air pump

Note that P_{out} from the Proportion-Air QVP1 is not necessarily the same as the converted V_{LOG} that is read back to the PC, and will almost certainly be different to that in the Duran bottle.

In the stability experiment outlined previously (see Figure 98) with a command flow rate of 2nL/s, the backpressure should have remained 70mbar throughout. In fact, the mean logged backpressure is 70.1mbar, but with a standard deviation of 2.8134 mbar. This is significant as it means the backpressure is itself a source of error. The flow rate feedback loop (see Figure 94) is forced to continually adjust to substantial transient changes in the backpressure.

Opposing QVP1 regulators

Here 2 regulators are commanded to provide opposing pressures. Each enters a Duran pressure vessel, and both vessels are connected by PEEK tubing with a flow rate sensor in-line. The backpressure is set at 70mbar while the forward pressure is set at 75mbar, and the data, including net flow rate, is logged for 45 minutes (see Figure 105). The flow rate is not used to adjust the pressures.

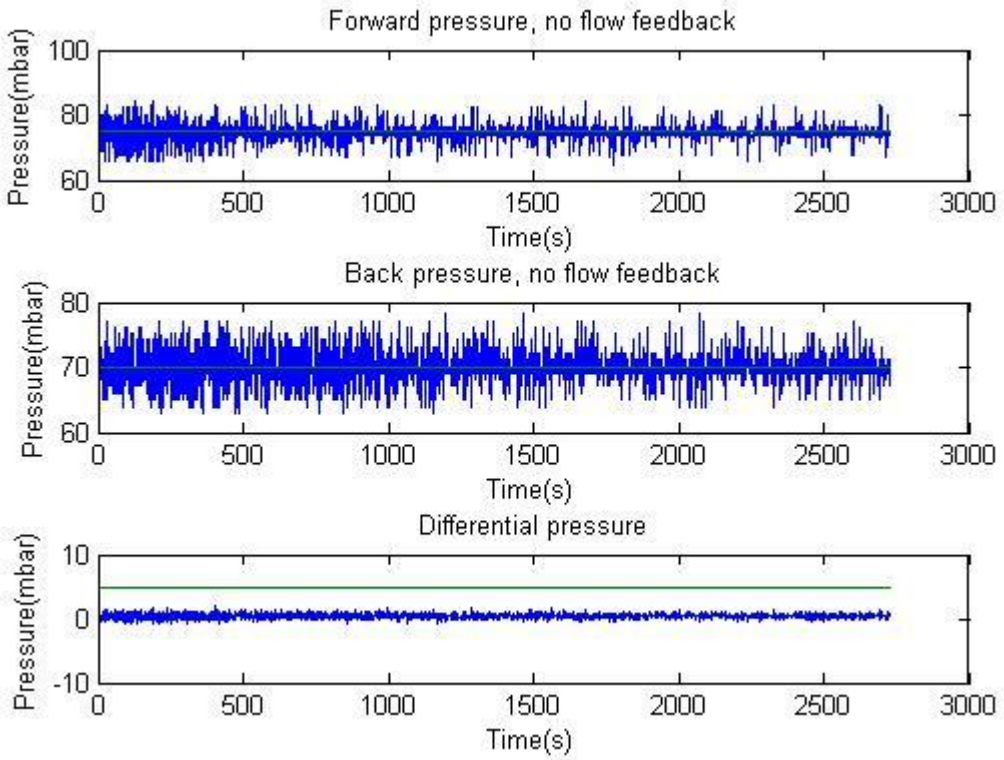

Figure 105 Both QVP regulator returned log values are recorded at 1.5Hz . The net flow rate was recorded but was not used to provide feedback to the system. The difference (subtracting backpressure from forward) at each time point is compared to the difference of the command values (5 mbar)

	QVP forward	QVP back	Difference
Mean (mbar)	74.09	69.89	0.42
Standard Dev (mbar)	1.83	2.14	0.28

Table 9 Comparing variance of the QVP pressures, and the average offset from the expected pressure difference.

The mean flow rate is 13.06nL/s, with a standard deviation of 3.47nL/s.

Noticeably despite the average pressure difference being logged as practically zero (see Table 9), the flow rate is over 13nL/s on average, so something is not being logged accurately, and as a result the precision metric (under 2nL/s, from section 4.1.1) is not being achieved.

By measuring the output of the manifold directly with a GE Druck PMP5074 pressure transducer, it was discovered that the value sent to the LabVIEW program by the QVP1 does not represent the output pressure value of the regulator, which is typically lower. When externally measured by the PMP5074, the QVP pressure output in the stable region of Figure 106, the regulator has a mean 64.814mbar, and standard deviation of 0.053mbar.

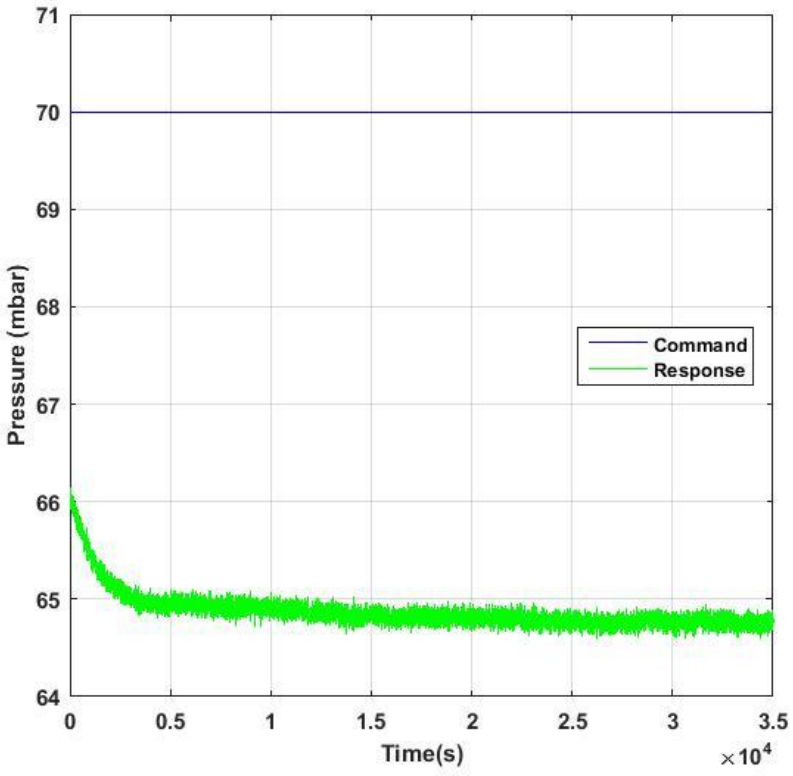

Figure 106 Externally measured output of the QVP1 regulator compared to the 70 mbar target

This appears to imply the issue is one of accuracy, as when measured by another sensor the output has far better standard deviation but an average significantly below what it is required. Currently these regulators cannot be used in the system, until the discrepancy is addressed.

The QVP is also capable of performing with much improved precision if addressed more effectively in LabVIEW (see Figure 107). Again the output is measured by a PMP5074.

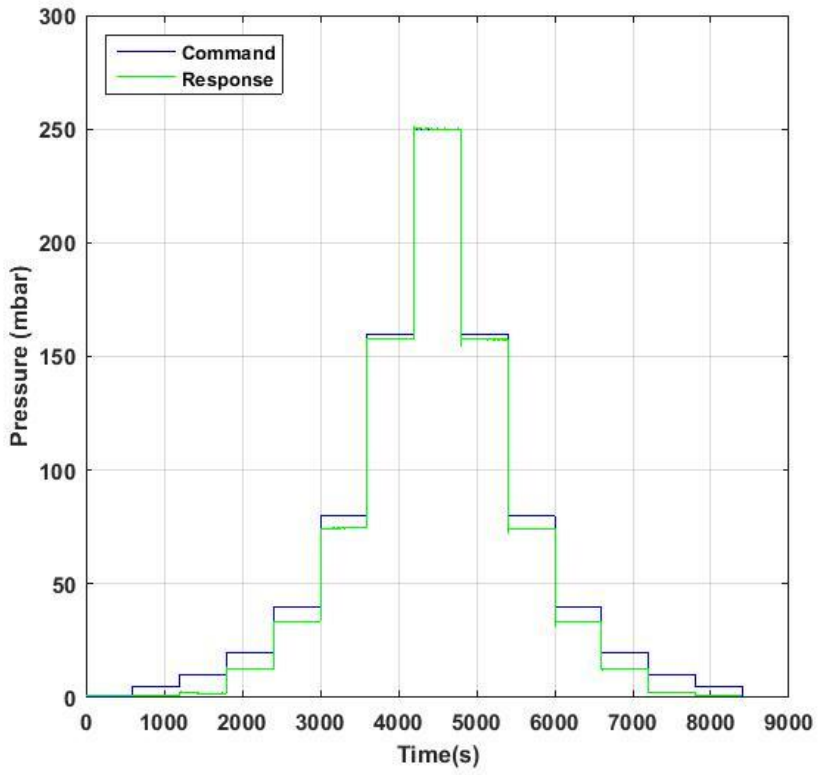

Figure 107 Comparing the commanded pressure response to the recorded pressure measured by a transducer at the regulator outlet, rather than the value returned to the PC by the regulator signal.

The best of the 3 QVP regulators has good pressure precision but a variable offset from the target. The offset is more pronounced at the lower end of the range, which may be due to the QVP's calibration being optimised for higher pressures.

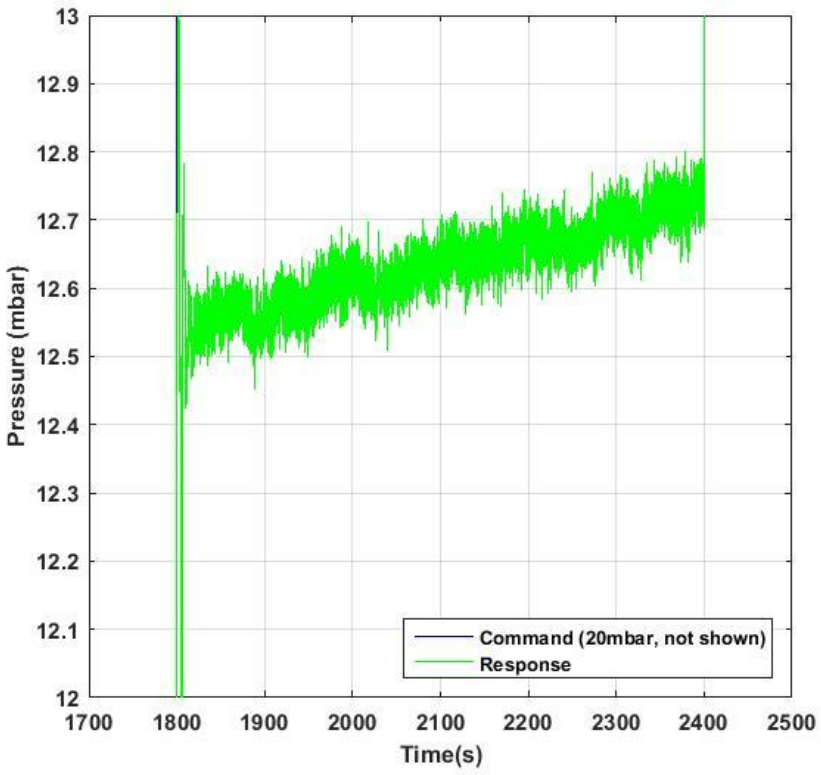

Figure 108 Pressure logged by QVP in response to a 20mbar pressure command, over 10 minutes.

Noticeably the pressure is drifting over time (see Figure 108), so that not only is it offset but constantly altering. This is a definite source of error and indicates that even with effective software control, the QVP does not provide constant accurate pressure, without feedback.

However, when flow rate feedback (as in Figure 94) is used with a command of 1nL/s and no opposing backpressure, the QVP is able to provide a constant flow rate with mean 0.99 nL/s and standard deviation 0.13 nL/s, far better than was achieved earlier.

Thus when the system is placed under flow PID control, the pressure offset is irrelevant as the regulators will provide whatever pressure is necessary to maintain the flow rate. But where an opposing pressure not under flow PID control is used, as for the backpressure, this is a problem.

We also emphasise again that the pressure returned by the proportion air manifold is not the same as is actually measured at its output, or by a second sensor downstream at the pressure vessel.

In conclusion, it is desirable to emulate the function of the Proportion-Air (pressure feedback) but build it ourselves, in order to gain complete knowledge control of the manifold performance, and get accurate backpressure. Thus a co-flow perfusion system composed of 3 custom-built pumps is required.

4.4.3.6 ***Clippard valves***

The Clippard valves are run by direct current up to 370mA from a 10V supply (5V per manifold), although PWM waveforms would have provided better control flexibility. This is because the 6008 DAQs available cannot support PWM waveforms from a digital output. The upshot is that there is noticeable hysteresis when commanding the valves (see Figure 109):

Testing the PASS valve

The VENT valve is shut off, and the current to the PASS valve is ramped up and down from 0 to 4.5 Amps (Figure 109). In this configuration all the input pressure should be passing to the output without loss. Next, the vent outlet (see Figure 92) is temporarily sealed and the same current ramping repeated.

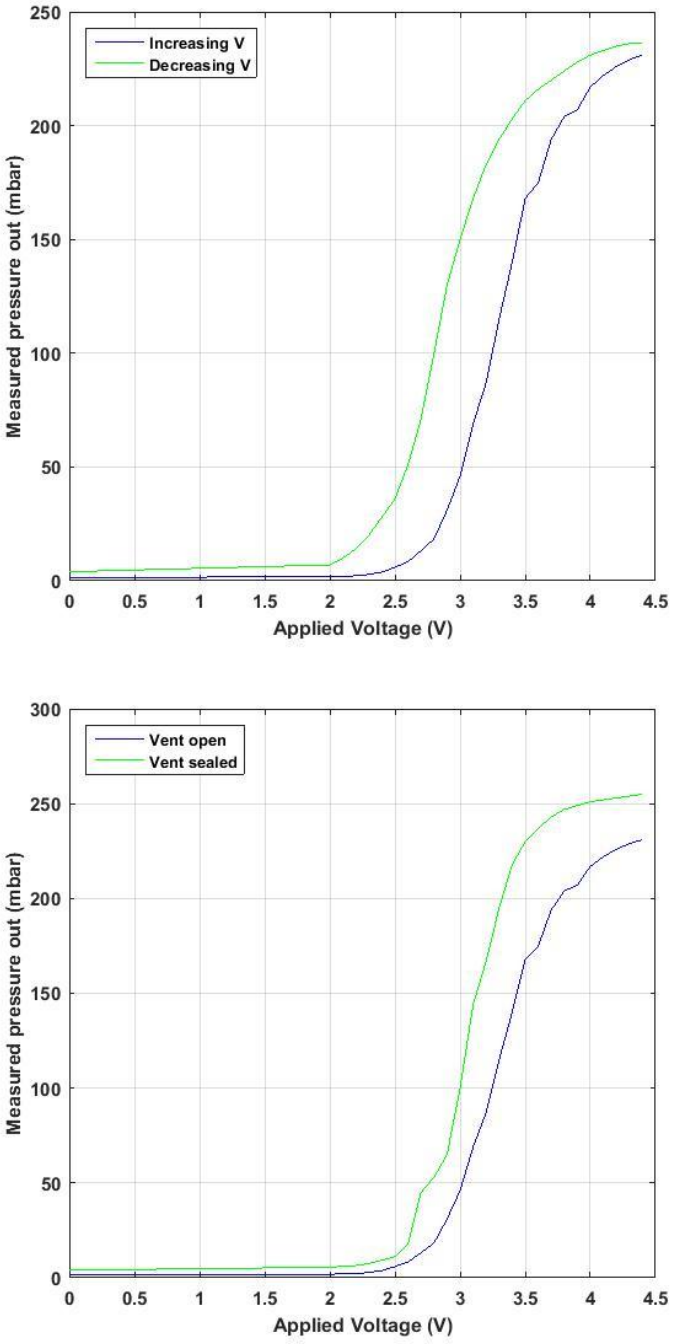

Figure 109 The Pressure output of the manifold showing hysteresis of the PASS valve when the VENT valve has no current to draw and should be shut (top), and the pressure retained when the VENT outlet is sealed (bottom). Available pressure at inlet: 263mbar.

It is evident that the pressure output alters for the same applied current depending on whether the valve current is increasing or decreasing. This leads to an unpredictable and asymmetrical system performance.

Also clearly the pressure retained in the manifold is higher when there is literally no escape route via the VENT outlet, so the VENT valve is leaking.

Testing the VENT valve

The PASS valve is fully open, and the pressure sensor registers how much pressure is lost at the outlet as the VENT valve current increases.

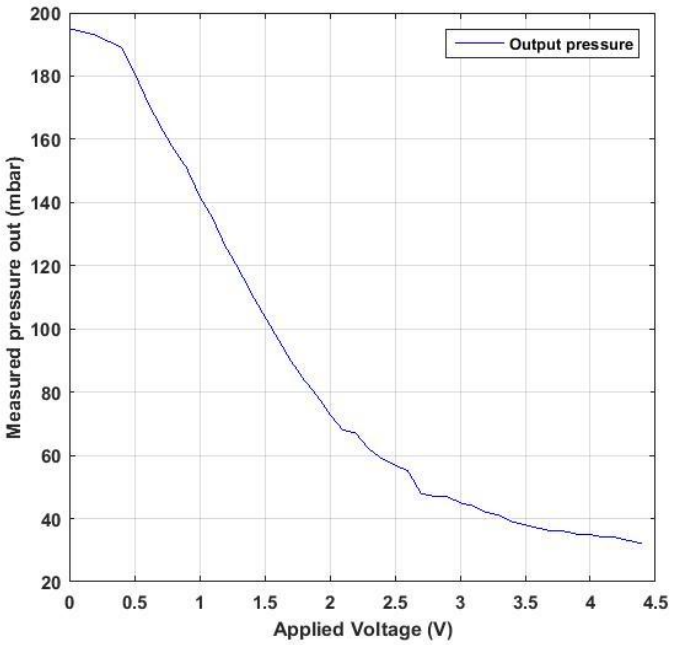

Figure 110 Output of the manifold with the PASS valve fully open and adjusting the VENT valve voltage from 0 to 4.5V. Available pressure at manifold inlet was 248mbar.

Even at zero Amps current, when it should be fully closed, the VENT valve appears to be losing at least 50mbar of the available 250mbar input pressure (Figure 110).

It is inferred that the valve / fitting for the Clippard proportional valve leaked air even when no current was available. The VENT valve was not only unpowered but not even connected (though this may mean it was partly open without being grounded. If so this is a design fault). This means that the full linear range supposedly available to the manifold is not utilised.

In addition, the 6008s only support 2 analogue outputs each, meaning that a 6008 DAQ is required per manifold.

In conclusion, different valves are necessary, together with a more useful / multifunctional DAQ. The USB-6259 multifunction DAQ can generate

deterministic PWM and has several analogue inputs, allowing many more than 2 sensors to be simultaneously polled.

4.4.4 Addressing stability by addressing the hardware

Much of the work for this iteration of the gas-driven system was undertaken by Mr Sorka Abanu, including design of the prototype LabVIEW code and current driver PCB**.**

4.4.4.1 *Hardware improvement*

Direct, reliable knowledge of the true pressure in the regulator is necessary, coupled with actuators that close completely when no current is drawn.

Valve change

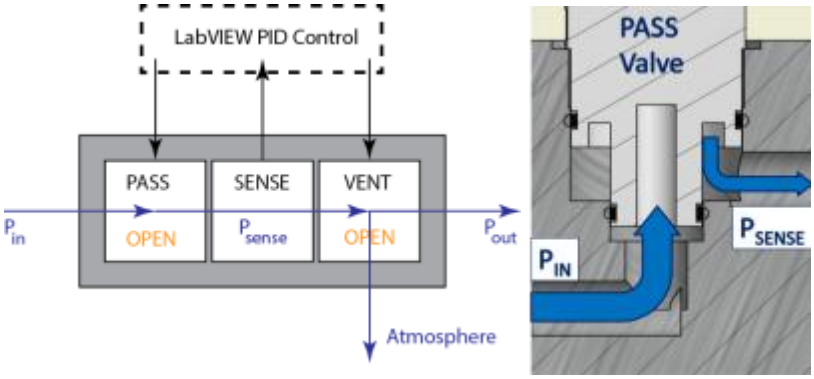

Figure 111 A direct measure of the manifold pressure is now available. This allows the actuators to be more finely controlled in a PID loop even without the flow rate data.

To overcome the issues of DC control of a valve that does not fully close when needed, a different valve was chosen: the Norgren EQIFIL Flatprop, which must to be run via PWM. The manifolds need to run on similar principles to the Proportion-Air QVP, which incorporates a pressure transducer between the valves. We will accept marginally worse latency as long as we keep similar precision. Our control over the PID settings for pressure and flow mean that stability should be much better. If the system is not functioning as expected, it is simpler to debug the components and replace or recalibrate the part.

Manifold Redesign

A new manifold was designed and fabricated (Figure 111), anticipating 2 EQIFIL valves and a pressure transducer. Because the chosen transducer may be damaged if exposed to pressures higher than 500mbar, and can only read up to 263mbar, a relief valve that prevent pressure build-up of higher

than 250mbar is also installed in the manifold (Figure 112, see Appendix 10.4.10 for dimensions and full schematic).

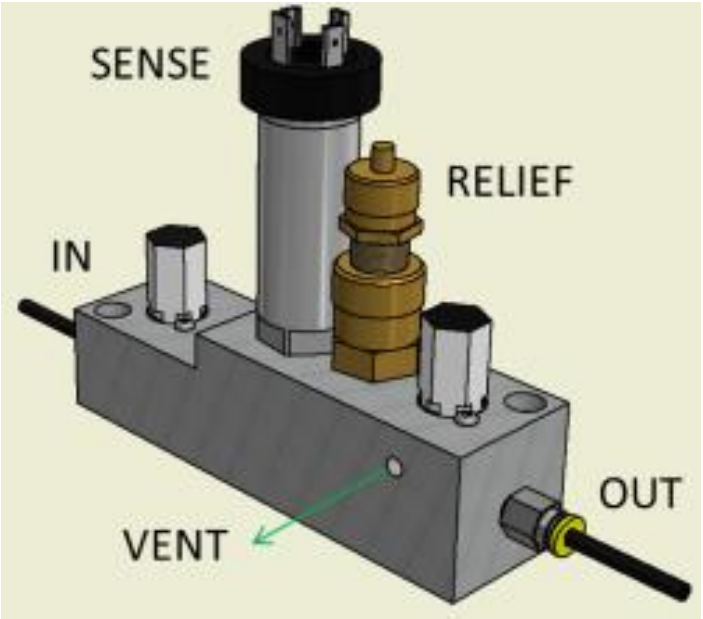

Figure 112 Schematic of the new manifold with all fittings installed.

Because the EQIFIL Flatprop is intended to be run using PWM control, a different current conversion board is necessary. PWM signals commanded in LabVIEW and generated by the DAQ card are sent to a multi-channel PCB capable of processing 8 valves (4 manifolds). The schematic and PCB of this new conversion circuit are in appendices 10.4.11.

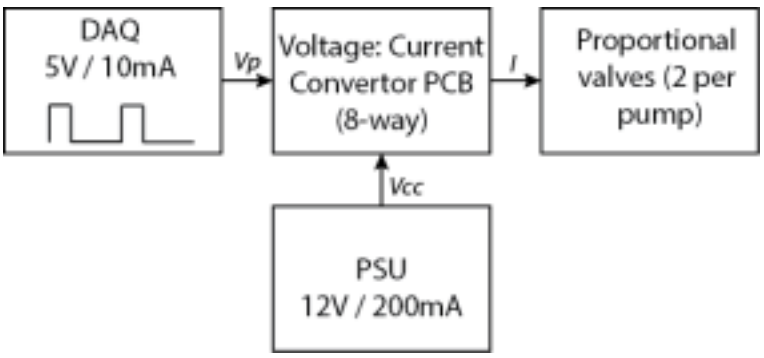

Figure 113 The electrical schematic of an individual PWM to EQIFIL conversion circuit.

This convertor board (Figure 113) was designed in –house and sent to PCB Train for fabrication.

The need for integration of vessel and sensor:

Although the latency and stability of the system are now both well within acceptable limits, there is still a mismatch between the pressure output by the manifold and the pressure imposed at the media vessel. A modified Duran bottle cap was used. Instead of a bulkhead permitting liquid egress, a second gas bulkhead leading to a pressure transducer was used. The pressure loss is shown below:

Latency response of the improved manifold system

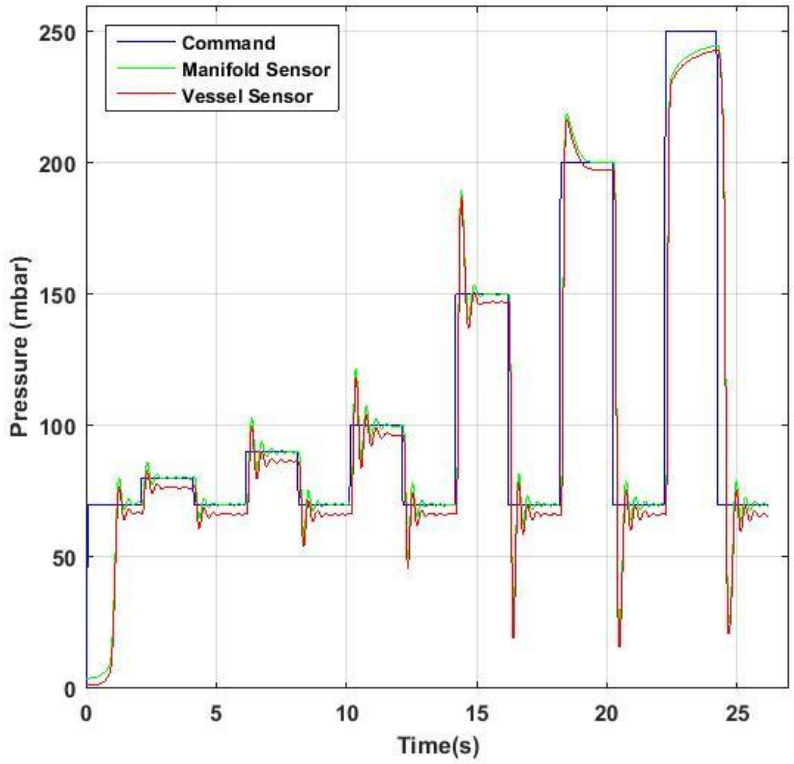

Figure 114 The offset of the second pressure transducer. Operating around 70mbar, it can be seen that the pressure in the manifold stabilises to the target, but the pressure vessel is consistently too low.

The modified manifold response Figure 114) to very fast pressure switching commands (2 seconds) is excellent: the sensor in the manifold meets the target within 2-3 seconds but the pressure vessel sensor is consistently up to 5mbar lower. The issue is not one of latency but pressure loss, possibly due to a leak in one of the many connections in the gas path.

4.4.4.2 *Long term stability over 10 hours*

To test stability, the manifold was subjected to two more tests. Firstly, the manifold was commanded to provide an output pressure of 70mbar into a pressure vessel with pressure loop but not flow loop feedback, for 10 hours. The logged pressure was on average 70.0mbar with a standard deviation of 0.07mbar.

Secondly, two manifolds were placed in opposition, as for the QVP experiment (Figure 105), with the backpressure set at 70mbar and flow PID control commanding a fixed 20nL/s flow rate. Over 10 hours, the average flow rate was 19.99nL/s with a standard deviation of 0.078nL/s.

4.4.4.3 *Summary of the new manifold performance*

The latency is currently slower than strictly required but can be rendered even faster with better PID response through the LabVIEW code, or by increasing the manifold orifice size to allow faster throughput of air in the valves. Here the object was to minimise overshoot and oscillation, which occurred at the expense of swift transition. Different code architecture such as gain scheduling may be necessary since a latency-critical application is the object.

The stability of the system is well within the desired parameters of 1nL/s precision.

4.4.5 Integrating the pressure vessel into the manifold

Based on prior behaviour it is evident that the pressure being directly controlled by the flatprop valves is different (higher) to that being measured at the vessel itself, which is a larger volume than the sensor space between the valves. Integrating the pressure vessel into the manifold (Figure 115) would be desirable both for tighter control of the system and for the ability to modularise the system into several manifolds run from one input. The dimensions of the machined manifold are in appendix 10.4.11.

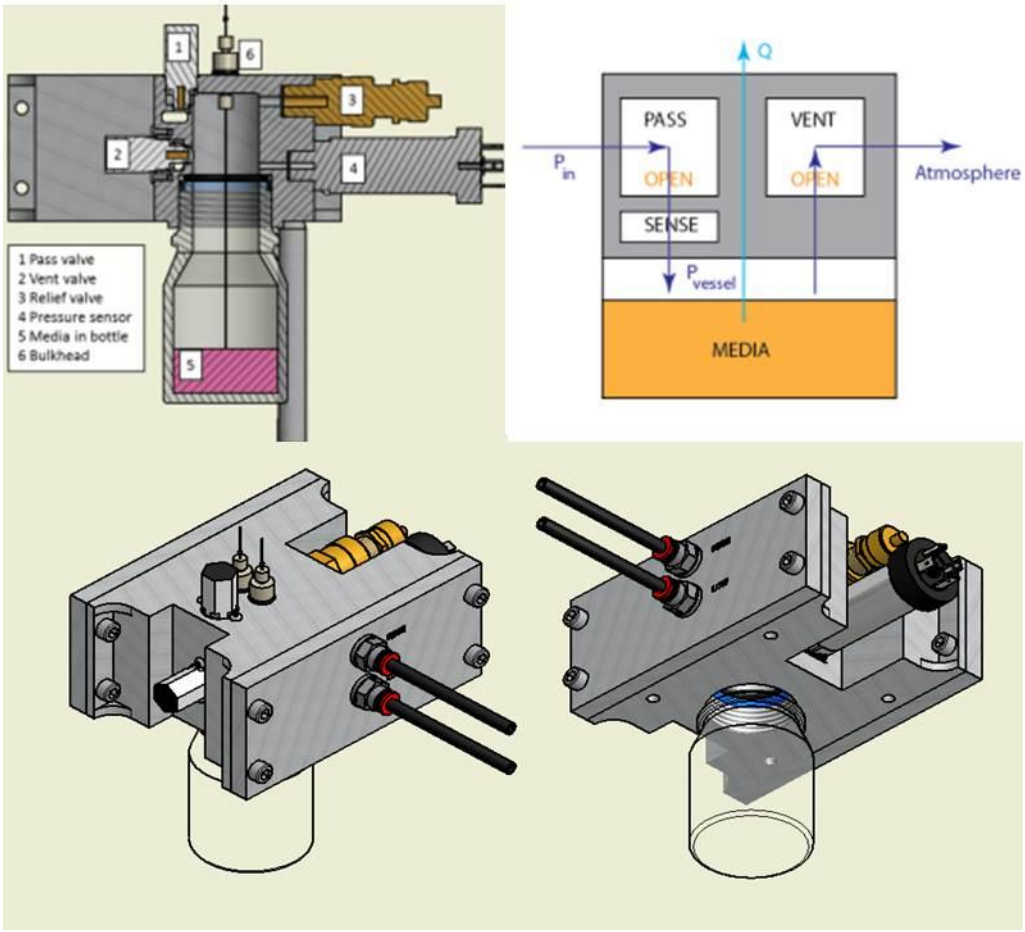

Figure 115 Cross-section of the integrated manifold / pressure vessel (left), and how it functions (right). The pressure P_{sense} is now the same as P_{vessel}. Multiple pumps are shown in Figure 122).

Multiple media outlets are also possible by having 2 bulkheads run from the same pressure vessel. This capacity is later put to use in chapter 6.5.8.

4.4.5.1 *Latency Flow and pressure with integrated pressure vessel*

Open loop flow control (pressure PID)

To compare the performance of the integrated system, the same command sequence is used (Figure 116) as for the previous manifold (Figure 114), only assessing pressure response at this stage.

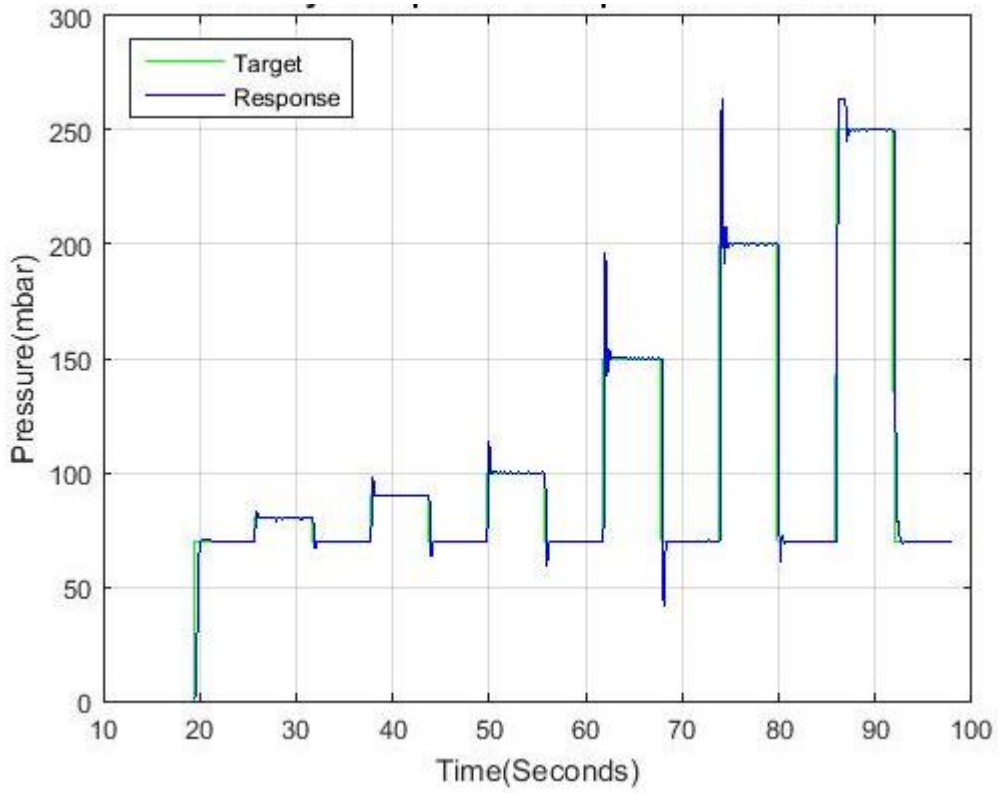

Figure 116 Pressure control of the system. Target levels 70, 80,70,90,100,70,150,70,200,70,250,70 mbar, held for 5 seconds at each level.

Although there is still some overshoot, it can be seen (that the commanded pressure does not consistently drop under the 70mbar threshold as the previous system did (Figure 117), since the pressure of the sensor and the vessel are equal.

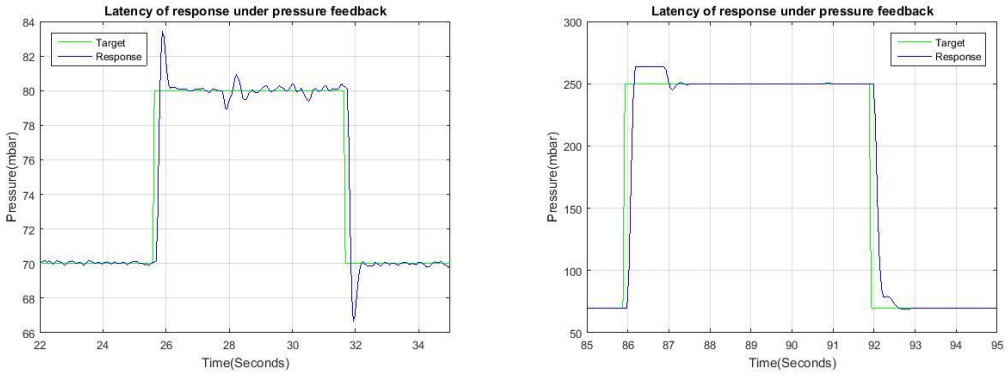

Figure 117 Pressure latency at low level switch (10mbar, left) and high level (right, 180mbar). In both cases the response is very prompt (<1 second), but the overshoot become more significant as the required level shift increases. Note that the sensor cannot read higher than 263mbar, hence the truncated overshoot for the 250mbar target.

Flow control PID

Now the flow rate control loop is used to directly control the flow rate (Figure 118) with different PID settings.

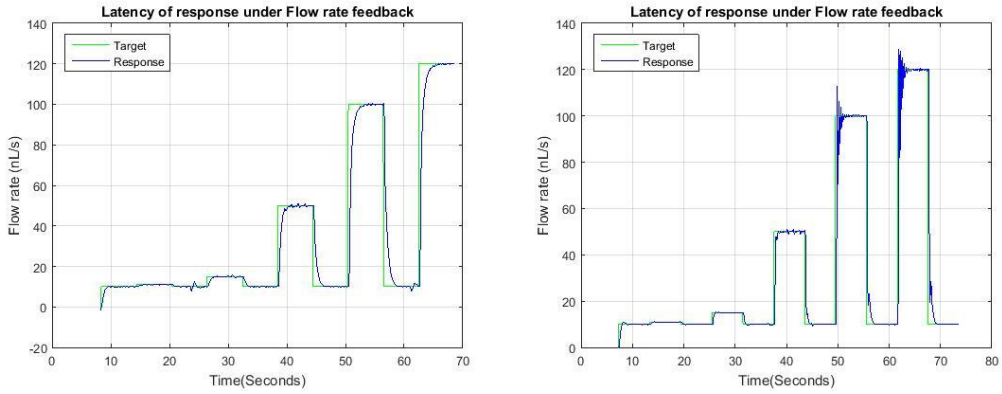

Figure 118 Flow control of the system with 2 different PID settings. The flow now consistently follows the target value with very fast response and short settling time. Target levels 10,11,10,15,10,50,10,100,10,120 nL/s, 5 seconds at each level

It can be seen now that the system is capable of very rapid (less than 2 seconds) latency, but that this comes at the expense of overshoot. Alternatively, if the latency can be tolerated up to 5 seconds, there is no overshoot. Gain scheduling, where the flow PID settings can be altered depending on whether rapid response or stability is preferred, could be used in future to ensure optimal performance both I steady state and switching operations.

The pressure response of the system now retains the latency of the previous version, but with an accurate pressure reading since there is no loss between sensor and media reservoir.

4.4.5.2 *Pressure and Flow Stability over 1 hour*

Finally the longer term stability of the integrated manifolds is recorded (Figure 119) for 1 hour, with standard deviations within 0.16mbar and 0.351 nL/s respectively.

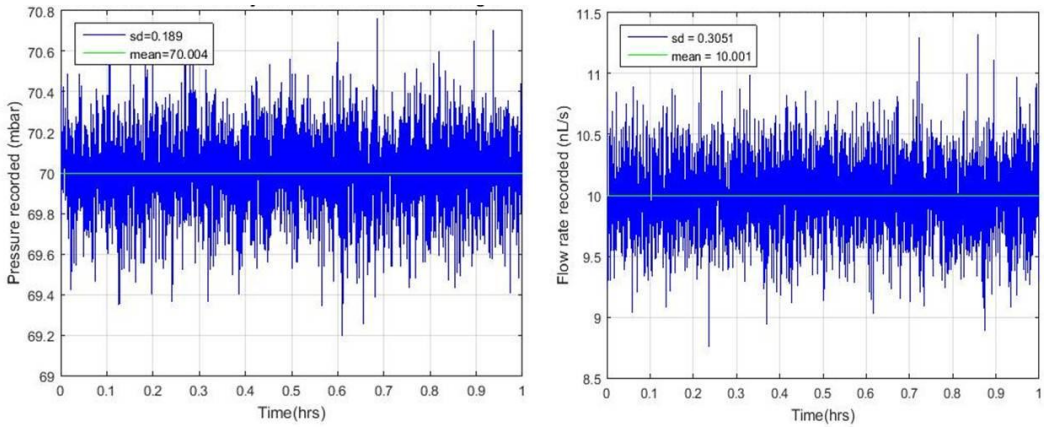

Figure 119 Stability measured Pressure (70mbar) and flow rate stability (10nL/s) over 1 hour.

4.4.5.3 *Pressure stability over 10 Hours*

One last test of long term stability is for the pressure control, since this was a major problem for the original gas perfusion system. As can be seen (Figure 120), it is now highly precise over long periods.

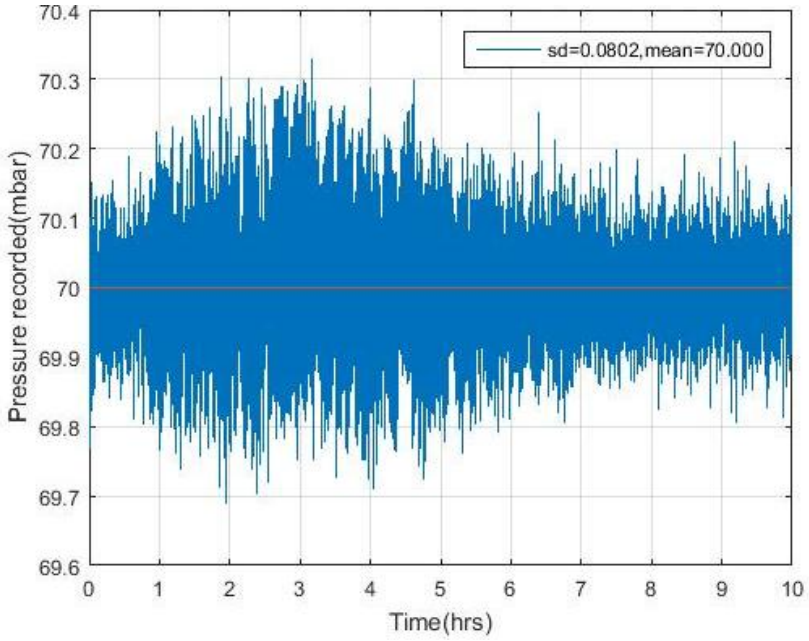

Figure 120 Pressure stability is within 0.4mbar and stabilises to within 0.3mbar after the first 4-5 hours.

The stability of the system is a significant improvement upon the commercial regulator (standard deviation 0.28mbar).

4.4.5.4 *Final system Specifications*

The final version of the perfusion system developed is compared to the original specifications in Table 10 below).

Parameter (unit)	Typical	Standard deviation	Target metric
Latency (s)	<1.5		<1
Stability (nL/s)		0.3051	1
Range (nL/s)	0-100		0-100
Parameter (pressure)	Typical	Standard deviation	Target metric
Latency (s)	<0.5		<1
Stability (mbar)		0.08	0.5
Range (mbar)	0-250		0-250

Table 10 Final specifications of the perfusion system and comparison to requirements

This version of the system has been utilised to wash Carbachol on and off a primary neuronal culture in under seconds, demonstrating the capacity of the system to provide prompt delivery of agonists. This was presented at the 18th International Conference on Minituarized Systems for Chemistry and Life Sciences (Herzog et al. 2014).

4.4.6 Successful alternative application of the system

An alternative use of the developed perfusion system was to make use of the stability and accuracy of the system to implement a slow, incremental change in the interface position (see Figure 121), rather than an abrupt switch as has been the goal for neuromodulator delivery.

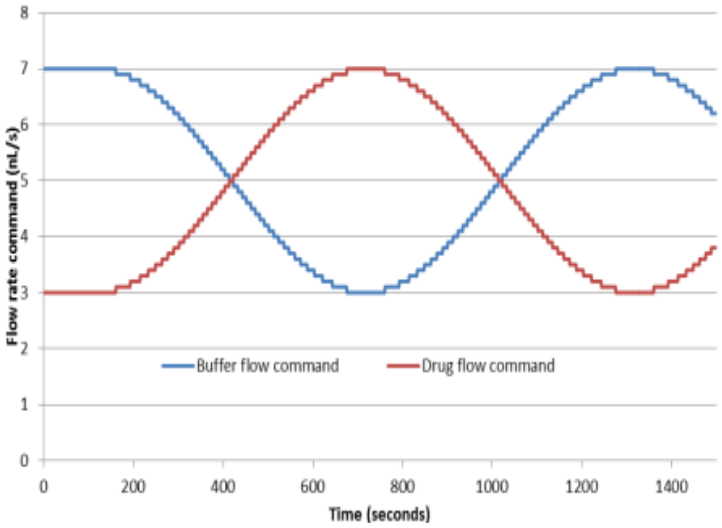

Figure 121 A varying command profile which swaps the drug and buffer flow rates over 25 minutes instead of under 1 second.

In an application that did not require the rapid response conditions required for reinforcing primary neuronal cells, the system was used in a 3 pump

configuration (see Figure 122) by Dr Tomas Bellamy and Dr Wayne Croft.

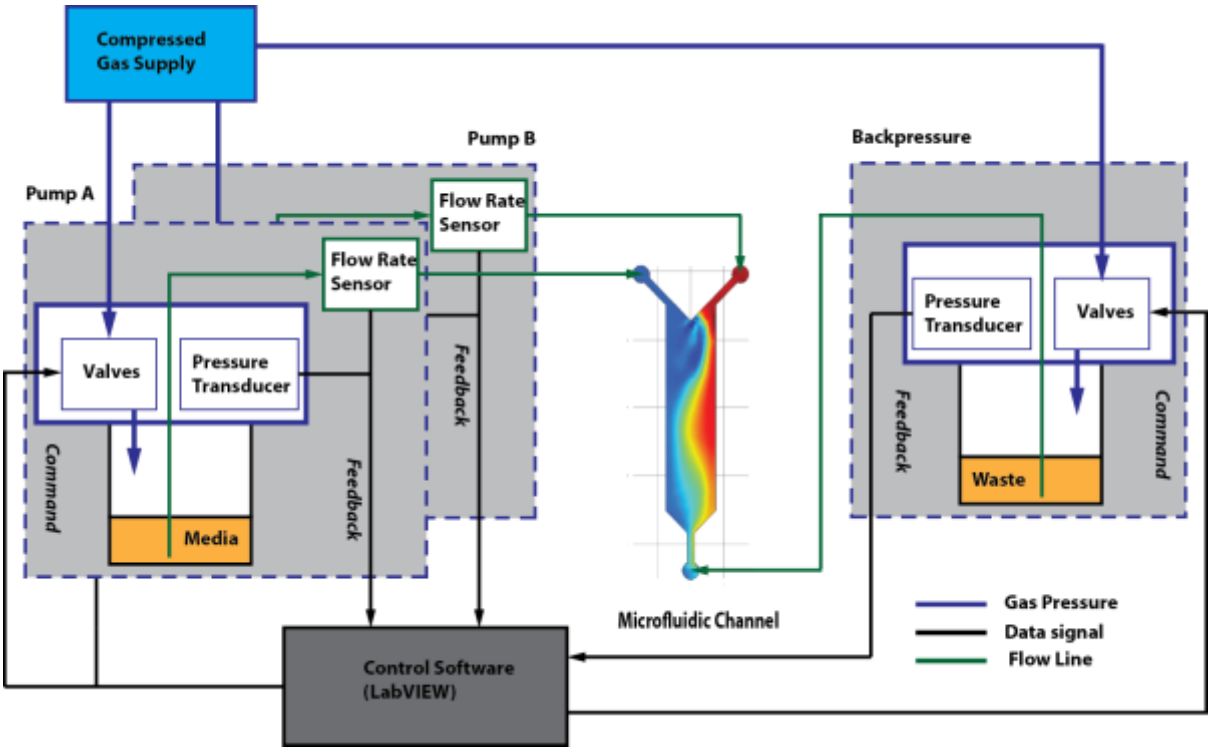

Figure 122 The full 3 manifold system, used to direct a gradient of Carbachol over HEK cells

A slow-switching sine wave over many hundreds of seconds was implemented, to periodically wash Carbachol over HEK and astrocyte cells cultured in microfluidic channels. The channels were assembled using the SU-8 moulding and stamp: stick methods described previously, and were fabricated by Mrs Marleen Groenen.

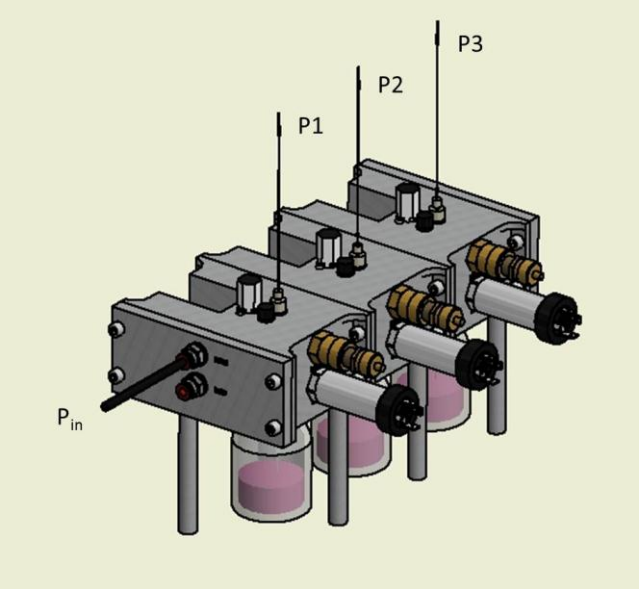

Figure 123 A 3D rendering of the pump system used, and the previous schematic. Each manifold is of the design shown in Figure 115.

The aim of this project was to investigate how populations of astrocytes encode information about time-varying stimuli in their environment, via calcium signalling. The calcium response of the cells to the Carbachol wave front crossing the channel was compared to the known actual flow rate profile (Figure 124). It was found that although individual cells could not respond with the temporal precision needed to encode the concentration change, the population of heterogeneous response did encode it very accurately, and this lead to speculation about the role of ensemble coding in calcium signalling networks (Croft et al. currently in press).

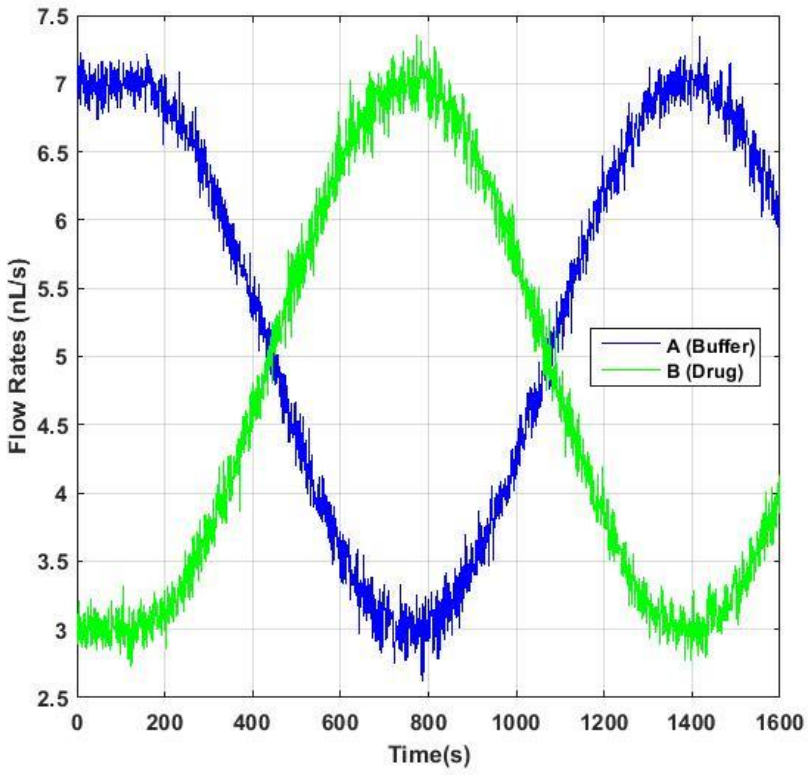

Figure 124 the logged flow rate values for Pumps A and B, summing to 10nL/s over the course of 1600 seconds (26 minutes).

The fidelity of the logged flow rates (Figure 124) compared to the command profile (Figure 121) was essential if the calcium response was to be meaningfully compared to the concentration profile predicted by COMSOL (see Figure 125).

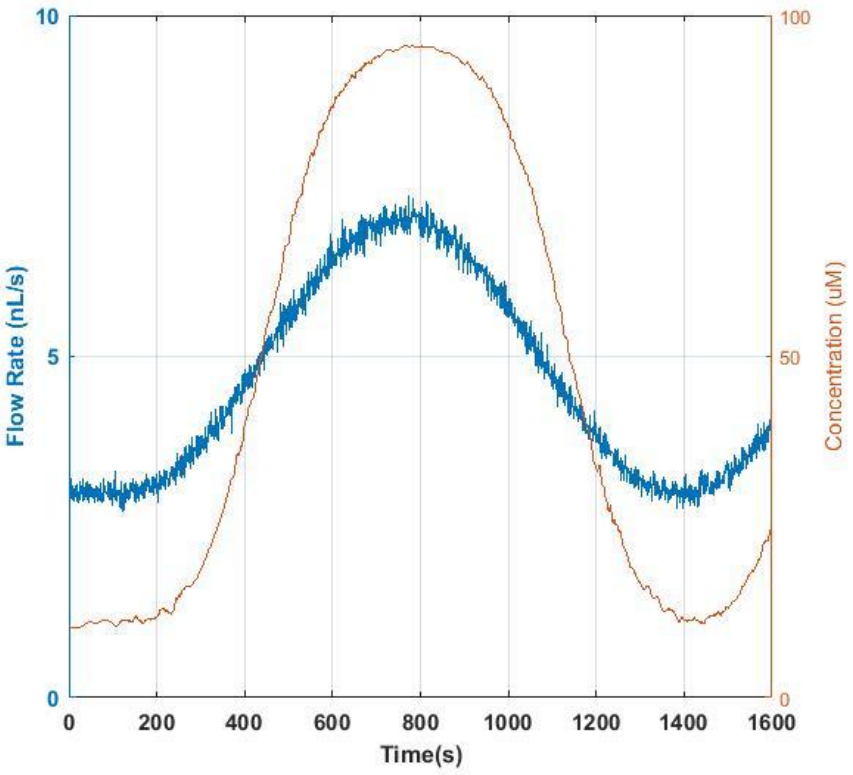

Figure 125 The modelled change in concentration over a point in the centre of the microfluidic channel, as the agonist flow rate slowly varies.

Because the aim for this work is to investigate the response to a slowly changing concentration, diffusion needed to be more significant in the channel compared to the Péclet regimes covered in chapter 3 (Pe = 50 to 200). Here, given the channel dimensions are identical but the flow rate is only 10nL/s (velocity = 66.7µm/s), the experiments were carried out in a Péclet regime of 20.8.

4.5 **Temperature clamp**

In order to secure the PDMS: glass microchannels when perfusing on coverslips rather than MEAs, a custom clamp system was constructed (see Figure 126 below). This clamp is designed to fit to a microscope, in place of a standard 60mm coverslip holder.

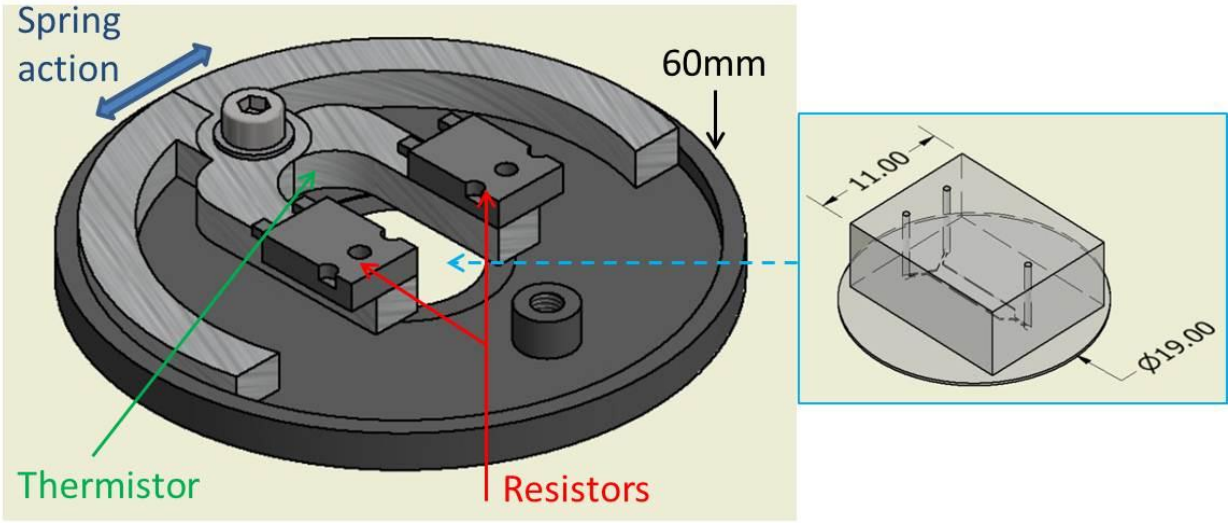

Figure 126 Schematic of the spring loaded clamp / temperature regulator. Wire spring under the arms and the thermistor are not shown here. Full dimensions are in appendices. See also chapter 7.1.4.5 for an image of the manufacture clamp after fabrication

While out of the incubator it is necessary to maintain the temperature of the cells in the microfluidic channel. The MEAs used elsewhere are heated from above and below, but this is impractical here since imaging will be done from below and perfusion tubing inserted from above. Consequently a system that grips the PDMS block on either side and imparts heat to it has been designed and built (see Appendix 10.4.4).

This design is simpler to use, which reduces the time spent integrating the channel into the perfusion system. This is critical, as an extended period without temperature and perfusion control will be detrimental to cell survival. In addition, the clamp should not damage the channel device.

The clamp consists of two thermally conductive aluminium arms, which naturally spring shut about a pillar due to a stiff wire inserted into a groove under the arms. This resists when the arms are pulled apart and acts to close them. The pillar and base plate are machined in black Delrin, which is mechanically durable and thermally insulating. A central hole permits imaging and illumination through the microfluidic device.

A 5Ω 15W TO-126 thick film resistor is thermally bonded to each of the metal arms (10Ω total), together with a single NJ28 NTC 10KΩ 1% thermistor. These interface with the temperature controller (Warner Instruments TC-

234B); the resistors heat up as current is supplied and the thermistor provides temperature feedback.

4.6 Chapter Conclusion

A gas-driven perfusion system, with pressure and flow rate feedback informing electro-pneumatic valves has been developed, comprising three pressure driven pumps. This provides real-time control of two flow rates for agonist and buffer, and a constant opposing backpressure to prevent bubble formation. All sensor elements and valves are monitored and controlled with a LabVIEW control program using PID feedback algorithms.

This system has the capacity to switch the ratio of laminar co-flows with high temporal precision. The flow rates can be adjusted by 100nL/s in less than 1 second, while the stability of the system when not switching is under 0.3nL/s.

To ensure the microchannel is maintained at the correct temperature, a spring-loaded clamp which heated the PDMS chip has been designed. This clamp can be placed at the sample plane of a microscope. Soluble gases are delivered within the media at 5% CO_2, to ensure CO_2 and pH levels are physiologically appropriate.

5 Confinement of culture extent

Previous chapters have demonstrated the capacity to fabricate microchannels capable of supporting neural cells indefinitely *in vitro* in the absence of perfusion, and a perfusion system has been developed capable of providing the flow switching spatiotemporal precision and stability necessary for the desired neuromodulator delivery profiles.

As was previously discussed, it is necessary to implement a spatial constraint on the network such that it occupies a relatively small region, while maintaining the plating density found optimal in planar channels (Figure 127). Without this limitation, it is not possible to capture or influence the entire network, electrically or pharmacologically.

Ultimately, culture area is constrained by extent of stimulation (electrical) and speed of global reinforcement (chemical).

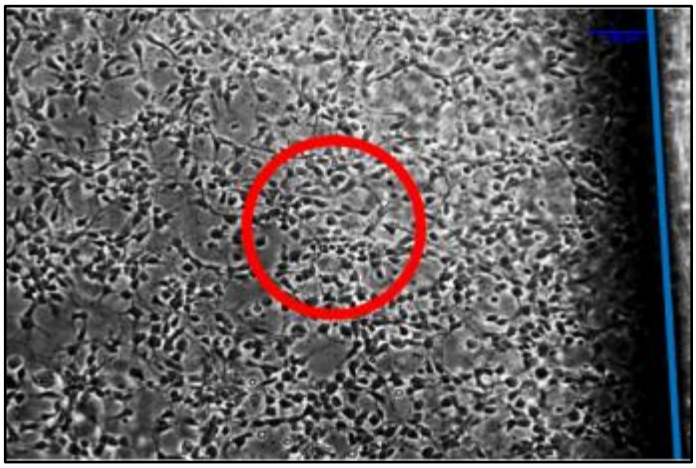

Figure 127 A confluent culture grown on PLL in a millimetric channel (boundary highlighted in blue). The plating density is correct, but the culture extends throughout the entire channel. It is necessary to have the cells constrained to a smaller region within the channel (red example) while keeping the same plating density. Scale bar (top right) is 200µm.

This is needed for the following reasons:

i) *Drug delivery*: In order for global neuromodulator delivery without lag between different parts of the network, the culture should only

occupy a small region. This region should be as close to the delivery inlets as is practical.

ii) *Plating density:* As has been seen previously, a low plating density does not lead to optimal culture development. Consequently although the culture region should be small, the number of cells in the region per mm^2 will need to be high, around $500/mm^2$.

iii) *Sensing imaging:* Whatever method of electro-optical detection is employed, it will have a finite region of effect. This is also true for the imaging optics employed for recording. Therefore the culture extent must be limited, so that data is not lost.

iv) *Stimulation:* Again, the stimulation method, whether electrical or optical, will work only within a small area, and if cells are able to migrate outside that region then they are no longer part of a deterministic feedback loop.

This chapter covers methods used to implement the confinement of culture into a single region for long term cell culture, and the adoption of an optimal method.

5.1.1 **Methods**

As discussed in the first chapter, it is simpler to use chemical pattering rather than topography to create the confinement region. Hence the first approach involved a patterned ligand where cells could grow, surrounded by a region where there was no ligand.

5.1.1.1 ***Metal Patterned surfaces***

It has been noted (Kleinfeld 1988) that patterned boundaries in a saline environment tend to lose their distinction over time – often within a few days (Kwiat et al. 2012). It is preferred, therefore, if relying solely upon chemical heterogeneity to impose a boundary, to use ligands which form strong covalent bonds with the substrate, namely *silanes* (if adhering to glass) or *thiols* (if adhering to gold). Silanes as ligands have not been used in previous chapters, and this represents a change in environment that would need to be tested independently. The thiol AUT has been tested, however, and found to work even in a bonded microchannel, so long as the density is sufficiently high. Moreover, it is advantageous to make use of a metal: glass distinction

since such a geometry will certainly exist in the final device in the form of sensors or stimulating electrodes. It is therefore efficient to utilise this by using a ligand which will bond only to the gold and leaving no attachment points on the glass outside the intended culture extent. If using gold, the AUT will not bond to the glass, but a silane such as fluorosilane may be necessary to prevent eventual cell growth on the gold.

A crude gold pattern on glass was formed from a low-resolution ink and acetate photomask (see appendix 10.4.7). The gold pattern was then was created by photolithographic patterning and evaporation, followed by AUT deposition (see methods 2.3.4 and Figure 128) as was previously done in section 3.5.4.2, except that the gold extent is reduced so that only part of the channel is functionalised. A better resolution chrome photomask was later designed for Surface Plasmon Resonance work (see chapter 7.2).

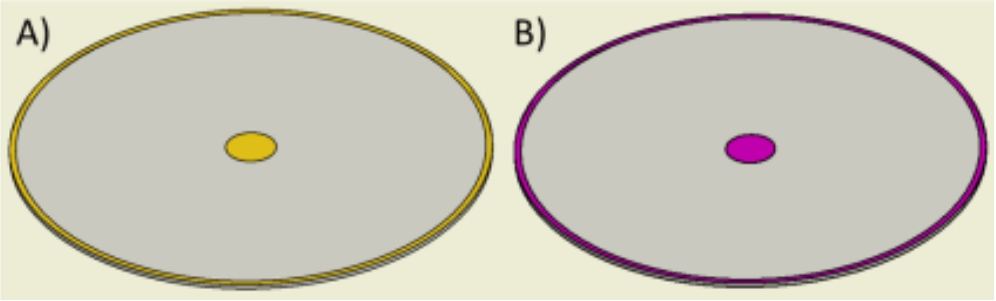

Figure 128 AUT deposition on a limited gold region without ligand on glass. The BPRS method and AUT methods were used. Coverslips were removed from the AUT solution, rinsed and dried on the day of the cell plating, in order to minimise the time the AUT ligand would be exposed to air.

This tests i) If the photoresists and developers have rendered the surface cytotoxic and ii) how effective the glass alone is at preventing adhesion, without a cytophobic / anti-fouling ligand such as fluorosilane.

It is preferable not to require such a ligand since it will be extremely difficult to integrate such a surface with any subsequent channel bonding: the presence of the silane will preclude plasma bonding altogether, and is expected to prevent robust adhesion if using the pre-polymer or tape adhesion methods. The Perfluorodecyltrichlorosilane (PTFDS) available could be laid down in an

anhydrous solvent such as IPA or Toluene, which would seriously affect the PDMS bulk and bond.

In addition (Figure 129) the gold and AUT pattern was integrated with a microfluidic channel using the shielded plasma bond technique. This was done prior to the adoption of tape channel fabrication, but given the results that follow it was deemed unnecessary to repeat the experiment with a tape channel.

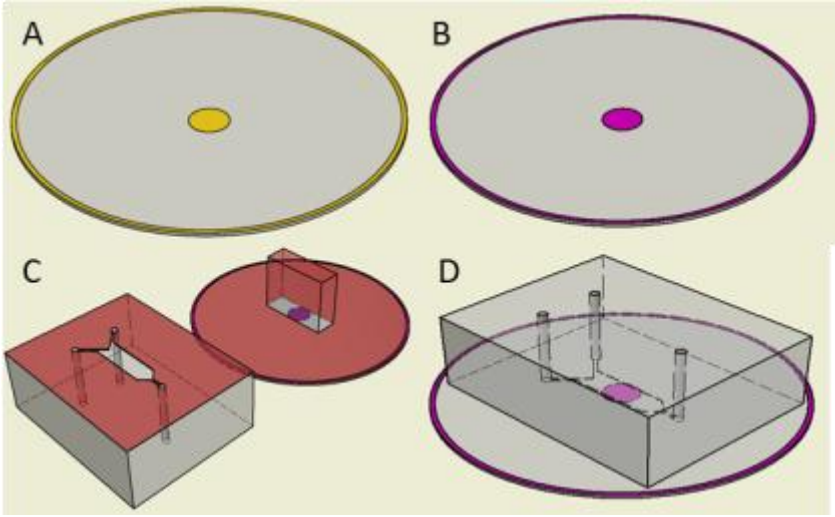

Figure 129 Plasma cleaned gold A) is functionalised with AUT as described B). The coverslip is then bonded to a PDMS channel. If plasma bonding is used C) then the AUT must be shielded during the plasma activation, typically with a block of PDMS over the area to be preserved. Once bonded D), AUT will only be on the gold surface.

5.1.2 Cells growing on patterned gold and AUT without a channel

The pattern is a gold region of roughly 500µm x 500µm, formed using the BPRS photoresist and gold evaporation methods described, and a crude ink: acetate mask with limited edge resolution (see appendix 10.4.6). A titanium adhesion layer was used to be certain the small gold region would definitely remain during photoresist lift-off. AUT was deposited onto the coverslip, and should have adhered only to the gold.

A droplet of 500µL cell suspension at density 150 cells/µL was deposited onto the gold region so that cells dropped onto both gold and glass.

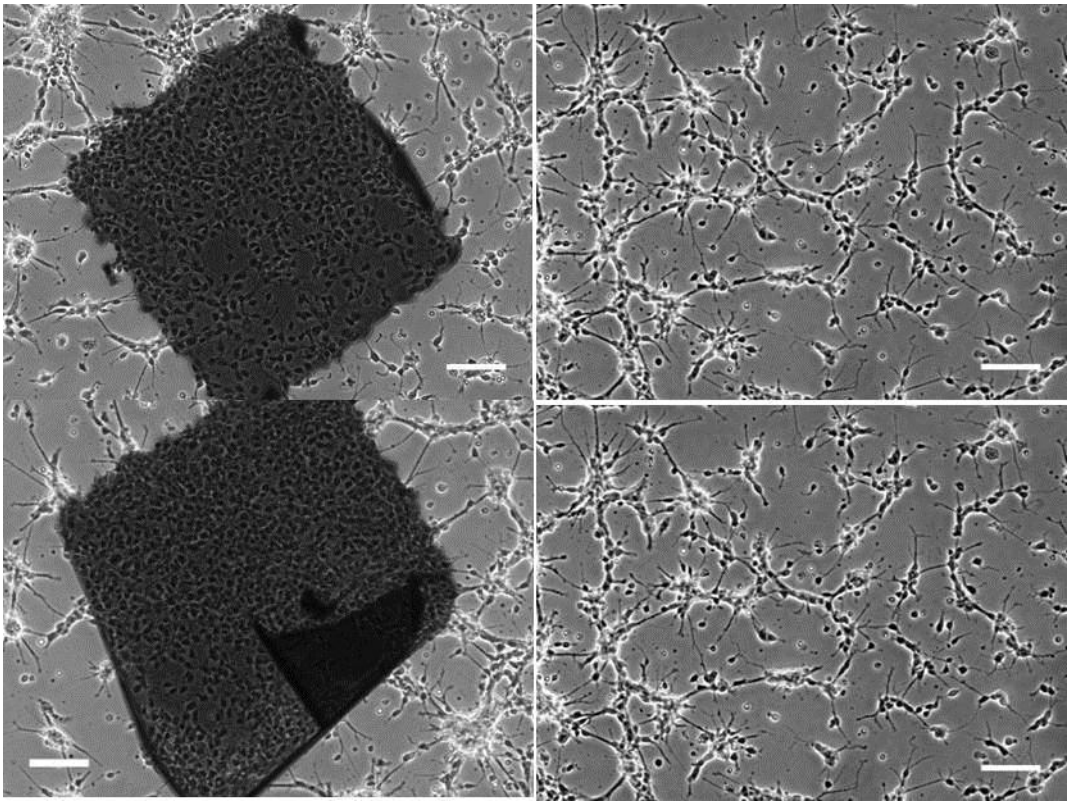

Figure 130 Gold spots on glass were plated at 150/µL. At 1 div, Top left and right on the same coverslip, bottom left and right on a different coverslip. Cells grow normally on the gold but have heavily fasciculated on adjacent glass regions. Scale bar 100µm.

At 1 div on the gold area (Figure 130), cells grow as expected, except that the density appears higher, while on the glass the adhesion is poor, comparable to the negative control surface.

It is important to note that where the cells have landed on glass they cannot be cleared from the surface without jeopardising the adhesion of the cells on gold. This would also be a serious issue in a microchannel, where the shear forces induced during the flushing out of unattached cells will be very significant.

At 7 div, the gold and glass region were compared to control surfaces of PLL on glass and AUT on gold, where plating density was around 300/mm^2.

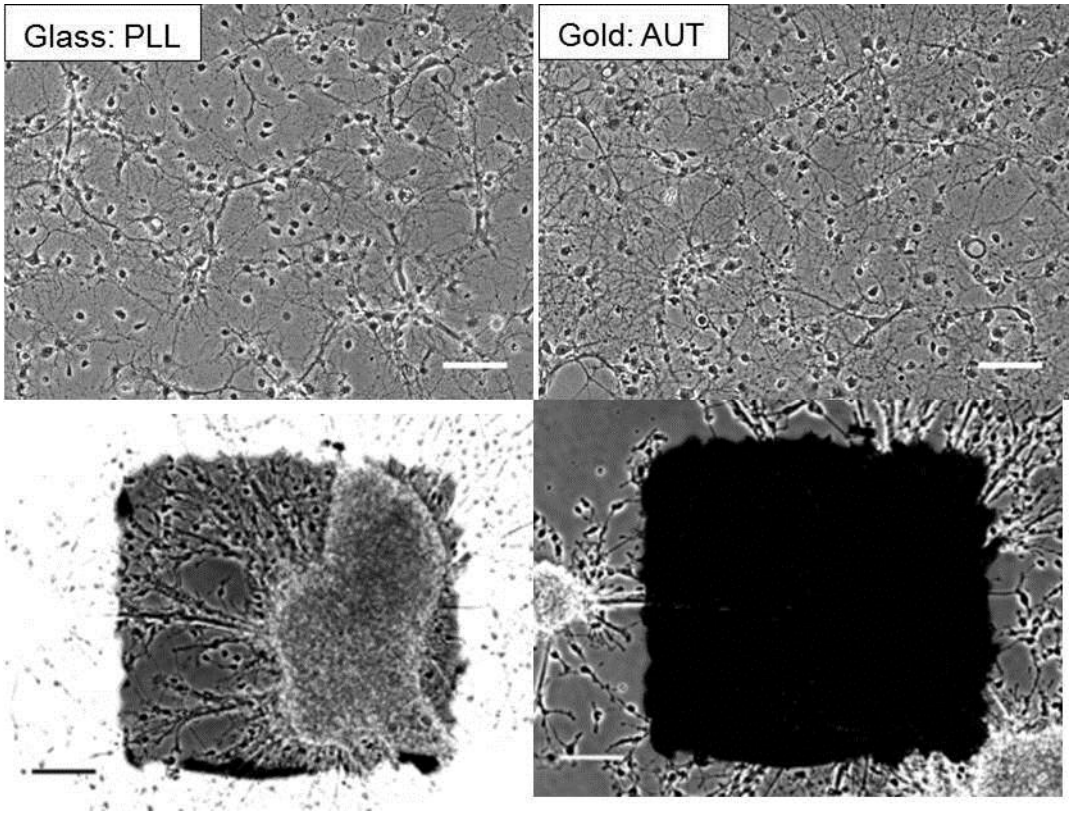

Figure 131 Top: Cells were suspended at the usual plating density, onto a 500µm crude Gold-on-Titanium shape functionalised with AUT. The darker region at the edges of the shape is the underlying titanium. At 1 div, cells grow healthily on the gold and fasciculate badly on the glass. By 7 div (bottom), the gold is very densely populated, and the cells are beginning to migrate out across the glass, though the network on both gold and glass is strongly fasciculated. Scale bars are 100 µm.

After 7 div (Figure 131), the cells have migrated en masse onto the gold region, forming a very confluent 3-dimensional network which is so dense that cells can no longer be discriminated in the image, and have survived long enough to presumably begin producing their own extracellular matrix on the glass region, which was not possible previously where there was no gold area to sustain part of the culture.

The highly dense network is not desirable as this means there is a considerable percentage of cells that cannot be directly monitored or stimulated. A planar 2 dimensional culture is necessary.

5.1.3 Combining the patterning step with a microfluidic channel

5.1.3.1 *Gold patterns in channels*

Microchannels were bonded over the gold spot using the deposition-then-bond method, with the gold: AUT region protected during plasma activation. Initially a lower plating density was used to see if the cell migration effect observed in section 5.1.2 could be used to reach a critical density on the gold, without any subsequent colonisation of the glass region, or the formation of a highly confluent 3D culture.

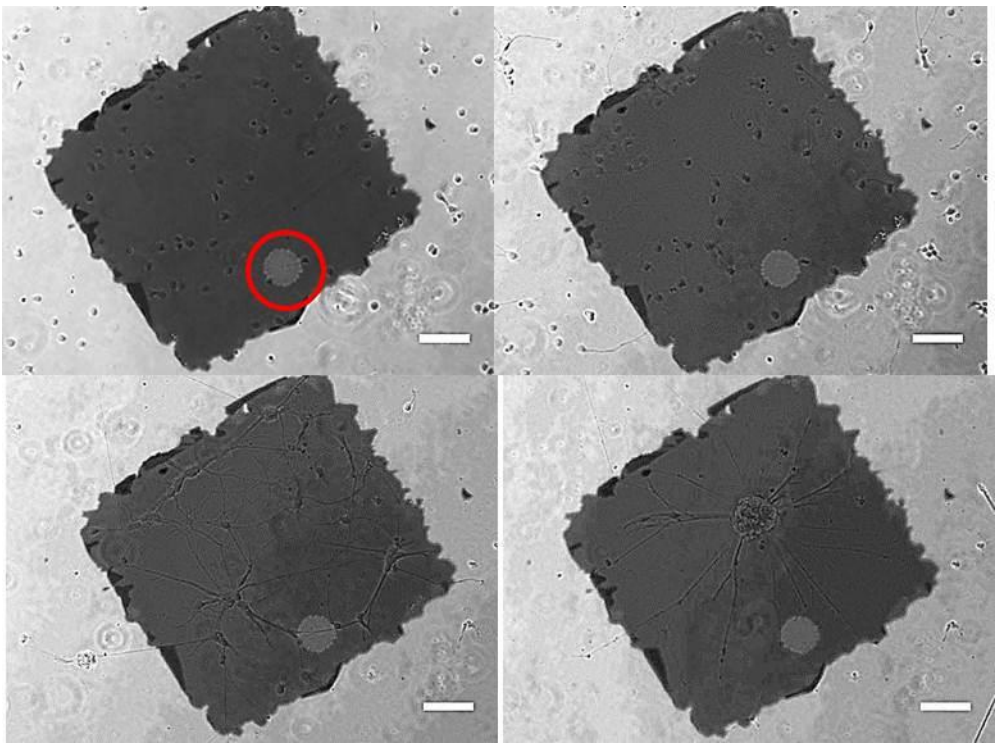

Figure 132 Cell suspension (300/µL) was injected into a bonded channel. Images were taken at 1, 2, 6, and 10 div. The reduction of plating density and extent has a clear effect. Scale bar is 100µm. Note the pale circle (highlighted red at top left). This was visible after the metal deposition and appears to be a substrate defect, rather than a biological growth.

The injection of cell suspension into a channel does not guarantee its deposition where needed. Although there is a large area of gold available for growth, only a small percentage will land on or near it (see Figure 132 above, where the cell suspension density (300/µL) is twice that used to seed a confluent culture (Figure 130) but the final plating density is much lower, with very few cells on the gold region.

Subsequently the remaining vast majority will die in situ, or may be flushed with the risk of removing the few cells that have landed on the gold. This last

would be a problem irrespective of the average plating density in the microchannel. Therefore further experiments with high volumetric density to achieve a plating density of over 500/mm^2 throughout the channel were not carried out.

In conclusion, it is determined that surface patterning can represent a precise method of constraining cell culture growth, but it is difficult to combine with channel fabrication, and it does not solve the issue of ensuring high plating density over the region of interest. Furthermore it will offer no mitigation of shear stress in the channel if necessary.

5.2 **Concept Microwell**

From the previous results it is necessary to plate the entire area at the same density, and then flush away all cells that are not in the region of interest. This requires a region of reduced flow rate with respect to the rest of the channel, so that cells can remain adhered while the flushing is carried out. A microwell is therefore needed (see Figure 133 below). The microwell is formed by adding another layer (denoted C in the figure). This layer has a gap (B in the figure) which aligns with the existing microchannel.

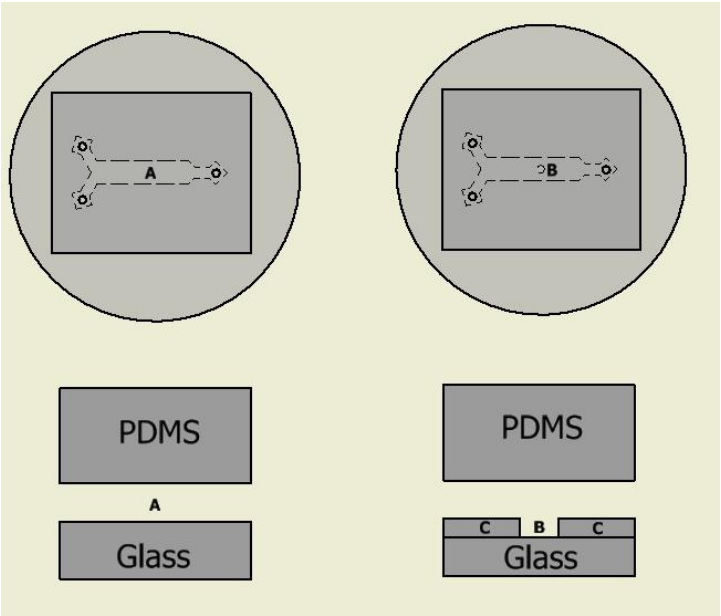

Figure 133 The existing microchannel A (left of figure) is altered by having an additional hollow space B (right of figure) incorporated into the design. The well is created by adding another layer C which bonds to glass below and the microchannel layer above.

This essentially effects cell confinement by creating a physical barrier the cell cannot surmount. As motile cells are perfectly capable of escaping a barrier of a few µm in height (Claverol-Tinturé et al. 2005), the height and extent of the barrier will need to be considerable, and the walls of the barrier should not be amenable to ligand deposition. Consequently this approach must be planned in conjunction with ligand deposition, taking care that the fabrication or attachment method of the various layers is not incompatible with depositing and protecting the ligand.

This method by necessity will create an additional distance for drug molecule to travel (the height of the well). In addition, it requires careful integration with surface deposition.

5.2.1 **Microwells Methods**

Microwells can be fabricated in several ways, but must ultimately be readily:

i) Bonded with precise alignment to the drug delivery and cell loading layers above

ii) Not counteract the chemical confinement, so no adhesion outside the well area, and optimal or acceptable adhesion inside the well.

5.2.1.1 ***SU-8 features:***

These were initially tested as an open coverslip with hard-baked wells <10um deep. The devices were thoroughly baked at 150°C for 30 minutes to remove all traces of the solvents originally present in the photoresist. This represents a logistical difficulty since bonding SU-8 to PDMS would be impossible with the usual oxygen plasma method. SU-8 does not readily bond to PDMS, though it can be done with Nitrogen plasma (Zhang et al. 2011). This is a longer plasma process (up to 5 minutes) and requires very pure (>99.9995%) nitrogen, so is more prone to oxygen contamination. The nitrogen activation produces amino rather than silane groups to form on the PDMS surface, and these are more stable, lasting many days. The amino groups can then bond to uncured epoxy groups in the SU-8. This is functionally similar to the bonding methods considered in chapter 6, where different materials are treated with amino and epoxy silanes (Tang & Lee 2010).

Potential issues are that the SU-8 may not be as mechanically robust as it has not been as thoroughly heat-treated, so that media immersion could cause breakdown of the material. In addition, if the device is heated past the temperature range quoted for this process (<110°C) then the epoxy may react, damaging the device and perhaps rendering it cytotoxic. Sterilisation of glass prior to cell plating is typically done at 160°C so this would have to be revised.

5.2.1.2 *PDMS Fabrication of microwells*

5.2.1.3 *Fabrication of thin PDMS films*

A spin-coater (SPS Europe Spin 150) was used to spread uniform thin films of PDMS on a silicon: SU-8 substrate. The relationship between film thickness, RPM and spin duration is assumed to be

$$\boldsymbol{H = k.\omega^{\alpha}} \qquad \textbf{[19]}$$

based on (Koschwanez et al. 2009), where H is the PDMS film thickness in μm, and ω is the spinner speed in rpm, for a given run time (in this case 30 seconds).

The thin PDMS film thicknesses were measured with a contact profilometer, averaging over 3 attempts at each spin program (see Table 11).

Spin ω (RPM)	Measured H (μm)	Average $\bar{H}$ (μm)
1000	63, 70, 66	66
1500	44, 41, 41	42
2000	25, 22, 25	24

Table 11 Measured PDMS film heights for 3 spin programs lasting 30 seconds

Taking the natural logarithm of all terms in the equation transforms the relationship to a linear equation:

$$\boldsymbol{\ln H = \ln k + \alpha \ln \omega} \qquad \textbf{[20]}$$

Constants k and α can thus be inferred from a least squares regression:

If $\ln \omega$ is denoted X and $\ln \bar{H}$ is denoted Y then

$$\boldsymbol{\bar{Y} = \alpha.\bar{X} + k} \qquad \textbf{[21]}$$

and

$$\alpha = \frac{\sum XY - (\frac{1}{n})\sum X \sum Y}{\sum X^2 - (\frac{1}{n})(\sum X)^2} \qquad [22]$$

which for the measured values gives the coefficients (see appendix 10.3), α = -1.366 and $\ln k$ = 13.63.

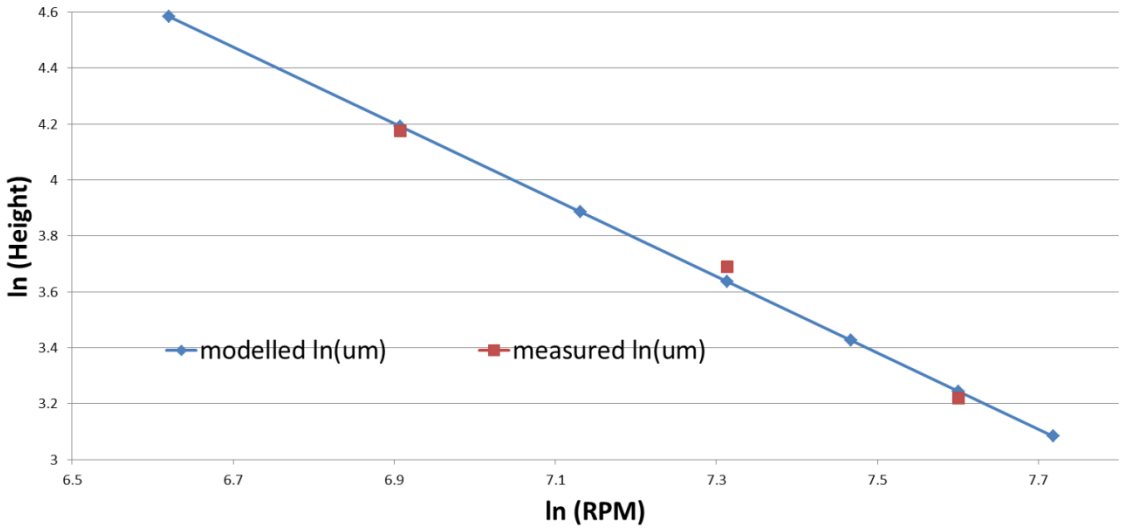

Figure 134 Fitting the regression line, logarithmic values of a range of PDMS film heights can be inferred based on the logarithmic RPM values. Predicted thickness values (blue) are compared to measured values (red).

Fitting the line

$$\ln H = 13.63 - 1.66 \ln \omega \qquad [23]$$

between the limits ω = 750 and 2250 RPM (3.0826 < ln ω < 4.5844) gives a model for all heights between those spin speeds (Figure 134).

Then both logged parameters are returned to linear values. An estimation curve of spin speeds (for 30s) needed to obtain PDMS heights between 20 and 70µm is obtained.

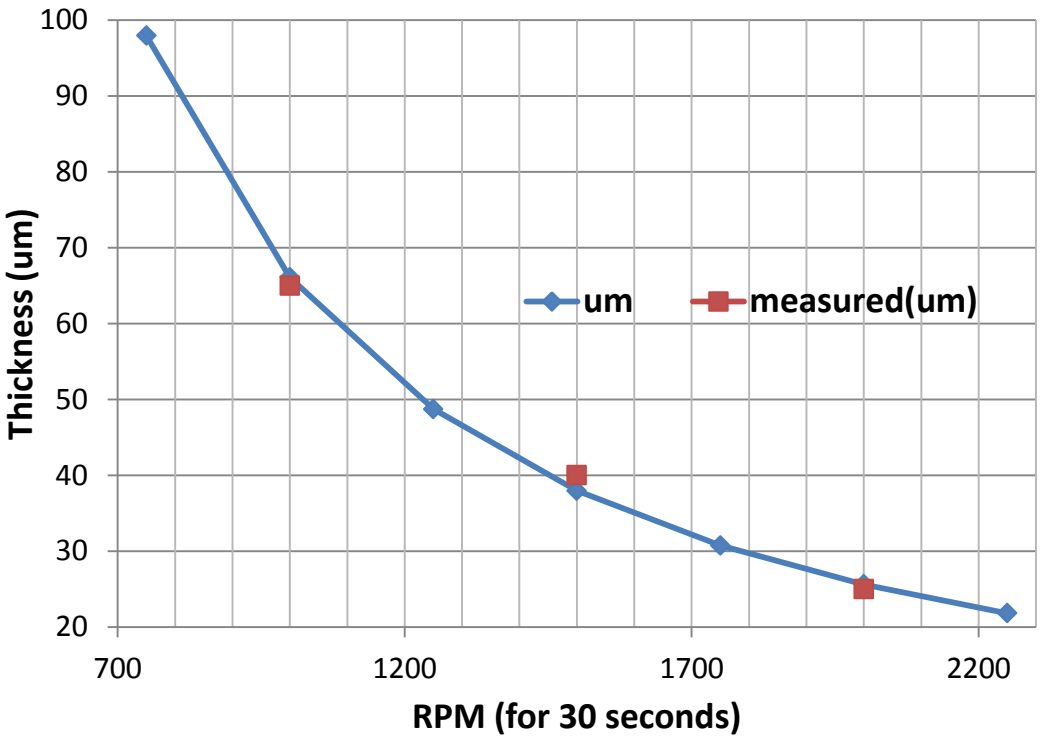

Figure 135 Returning to linear values for both parameters, PDMS thickness values are predicted between 20 and 100µm.

For values higher than 70µm the curve (Figure 135) is extrapolated and may not be as reliable, but the values of interest are in the region of 50µm, for which a spin speed of 1220RPM is predicted.

5.2.1.4 *Assembly of PDMS layers*

The bulk PDMS mould was cast as usual, as for SU-8 microchannels in previous chapters, and the two upper connection ports were punched and cleaned. Following the process of (Kang et al. 2009a), the lower 50µm thick layer was spun at 1220RPM and the SU-8 features freed of overlapping PDMS film by a nitrogen jet at 10kPa through a needle tip (27 gauge, 0.4mm internal diameter). The PDMS was permitted to reflow while the substrate was placed on a level hotplate for 5 minutes, before heating to 100°C for 15 minutes to harden the PDMS film. Trails of thicker PDMS were then laid down several mm from the edges of SU-8 features and similarly heat hardened, so that the PDMS film could be removed and handle by the thicker edges without tearing or crumpling.

Plasma bonding

The bulk layer could be plasma bonded to the lower PDMS film by exposing both surfaces to oxygen plasma as for PDMS as for glass bonding (50W, 0.28mbar, for 30 seconds). The bulk layer was placed surface side up in the field of view of a dissection microscope and the film layer was flipped over so the active surface came into contact with the bulk PDMS. A droplet of methanol was used to defer the bonding while re-alignment was done. The assembled layers were cured in an oven at 60°C for 1 hour, as they could not yet be flipped over and placed on a hotplate.

The two lower connection ports were then punched though both the film and bulk PDMS layers, and cleaned. The PDMS surface and a glass coverslip were then plasma activated as before and brought into contact. As alignment was not as critical for this step, the dissection microscope and methanol were not needed. The complete device was cured on a hotplate at 60°C for 1 hour.

Pre-Polymer bond

This process could be carried out as above, except that the bulk PDMS, and later the assembled PDMS layers, were coated with a spun layer of PDMS pre-polymer instead of plasma activated. Methanol was not used to defer bonding, as realignment was possible by lifting and repositioning the layers. However, as this could introduce air bubbles and smear polymer into the final flow cell space, it was preferable to align as correctly as possible at the start.

Initially the wells required soft lithography of a designed SU-8 feature, and subsequent plasma or polymer fusing of the device. The 40-50 µm thick PDMS films developed were utilised here, with a simple SU-8 feature; a square several hundred microns on a side. These experiments were undertaken in collaboration with Mr Nitzan Herzog, and are designed in part to interface with higher-density MEAs, where 2 networks of densely grouped electrodes (10µm and 30µm pitch, in 6x5 arrays, 500µm apart) are used instead of the larger MEAs encountered previously.

Because of the toxicity issues reported for pre-polymer devices, these wells were not suitable for cell culture, but were used instead to refine the alignment of different well geometries.

5.2.1.5 *The use of silicone tape*

This creates well features with xurography and allows a uniform ligand layer to be deposited on the glass surface, followed by robust bonding of the well layer.

This method in effect is an equivalent solution to the plasma shielding previously mentioned. Because the adhesive tape does not require covalent bonding as the plasma bonding and pre-polymer bonding methods do, it can be placed down onto a PLL layer and will adhere through it.

Experiments by Nitzan Herzog, involving microchannels tape bonded over uniform PLL surfaces and subsequently perfused, implies that 100nL/s flow regimes with 70mbar backpressure do not delaminate or leak even over many hours and rapid pressure shifts.

The resolution of the xerographic cutting system (Silhouette Cameo, Graphtec Inc.) is in theory under 100µm, but this assumes rigid, non-compliant materials such as paper and cardboard. The silicone tape is compliant and can tear or deform much more easily, so that the smallest feature that can be reliably excised is likely to be much larger.

5.2.2 **Microwells results:**

5.2.2.1 ***SU-8:***

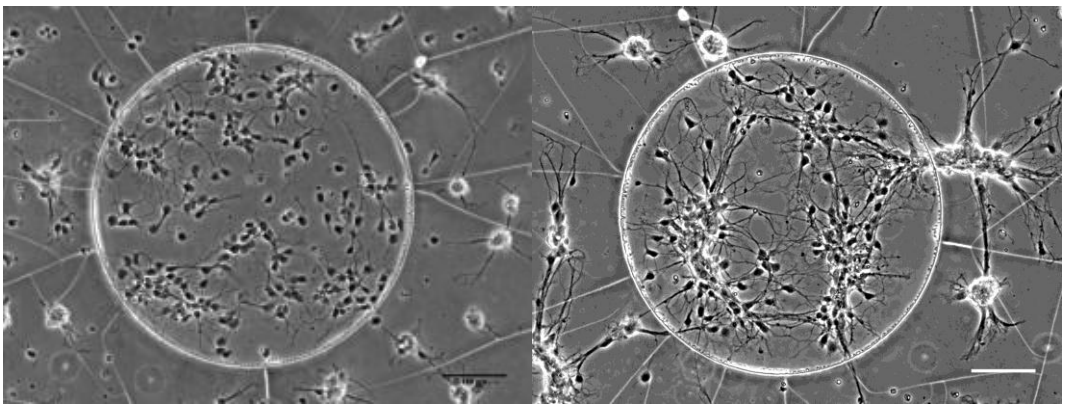

Figure 136 SU-8 5 (nominally 5um high) with PLL deposited on both SU-8 and glass. At 1 div and 3 div, scale bar 100µm

SU-8 cannot be laid down over the PLL and it is thus deposited everywhere, allowing cell growth outside the well. Cells grow healthily on the glass region and do not adhere well on the SU-8. Within 3 days most of the cells on the SU-8 have died, except for a few aggregates in contact with the healthier

culture in the well. In addition, the 5µm well height is too small to inhibit cell migration.

5.2.2.2 *PDMS wells:*

These need to be manufactured using a gas gun concept (Kang et al. 2009b), in which the PDMS is spun to the desired depth on top of SU-8 features, before compressed nitrogen at low pressure is applied via a needle. This displaces the PDMS on top of SU-8 structures, and the PDMS can then reflow before it is cured. After detaching from the mould there will gaps where the SU-8 features were located. The bond to the underlying substrate (an MEA) cannot be permanent, since the MEA must be reused, and thus some leakage under perfusion was reported.

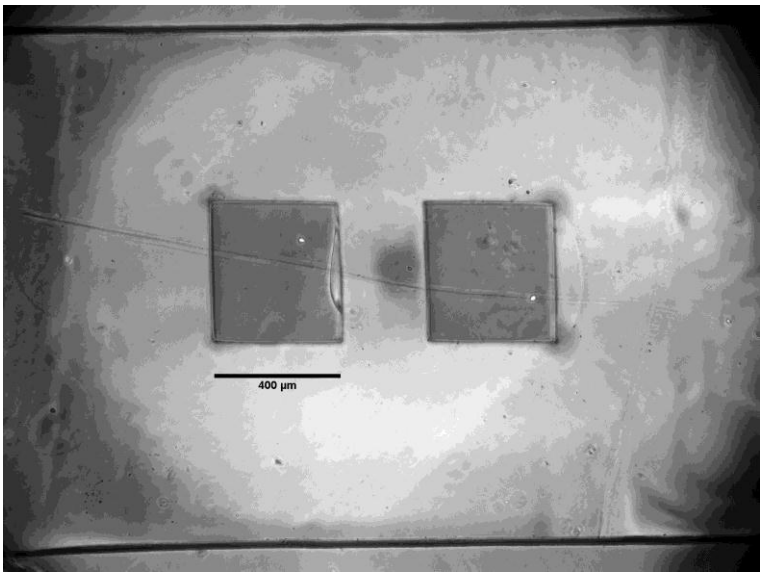

Figure 137 200µm wells separated by 500um, forming the floor of a PDMS microchannel. This device is wholly formed of PDMS. Scale bar 200µm.

Of interest is the ramping of the PDMS feature at the edge of the well, where the PDMS has either cured in a visibly raised lip (Figure 137, to the right of each well) due to capillary action next to the SU-8, or has not laid down flat to the glass.

This may be advantageous during flushing of the channel to remove unwanted cells, as it will provide additional shielding of the microwell region.

Cell culture in PDMS microwells

All devices are now functionalised using the deposition followed by bond technique described in section 3.5.3. The PLL is deposited first, and then the

PDMS or tape layer is placed over it. This ensures that the ligand will only be located at the bottom of the microwell, so cells cannot adhere in any other location within the microfluidic device.

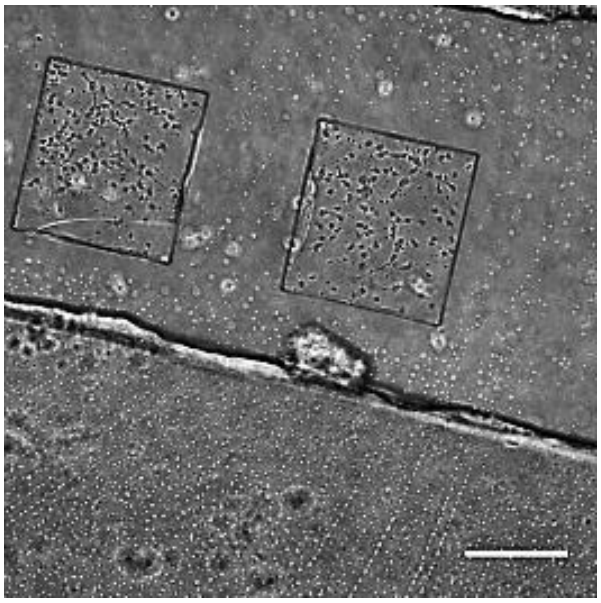

Figure 138 Cells grown by Mr Nitzan Herzog in 400µm wells intended to work with high-density MEAs. At 1 div, after plating with cell suspension at 20k/µL and flushing the suspension out of out the main channel. Cell density in the well 400/mm^2. Scale bar is 300µm.

Cells could be grown in the PDMS microwells (Figure 138), but their survival was poor. It is not known if this was the result of oligomers in the PDMS around a small number of cells, which will be more of a problem than for a larger cell culture in a microchannel.

5.2.2.3 *Making wells in Silicone tape:*

It was found that using the 50µm thick tape is problematic, since to seal a tape microchannel device pressure must be applied, and if the floor of the microchannel is adhesive then it may stick to the PDMS channel roof, sealing the channel.

Also, the 50µm tape is very prone to tearing when handled, and cutting very small features in the tape is not feasible, as it rips and distorts easily, leaving a jagged, messy hole (Figure 139). The smallest replicable feature must be least 500µm across, and usually 1mm is selected.

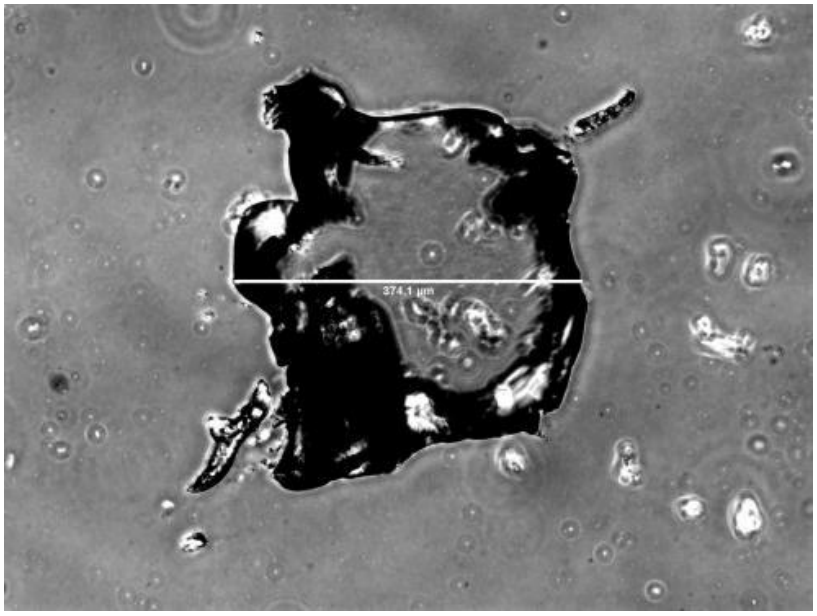

Figure 139 Attempting to cut a small size microwell in the silicone tape. The silicone rips and distorts, leaving an irregular shape with randomly jagged edges which cannot be replicated. Considerable debris is also left around the edges of the well on both tape and glass. Scale bar (centre) 374 µm.

The 125µm tape was found to be much less problematic, and could be routinely combined with microchannels and substrates (Figure 140). Because of the liner protecting it, the tape can be flattened to the glass to ensure it is sealed, which is not the case for PDMS films.

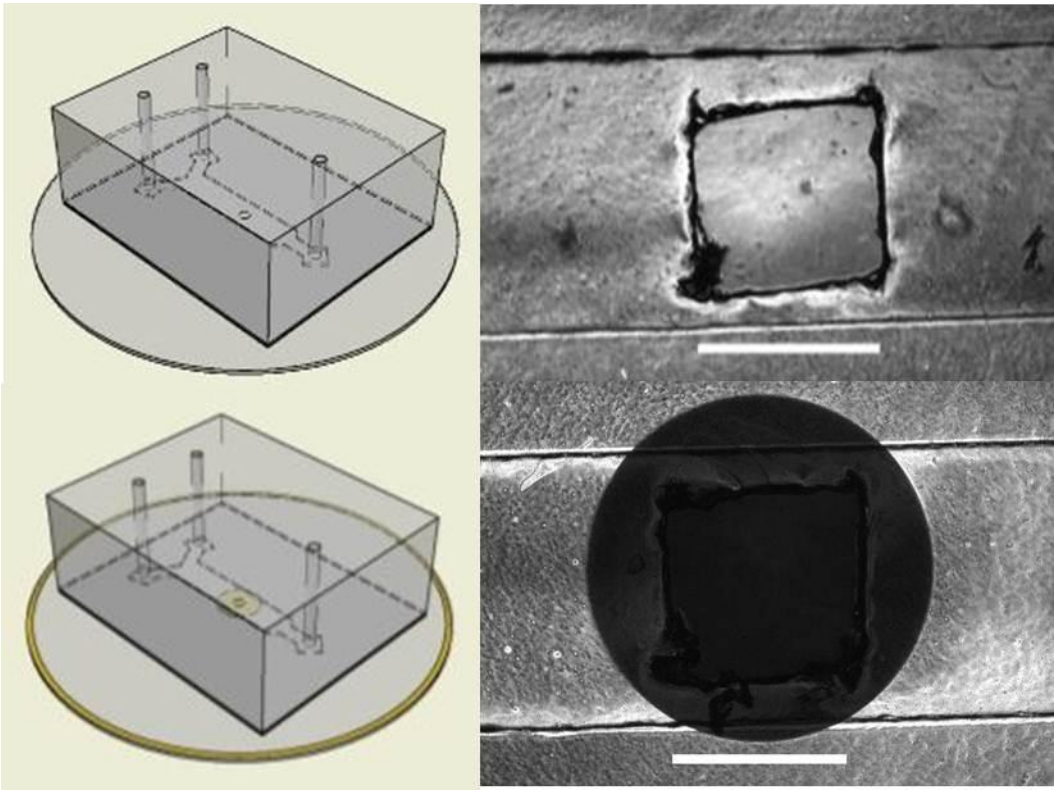

Figure 140 1mm square well cut in tape and the same on a 2mm gold spot. Thus this process is compatible with both PLL and AUT, as both ligands can be laid down as a monolayer across the entire coverslip before the tape is positioned. Scale bar is 1mm.

Cell culture in tape microwells

Cells were cultured on glass with the ligand PEI. Control coverslip cultures (Figure 141)were compared to microchannel (Figure 142) and microwell cultures (Figure 143), to check the plating densities that would be achieved.

GLASS Control coverslip

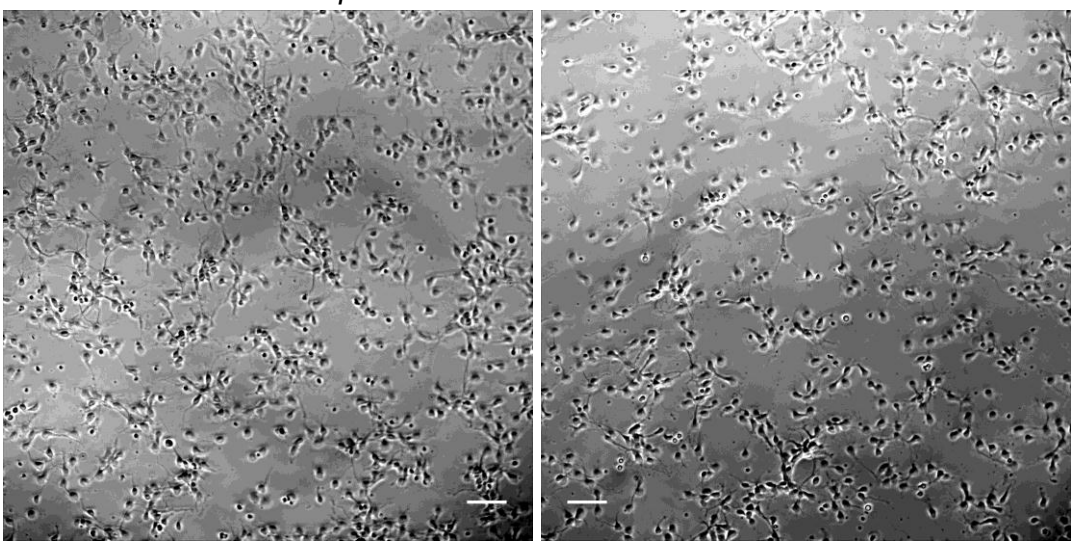

Figure 141 Control surface, glass and PLL coverslip at plated at 300/µL Scale bar 50 µm.

125µm Channel only

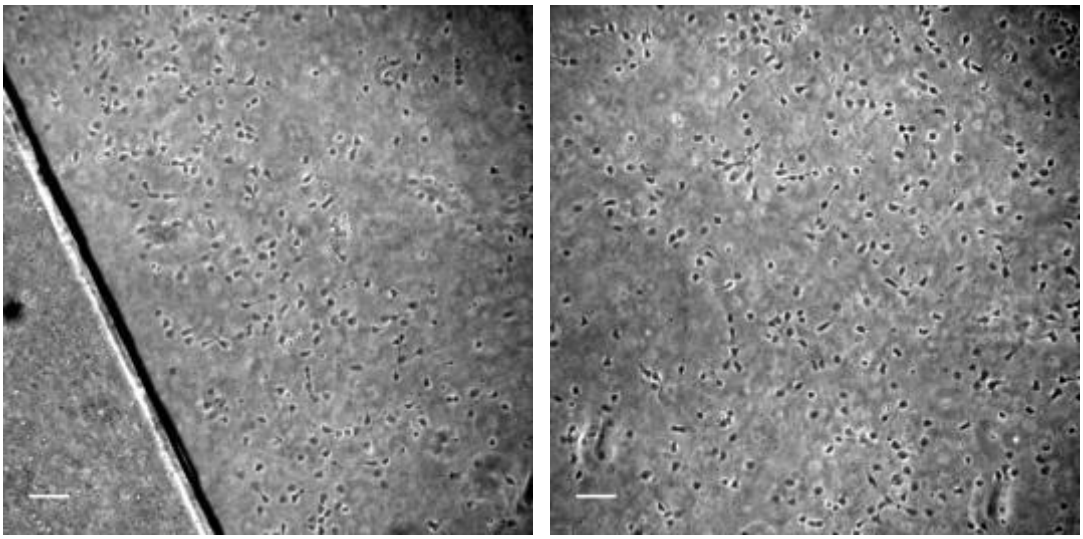

Figure 142 125µm channels plated at 4k/µL. Total height 125µm. Scale bar 50 µm.

125µm Channel and 125µm well

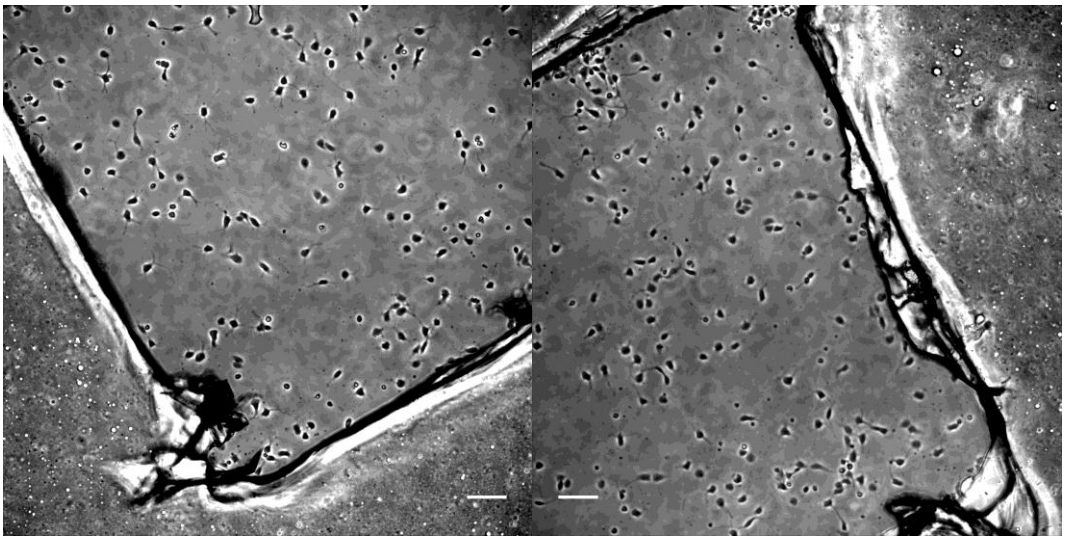

Figure 143 125µm channel with 125µm wells plated at 2k/µL. Note no cells remain on channel floor outside well. Scale bar 50 µm.

It was assumed from earlier work with channels of greater than 100µm, that the volumetric suspension density could be reduced, since the volume of the well would be greater than in the adjacent channel (Figure 144), and thus the number of cells dropping into it would be higher.

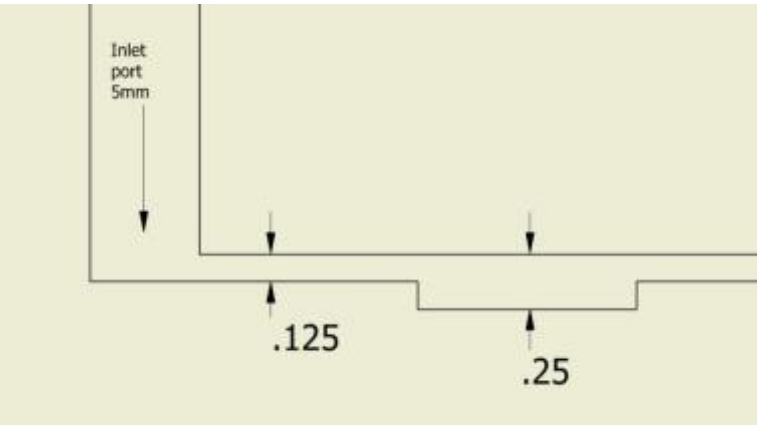

Figure 144 Cross section of wells in channels using 125µm tape. Note that the inlet ports in the bulk PDMS are several (up to 5) mm high. Dimensions in mm.

Based on this, the suspension density plated in channels containing microwells was reduced. The plating density of both control and channel cultures was below what would have been predicted (see Table 12 below), and this may because the true suspension densities were below what was intended, but this is proportionally more severe for the channel cultures.

GLASS Ligand PEI	Total h, µm	Suspension Volume density	Plating expected	Plating actual
Control	0	300/µL	560/mm^2	393/mm^2
125µm Channel	125	4k/µL	500/mm^2	193/mm^2
125µm Well	250	2k/µL	500/mm^2	97/mm^2

Table 12 Expected plating density based on geometry, and actual density

In order to obtain the correct suspension density in a 125µm high channel at 500-550 cells/mm^2, the density needed to be higher instead of the 4k/µL anticipated by volumetric considerations alone.

Similarly, a volumetric density of 2k/µL would be needed to get 500-550/mm^2 in a 125µm well under that 125µm channel. Thus an additional 'overhead' of suspension density is needed to guarantee the minimum plating density desired. This needs further investigation.

The microwell approach is wasteful of cells since only a fraction ends up the well and the density must be very high to endure this. However, it is the most effective method for constraining cells to one region and removing cells from any other region in the same channel.

5.3 **Chapter Conclusion:**

Using photolithographic techniques to selectively place ligands on gold regions was found to be insufficient for creating a viable culture on the region of interest. A combination of low plating density and cytotoxic ethanol residue in the PDMS prevented cells survival in the channel, due to the order of channel bonding followed by AUT functionalization of the gold.

While a sufficiently high plating density was achieved in the absence of a channel, the cells were observed to migrate onto the gold after 2-3 div, having altered the glass surface with expressed glycoproteins so that they could grow on it.

The surface chemistry approach was therefore unsatisfactory both in terms of culture survival in one region of a microchannel, and of subsequent confinement to the region.

Cells were however successfully confined and cultured within a microwell formed by an aperture in a thin layer of PDMS or silicone tape. The plating density in the microwell could be adjusted to the correct level, by adjusting the suspension density per volume. Careful flushing of the liquid volume in the main microchannel removed cells from all other regions except the well.

It was noted however that by adding the well, an additional latency has been added to drug delivery, as the agonist must now travel the height of the well in order to stimulate cells at the bottom. This effect was explored in the following chapter.

6 Perfusion of neurons in microchannels

6.1 Chapter recap

This chapter brings together preceding work, combining healthy constrained culture with controlled perfusion. Thus far: i) previous chapters have demonstrated the capacity to fabricate microchannels capable of supporting neural cells indefinitely in vitro in the absence of perfusion, ii) a perfusion system has been developed capable of providing the flow switching spatiotemporal precision and stability necessary for the desired neuromodulator delivery profiles, and iii) the ability to condense the culture into a limited region of suitably high density has been demonstrated.

6.1.1 Culture and constraint

The primary neuronal cultures can survive for several weeks in the fabricated microchannels on functionalised surfaces, and form healthy cultures provided that the plating density per mm^2 is sufficiently high (>250/mm^2). This is established in the absence of continuous volume replacement. Factor exchange via bulk media change (‘feeding’) is done in the first 2-5 days at intervals of 48 hours; culture contents are typically not adjusted thereafter.

It is further demonstrated that these same preferred cell densities can be replicated in a constrained region within a microfluidic channel, by the use of a microwell of appropriate size, and by adjustment of the cell suspension density. The effect of this microwell on shear forces and drug delivery time is investigated in COMSOL.

To begin with however, planar device cultures without cell constraint will be perfused at flow rates deemed appropriate (1-100nL/s). It is anticipated that a confined culture even at optimal plating density may be more susceptible to degradation under flow than a large, channel-wide culture, since there are fewer cells to express extra-cellular matrix and neurotrophic factors.

Thus it is expected that the viability of a confined culture will be reduced. Consequently, measures will need to be taken to improve the viability back to

planar culture levels by mitigating the effect of flow, without impeding the ability to deliver agonists rapidly.

6.1.2 Perfusion over cells

The media vessels, flow lines (including fluid bulkheads) and flow sensors were sterilised with ethanol and/or high temperature. Deionised water was flushed through afterwards to remove any ethanol that might induce protein crystallisation out of the culture media. Failure to do this could lead to blocking of flow lines and sensors. Then culture media was used to prime the flow paths.

Cells that had been cultured for several days were attached to the flow lines as described above, with care taken to ensure that no high unopposed flow rates were imposed. This was achieved by slowly ramping up the opposing flow rates over several seconds rather stepping them from zero to a significant final operating point.

6.2 Planar channels (initial geometry)

6.2.1 Methods – Fabrication, seeding, analysis

Planar microchannel devices as described previously were formed and plasma bonded to glass. PLL was infused to treat the glass before cells were loaded as before.

Initially devices were seeded with equivalent volume density (150/µL) as would be needed to obtain ‘single’ plating density (around 260/mm^2) on a 19mm open coverslip. In the 1µL volume of the channel, which has a surface area of over 8mm^2, this translates to well under 100 cells per mm^2.

Other devices (principally those of Mr Nitzan Herzog) were plated at a high volumetric density of several thousand per µL, to ensure a plating density of several hundred per mm^2. See previous section 5.2.2.3 on correlating device geometry with intended plating density.

Initially, cells were subjected to continual perfusion on the day they are plated. The theory was that cells should be acclimatised to a flow regime early, so that when their activity is monitored around 14 div their behaviour is not masked by flow response.

This does bring up the problem that such a culture would need to be perfused continually from the beginning, which prevents any other experimental work being done, and has the logistical issue of replacing reagents in reservoirs while the pumps are operating. While such experiments were being considered, only the one prototype perfusion system existed.

An alternative approach was to culture cells under static conditions. The cultures were incubated for 14 days after plating, with media left unchanged after the first 2 days. After this the culture in device was attached to the perfusion system. This was to test the effect of the flow on cultures which had succeeded in establishing synaptic connections before the flow regime was applied.

For all planar devices described, the flow rates Q always lay between 4nl/s, the minimum sensitivity of the Elveflow flow rate sensors; and 40nL/s, the next order of magnitude.

Live/dead assays were not undertaken for the initial experiments; assessment of the culture viability was done entirely by eye, by counting the numbers of apparently healthy and unhealthy/dead cells.

Later higher density experiments undertaken in collaboration with Mr Nitzan Herzog were assessed with Brightfield cell count and fluorescent dead cell assay (using Propidium Iodide to penetrate the membrane of dead cells and highlight them).

6.2.2 **Results for sparse density cultures (less than 100cells/mm^2)**

Firstly, low density cultures growing in planar channels are subjected to flow. This was done with the original perfusion system and lower than optimal cell densities, before a better understanding of the necessary perfusion and culture condition was achieved. As these sparse cultures do not go on to form dense, healthy cultures in static conditions (see chapter 3.4.2), it is expected that they will not survive long under flow. Their longevity can be subsequently compared to that of higher density cultures.

6.2.2.1 *Flow regime from day 1*

Cells plated at suspension density 150/µL (see Figure 145 for a representative culture), were loaded into a channel of volume 1µL and surface area of around 9mm^2, so the plating density was under 17 per mm^2. Such cultures were then within 1 hour connected to the prototype perfusion apparatus (see chapter 4.4.2), where they were perfused for several hours at a constant command rate of 10nL/s.

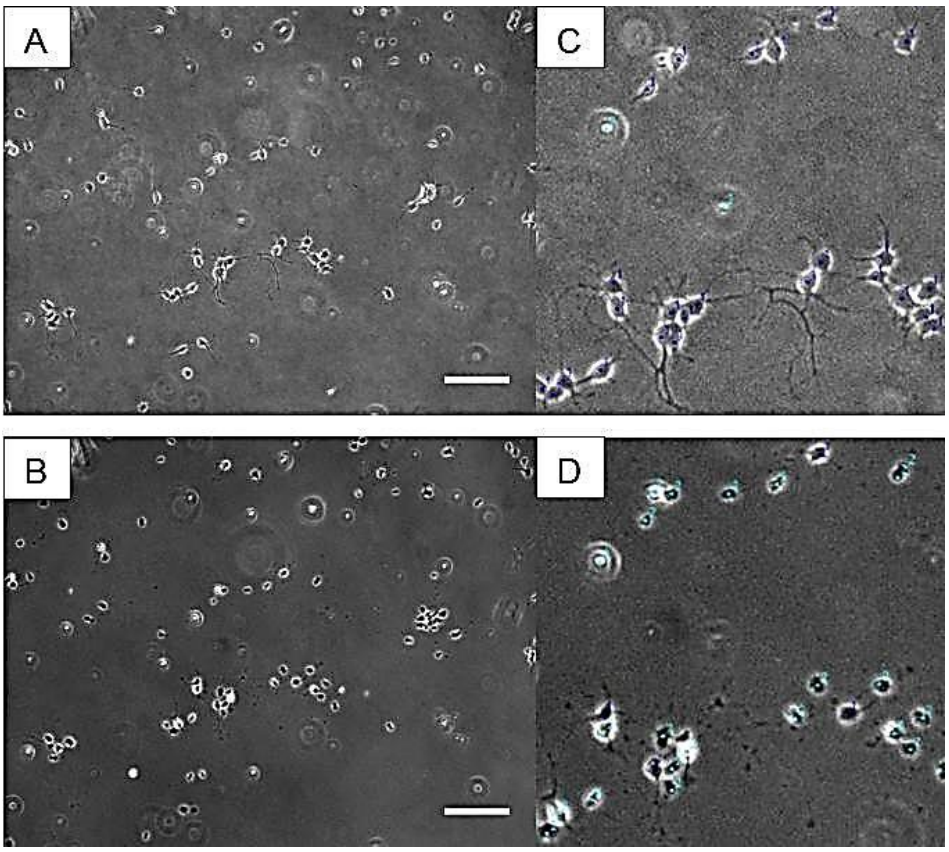

Figure 145 Primary cells at 1 div. (Scale bar 100µm). A) At 0 hours flow of 10nL/s, C) at 8 hours flow. Cells with (dark blue) and without (light blue) growth cone processes (close-up B and D) are counted with imageJ at 2 hour time points.

A metric for culture death was arrived at by counting the number of cells visible and healthy (dark blue in Figure 145) in the field of view at the point when perfusion began. As the cells die, they apoptose into small dark spots with no visible outgrowths (highlighted light blue in Figure 145). The point at which the number of dead cells reaches 80% of the original counted in the microscope field of view is taken as the point of non-viability.

Timepoint	Viable / healthy (processes)	Invalid (no process/apoptosed)
0 hours	51	29
1	51	25
2	51	21
4	43	29
6	33	36
8	9	66

Table 13 Visual comparison of number of healthy cells with axons, and apoptosis or cells.

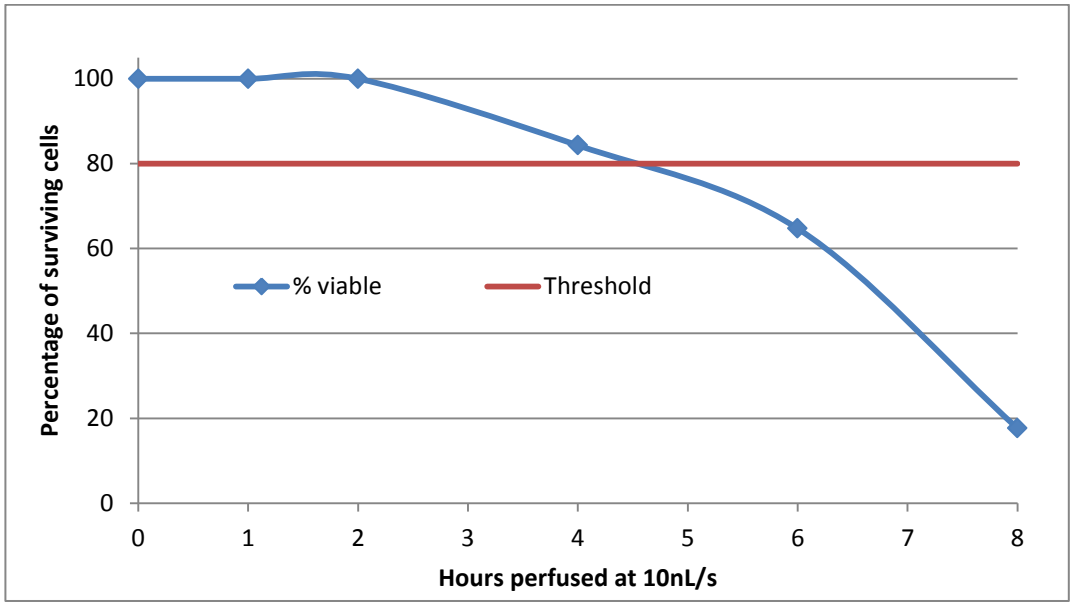

Figure 146 A graphical representation of the observed cell death, using the numbers tabulated above.

The threshold point occurs – in the instance shown relating to Figure 145 – at around 4.5 hours (see Table 13, and Figure 146). The arbitrary threshold choice of 80% was taken after discussion with Mr Tim Smith and Mr Nitzan Herzog, both experienced cell culture specialists.

Several attempts were made to use the prototype perfusion apparatus, which was found to have many systemic faults (see also section 4.4.3.1). The cumulative failure rate of the many issues encountered meant that the system needed to be significantly revised.

6.2.3 Perfusion System Failure Modes

6.2.3.1 *Control software crashes*

The system is on occasion interrupted as a result of the Sensirion™ flow rate sensor crashing the system, or LabVIEW freezing when the power supply is tripped.

6.2.3.2 *Tubing blockage*

This occurs when a kink (tight bend) occurs in the tube, or a plug of solute is formed in the tube, due to protein or salt crystallisation. Of particular concern is when solute blockage occurred in the flow rate sensor itself, as it required aggressive solvent or pressure removal, sometimes by the company itself.

6.2.3.3 *Bubble formation*

Bubble too large to effectively removed by the backpressure, or continually introduced at a point on the flow line. Often due to failing to prime the system lines correctly, but tended to become more frequent as the experimental duration increased, due to the pressure gradient and nucleation in the tubing around bulkheads and sharp internal corners. When cells were present in the system there was a very limited time to recover the situation before cells were killed by the air bubble, and of course this was only possible if the operator is present during the bubble formation. Over a several hour or overnight experiment this is not guaranteed, and so many cultures were killed off with this only becoming apparent many hours later. This is why the average experimental time often exceeds the average cell survival time (estimated, see Table 14).

6.2.3.4 *Gas runs out*

On occasion the compressed gas source (cylinder 5% CO2 / balance air) ran out during an overnight experiment.

6.2.3.5 *PDMS ruptures during tubing insertion*

The PEEK tubing was cut with a sharp blade to the length required. This sometimes resulted in a sharp edge at the end of the tube, which could tear the PDMS during insertion into the channel ports. This meant the device could no longer be used for perfusion purposes.

6.2.3.6 *Device delaminates or glass cracks during system setup*

If the glass is not balanced against a solid surface when attaching the HPLC tubing, the glass can crack, leading to leakage of fluid. This was especially likely when using the original temperature clamp which required tubing to be inserted after installation in the clamp. The revised spring loaded clamp allowed for tubing installation before the device was placed in the clamp.

Attempt (on the prototype perfusion rig)	System run time before halting the experiment	System Problem (Known or theorised)	Cell survival (80% metric) as observed in Brightfield only
1	Under 1 hour	Software failure	2 hours
2	Did not start	Tubing blockage / sensor failure	n/a
3	24 hours	Eventual CO_2 used up	<4 hours
4	6 hours	Instability in flow, due to unstable / drift issues in software	Under 1 hour, may have been dead to begin with
5	Did not start	Bubbles in lines	n/a
6	Did not start	PDMS tore at insertion	n/a
7	Over 24 hours	None noted	3-4 hours
8	7.5 hours	pH may have changed	4.5 hours

Table 14 A comparison of the average time cultures perfused at 1 div perfused survive, attributed to all known causes.

In summary, the prototype perfusion system and device handling protocols used initially contributed a range of failure modes which led to an average culture survival time of less than 3 hours. At this point it was unclear if this was entirely due to the perfusion system, or if the cell culture was simply too

undeveloped to survive. Accordingly, more mature cultures of the same sparse density but incubated for 14 days were used instead

6.2.3.7 *Flow regime at 14 days*

Established cultures at low density (150/µL) were placed under a low perfusion regime. Again cells are subjected to 10nL/s flow for 8 hours.

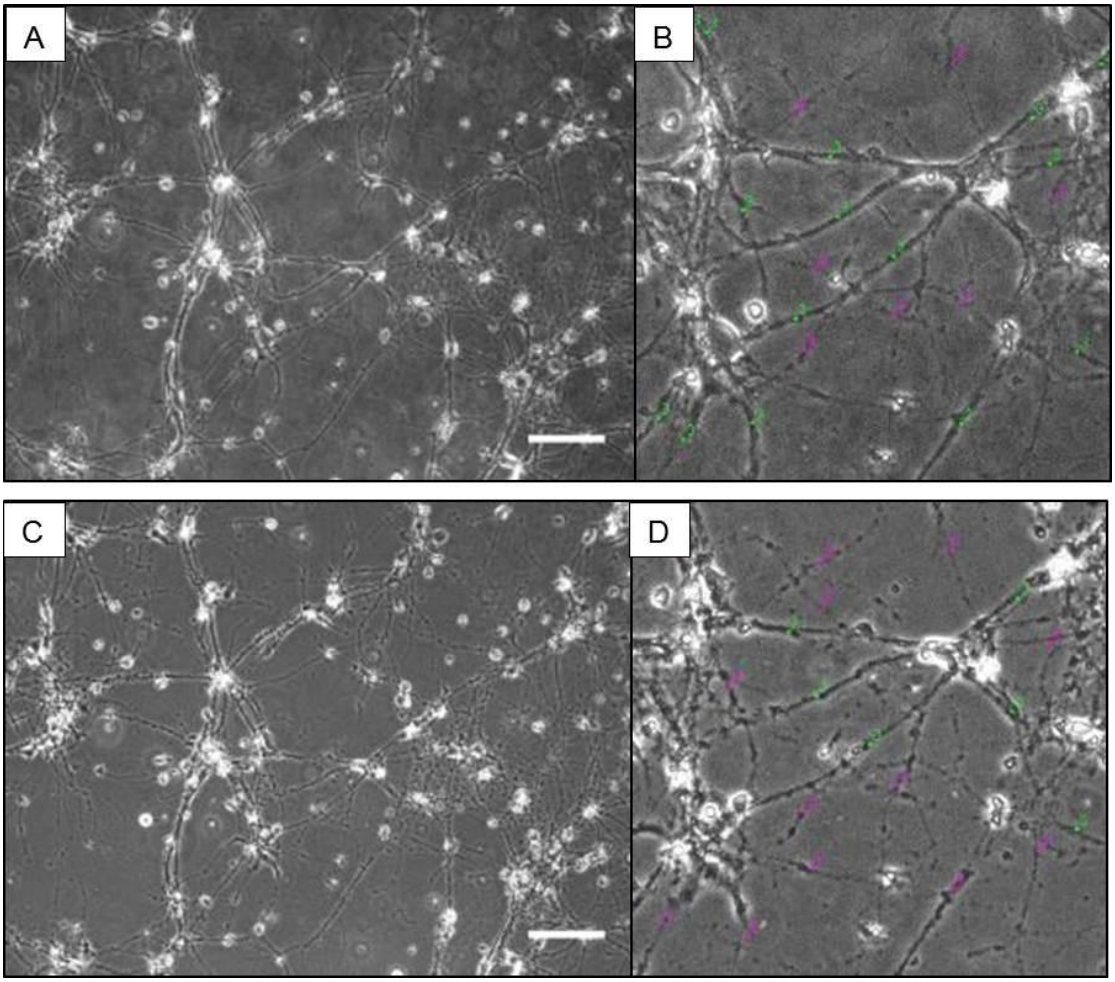

Figure 147 Primary cells plated at low density (150/µL, equating to 305cells/mm^2) at 14 div, scale bar 100µm. A) At 0 hours flow of 10nL/s, C) at 8 hours flow, using the prototype perfusion system. B) and D) are respective close-ups. Unbroken links between cells (green) and broken/granulated links (pink) are counted in the field of view at 2 hour intervals. Again the point of severe degradation occurs after 6 hours.

Timepoint	Viable links	Broken links
0 hours	16	7
2	16	7
4	16	7
6	15	8
8	8	12

Table 15 Visual comparison of number of healthy cells with growth cones, and unhealthy cells with broken links.

Thus using a metric of the number of viable links falling below 80% of the initial number of starting, even established cultures are considered defunct after 6 hours of supposedly continuous low flow (10nL/s). From this progression, having overcome system faults and setup, it becomes clear that even when the system is running correctly for long periods without noticeable flow perturbation (quantified by observing the logged flow rates) the cells do not survive past 6-8 hours. Therefore there is an issue with both the perfusion control, which is only intermittently stable, and the culture channel, which is not sustaining cells under flow.

6.2.4 **Using higher density cultures**

After better understanding of the necessary culture densities (see chapter 3), cultures were grown at higher densities in channels both on MEAs (see Figure 148) and coverslips, before being subjected to perfusion.

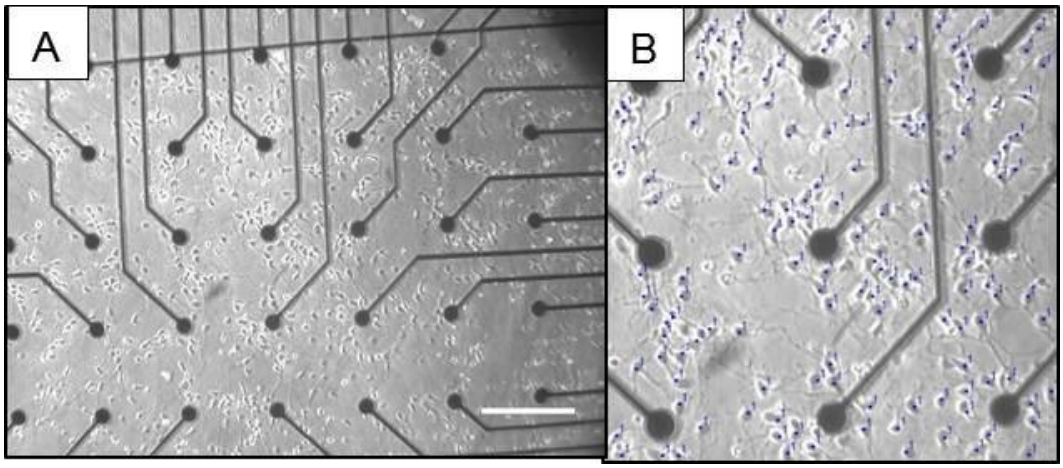

Figure 148 At 2 div, cells have been plated (A) in a planar microfluidic device plasma bonded to an MEA. Counting in a 500µmx500µmregion (B, each blue spot indicates a counted cell) gives a plating density of 596 per mm^2. Scale bar is 200µm.

The particular culture shown is not subjected to flow, but demonstrates successful high –density plating on an MEA (see also chapter 3.4.2). The original images and cell culture were carried out by Nitzan Herzog.

Conditioning and perfusion of such channels was undertaken by Nitzan Herzog with an alternative Elveflow™ OBI fluid handling system while the perfusion system developed in chapter 4 was improved.

One parameter considered here which becomes important later is the condition of the media being used to perfuse the culture in the microchannel.

For experiments where perfusion begins on day 1, the media would necessarily be fresh from the source vessel. For experiments where perfusion begins at 14 div, however, there are two options. The first is once again to use media directly from the source. The second is to use media (at least 5mL) from a bath coverslip culture in which at least $3x10^6$ cells have incubated for several days, and which contains their excreted neurotrophic factors. These two options are called *fresh* and *conditioned* (to several div) media respectively.

A comparison of both different flow rates and different media composition is shown below in Table 16. Of note is that the flow rate used appears far less significant than the conditioning level of the media.

Media condition level	Flow rate (nL/s)	Hours beyond which <80% surviving	No. of attempts
10 div	4	6 hours	>3
10 div	40	8 hours	>3
Fresh	4	3 hours	>3
Fresh	40	3 hours	>3

Table 16 Comparison of longevity of dense (more than 600/mm^2) planar cultures. Results were derived from work done by Nitzan Herzog.

At flow rates around the ranges estimated previously (10-100nL/s) cultures do not survive (based on the 80% metric) for more than 8 hours, even at high density and low flow rate. This was derived by Nitzan Herzog from a dead cell assay, where the chemical *propidium iodide* only penetrates the membranes of cells which have died. The dead cells then show up under fluorescence (TRITC 536nm excitation / 617nm emission).

6.2.5 **Effect of media content, inferred results**

From the planar culture results in Table 16, it appears that although increasing flow rate does reduce the average survival time, conditioned media dramatically increases the lifetime. This implies that while shear stress, which was the original channel design consideration (see chapter 3), is clearly an important parameter, the media conditioning level may also be critically important.

6.3 Explanatory Theory 1): that shear stress is the critical parameter

Shear stress can be investigated in COMSOL and to some extent compared with known/expected values without needing to physically redesign devices,, so this is the first choice of investigation. At this point, the theory is that it is uncontrolled changes in shear rate that are killing the cells, and thus shear reduction is essential going forward. While the perfusion system was undergoing improvement, this was the separate line of enquiry in on-chip planar cultures. This approach is in agreement with literature (Millet et al. 2007) where measured or calculated values of much less than <10µm/s flow and thus shear stress under 1mPa are associated with long-term viability.

6.4 Mitigation strategy 1) Microwells

Since we have elected to use a microwell (from chapter 5) in order to effectively constrain the cells into one region without complex surface patterning or flow control, the efficient solution is to make use of that microwell as the built-in shear mitigation element (Figure 149).

6.4.1 Methods: Microwell as shear stress reducing element

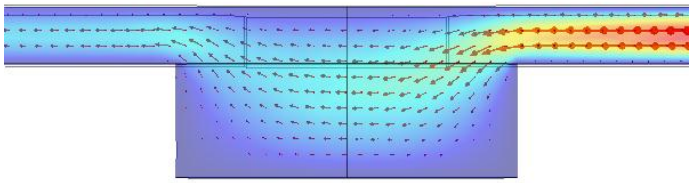

Figure 149 COMSOL representation of the velocity reduction expected in a microwell seen from the side. The red arrows indicate magnitude, and are clearly smaller in the well than the channel.

6.4.1.1 *Smaller PDMS wells*

Given the baseline for best survival was with the protocols developed by Mr Nitzan Herzog, it was logical to proceed by jointly developing devices he then seeded. Initially there were concerns the tape would not be removable from the MEA without leaving residue or damaging the surface, so PDMS wells were used. The wells could be made smaller, as discussed in chapter 5.2.2.2, and the culture size was constrained assuming that a high aspect ratio would reduce shear stress.

These results are as below. These microwells were squares of dimensions 200µm, 300µm, or 400µm, designed by Nitzan Herzog for use with MEAs. All were of depth <100µm in PDMS.

All well cultures are self-conditioned: the media in the well plate they incubated is subsequently used to perfuse them. This is a refinement to the conditioned media used previously (section 6.2.4).

6.4.1.2 *Larger tape wells*

Other wells were made from 125um tape (see chapter 5.2.2.3), once the xerographic process became more widely used. The minimum well size is 1mm, as previously discussed, and the height is fixed at 125µm.

6.1.1 COMSOL shear stress simulations

COMSOL modelling was used to indicate the depth of well needed to impose a reduction in shear, and predict what size of well would be optimal. Recall that the cultures surviving longest have reported shear stress values of less than 10mPa (Joanne Wang et al. 2008), and ideally less than1mPa (Kolnik et al. 2012b). The flow rates used in previous design (1, 10, and 100nL/s) were used again, and the shear stress at points 6µm off the floor of the channel and the well (see Figure 150) was noted.

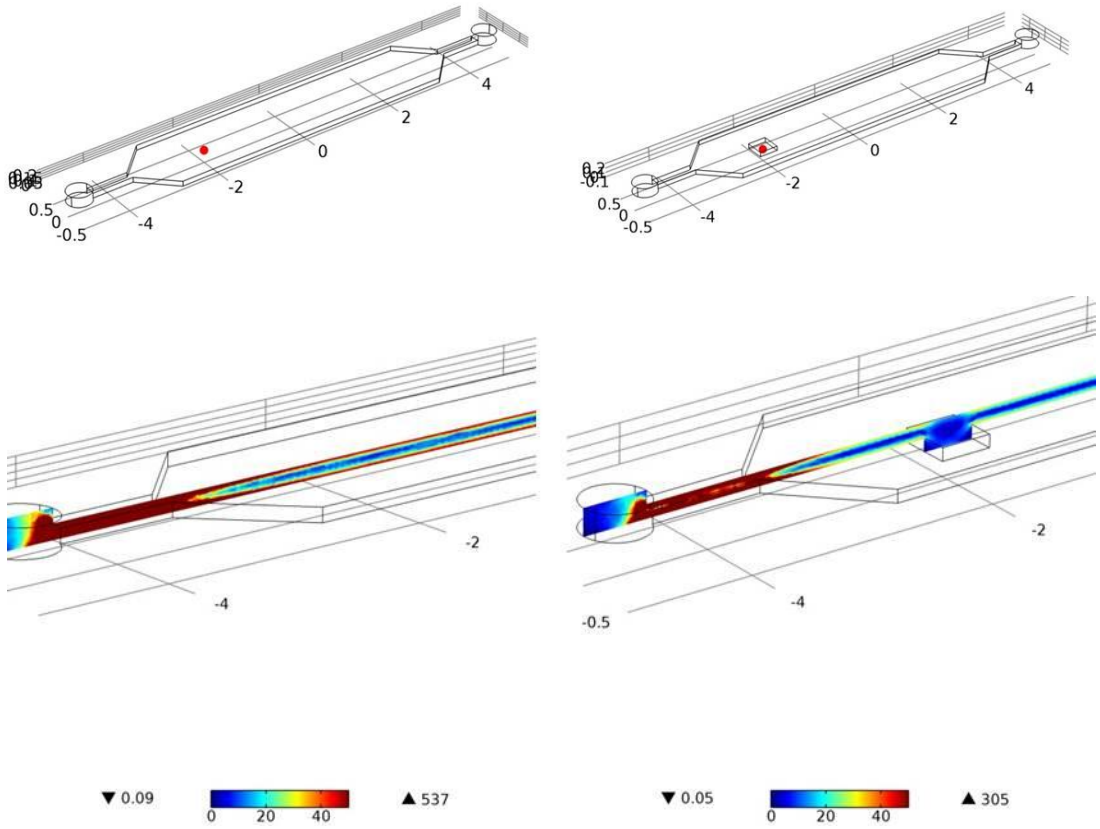

Figure 150 Top: Shear stress is measured in a microfluidic channel (top left) and in a microwell (top right). False colour planes of shear stress though the microfluidic channel (bottom left) and in the microwell (bottom right). The shear stress in the microwell is clearly lower than in the channel. The units in the legends are in mPa.

All measured shear stresses are taken at the data points indicated in Figure 150.

Flow rate (nL/s)	Well width (µm)	Well height (µm)	Shear stress (mPa)
1	0	0	0.2419
	200	100	0.023
	300	100	0.089
	400	100	0.117
	1000	100	0.094
	1000	250	0.038
	1000	500	0.013
	1000	1000	0.001

Flow rate (nL/s)	Well width (µm)	Well height (µm)	Shear stress (mPa)
10	0	0	2.419
	200	100	0.242
	300	100	0.926
	400	100	1.175
	1000	100	0.937
	1000	250	0.368
	1000	500	0.131
	1000	1000	0.011

Flow rate (nL/s)	Well width (µm)	Well height (µm)	Shear stress (mPa)
100	0	0	24.195
	200	100	2.350
	300	100	9.332
	400	100	11.752
	1000	100	9.373
	1000	250	3.681
	1000	500	1.306
	1000	1000	0.105

Table 17 Comparison of modelled shear stress in different geometries at 3 flow rates

Recall from chapters 1 and 3 that the reported range of acceptable shear stress is primarily between 0.5mPa and 20mPa, and that the longer-term perfusion experiments reported are around 1mPa. From Table 17, the wider 1mm wells must be at least 500µm deep in order to keep the shear stress in this range for all higher flow rates. From a shear stress criteria alone, the smallest wells would appear to be the most effective.

6.4.2 **Cell survival under flow**

As for the planar devices tested previously (Table 16)., the flow rates always lay between 4nl/s, the minimum sensitivity of the Elveflow flow rate sensors; and 40nL/s, the next order of magnitude.

Again, to quantify the longevity a dead cell assay was used, with Propidium iodide, and time lapse images taken every hour. The established metric that 80% of the visible cells must be viable was again used. Once the number of cells stained as dead exceeded 20% of the number of viable cells counted initially in a Brightfield image, the culture was declared dead. This work was carried out by Mr Nitzan Herzog.

W x H (µm)	Flow rate(nL/s)	Time for >20% to die (hours)
400x40	4nL/s	<3
400x40	40nl/s	<3
300x40	4nL/s	<3
300x40	40nL/s	<3
200x40	4nL/s	<1
200x40	40nl/s	<1
1000x125	4nL/s	>6
1000x125	40nl/s	>6

Table 18 Longevity estimates (provisional) of cells in microwells. Compare to Table 14 and Error! eference source not found.

These devices were again perfused at 14 div on MEAs. From Table 18, it is seen smaller micro-cultures (under 400µm) do not survive very long irrespective of flow rate or conditioning factor. Consequently a minimum size of 1mm is apparently needed. Referring back to Table 18, it seems apparent that the size of the well, and thus the number of cells it can support, is even more critical than the depth of the well.

6.4.2.1 *COMSOL latency simulation*

Models were then tested as before with the flow rates needed for unambiguous agonist: buffer distinction, to determine what additional latency of agonist onset is imposed by the microwell, and if the switching timescale requirement of 1-2 seconds is still feasible.

The microwell poses a serious problem for drug delivery timing, illustrated in Figure 151 and Figure 152.

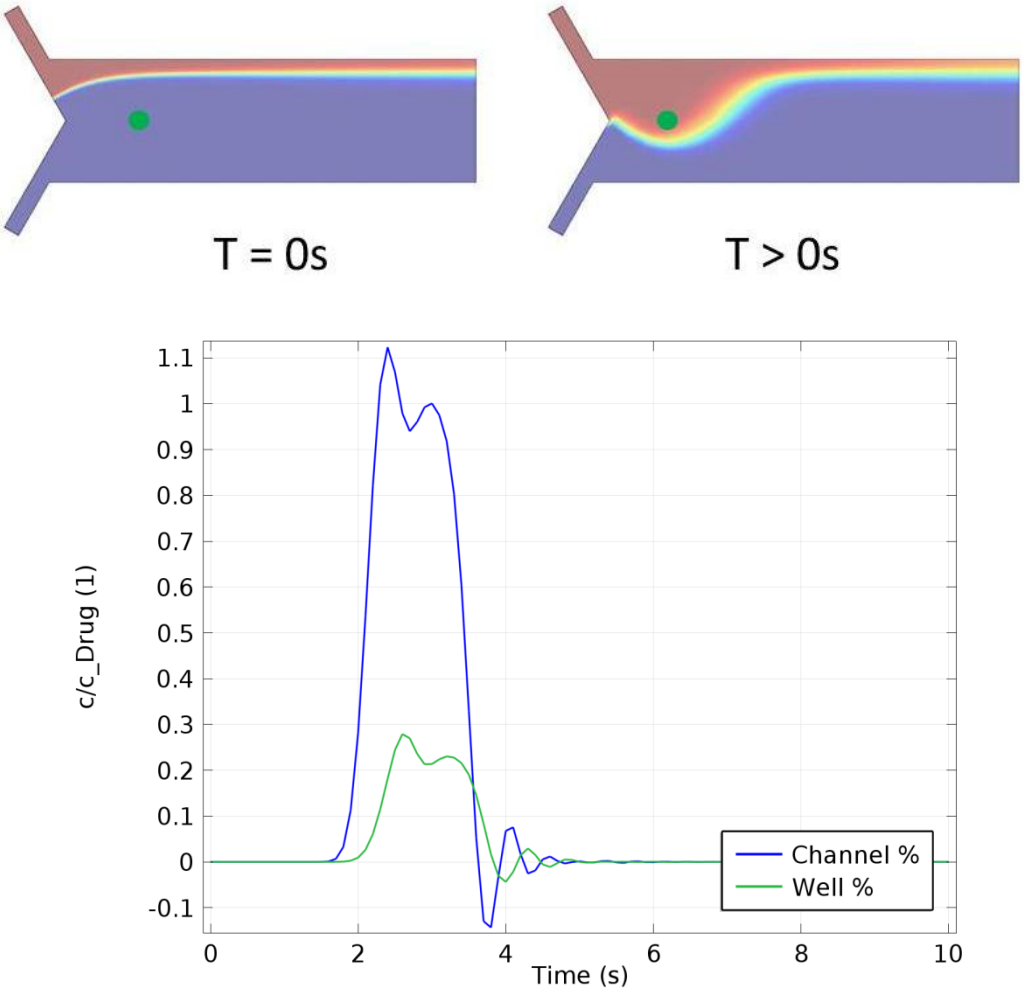

Figure 151 Top: Concentration is modelled at the green area at two different heights as in Figure 150). Bottom: Profile of drug concentration as a fraction of 100µM in the channel (blue line) and in a 125µm deep microwell (green line) during a commanded flow rate switch (right). The total flow rate is 100nL/s throughout.

Because the volume change in the well is effected less by advective transport and more by diffusive transport, the time taken to change the concentration to the extent previously possible is increased. In Figure 151, the microwell concentration peak is much lower than that of the channel concentration, because in the time required for the agonist to descend into the well, the interface has already receded in the channel, so that only a reduced concentration level ever reaches the cells. The lag in concentration change is illustrated in Figure 152. The well should therefore be as shallow as possible for rapid agonist delivery, but this requirement conflicts with the need for shear mitigation.

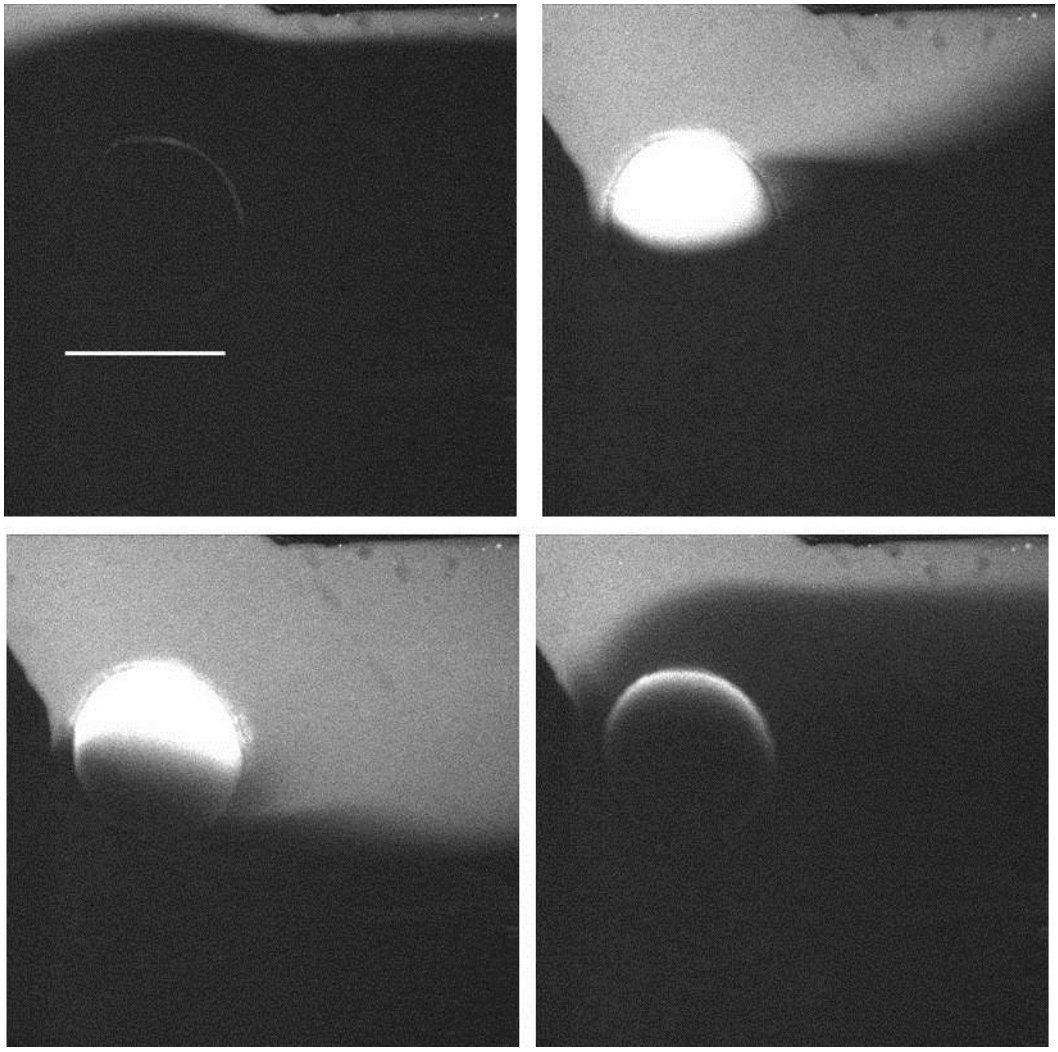

Figure 152 Time lapse of a fluorescein pulse sweeping the channel and back over the course of 5 seconds. The scale bar (top left) is 500µm. Note the fluorescein in the 125µm deep well lagging the wave front in the channel.

To mitigate shear to an acceptable degree, with the flow rates necessary for rapid drug delivery, the well would need to be at least 500µm deep, as already indicated. Thus the advantages accrued with the perfusion apparatus and to some extent the placement of the well in the channel, are negated, because the drug must now travel an extra distance in height.

The flow turnover will lag the flow gradient in the channel, and thus may not reach the cells in a timely fashion or at a sufficiently high concentration, and equally it may not depart quickly as the turnover will be diffusion dominated. This is exactly what we want in order to minimise shear stress to the cells, but it conflicts with the requirement of fast agonist delivery.

Conversely it is extremely difficult to make a well much deeper than 125um, and in doing so the latency of the drug response drops below the metric achieved with the perfusion and channel design to date. A microwell alone is not capable of reducing shear stress while maintaining the capacity for rapid drug delivery.

6.5 Mitigation strategy 2): Semi-permeable Membranes

An alternative for minimising shear is to decouple the cells from the flow itself, while ensuring the transported chemicals still reach the cells. A multi-layer structure is proposed to achieve this, separating the fast-moving flow rates of the existing drug delivery system from the agonist being transported by it.

The proposed method for this involves the development of a 2-compartment channel (see Figure 153) in which the cells are loaded and housed in a lower channel under the drug flow, separated by a thin membrane with perforations or pores through which chemicals can pass primarily by diffusion, since the size of the pore should be sufficient to permit free transport of the drug molecules, but sufficiently narrow (particularly with respect to the membrane thickness) that advection transport across the membrane is greatly reduced.

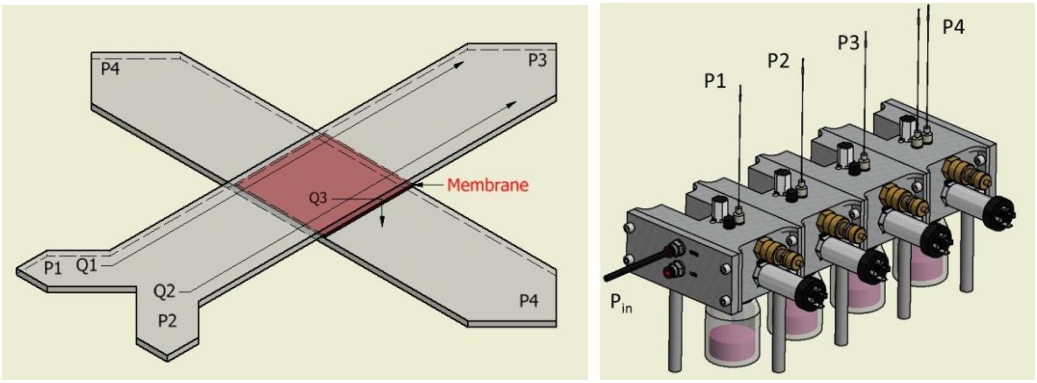

Figure 153 Left: Cross-section of the proposed two-layer microfluidic device with membrane (red) between layers. Right: expansion of the perfusion system to provide all necessary pressure (compare with Figure 123)

From the figure, the existing the drug delivery channel has flow rates Q1 (drug) and Q2 (buffer) due to the difference between P1 + P2 and the backpressure P3. All the pressures P1 to P3 must be higher than the fourth pressure P4 in the second cell culture channel so that a smaller flow rate Q2 crosses the membrane.

6.5.1 Why it is needed and how it should function

As discussed, a microwell is of limited use as a shear reduction approach in a system that is intended to deliver drugs with minimal latency, since the height of the well is an advantage for reducing shear but a disadvantage for timely chemical transport.

If the membrane decoupling the channel compartments is sufficiently flexible, however, then the pressure difference between the upper and lower compartments should stretch the membrane down so that it comes into close contact with the cells. This would reduce the diffusion distance required to deliver drugs on to the cells. Furthermore, this decoupling should allow the perfusion system to run at higher flow rates and with more tolerance for transient overshoots during flow rate switching events. Consequently the switching time can in theory be reduced to less than 1 second, as desired.

Thus the cell compartment could be made very shallow. However, in order to bring back the confinement of chapter 5, the cell compartment would have to include 2 layers, one for cell loading and subsequent pressurisation, and one for the actual microwell.

The flow rate Q2 across a semi-permeable membrane due to a pressure difference (the *transmembrane pressure*) can be described with Darcy's Law

$$\boldsymbol{Q} = \frac{\boldsymbol{kA(P_H - P_L)}}{\boldsymbol{\mu L}} \qquad [24]$$

where the flow Q across the membrane is proportional to the transmembrane pressure (P_{High} - P_{Low}), the membrane area A and the permeability k which is a measure of how easily liquid can cross it, with units of m^2. Q is inversely proportional to the fluid viscosity μ and membrane thickness L.

6.5.2 What is needed to make it function

Most of the system elements already exist, albeit in a less complex form than will be needed. The perfusion system built in chapter 4 can be expanded (see Figure 158) to incorporate an additional pump, which will have two fluid outlets at equal pressure. It has also been established that multiple layers of

tape and PDMS can be built up, as for the microwell devices in the previous chapter. The membrane and perfusion control needed are now explored.

6.5.3 Necessary properties of the membrane and materials available

As with all the materials used so far, the membrane should be optically transparent, and biocompatible.

The membrane will function to permit agonist molecules through promptly while protecting the cells from the drug delivery domain in which shear is higher, meaning pores with diameters much smaller than their length. Since the membrane should not be more than a few microns thick, or it loses any advantage gained by coming into close proximity to the cells, this mean the pores must be no more than 1 micron wide and ideally much smaller. The number of pores and the density per unit area should also be very high, so that every cell is close to several pores.

This immediately casts doubt on the possibility of using PDMS as a membrane. This would be the preferred material as it is elastically stretchable and can be plasma bonded to both PDMS and SU-8. It has also been established (see chapter 5.2.1.3) that PDMS thin films can be made, and the thickness can be reduced to under 10um with higher RPM and longer spin duration.

However, bonds between layers of PDMS are often less robust than glass: PDMS bonds (Eddings et al. 2008). Furthermore, such films are typically gas-permeable only, and will not permit soluble molecules to cross.

A perforated PDMS membrane of <50µm (Luo & Zare 2008), 10µm (Chueh et al. 2007) (Huh 2010) or even 7µm (de Jong et al. 2006) thickness is possible. Some methods involve mixing polystyrene spheres into the PDMS mixture before spinning, and later dissolving the spheres with a solvent such as acetone (Ou et al. 2010) (Shameli et al. 2011) The pore sizes reported are at least 1um across, with no real control over pore distribution.

Photo-patternable PDMS (Delivopoulos et al. 2011) is also possible, where instead of dissolvable polystyrene, a photo-initiator is placed within the PDMS

mixture. After curing of the thin film, a photomask activates some regions, allowing selective removal with an appropriate developer.
Unfortunately the features cannot be resolved below 50µm and so it would not be suitable for perforated membranes, and the photo initiator and developer used for this protocol are very cytotoxic, requires significant leaching with isopropanol.
The alternative is to make use of a commercially manufactured track-etched membrane. These are thin sheets of plastic which have been bombarded with thousands of high-velocity ions, punching holes right through the sheet. Such membranes are already used in cell culture (Sip et al. 2014; Cate et al. 2010; de Jong et al. 2006), and the cells are cultured directly on either side of such a membrane, so there is zero distance between pore and cell. This is not feasible for the purposes of this project, as the cells must grow on a substrate which permits their electrical activity to be recorded.

Some work has already been carried out (Morel et al. 2012; Cate et al. 2010) for the purpose of delivering molecules to cells without high shear stress, and the membranes typically used are around 20µm thick with tens of thousands of pores per mm^2. The average pore size can range from a few nm to a few um, but typically a few hundred nm is reported.

Accordingly, Whatman™ polycarbonate membranes of average pore size 0.1µm were used.

The difficulty arises in effectively bonding such a membrane into the device, since it is made of a plastic (such as polycarbonate) that cannot be fused with the existing silicone and glass structures by any of the means (oxygen plasma, PDMS pre-polymer stamp-and-stick) already used. The plastic has no silanes to bond to and so an alternative strategy is needed.

6.5.4 **Available strategies for bonding the membrane into a microfluidic device**

Initially, the route explored was silane functionalization of the plastic, to add a ligand capable of bonding to the PDMS. Such an approach has the advantages of reportedly very robust bonds, and does not add any height to the device as an adhesive might do.

Functionalization with Two silanes (Tang & Lee 2010)

This method (see chapter 2.5.5) creates oxygen plasma activated silane bonds with two groups: APTMS, an amino-silane, and GPTMS, an epoxy-silane. Immersion of the two activated surfaces in the dilute silane solutions creates strong bonds to the silane groups, where the plasma bond directly between PDMS and plastic would be short-lived and weak.

After rinsing of the silane solutions off the surfaces, they can be brought together once completely dried (Figure 154) and will fuse *in situ,* much as plasma activation of conventional silane surfaces creates a bond.

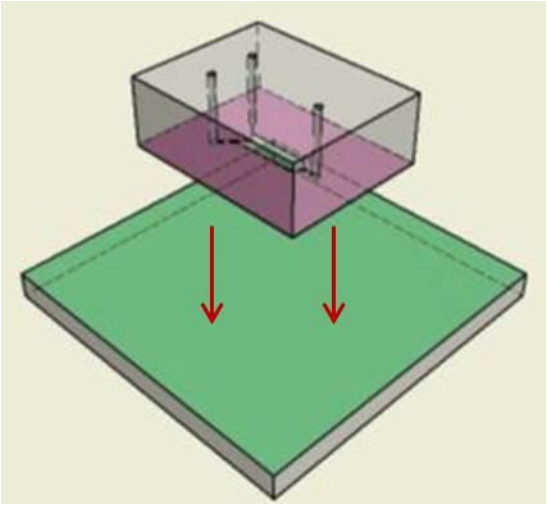

Figure 154 APTMS (pink) on is deposited on plasma-activated PDMS and GPTMS (green) deposited on plasma-activated polycarbonate (PC) sheet. The two ligands fuse together on contact.

Initially, instead of the membrane, the channel was bonded to a flat sheet of polycarbonate. This is used as a test of the efficacy of bonding PDMS to polycarbonate (PCTE), prior to committing to purchasing the membrane.

The strength of the bond is to be tested by flowing liquid through the channel as rapidly as possible, using a syringe driver capable of far higher flow rates than the pressure driven system previously built in chapter 4.

Devices were tested by flowing liquid through via syringe driver, at rates up to 4mL/minute. The stiffness of the tube (0.5mm diameter PEEK or 1.5mm diameter FEP) has an effect on the bonding strength after short curing times,

while the duration and temperature of the curing schedule affected the final strength.

Short cure schedule (1hour)	**Failure rate (µL/minute)**
At room temperature	200
At 80°C	4000
Long cure schedule (>24 hours)	**Failure rate (µL/minute)**
At room temperature	1000
At 80°C	4000

Table 19 flow regimes used to test bond strength of the silane method. The syringe driver nominal flow rate is incremented from 100 to 4000µl/minute.

The metric in Table 19 is the highest rate delivered (in µL per minute), prior to the device failure or prior to the syringe driver stalling, which ended the test.

If the bonding is of short duration at room temperature, the flow rate limit is very low (<200µL/minute). If the bonding is of long duration at room temperature or even long duration at 80°C, the flow rate limit is higher (1000µL/minute), but the device may still fail.

It is inferred that the initial contact between the two surfaces is most important; since the bonds are only a few atoms long any imperfection the flatness will prevent a true bond. Furthermore, the epoxysilane group can be rendered inert by any contact with water, preventing it from bonding to the aminosilane. Thus the solvent for the epoxysilane must be a solvent such as hexane.

This proved critical for thin membranes which crumpled during pressure changes in the plasma oven, and/or did not immerse properly in the silane. Flat contact was almost impossible with membranes, and none successfully bonded using this method.

It was deemed preferable to reduce the number of plasma activation and sensitive functionalization steps needed, by using a single ligand instead of two.

6.5.4.1 *Tape adhesion*

With the use of adhesive transfer tape to form channels (Thompson & Abate 2013), there is no longer an issue bonding PCTE to PDMS. A configuration of stacked tape and PCTE membrane layers is now easily fabricated (see Figure

156 below). This stack is compressed at 45°C overnight (under a weight on a hotplate).

After this heat and weight curing step, the bonded channels are capable of withstanding 250mbar pressure (the perfusion system operating limits). This was tested by flowing liquid though a single inlet/ single outlet tape channel with a membrane floor. The membrane was in turn attached to a featureless layer of tape backed onto glass, to give the structure rigidity and so that liquid could exit the device only via the channel path. Opposing pressures of 250mbar and 150mbar were applied to each inlet for 1 hour. No evidence of delamination was observed in the devices.

Creating channels directly out of adhesive silicone tape and using the tape adhesive to attach the membrane is logistically simple and reliable. Although the functionalization method does result in a very strong bond to solid plastics, this does not translate well to the membranes intended for use in the microfluidic devices.

Assembly of devices including the membrane

Having established that there is a simple and robust method for attaching the membrane to tape on each side, it is now necessary to correctly position the different geometries with respect to each other, particularly where the channel may be attached to an MEA or over a microwell.

6.5.4.2 *Cutting out and alignment*

A metal alignment tool was designed and sent to the engineering workshop for fabrication. The device is a flat square of metal with protruding pillars 3mm wide and 30mm apart (see

Figure **155**). Sections of tape which incorporate 3mm holes 30mm apart can thus be precisely aligned with each other, and a 3mm biopsy punch was used cut both PDMS and the membrane.

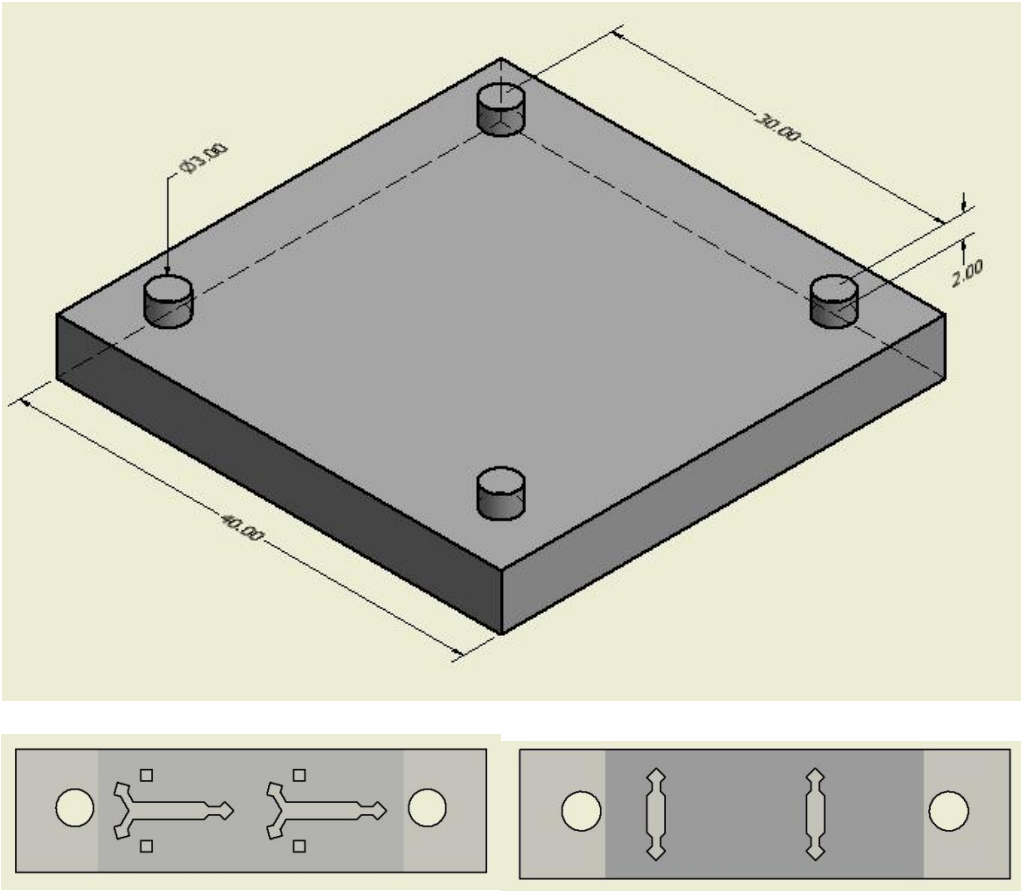

Figure 155 Top: The alignment tool, composed of a single piece of metal. The pillars act to position any tape piece with corresponding holes. Bottom: Two such pieces can be aligned and then diced into single devices.

It was found however that the 125µm and 50µm tapes deform and tear badly when attempting to pierce them with a biopsy punch, so where access ports must pass through a layer of tape, a hole is cut in the layer during the xurographic step. Due to the resolution limit of the cutting blade, such holes are 1mm squares (see Figure 156).

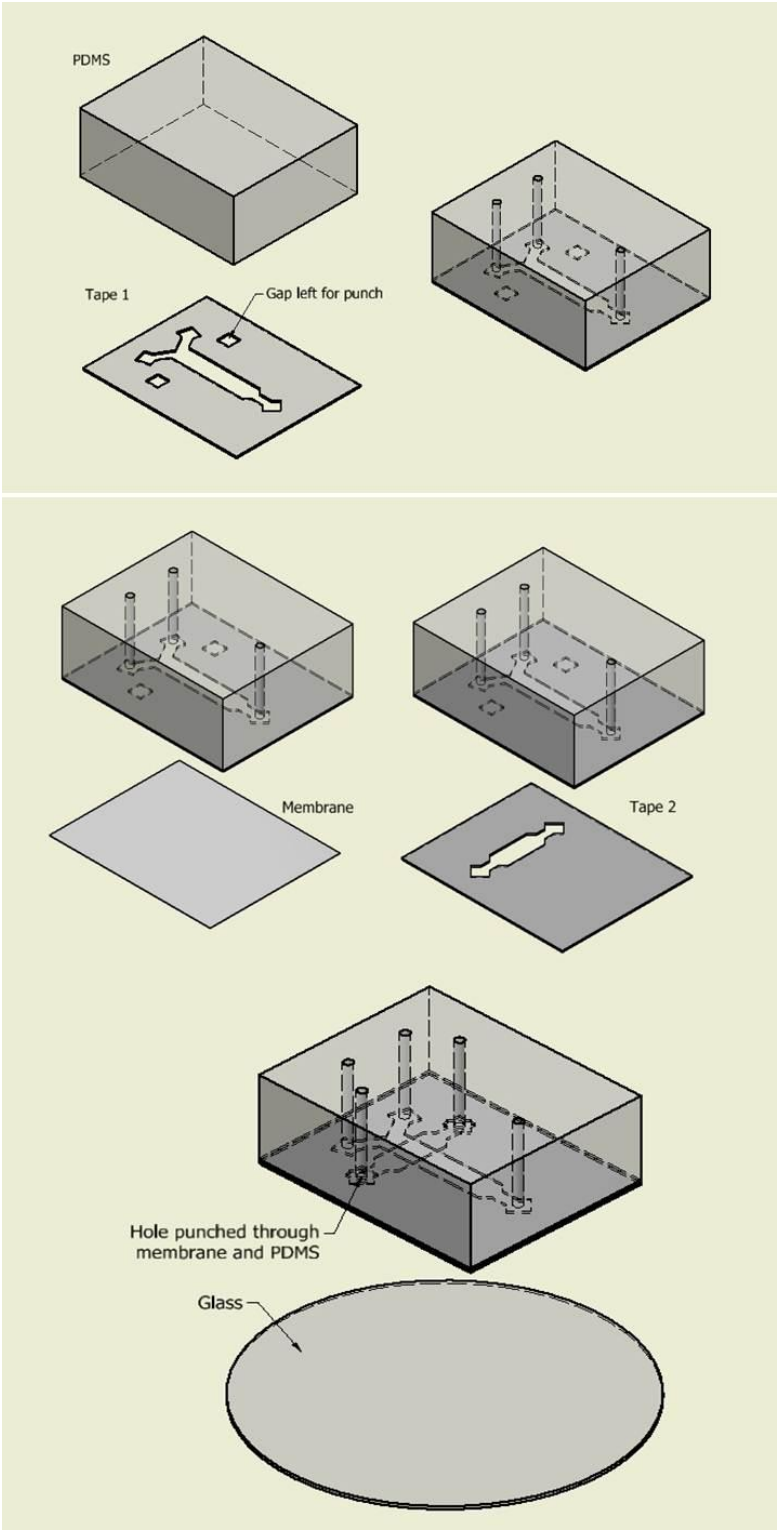

Figure 156 Top: a block of PDMS is attached to a pre-cut layer of tape and access ports punched, as described in chapter 2.5.7. Middle: the membrane and a second tape layer are added, and more access ports punched though. Bottom: the assembled device is brought down onto a substrate such as glass.

6.5.5 **Geometry of the channels**

The channel geometries in the previous figures are representative only, demonstrating the functionality of the device, or how additional layers are added to existing device designs.

Because much of the microfluidic design and cell culture work described in this chapter was done in collaboration with Mr Nitzan Herzog, it needed to be compatible with culture and recording on MEAs.

As described in previous chapters, the channel width should therefore be at least 2mm, to ensure the 60 electrode array is completely enclosed in the channel, and should be long enough to include the reference electrode. Conversely, because the reference electrode no longer needs to be included in the drug delivery channel, this channel can now be made much shorter (see Figure 157).

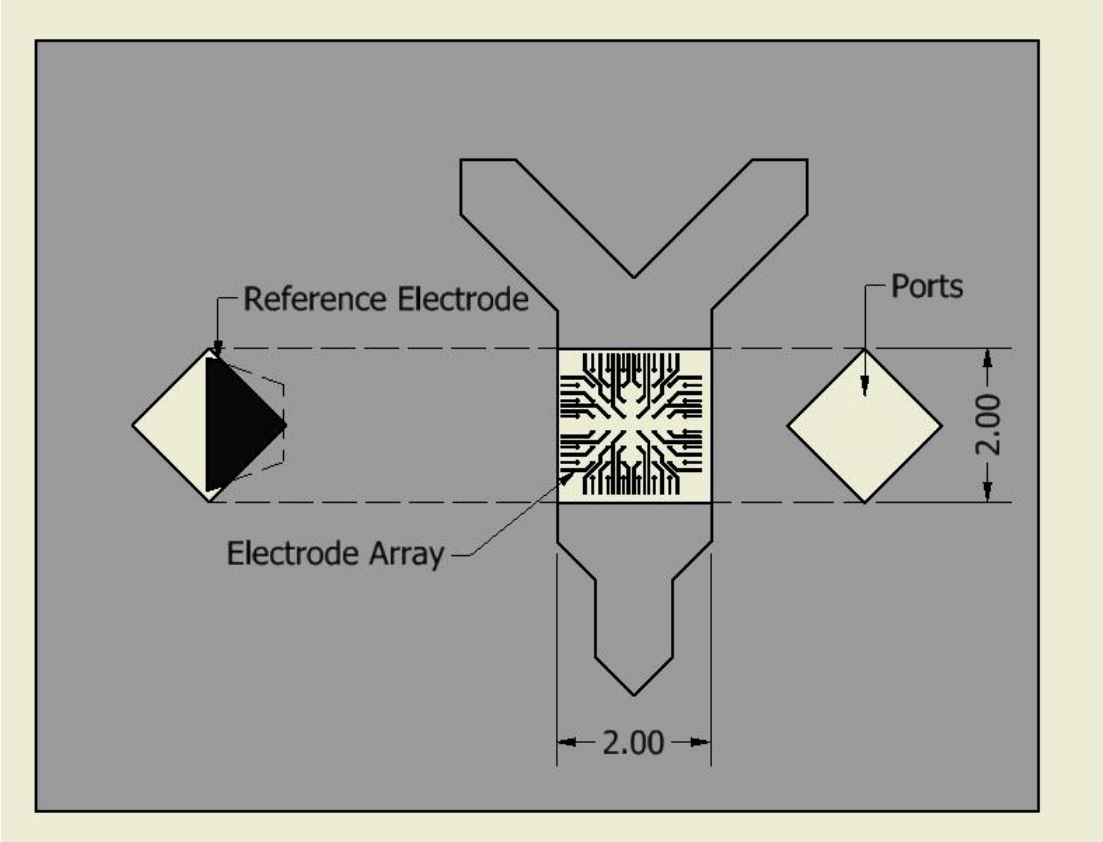

Figure 157 Top: a device built using the alignment method previously described, intended to interface with an MEA. See also Figure 163 for a fabricated device of this type in use.

Thus it is now routine to fabricate a multilayer channel comprising a drug delivery channel and a cell culture channel, designed to interface with a

commercially available cell recording technique and a custom-built perfusion apparatus. The next step is considering how to control the perfusion apparatus successfully.

6.5.6 **Necessary perfusion control**

A more complex set of control algorithms will be needed to balance all the pressures and flow rates anticipated from Figure 153 while maintaining the capacity for both rapid interface shifting, and this has not yet been addressed. Figure 158 shows the complexity of hardware required, and the need for not just two but ideally four flow rate sensors.

The flow sensors attached to pump 4 and measuring the flow Q3 will, if the system functions correctly, need to be much more sensitive than the sensors measuring Q1 and Q2, since the orders of magnitude should be very different.

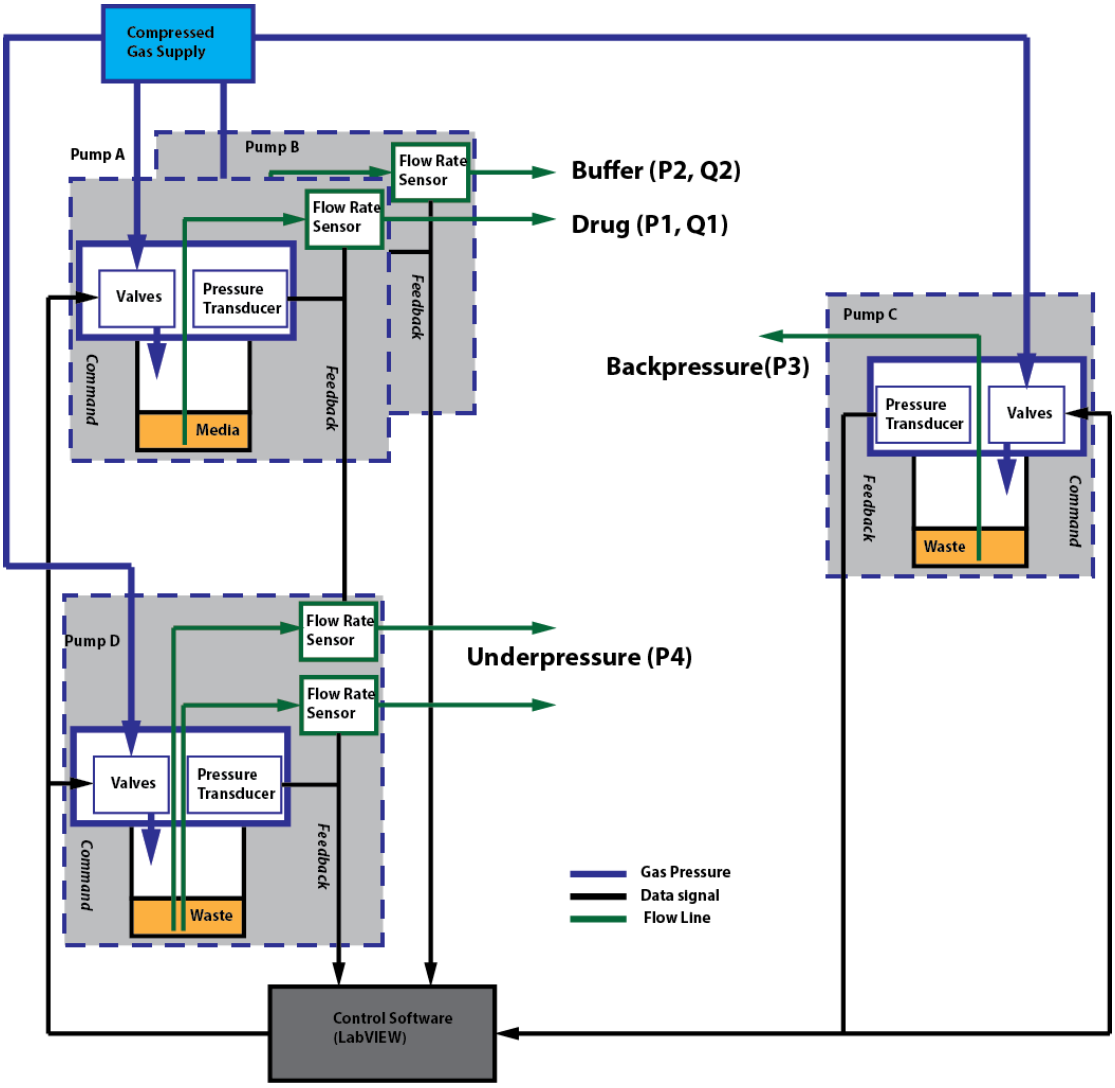

Figure 158 The arrangement of perfusion control elements needed to regulate the microfluidic device proposed in Figure 153. Contrast this with the simpler arrangement used in chapter 4 (Figure 122).

In initial calibration operation, the system may also need a fifth flow rate sensor for pump 3, to check that all flow rates sum to zero. Recall the 'water circuit' analogy (see equations 16 and 17), where pressure is analogous to voltage and flow rate to current. As discussed in chapter 4.2.1, the sum of all flows entering the device must equal the sum of all flows exiting it and thus

$$Q1 + Q2 = Q3 + Q4$$

Where Q1, Q2 and Q3 are the flow rates illustrated in Figure 153, and Q4 is the flow rate from pump 3. If it is not measured, then there is the possibility that the device may partially delaminate and leak without this being apparent from the logged Q1 and Q2.

Given that the perfusion culture experiments to date have worked with a backpressure of 70mbar to minimise the possibility of bubbles nucleating in the channel near the cells, the 'underpressure' P4 must be no less than this value. The pressure over the membrane must be regulated such that it is only a little higher than 70mbar, to ensure that Q3 is kept very small (from equation 24).

Materials for which permeability is known range from 1 to 50,000milliDarcys, (where a Darcy is $10^{-12}m^2$), so between $1x10^{-15}$ to $5x10^{-11}m^2$. From equation 24, the known values are viscosity μ = 0.6913mPa.s, membrane thickness L = 20µm, the area across which the membrane would be permeable is 2mm x 2mm (see section 6.5.6), and the lower pressure is 70mbar or 7000Pa.

Thus, aiming for a Q2 of under 10nL/s ($10^{-11}m^3/s$), the pressure would need to range between 7034.565Pa (70.35mbar) and 7000.00001Pa (≈70mbar).

This implies the transmembrane pressure required to maintain a neuron compatible cross-flow is very small, at most 0.35mBar. From chapter 4.4.5.4 (Table 10) the system has a pressure standard deviation of 0.08mbar, so this would be on the very edge of what is feasible.
Because of the difficulty in obtaining all the flow rate sensors needed, and developing a new LabVIEW control program to run all 4 of the pumps needed, and because from the theoretical conclusion that the level of pressure control needed might not be possible, the complete development of the system shown in Figure 158 was not undertaken.

Instead, simpler tests that could be carried out with the available and established resources were attempted instead, and these are subsequently described. This was in hindsight a mistake, and attempts should have been made regardless of the perceived difficulty in doing so. The complete development and integration of the perfusion system and a multilayer microfluidic device remains future work.

6.5.7 **Ability to deflect under pressure difference**

In order to test how far the membrane would deflect due to a pressure difference between compartments, a simpler pressure control setup was established (see Figure 159). Only 2 pumps were used, each with two flow line outlets at equal pressure. Furthermore, a less complex delivery channel was used, with only one inlet port. The tape used for the cell compartment was either 50µm or 125µm.

The difference between the pump pressures was slowly incremented, with the delivery channel pressure increasing while the cell channel compartment was kept at 70mbar.

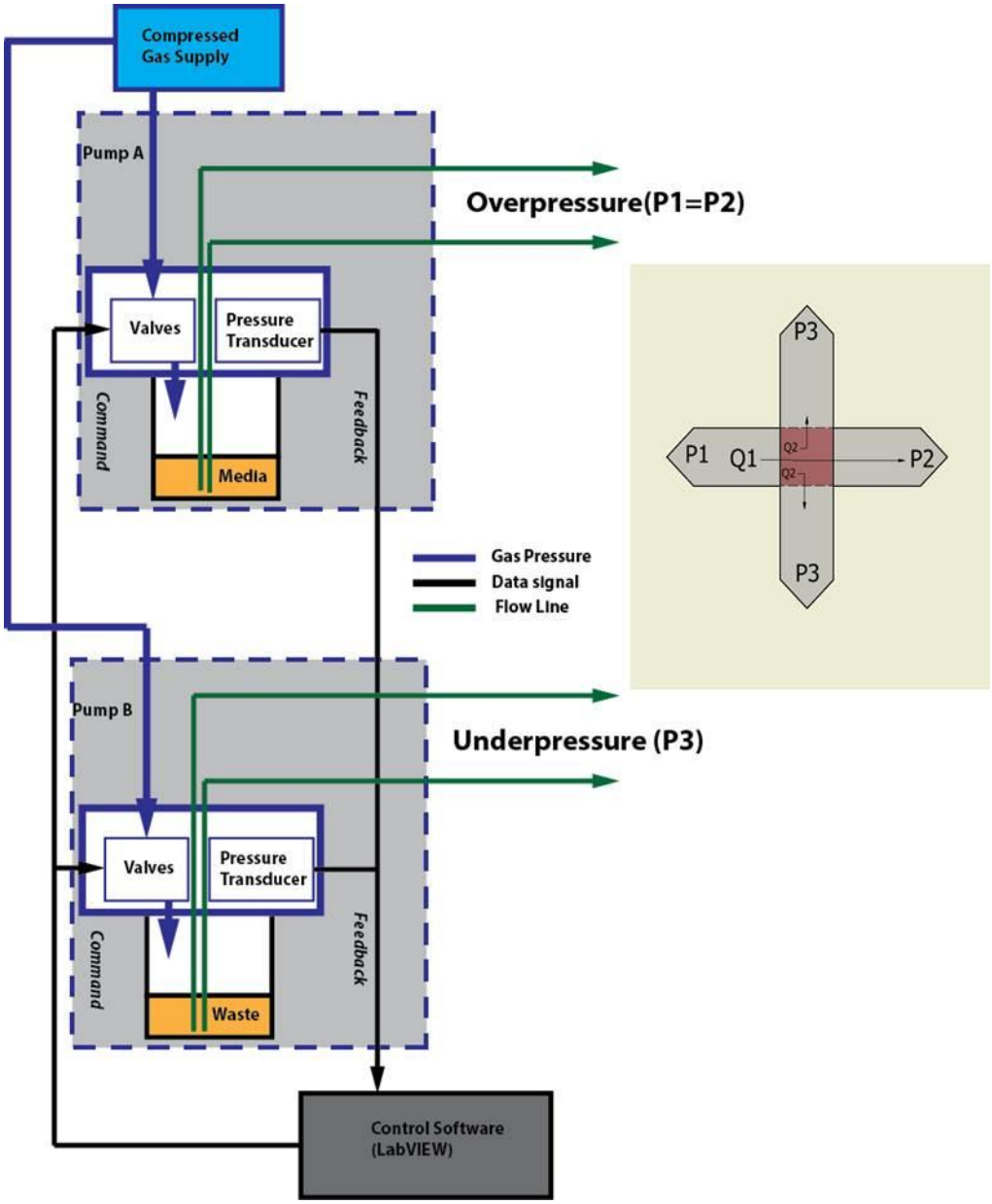

Figure 159 The simple trans-membrane pressure test. Note that only 2 pumps with dual outlets are used, as opposed to the functionality required for Figure 158. Because P1 = P2 , there is no net flow rate Q1 for this experiment.

To establish how much the tape had deflected, during fabrication the device had a spot of ink placed on the membrane. An image was taken at the plane of the membrane with the ink spot in focus. No pressure difference was implemented for this image. The microscope was then adjusted to the plane of the glass substrate, and the pressure difference applied until the ink spot came back into focus.

50µm cell channel height

For this tape thickness the available system pressures were adequate to completely deflect the membrane down to the surface where the cells would be located (see Figure 160).

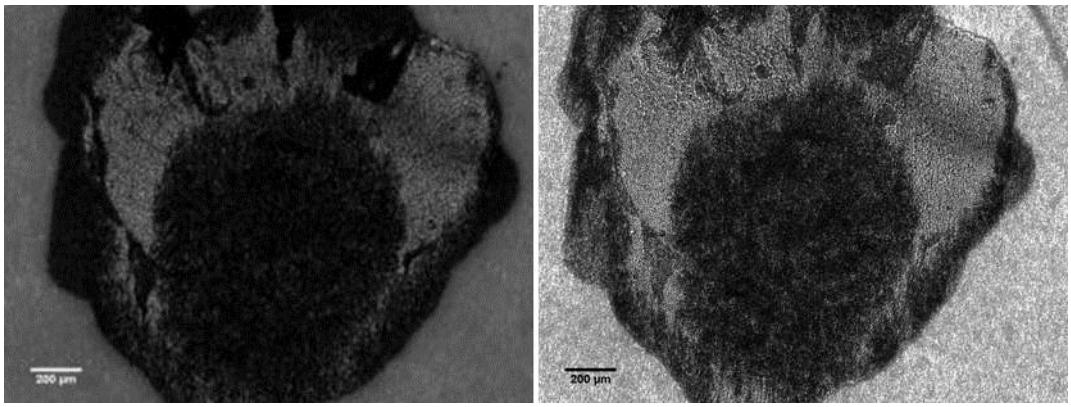

Figure 160 Left: An ink spot on the membrane in focus 50µm above the glass surface. Right: The same ink spot in focus again at the glass surface, after 60mbar pressure difference is applied.

125µm cell channel height

For this tape thickness, however, the perfusion system is not able to fully deflect the membrane (see Figure 161). Recall that the maximum available pressure that can be provided is 250mbar, and that the cell compartment is to be kept at 70 mbar, in accordance with previous experience that bubbles may form in the device if the pressure is lower than this. Thus the maximum pressure difference that can be applied is 180 mbar.

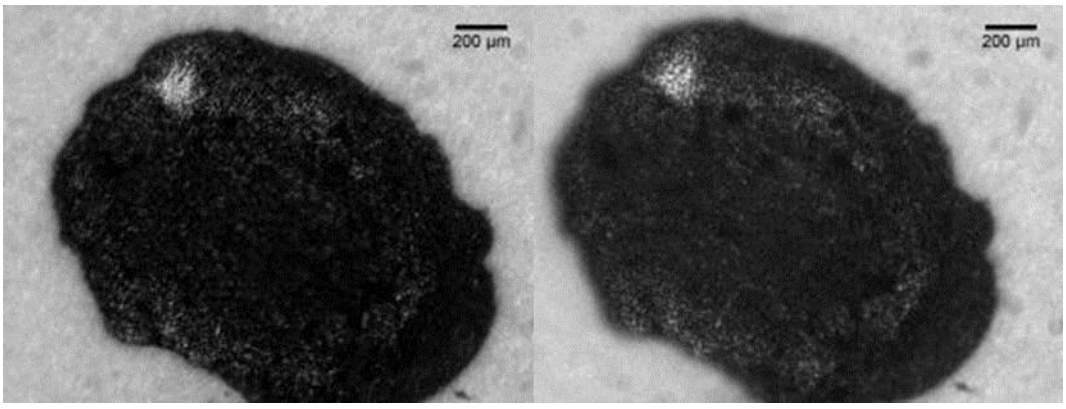

Figure 161 Left: An ink spot on the membrane in focus 125µm above the glass surface. Right: the same ink spot with 180mbar pressure difference applied is still not in focus at the glass surface.

A channel of 50µm is therefore preferred, but what has not yet been included in these devices is the constraining microwell that would keep the culture in one place over the electrode array. This would add another 50µm layer of

tape, so that the total distance that the membrane must be deflected is 100µm.

6.5.8 **Perfused cell survival in multilayer devices**

Multi-layer devices were fabricated, heat-sterilised and issued to Mr Nitzan Herzog, who undertook all cell culture and labelling processes described later.

As for previous cultures, the cell compartment consisted of a functionalised surface and tape channel, with a plating density of at least 500/mm^2. After cells were loaded into the lower compartment, the ends were sealed (see Figure 162), so that further nutrients and gases could only reach the culture via the membrane.

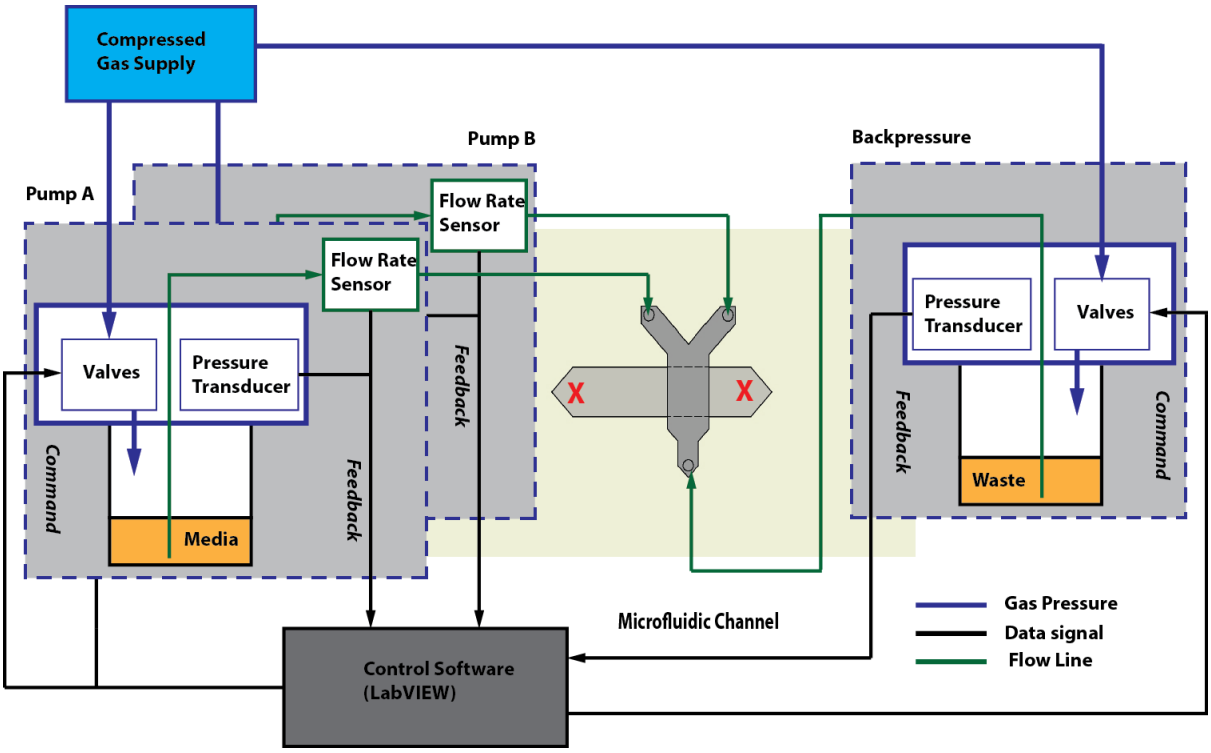

Figure 162 The perfusion setup used in the experiment. Note the identical setup to chapter 4 figure 122, except that the device is different. The ports of the cell compartment were blocked (red crosses) after it was primed with liquid.

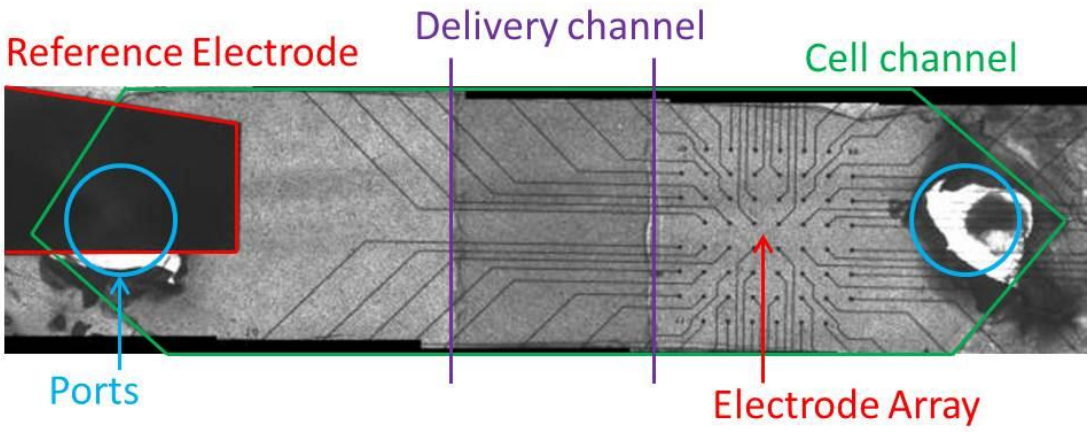

Figure 163 Annotated composite Brightfield image of cultured cells growing in a multi-compartment device. The channel width is 2mm. See also Figure 157 for the intended placement of the delivery channel. This image was taken before the ports were blocked.

Because this configuration (Figure 163) represented a new environment, it was decided that the culture should initially be large, rather than a confined microwell, so that the cells would have a strong chance of survival during incubation. Ultimately the cells showed no signs of ill health prior to the perfusion, so it will be possible in future to incorporate a microwell under the membrane, as discussed previously.

At 14 div, perfusion commenced with a flow rate of 100nL/s in the top compartment, using the same media in which the cells had incubated. To evaluate the effect of flow on viability, a live/dead assay was used. This assay includes not only the Propidium Iodide used to label dead cells, and which was used previously as a metric for deciding if a culture was still viable, but also a Calcein-AM marker which will only bind to certain esterase groups in living cells, not dead cells.

The Propidium Iodide was added to the media at the beginning of perfusion, and time lapse images (Figure 164) all along the length of the channel were taken every hour for 7 hours, with a TRITC filter cube (536nm excitation / 617nm emission). After this the Calcein-AM was added for 1 hour of flow at 100nL/s, and an image (Figure 165) taken with a FITC filter cube.

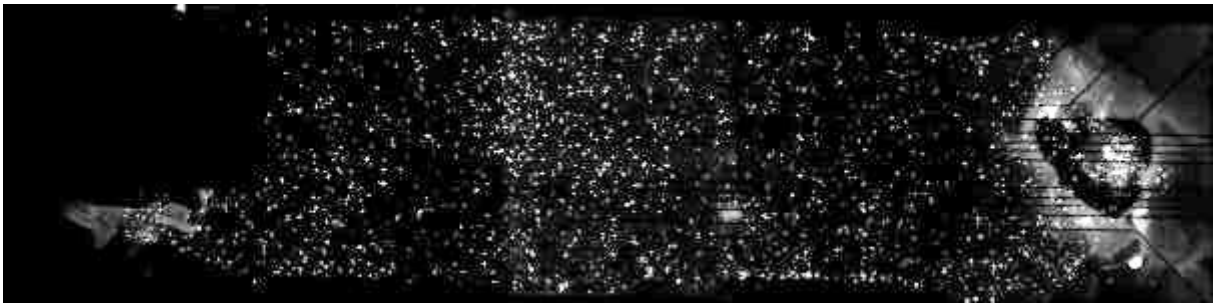

Figure 164 Propidium Iodide / TRITC image for dead cells, after 8 hours flow at 100nL/s in top compartment.

After 8 hours dead cells were visible throughout the device, though average density was higher nearest the intersection with the channel (see also Figure 163). This might indicate the cells under the membrane are less healthy than elsewhere in the channel, but Figure 165 below shows a high density of living cells in the same region.

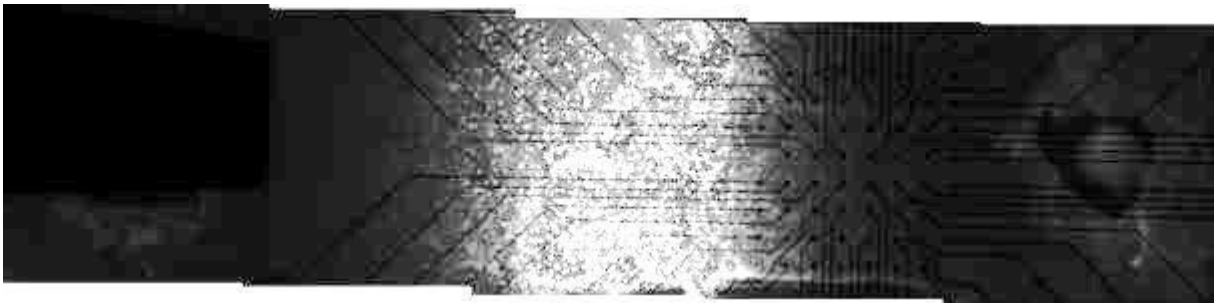

Figure 165 Calcein-AM / FITC image after 1 hour flow at 100 nL/s flow in top compartment.

Conversely, live cells are evident mostly only under the intersection of channels (see Figure 165). What is evident is that the majority of the cells under the membrane are still alive even after 8 hours. This should not be taken to imply that all cells in other regions of the channel are dead. The density of cells was uniform throughout the channel, so the density of dead cells in Figure 164 should be far higher if this was so.

The channel is several mm long and diffusion alone would take several hours to carry the Calcein-AM to the ends.

Unfortunately only limited information about the effect of the membrane using cell electrical activity is possible with the culture shown, as the delivery channel is not situated over the electrode array.

Further experiments with perfusion over cultured cells under membranes were carried out by Mr Nitzan Herzog, with adjusted devices where the delivery channel is correctly situated over the electrode array, as in Figure 157). The

longevity of such cultures is shown in Table 20 below, and can be contrasted with the longevity of planar channels (Table 16), which is essentially the same.

Dimensions W x H (µm)	Flow rate (nL/s)	Hours for >20% to die	No. of attempts
2000x125	4	7	2
2000x125	40	8	2

Table 20 Longevity of cell culture in a culture benath a membrane.

From this it can be seen that adding a membrane to the device has fractionally improved the longevity of the device at low flow rates, by 1-2 hours, and not at all at higher flow rates. Thus it has not had the significant improvement hoped for, and this suggests there is more to the problem than shear stress alone.

6.6 Explanatory Theory 2): that conditioning factor loss from the local extracellular volume is the critical parameter

Cells *in vivo* are tightly packed together with only a small extracellular volume. The ratio of intra and extra cellular volume is around 1:1, if not in favour of intracellular(Duong et al. 2001). This allows for tight electrical coupling, and rapid uptake and removal of neurotransmitters, without dilution or attenuation of electrical signals in a large liquid volume. Since the volume is small, the neurotrophic factor need not be expressed at high levels in order to achieve the concentration required.

In vitro, particularly in a well plate of several mL, the extracellular volume is effectively infinite; many thousands of times that of a picolitre cell volume. Thus we may logically infer (but not empirically prove) that the cells are obliged to express far more conditioning factors than *in vivo*, in order to condition their environment, and that intra-cell signalling is more difficult due to diffusive dilution of chemicals.

From results reported in this and other chapters, the conditioning of the perfused media has a significant effect on the longevity of the culture. Furthermore, as reported by Mr Nitzan Herzog, the electrical activity of a culture grown on an MEA drops significantly within 1 minute of perfusion

commencing. This is in spite of the membrane separating delivery and cell compartments. An alternative mechanism to shear may therefore be the rapid loss of accumulated molecules essential to cell signalling via diffusion.

6.6.1.1 *Rate of concentration change and implied molecule size*

Assuming the molecules near the cell culture are displaced solely due to diffusion, they must be transported at least 145µm (125µm tape + 20µm membrane) in the reported time of 1 minute. The Einstein-Stokes relation is therefore used,

$$\boldsymbol{D} = \frac{\boldsymbol{k_B T}}{\boldsymbol{6\pi\mu r}} \qquad [25]$$

which relates the diffusion coefficient ***D*** of a particle to its hydrodynamic radius ***r*** (in m). This is the radius of a theoretical perfect sphere that would diffuse at the same rate (in the solvent of viscosity ***µ***) as the non-spherical molecule it represents. A range of diffusion coefficients across several orders of magnitude is shown in Table 21, together with their hydrodynamic radii and the estimated time required to diffuse from cells to drug delivery compartment.

Temperature ***T*** is assumed 310K (37°C), and Boltzmann's constant is rounded to $\boldsymbol{k_B} \approx 1.38\text{x}10^{-23}$ J/K (Pa.m^3/K)

$$k_B.T = 4.28\text{x}10^{-21}\ \text{Pa.m}^3 \qquad [26]$$

Viscosity ***µ*** for water at 37°C ≈ 0.6913 mPa.s, so

$$6\mu\boldsymbol{\pi} = 0.013\ \text{Pa.s} \qquad [27]$$

Thus $D = 3.24\text{x}10^{-19} / r$ [28]

and conversely $r = 3.24\text{x}10^{-19} / D$ [29]

D*iffusion Coeff* *(m^2/s)*	*Particle **r**adius* *(nm)*	*Typical for*	*Time to diffuse 145µm (s)*
$4.5\text{x}10^{-12}$	72	Immunoglobin	4672
$4.5\ \text{x}10^{-11}$	7.2	Hemoglobin	467
$4.5\ \text{x}10^{-10}$	0.72	Fluorescein	46.7
$4.5\ \text{x}10^{-9}$	0.072	Ions	4.67

Table 21 Typical Diffusion coefficient and associated particle radius for 4 scales.

For reference, Fluorescein ***r*** = 0.7nm, Calcium and Chlorine ***r*** = 0.18nm, Sodium ***r*** = 0.1nm, Potassium ***r*** = 0.14nm.

From this it can be inferred that if the cell electrical activity change is due to concentration changes, the relevant molecules must be under 1nm across. This includes both ions and neuromodulators, which are essential to action potentials and inter-cell signalling. The concentration gradient between the cell culture and the drug delivery compartment is very high, which suggests the molecules are not present even in the conditioned media the cells were incubated in.

It is not surprising that any net diffusive transport would be from the cells, which are the source of the molecules, to the delivery channel, which is acting as a sink. As there is no transport due to advection between the compartments, given the dead volume of the cell compartment, no mechanism exists to oppose the concentration gradient.

It would have been more instructive to fully realise the potential of the cross-flow device with transmembrane pressure, but this was not done. A possible outcome is that the molecules would have exited the cell compartment via the punched access ports, instead of across the membrane.

This section is entirely hypothetical, since there was no available empirical means of labelling and tracking the molecules of interest, but it is a line of enquiry that should be followed up in future, given the demonstrated importance of media conditioning on culture survival.

6.7 **Chapter Conclusion:**

Existing work was integrated such that the perfusion apparatus and microfluidic devices previously built and tested were used simultaneously. Contrary to expectations, cells did poorly in the devices, even when a dense network had many days to form a network before perfusion. Some issues could be attributed to the prototype perfusion rig, but the available commercial pump (Elveflow) did no better. The issue is apparently due to the flow in the chamber.

It was found through live/dead assays of the perfused cells, and using a metric of 80% survival in the observed region as a benchmark of viability, that cultures grown in the originally designed microchannels did not survive more than 6 hours.

The working theory, in accordance with prevailing literature theory, is that the shear stress imposed on the neurons by the flow was considerably more significant than had been accounted for in prior channel design. Thus mitigation of the shear stress was attempted, by using a microwell to create a region where flow rate would be much reduced.

Microwells are shown to be capable of mitigating the shear effect of direct perfusion, but this comes at the expense of increased latency, given that diffusion is now expected to more significant in the microwell. This negates the response time of the perfusion system. The cells grown in microwells up to 125µm deep did not survive any longer than those in simple channels.

A semi-permeable membrane approach was next attempted, in which a porous polycarbonate sheet under 20µm thick was interposed between the co-flows and the cell culture. This was expected to decouple the flow rate from the pharmacological content. The key advantage that would emerge if successful is that the flow rates could now be increased in magnitude without perturbing the cells, possibly reducing the interface switching time to under a second.

The longevity of the cultures appears to fractionally improve in cultures perfused under a membrane, but it appears that shear stress is not the critical issue for cell signalling. At the same time, an interesting phenomenon appeared in the electrical activity of perfused cell cultures under membranes, implying that even in an environment in which shear stress was supposedly very low, cell electrical activity was affected by perfusion. A theoretical section explores if this could be due to loss of molecules important to cell signalling via diffusion along a concentration gradient, concluding that it is feasible, but this is not proven.

What should have been followed up, as discussed, is the complete integration of the perfusion system and developed multi-layer devices, so that fully controllable transmembrane pressure and rapid drug: buffer interface shifting above the membrane could be realised in the same microfluidic chip. This remains future work.

To date, it has not proven possible to keep cultured neurons alive in the microfluidic devices for more than a few hours, in spite of optimal surface and plating density conditions, and despite implementing strategies to reduce shear stress. This indicates that the long-term solution to this problem will need to address the concentration and retention of essential neurotrophic factors in the media, which clearly has an impact which is not yet fully understood.

7 Integrating alternative recording methods

As discussed in the introductory chapter, as part of the overall goal of understanding neuronal encoding of information, it is vital to record in real time as much of the network activity as possible, over an indefinite period of time.

In preceding work (Chapter 3) it was established that the micro-electrode arrays (MEAs) purchased from Multi Channel Systems (MCS), which are composed of titanium nitride (TiN) electrodes insulated with silicon nitride (Si_3N_4), are fully compatible with neuronal cultures grown in a microchannel.

However, the MCS MEAs used have a relatively low spatial resolution (200µm apart) (Multichannel Systems 2014), meaning that much of the network information is likely not perceived. Furthermore, high-resolution microscopy of greater than 20X magnification might not be possible since the MEA glass is 1mm thick, and the working distance of the microscope objective may be smaller than this (Nikon Instruments 2016).

In addition, both the MEAs and the associated head-stage in which the MEAs are placed during signal recordings are very expensive. The MCS system only permits recording from one culture at a time, which is already a bottleneck for the 8 hour perfusion experiments achieved to date and would be insupportable for the ultimately desired long-term experiments lasting many days or weeks. Until the adoption of the adhesive transfer tape method of microchannel fabrication, any bonding of the channel to an MEA could prove irreversible, and was not often attempted.

7.1 Developing an alternative electrode recording apparatus

7.1.1 Rationale

It would be desirable to have a far cheaper and easily replaceable recording substrate developed in-house, together with a compatible signal reader which can be repeatedly built. This would permit parallel recording of cell cultures,

which is essential once it becomes possible to sustain perfused cultures indefinitely.

The MCS head-stage available consists of more than a signal reader. To usefully capture and discriminate the action potentials, the head-stage must pre-amplify the signal, then filter out signals below 100Hz (such as electrical mains noise) and above 15kHz (Multi Channel Systems 2014) and amplify again.

Within the scope of this thesis and given the other requirements which take precedence, it is therefore not realistic to develop such a system in its entirety, so the aim is the development of an alternative electrode patterned substrate and associated signal reader which can successfully relay the action potentials to an as-yet undeveloped filtering stage. It is not intended within the scope of this thesis to build a fully functioning microarray and amplifier for spike detection, What is tested here is solely the capability to construct metal geometries that can be used to record electrical activity, and incorporate them into a microfluidic device that remains conducive to healthy cell culture, with the theoretical ability to read off the signals. This requires a custom-built circuit board that can reversibly attach to the electrodes on the substrate.

7.1.2 **Materials and Methods for electrodes**

It has been established (chapter 5.2) that it is possible to fabricate metal patterns in gold and titanium which are compatible with microchannel and microwell fabrication, and which in conjunction with microwells can be used to confine a healthy culture of cells.

As TiN and Si_3N_4 were not readily available, gold and titanium were used instead for the electrodes. SU-8 and the silicone tape (as also used in chapter 5.2) were both considered to form the layer which will jointly act as microwell and electrode insulation.

Silicone polymers 50µm thick have dielectric strength of around 600V/µm (Zakaria et al. 2014). SU-8 5, the particular SU-8 product used, has a dielectric strength of around 500V/µm (Melai et al. 2009), while Si_3N_4has a breakdown of 1kV/µm (see Table 22).

Thus in order to have the same breakdown voltage – 500 volts – as 500nm of Si_3N_4, which is the insulation layer thickness used by MCS (Multichannel Systems 2014), at least 1 µm of SU-8 or 1µm of silicone tape would be needed. As the tape is at least 50µm thick and the SU-8 used at least 5µm thick, this should be more than sufficient.

Material	Strength (V/µm)	Thickness (µm)	$V_{Breakdown}$ (V)
Silicone polymer	600V	0.83	500
SU-8	500V	1	500
Si_3N_4	1kV	0.5	500

Table 22 Comparison of different insulating materials

Although the ultimate aim is to improve the spatial resolution of the electrode array, for the purposes of this thesis it was considered sufficient to match it, so the designed electrode geometries are identical in size (30µm) and spacing (200µm). Typical 30µm electrode resistance for TiN and gold electrodes of MCS production quality is less than 100kΩ (Multichannel Systems 2014).

This custom built array is to act as a proof of fabrication concept, and the task of increasing the array resolution and complexity is left as future work.

In addition, since the preferred substrate is another existing item – the 0.17mm thick, 19mm diameter glass coverslip – it is not feasible to attach 60 electrodes to it, and so only 4 electrodes are built. Again this is considered a proof of concept subject to future improvement.

7.1.3 **Geometry Design**

The geometries (see Figure 166 and Figure 167) were designed in Autodesk Inventor and sent to the photomask production company JD Phototools Ltd, to be rendered in glass and chrome. The electrode photomask is intended for use with a positive photoresist such as BPR-100 (see Chapter 2.4.3).

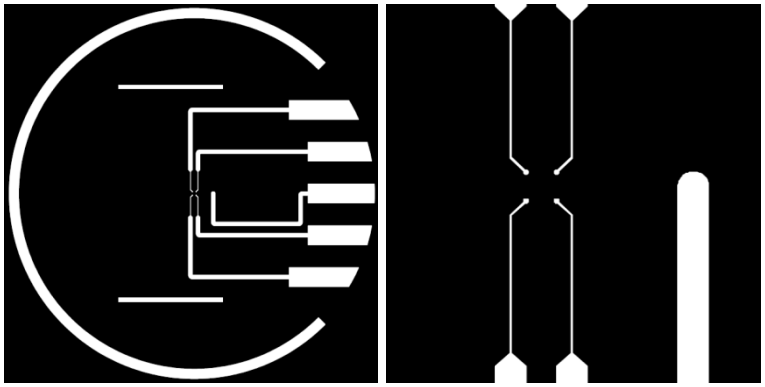

Figure 166 Photomask design for the custom-built electrode arrays. Left: the entire pattern is 19mm across, with 4 signal electrodes and one reference electrode. Right: each track narrows to 10µm ending in a 30µm pad, pitched 200µm apart. The reference electrode (200µm wide, left of image) is placed 1mm from the array, permitting a shorter microchannel if required.

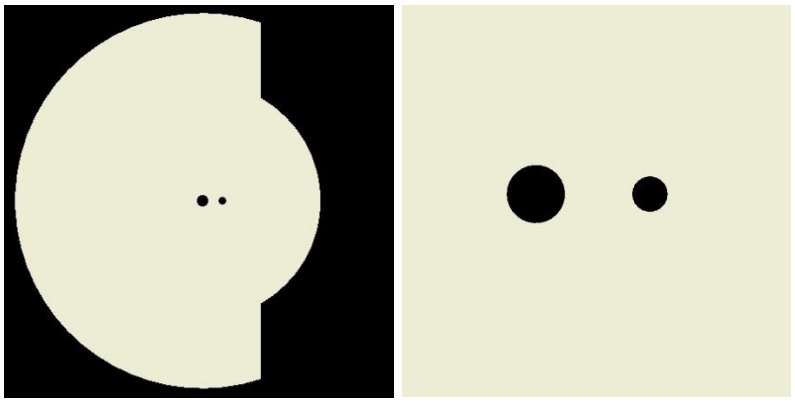

Figure 167 Photomask design for the insulation layer, to be rendered in the negative photoresist SU-8. Left: Again the pattern is 19mm across, with the left part of the coverslip not insulated so electrodes can be read. Right: Two gaps in the photoresist 1mm apart are left for the reference electrode (300µm across) and the 4 signal electrodes (500µm across).

The concept of these two photomasks is that they can be aligned (see Figure 168 below) to create an insulated region where only the ends of the electrodes are exposed, though there is the 500µm region between the signal electrodes that is not insulated, and was considered for use as a microwell.

As discussed in chapter 5.2.2 however, this technique is incompatible with a finite region of deposited ligand, and so cells will readily grow everywhere, including the insulated areas.

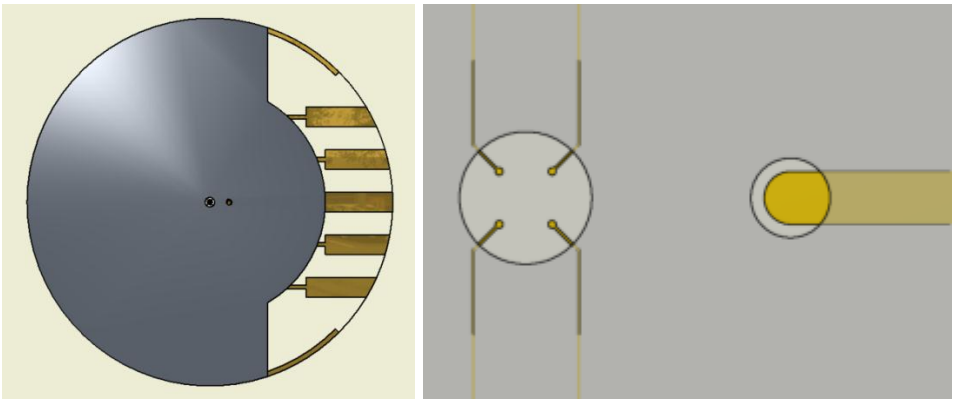

Figure 168 Concept (left) and close-up (right) of the SU-8 insulation over gold track. SU-8 is false-coloured blue to distinguish it from the glass substrate.

7.1.4 **Results**

The outcome of these fabrication methods are as follows:

7.1.4.1 ***Electrode layer fabrication***

Electrodes were formed by using the photolithographic protocol for BPR-100 (see chapter 2.4.3) and evaporating first 7nm titanium and then 20nm gold onto the glass (see chapter 2.3.3). These had mixed results (see Figure 169 and Figure 170):

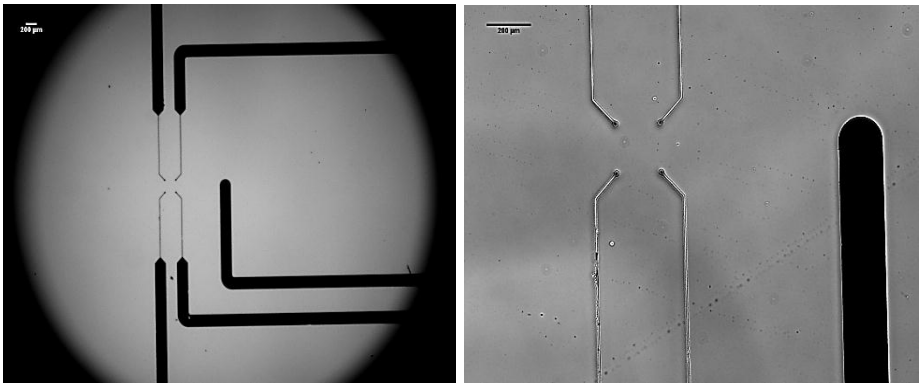

Figure 169 Left: a 1X magnification image of fabricated gold tracks. Tracks are composed of 20nm Au and 7nm Ti. Scale bar is 1mm. Right: a close-up of the electrode, scale bar 200µm. Signal tracks are 10µm wide and the reference is 200µm wide.

Some tracks formed mostly well-defined regions where metal had deposited as expected, as in Figure 169 above. Where the tracks appeared to have deposited as expected and all photoresist removed, impedance values were to be measured by placing a channel over the electrodes and filling with Neurobasal, then measuring the total resistance between the contact pads.

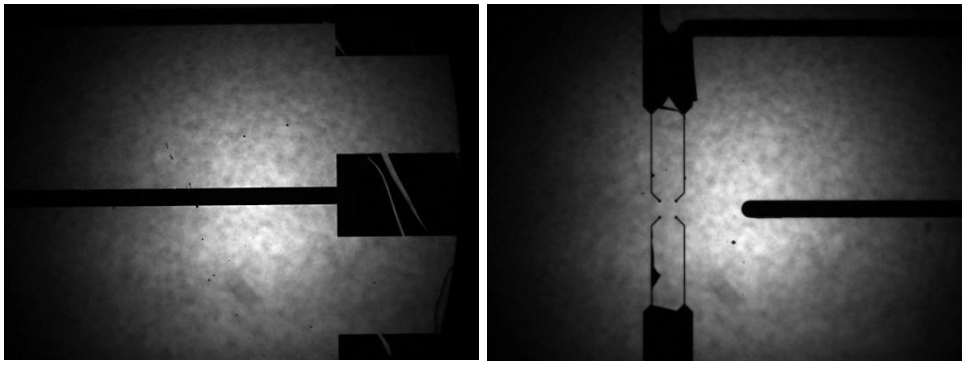

Figure 170 Left and right: different defects in the gold evaporation and lift-off. Left: a scratch or crack has appeared in the gold, as glass is visible behind the metal. The track is 200µm across and the pad is 1mm across. Right: where the tracks run together in parallel, photoresist with gold has not been successfully removed.

However, nearly all attempts revealed that after the photoresist lift-off step one of two issues was very common: either there was a gap in the track where metal should be, or the photoresist between tracks in close proximity has not been successfully removed.

Both open circuits and short circuits were thus formed in the tracks. Almost no tracks were fabricated completely free of these defects, particularly open circuits, and thus a robust quantitative assessment of their impedance was not possible. Of the few that were measurable, the recorded impedances were in excess of 1MΩ, indicating the gold features had not been deposited correctly.

This is an unfortunate result that should be addressed by reviewing the photolithographic steps taken, and isolating what step is causing the problems of broken or fused tracks.

7.1.4.2 *Insulation Layer fabrication*

The concept of aligned masks shown in Figure 168 worked well, with close alignment between SU-8 and gold features (Figure 171).

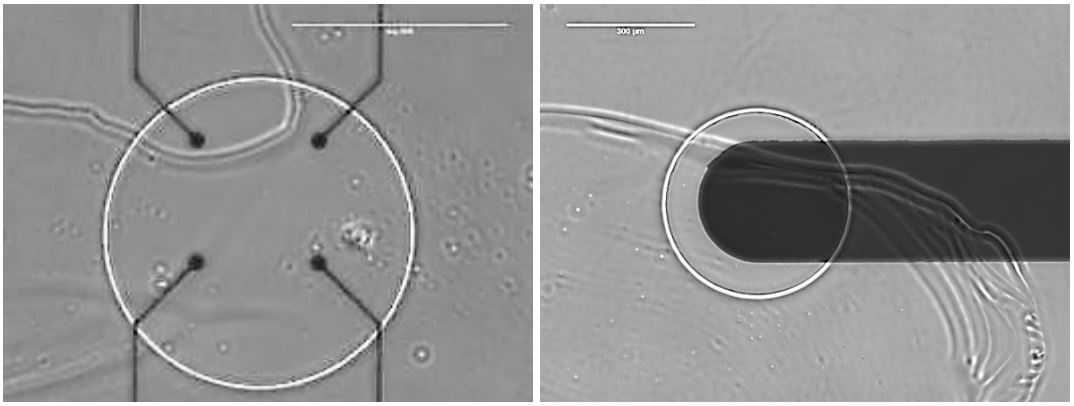

Figure 171 Image of SU-8 insulation aligned over evaporated gold tracks. Left (scale bar 500µm) are the four signal electrodes, while right (scale bar 300µm) is the reference electrode. Some residue and debris on the other side of the glass coverslip is visible in both images

A tape insulation layer was also possible and the concept is demonstrated in Figure 178, with a gold spot instead of electrodes. Thus there are reliable ways to construct insulated electrodes, though the electrodes themselves need to be improved, as discussed.

7.1.4.3 Electrode integration with microchannels

Electrode patterns were readily integrated with PDMS microchannels using any of the methods already described. A typical example is shown in Figure 172, using oxygen plasma and moulded channel formed previously with soft lithography.

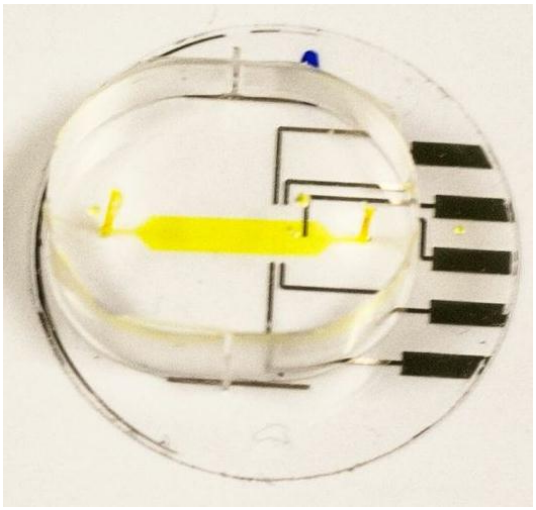

Figure 172 Electrodes in channel (which is highlighted with green food dye).

However without the insulation layer, the electrodes will not function correctly, as any mismatch in the length of track exposed to the media would have an effect on the track resistances.

7.1.4.4 Insulation integration with microchannels

This could have been done with an SU-8 layer using the nitrogen plasma bond method ((Zhang et al. 2011), see chapter 5.2.1). However, as for the microwell considerations outlined there, it was ultimately determined that using the tape would be logistically easier, especially with regard to integration with both the PDMS layers and deposition of a suitable cell ligand.

Conversely, the tape would not have been a precise track insulator due to the poor feature resolution (see chapter 5.2.2), given that the smallest feature that can be reliably cut is 1mm across.

A hybrid of the two techniques was feasible, in which electrodes were fabricated and then insulated with SU-8, before a tape microfluidic channel was attached to the SU-8. This was not ultimately done, however, and remains an option for future work.

7.1.4.5 Electrode read-off and voltage buffer amplifier circuit

In order to couple the action potentials from the gold electrodes to a suitable amplification and filtering stage, a connection similar to that used in the MCS 1060 head-stage is required. It must be able to reversibly attach to the microfluidic device, as depicted in Figure 173 below.

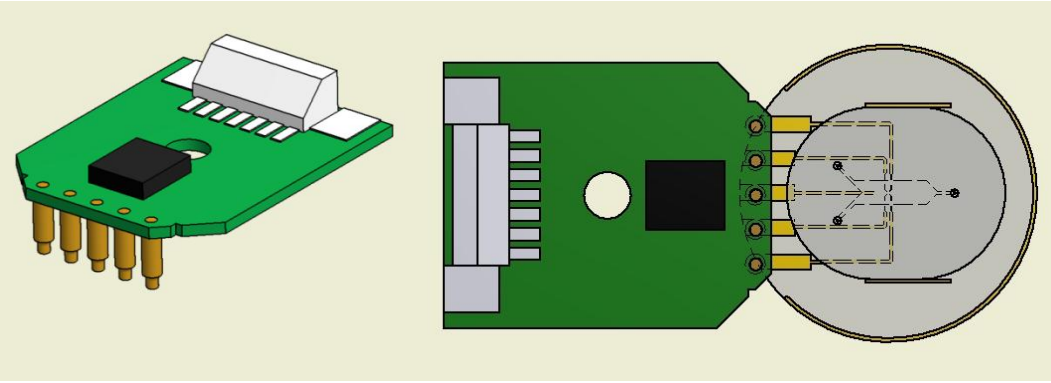

Figure 173 Concept of the signal read-out circuit. The board has 5 spring-loaded pins at the inputs and a 7-way socket to carry the signal outputs and power for the integrated circuit. The hole in the centre allows it to be mounted on a pillar (see later).

However, the circuit must be more than a simple connection. Each of the 4 input signals passes through a separate voltage follower circuit (see Figure 174). The LM339 op-amp in its voltage follower configuration acts as a bridging connection, and relays the input voltage without any gain, so that the

output voltage is identical. The circuit is necessary as it has very high input impedance to counter the high output impedance of the electrodes, and thus draws very little current from the electrode array. Conversely, it has very low output impedance, so the noise added is reduced, the current output is boosted, and crosstalk is avoided.

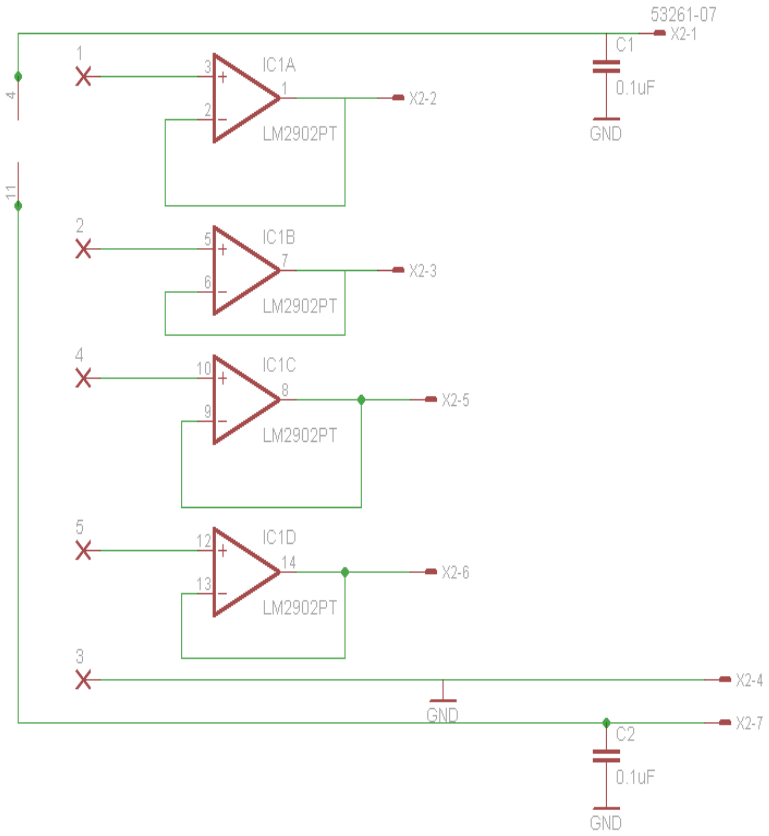

Figure 174 Schematic, designed in Eagle PCB software, of the 4-channel signal pre-amplifier. Decoupling capacitors are added to isolate the LM339 microchip (designated LM2092PT in schematic) and inputs from any high frequency signals in the power supply.

The completed PCB is designed to interface with the electrodes as spaced on the coverslip (Figure 175).

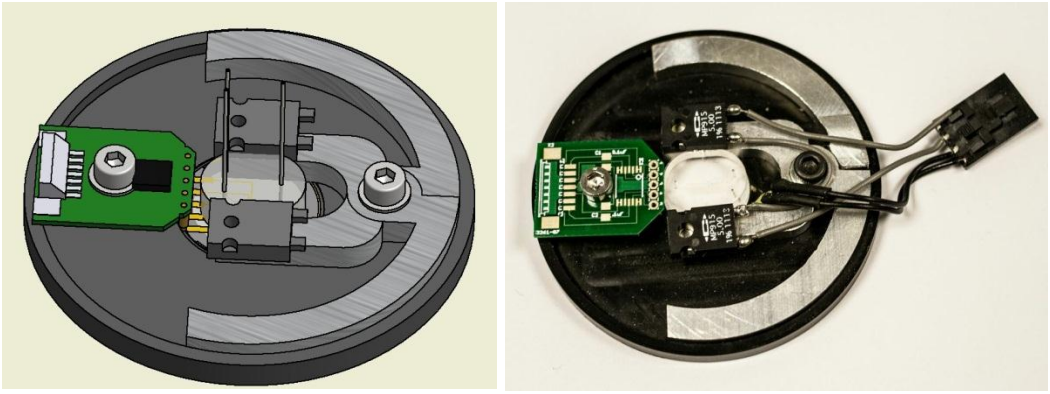

Figure 175 Left: 4-channel voltage follower circuit that can read off the voltage signals on the glass coverslip electrodes, by mean of spring loaded contact pins. Right: a photo of the PCB in position, without components.

The signals are relayed to the connector at the back, which leads to subsequent amplification and filtering stages. Design and fabrication are credited to Mr Gabriel Su. A channel of this type can be loaded in to the temperature regulation clamp and the PCB swung into position to interrogate the electrode pads. Further information is in appendix 10.4.5

7.1.5 Integration of an alternative recording method (SPR)

Recording action potentials with electrodes is often difficult to parse the activity of individual cells, because two neurons in close proximity to an electrode, or whose activity reaches the electrode at the same point in time, are indistinguishable. Highly complex analytical software is used to determine which neuron may have undergone the AP which is recorded at a particular electrode – this is known as ‘spike sorting’ (Rieke 1999) and is limited by the inability to detect all of the Action Potentials in a conventional neuronal culture, although this would be mitigated in a constrained (<500µm) area.

Improving resolution is possible, as mentioned in chapter 1.4.2, by placing more electrodes in the same space closer together, but this means making the electrodes smaller and hence increasing their impedance, and also greatly increases the difficulty of providing tracks to each electrode and recording from them all simultaneously.

7.1.6 Gold spots (SPR)

The alternative to electrode recording, as discussed in chapter 1.9, is to make use of the phenomenon Surface Plasmon Resonance (SPR) to detect changes in cell membrane permeability, and hence action potentials. The gold

layer is interrogated by a laser at 600nm. Because of the wavelength dependent dielectric constant of gold, which is 55nm at 580nm (Kuryoz et al. 2013b), the gold thickness must be around 50nm.

This has the advantage of requiring a simple geometry and no connecting tracks or insulation, and in theory very high spatial resolution. However, SPR cannot be used with a titanium adhesion layer, due to the loss of signal sensitivity caused by the titanium boundaries (Aouani et al. 2009), and consequently the ligand (3-mercaptopropyl) trimethoxysilane (MPTS) was used to form a metal-free wetting layer for the gold.

7.1.7 Design

As for the electrodes in the previous section, this was undertaken with a chrome photomask designed by JD Photo Tools Ltd based on an Autodesk Inventor design (see Figure 176).

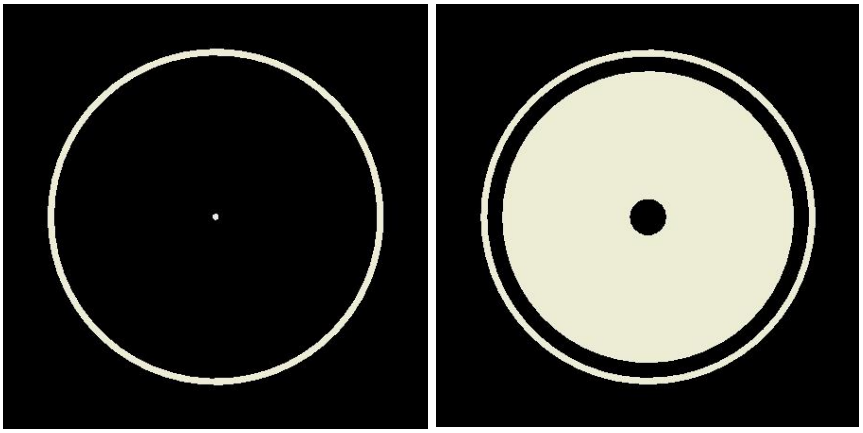

Figure 176 Photomasks for the 0.5mm (left) and 2mm (right) gold circles. In both cases a ring between 18.5mm and 19.5mm is left to permit concentric alignment of the gold on a 19mm coverslip. The 2mm design must be used with a negative photoresist such as AZ5214E.

A circle was chosen as it is a simpler shape to evaporate, and the field of view of most optical systems is circular. The sizes were chosen taking into consideration the expected field of view that could practically be realised with the optical elements available, and the microwell sizes found to be feasible in chapter 5.2. Specifically, the SPR camera scan limit is 0.5mm at 18X magnification, which is the optimal compromise between field of view size and the ability to discriminate individual neurons. In addition, the high speed (10kHz) camera developed by Dr Bo Fu (Fu et al. 2011) for high temporal

resolution has a field of view that is practically limited to 300µm across, with a pixel size (5µm) adequate to discern neurons (typically at least 10µm across). Thus a 500µm circle would have been best for optical purposes. However, as found in chapter 5.2, the tape microwells cannot be reliably cut to less than 1mm resolution, and so a 2mm circle was also considered.

7.1.8 Methods

The protocol for MPTS deposition (see chapter 2.3.2) was used to form the wetting layer. For the 0.5mm spot, the recipe for BPR-100 positive photoresist (section 2.4.3) while for the 2mm spot the image needed to be reversed and the image reversal resist AZ5214E was used (section 2.4.4). Photolithography was followed by gold evaporation as described in chapter 2.3.3, to a depth of 50nm.

7.1.9 Results

7.1.9.1 Evaporation of gold features onto MPTS

A comparison of the same feature on both titanium and MPTS wetting layers was carried out (see Figure 177), to check that the chemical ligand does not induce a degradation in the quality of gold attachment.

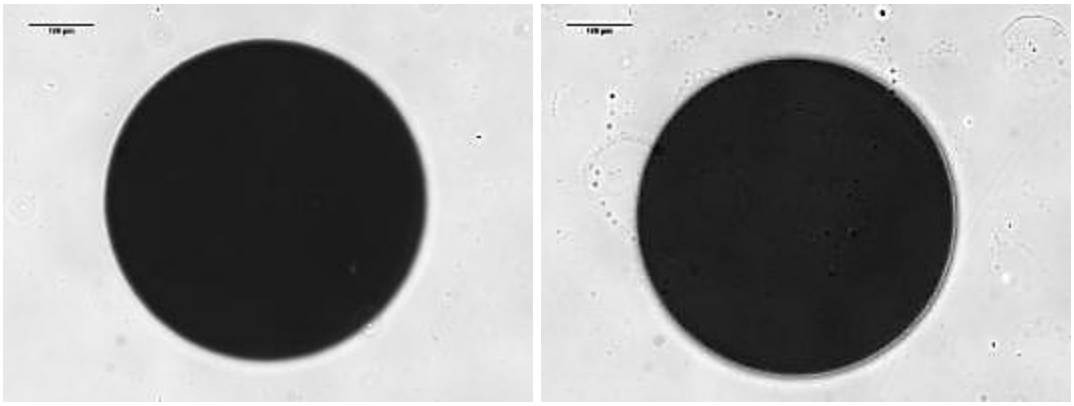

Figure 177 A 500µm circle of 20nm gold was evaporated onto (left) 7nm of titanium and (right) onto a deposited layer of MPTs. Scale bar is 100µm.

No noticeable change in feature quality was observed, suggesting that the gold adheres equally well to both surfaces. This is in contrast to the poor outcome of the electrodes (see Figure 170), and may indicate that small feature size and complex geometries are harder to fabricate successfully.

7.1.9.2 Integration with microwell

The cutting tool for tape microwells (Silhouette Cameo) cannot cut reliably a circular shape without distortion. Consequently a 1mm square is used instead (see Figure 178). The bond between the microwell tape layer and glass is strong, implying that the MPTS ligand does not affect subsequent layer adhesion.

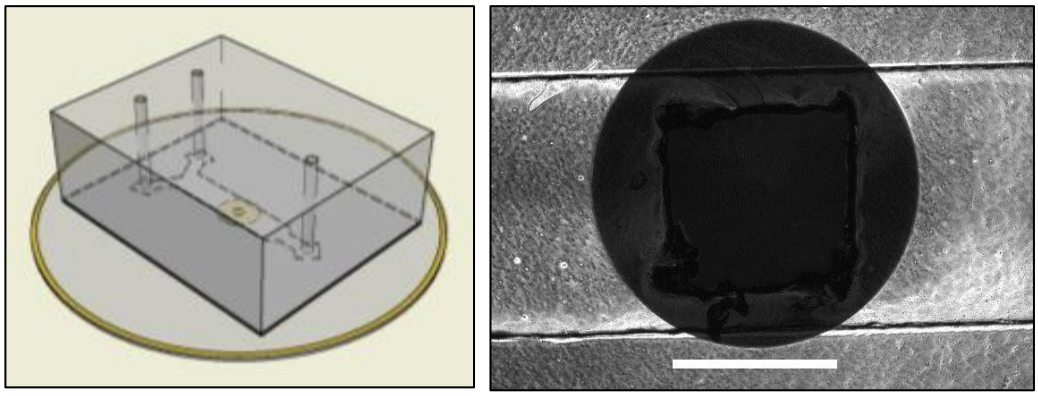

Figure 178 A 1.5mm wide microchannel and 1mm microwell formed with the tape xurography method, placed over a 2mm gold spot evaporated onto MPTS. Scale bar is 1mm.

Consequently it is clearly possible to grow a finite culture of neuronal cells in a microwell on a functionalised gold surface (see also chapter 5.2.2 for the growth of cells in such a microwell), where the gold is attached to the glass substrate in a fashion that does not impede interrogation using Surface Plasmon Resonance, and thus ultimately an electrode-free technique for recording all action potentials in a microfluidic cell culture is possible.

7.2 Chapter Conclusion

Gold electrodes and regions for SPR can be constructed and readily incorporated into the channel. The electrodes constructed demonstrate that it is possible to build an array of tailored size and geometry on the coverslip, though the general quality of the electrodes made indicates a change to the design and / or methods used may be necessary, in order to minimise the number of defects.

The metal geometries were readily integrated into microchannels with the use of silicone tape. A simple read-off circuit board to relay any action potentials recorded in the channel was designed and built, to interface with the temperature clamp previously built.

The quality of the bespoke electrodes was not optimal, with many track breaks and short circuits observed. However, if the photolithographic protocols could be adjusted to remove such defects, there is no reason why the electrodes could not be used in future.

Further, a system has been developed permitting the read-off of recorded signals from electrodes. This lays the groundwork for future development of bespoke micro electrode array development compatible with microfluidic cell culture.

In conclusion, such patterns can be deposited on glass and integrated with complex microfluidic geometries (microwells) with no loss of culture viability. The electrodes were not functional due to shorts and breaks in the tracks. Better fabrication protocols are needed if functional bespoke electrode arrays are to be utilised. At the time of thesis completion, this was a non-essential goal (given the availability of commercial MEAs which could be reversibly integrated with silicone tape microchannels), rather than an urgent necessity, and so it was not prioritised over ascertaining the reasons for inevitable culture death under perfusion (chapter 6). It is thus incomplete.

Future work is necessary in order to make viable electrodes and emulate the noise-shielded amplification and filtering stages already available in the MCS head-stage.

8 Discussion, conclusions, and future work

8.1 Aims and Outcomes of the thesis

This work aimed to provide a platform for research into reinforcement learning in neuronal networks, as part of a multidisciplinary investigation into the nature of *in vitro* neural signal encoding, and the formation of memory.

To achieve this, an essential element is the capacity to tightly couple the occurrences of electrical signalling and chemical reinforcement, so that a subset of the network connections was consistently reinforced while others were not. Based upon existing estimates of the time window necessary for the temporal correlation to be meaningful, it was clear that merely adding small agonist volumes to a much larger hydrostatic volume of culture liquid, as is typically done in many dose-response experiments, would not be adequate, due to the domination of diffusive transport over distances where the phenomenon is simply too slow to be useful. A hydrodynamic methodology was decided upon, where continually moving liquid containing the agonist could be brought into proximity with the cultured cells and then removed again in a short timescale. The approach was implemented by utilising microfluidic cell culture and fluid handling.

The overarching approach taken was two-fold:

i) Fabrication of a microfluidic chamber in which primary cultured neurons could grow in physiologically stable conditions indefinitely, confined to a single region that was completely accessible to electrical recording.

ii) Development of a fluid handling system that was capable of providing the flow rate transitions necessary to induce the spatiotemporally precise delivery and removal of a soluble agonist.

8.1.1 Primary cell survival in microfluidic devices

Firstly, a set of design criteria for the microchannels was arrived at, taking into account the intended functionality of the channel for rapid switching. The

geometry of the microchannel and the range of flow rates were explored using COMSOL modelling to find an optimal set of parameters. In particular, the latency of agonist delivery to a surface region within the channel following flow rate transition, the concentration gradient distinction achievable at different flow rates, and the range of flow rates compatible with neuronal survival (based on a literature emphasis of maximum permissible shear stress) were juggled to find the best compromise. As rapid switching for reinforcement on timescales relevant to synaptic plasticity is the overall point of the thesis, the latency parameter had the strongest weighting.

From this, a range of flow rates was arrived at, and regardless of the perfusion strategy that would be needed to implement the flow rate switching, it was evident that the channel fabrication method would need to ensure no leakage or device failure during perfusion.

As the microchannel must be compatible with electrical recording, the substrate on which metal patterns and ligands are deposited must be separately built to the microchannel, and a robust bond between channel and substrate is therefore critical.

Because of the range of chemical processes that would be performed on various aspects of the substrate and channel in order to create the microfluidic chips, it was necessary to confirm that it was possible to culture primary neurons in the assembled microfluidic devices independently of perfusion.

It has been demonstrated that the neurons are compatible with all photolithographic processes currently used, and can survive indefinitely on open coverslips. Barring a significant alteration to the processes used in the optimisation of surface patterning and electrode performance, there is no compatibility issue with any of the materials that were used.

It has also been demonstrated that the neurons are capable of surviving indefinitely in a microchannel, provided that the plating densities are comparable to open bath culture, namely more than 250 cells per mm^2. This was achieved by increasing the volumetric suspension density from under

500cells per µL to over 10 thousand per µL. The longevity of cells in these devices is not consistently worse than open culture (without a microchannel), as assessed by the morphology and density of connections at 14 div. Thus there is no inherent compatibility issue with the channel materials, channel geometry or adhesion surface treatments.

In order to interface with existing recording technologies such as the MEAs, different securing methods were used to reversibly attach the microchannels to the MEA. The method finally chosen was the use of silicone tape which can be removed without damaging the MEA or leaving residue. All methods used were found to be compatible with optimal cell growth, provided an appropriate plating density was subsequently used.

8.1.2 **Fluid handling system for perfusion and agonist delivery**

Based upon the design considerations arising from the previous chapter, it was clear that the fluid handling apparatus must be run at a flow rate between 10 and 100nL/s with a precision of 1nL/s in order to ensure unambiguous drug delivery, and that a switching time of less than 1 second was preferable. Excessive latency of more than 2-3 seconds would not be desirable, and any uncontrolled noise or drift which caused the interface of neuromodulator and buffer to fluctuate must be minimised, since the fluctuations could cause the interface to cross the network region and induce unintended reinforcement.

A syringe driver, the most readily available perfusion apparatus, was tested and found lacking in both stability and latency, since it oscillated about the target flow rate and took many tens of seconds to respond to a command change. A gas driven system, with pressure and flow rate feedback informing electro-pneumatic valves was instead developed, in collaboration with Mr Solomon Idinyang and Mr Sorka Abanu. It comprised three pressure driven pumps; with real-time control of two flow rates for agonist and buffer, and a constant opposing backpressure to prevent bubble formation. All sensor elements and valves were monitored and controlled with a LabVIEW control program using PID feedback algorithms. A prototype of this system was available, but was found to be critically unstable over long perfusion periods,

as the flow rate drifted away from the target before oscillating so drastically that cells were detached from the surface.

This system was then iteratively improved so that it now has the capacity to switch the ratio of laminar co-flows with high temporal precision. The flow rates can be adjusted by 100nL/s in less than 1 second, but this requires at least one of the two inlet pumps to be perfusing at 10nl/s, which is the high end of what was intended for shear tolerance. The stability of the system when not switching is under 0.3nL/s. The latency of the interface shift in the microchannel is slower than desired, around 3 seconds, but this is partly due to the distance the interface is required to move. That distance is determined by the extent of the electrical recording array the channel interfaces with. A smaller array would permit a narrower channel width and thus faster switching.

To ensure the microchannel was maintained at the correct temperature, a spring-loaded clamp which heated the PDMS chip was designed. This clamp could be placed at the sample plane of a microscope, and was also designed so that electrical recording from bespoke electrodes printed on a coverslip would be possible.

Soluble gases were delivered with the media at 5% CO_2, to ensure CO_2 and pH levels were physiologically appropriate.

8.1.3 **Network spatial confinement**

It was necessary to constrain cell culture to a single region, in order to ensure complete network activity recording and simultaneous agonist delivery. The plating density of this reduced region needed to be indistinguishable from the densities found to ensure healthy culture development in the previous chapters.

Using photolithographic techniques to selectively place ligands on gold regions was found to be insufficient for creating a viable culture on the region of interest. Initially a combination of low plating density and cytotoxic ethanol residue in the PDMS prevented cells survival in the channel, due to the order of channel bonding followed by AUT functionalization of the gold.

While a sufficiently high plating density was achieved in the absence of a channel, the cells were observed to migrate onto the gold after 2-3 div, having altered the glass surface with expressed glycoproteins so that they could grow on it.

Consequently even after the plating density and fabrication issues were resolved for gold patterns in microchannels, it was determined that confinement would only be possible with the use of an anti-fouling ligand such as fluorosilane, which would be incompatible with subsequent robust attachment of the channel to the patterned substrate.

The surface chemistry approach was therefore unsatisfactory both in terms of culture survival in one region of a microchannel, and of subsequent confinement to the region.

Cells were however successfully confined and cultured within a microwell formed by an aperture in a thin layer of PDMS or silicone tape. The plating density in the microwell could be adjusted to the correct level, by adjusting the suspension density per volume. Careful flushing of the liquid volume in the main microchannel removed cells from all other regions except the well.

It was noted however that by adding the well, an additional latency has been added to drug delivery, as the agonist must now travel the height of the well in order to stimulate cells at the bottom. This effect was explored in the following chapter.

8.1.4 **Perfusion and Culture Protection**

Neuronal cultures at 14 div grown in microchannels, with and without microwells, were perfused at the flow rates deemed acceptable in prior chapters. In particular, given the need to perfuse at relatively high flow rates in order to achieve the rapid interface shifting, cell survival at flow rates of 100nL/s was critical. This work was undertaken in collaboration with Mr Nitzan Herzog. It was found through live/dead assays of the perfused cells, and using a metric of 80% survival in the observed region as a benchmark of viability, that cultures did not survive more than 6 hours.

The working theory, in accordance with prevailing literature theory, is that the shear stress imposed on the neurons by the flow was considerably more significant than had been accounted for in prior channel design. Thus mitigation of the shear stress was attempted, by using a microwell to create a zone where flow rate would be much reduced.

It was determined through COMSOL modelling that microwells are capable of mitigating the effect of direct perfusion which prevents long term survival under flow, but this comes at the expense of increased latency, given that diffusion is now much more significant in the microwell. This negated the response time of the perfusion system, since a well deep enough to reduce shear to the level reported in literature would be so deep that it would take the agonist several seconds to diffuse into it.

A semi-permeable membrane approach was next attempted, in which a porous polycarbonate sheet under 20µm thick was interposed between the co-flows and the cell culture. This was expected to decouple the flow rate from the pharmacological content. The key advantage that would emerge if successful is that the flow rates could now be increased in magnitude without perturbing the cells, possible reducing the interface switching time to under a second.

The fabrication of such devices required the selection and integration of the polycarbonate membrane into a device with many layers. Precise orientation of the features in the layers was necessary, and this was addressed with a custom-built alignment tool which ensured all features were in the correct place.

Consideration was given to the perfusion apparatus needed to successfully control the developed multi-layer channels. Because of the perceived difficulty in procuring the flow rate sensors and developing a complex software architecture that could ensure rapid interface shifting above the membrane and stable low flow rates across the membrane, and because the pressure sensitivity estimated was barely achievable, the full potential of the multi-layer devices was not realised.

Some experiments were carried in the multi-layer devices to establish if the membrane would deflect under pressure into close proximity with the cells, and to see if cell longevity during perfusion under a membrane was improved. Because the cell compartment was sealed during these experiments, they cannot be used to infer what would happen in a device where there is some flux due to advection across the membrane.

Again, live/dead assays were used to assess whether the longevity of the culture was improved when perfusing at 100nL/s, but no significant improvement was observed. In addition, the electrical activity of cells in identical microfluidic devices with the polycarbonate membrane was monitored by an MEA both before perfusion commenced and for some time afterwards. In several instances, the average spike frequency fell to almost nothing within 1minute of flow beginning. Since it was considered unlikely that this could be due to shear perturbation as the convective transport was insignificant, the possibility of rapid concentration changes affecting cell signalling was explored.

A brief theoretical study suggests it is possible that essential cell signalling molecules, perhaps ions or larger molecules the size of dopamine, are lost by diffusion when the concentration in the drug delivery channel changes during perfusion, creating a steep concentration gradient that draws molecules away from the cells. However, this is speculative and cannot be proven here.

Overall, the many attempts to reduce shear stress have not resulted in any significant improvement in culture longevity; but altering the conditioning level of the media, and hence the concentration of neurotrophic molecules, does seem to have a significant impact on the cell longevity. This implies that the principal issue with using high flow rates when perfusing cultures of primary cells may not be the shear stress imposed, but the inability of the cells to maintain a physiologically appropriately high concentration of the neurotrophic factors needed to correctly exchange chemical cures with each other.

8.1.5 **Integration of novel recording strategies**

Because of the low spatial resolution of existing MEAs, and the thickness of the glass substrate, it was desirable to have the option of printing bespoke

electrode arrays on thin coverslips. Gold electrode geometries were printed on glass, as well as simpler gold spots on the MPTS ligand, for the potential use of surface plasmon resonance imaging.

The metal geometries were readily integrated into microchannels with the use of silicone tape. A simple read-off circuit board to relay any action potentials recorded in the channel was designed and built, to interface with the temperature clamp previously built.

The quality of the bespoke electrodes was not optimal, with many track breaks and short circuits observed. However, if the photolithographic protocols could be adjusted to remove such defects, there is no reason why the electrodes could not be used in future.

8.2 **Overall conclusions**

Neuronal cultures of a finite size were successfully grown in microchannels, on substrates capable of recording their electrical activity. Thus it was possible to create a small cultured network in which all the network activity can be detected, if integrated with a recording technique with sufficient spatial resolution. Although this is not a new result, it was important to establish the capacity to grow physiologically healthy cells before any assessment of neuromodulator could be considered.

Although the fluid handling system has not yet been successfully employed to perfuse over primary neurons without affecting their signalling, it is demonstrably capable of inducing precise spatial variation of a concentration gradient exposure over many minutes, and has been used for this purpose with cultured HEK cells, which respond to the measured gradient on a timescale indicating their sensitivity to low agonist concentrations.

Flowing media over the cultures in the microchannels has unfortunately affected neuronal network activity so drastically that the effect of chemical reinforcement pathway cannot be independently evaluated. All efforts to date seem to imply that the problem is not simply one of shear stress, but the concentration of neurotrophic factors and signalling molecules in the vicinity of the cells, though this is very speculative and further investigation is necessary.

This seems to draw a line under the possibility of using convection dominated delivery system *in vitro* to emulate what *in vivo* is a diffusion-dominated phenomenon. The delivery of neuromodulator to an entire network simultaneously in order to selectively reinforce certain connections has not been replicated here.

8.3 Potential future directions

In order to further the work achieved here and develop it into a key part of the larger project investigating neuronal encoding *in vitro*, a number of possible research directions could be followed:

8.3.1 Decoupling gas content from flow rate, and adding on-chip sensors

While the flow rate and temperature are directly measured, other crucial physicochemical parameters such as pH, oxygen and carbon dioxide levels are not directly measured, but assumed to lie in physiologically appropriate ranges due to the use of gas with 5% CO_2 and Neurobasal culture media. It would be prudent in the longer term to have a means of checking such parameters on-chip, by incorporating sensors in the microchannel. These could be in the form of ratiometric sensors which fluoresce according to the range of a parameter such as oxygen (Webster et al. 2007) or pH level (Nielsen et al. 2010)

Also, from the work done to date it emerges that using compressed gas to induce flow is inherently prone to bubble formation over long periods, since the channel is always at a lower pressure than the pressure vessels in which the gas is first dissolved into the liquid. Consequently, gas will eventually nucleate in the connecting flow lines and propagate into the culture region after several hours.

An alternative considered is to retain the linear, precise control afforded by the gas-over-liquid pumps developed, but to decouple the degassed liquid from the compressed gas by having a collapsible, airtight sac inside the Duran bottle.

This now means there is no gas content in the media as it is delivered. To provide the O_2/CO_2 levels necessary, a separate perfusion system of mixed

gases could flow through a separate microchannel network, separated from the liquid by a thin layer of gas-permeable PDMS (see Figure 179), by advancing the concept of multi-layer microfluidic chips demonstrated in chapters 5 and 6.

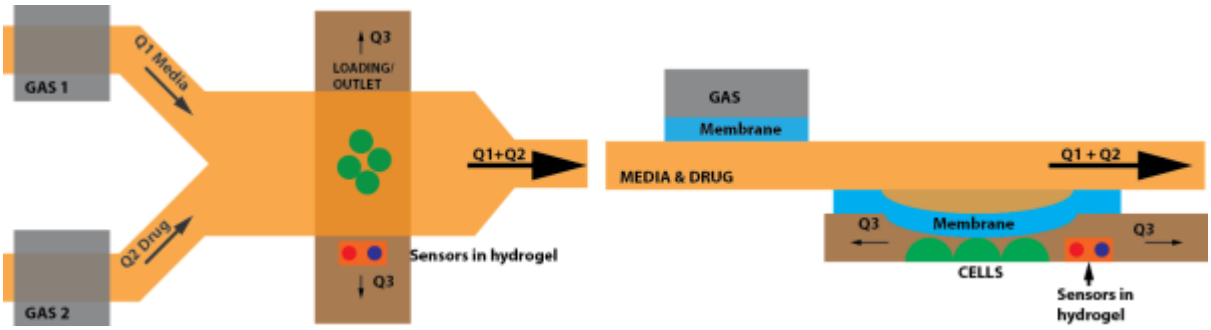

Figure 179 The concept of gas on chip. Different compressed gases can be added independently to the gas lines (grey) which passes over a thin (<100µm) PDMS region.

The gases can be diffused through a PDMS layer, into the media directly next to the cells(Chang et al. 2014). The diffusion coefficients of oxygen and carbon dioxide through PDMS are of the order of $5x10^{-6}$ cm^2/s (Lu et al. 2012), implying a maximum diffusion time of 100ms through 10µm thickness.

8.3.2 Optogenetic stimulation

Using electrodes to stimulate the neurons has several drawbacks. An electrode cannot record and induce activity simultaneously, and the current injected during stimulation can affect several cells within an area of effect, rather than a single specific neuron. A method of stimulation with very spatial precision that is completely decoupled from the recording technique would be preferable.

Recently, developments in Optogenetics (Zhang et al. 2006; Yizhar et al. 2011) have provided a way to stimulate neurons by transfecting them with light-sensitive molecules, which form photosensitive ion channels in the cell membrane. The transfected cells can subsequently be stimulated *in vitro* by exposing them to specific wavelengths of light which depolarise (at 480nm) or hyperpolarise (590nm) the neurons.

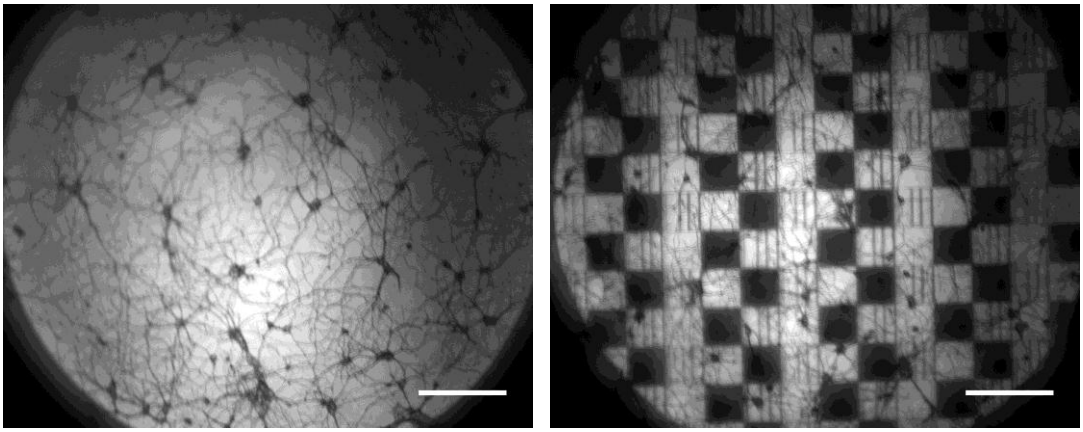

Figure 180 Images 1) A culture of fixed cells on a coverslip at the sample plane of the SLM, 2) Superimposing a simple light pattern onto the fixed culture. The vertical lines are a single pixel in width, demonstrating the spatial precision of the SLM. Scale bar 500µm.

A light projection system based upon a spatial light modulator (SLM) with these properties has been adapted (Fu 2012) (Johnstone 2011), which is capable of projecting patterns of light at both wavelengths with a spatial resolution of under 10µm (see Figure 180). Currently it can stimulate only at a few dozen Hz rather than the kHz needed, but this is a solvable issue with a sufficiently fast microprocessor. The patterns generated could be arbitrarily adjusted to target individual neurons while not affecting their neighbours.

8.3.3 Software integration for deterministic synchronisation of activity and reinforcement

The integration of software to deterministically combine electrical recordings and chemical reinforcement in response to those recordings was not attempted in this thesis. Since the perfusion system is controlled in LabVIEW and the same software can be used to control both the SLM and an SPR monitoring system, ultimately these three elements should be integrated under a common control program (see Figure 181). This is essential in order to finally achieve the electrical and reinforcement signal synchronisation, and begin answering the questions of behaviour and encoding of memory.

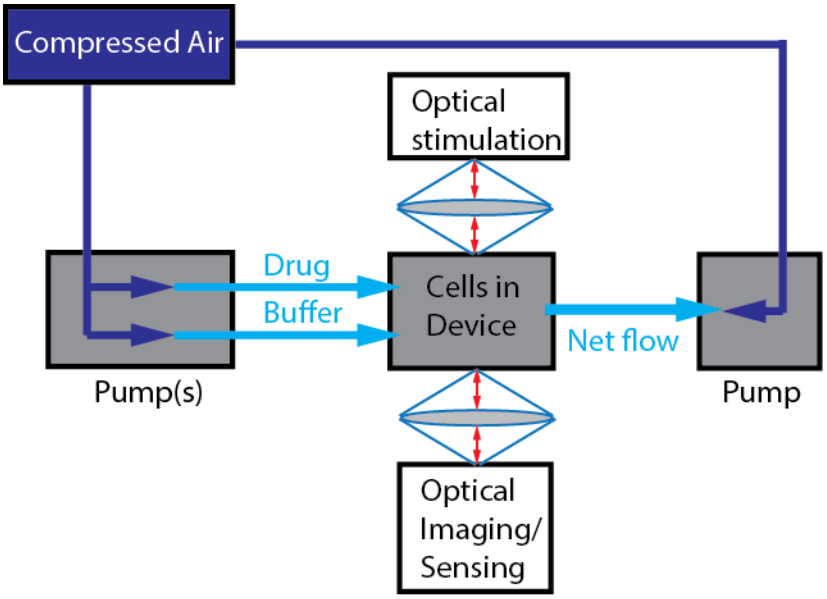

Figure 181 The complete integration of methods the microfluidic device has been designed to interface with, incorporating the concepts of optical recording (SPR) and stimulation (SLM).

It should possible to integrate the code running both the perfusion control and the recording rig, so that a simple neuronal activity metric, such as the average firing rate, or average firing inter-spike interval in a subset of the recorded cells, could be compared to an adjustable target which initiates a flow rate switching event. More complex reinforcement triggers could later follow based on increasingly more specific patterns of network activity.

8.4 Where does this work stand with regard to field of study

The later perfusion results indicate that the perturbation of primary cultured neuronal networks under flowing liquid in a microchannel, is due more to the loss of the chemical microenvironment through concentration change than to imposed shear stress on the cells. Many emerging microfluidic device publications claim an advantage for cell culture by mitigating shear stress without attending to the preservation of the chemical environment, but the latter appears to be an equally significant consideration.

Although the system as it stands has not been able to implement a reinforcement pathway that can deliver neuromodulators to primary cultured neurons without adversely affecting their signalling activity, the microchannel devices and fluid handling system developed during this thesis can both be readily applied to other experimental questions. The implications of successful

implementation of this fluid handling system are considerable. The ability to reliably deliver and wash off precise volumes of drugs in a matter of seconds, with no dilution of the intended concentration, will be of great benefit to researchers investigating the response of various cell types to different agonists.

9 References

Abaci, H.E. et al., 2012. Microbioreactors to manipulate oxygen tension and shear stress in the microenvironment of vascular stem and progenitor cells. *Biotechnology and applied biochemistry*, 59(2), pp.97–105.

Albutt, D.J., 2013. *Surface Chemistry Modification of Glass and Gold for Low Density Neural Cell Culture (PhD thesis)*. University of Nottingham.

Aouani, H. et al., 2009. Crucial Role of the Adhesion Layer on the Plasmonic Fluorescence Enhancement. *American Chemical Society Nano Letters*, 3(7), pp.2043–2048.

Arbuthnott, G.W. & Wickens, J., 2007. Space, time and dopamine. *Trends in neurosciences*, 30(2), pp.62–9.

Bae, A.J., Beta, C. & Bodenschatz, E., 2009. Rapid switching of chemical signals in microfluidic devices. *Lab on a chip*, 9(21), pp.3059–65.

Baigl, D., 2012. Photo-actuation of liquids for light-driven microfluidics: state of the art and perspectives. *Lab on a chip*, 12(19), pp.3637–53.

Balasubramanian, S., Revzin, A. & Simonian, A., 2006. Electrochemical Desorption of Proteins from Gold Electrode Surface. *Electroanalysis*, 18(19-20), pp.1885–1892.

Barbulovic-Nad, I., Au, S.H. & Wheeler, A.R., 2010. A microfluidic platform for complete mammalian cell culture. *Lab on a chip*, 10(12), pp.1536–42.

Bartholomeusz, D.A., Boutté, R.W. & Andrade, J.D., 2005. Xurography : Rapid Prototyping of Microstructures Using a Cutting Plotter. *Journal of Microelectromechanical Systems*, 14(6), pp.1364–1374.

Beta, C. et al., 2007. Flow Photolysis for Spatiotemporal Stimulation of Single Cells translocation of fluorescent fusion proteins in chemotactic. *Analytical chemistry*, 79(10), pp.3940–3944.

Bi, G. & Poo, M., 2001. S YNAPTIC M ODIFICATION BY C ORRELATED A CTIVITY : Hebb ' s Postulate Revisited. *Annual Review Neuroscience*, 24, pp.139–166.

Bi, G. & Poo, M., 1998. Synaptic Modifications in Cultured Hippocampal Neurons : Dependence on Spike Timing, Synaptic Strength, and Postsynaptic Cell Type. *The Journal of Neuroscience*, 18(24), pp.10464–10472.

References

Biffi, E., Piraino, F., et al., 2012. A microfluidic platform for controlled biochemical stimulation of twin neuronal networks. *Biomicrofluidics*, 6(2), pp.24106–2410610.

Biffi, E., Menegon, A., et al., 2012. Validation of long-term primary neuronal cultures and network activity through the integration of reversibly bonded microbioreactors and MEA substrates. *Biotechnology and bioengineering*, 109(1), pp.166–75.

Björklund, A. & Dunnett, S.B., 2007. Dopamine neuron systems in the brain: an update. *Trends in neurosciences*, 30(5), pp.194–202.

Bliss, T. & Lomo, T., 1973. Long-Lasting Potentiation of Synaptic Transmission in the Dentate Area of the Anaesthetised Rabbit following Stimulation of the Perforant Path. *Journal of Physiology*, (232), pp.331–356.

Breier, J.M. et al., 2010. Neural progenitor cells as models for high-throughput screens of developmental neurotoxicity: state of the science. *Neurotoxicology and teratology*, 32(1), pp.4–15.

Brewer, G.J., 1997. Isolation and culture of adult rat hippocampal neurons. *Journal of neuroscience methods*, 71(August 1996), pp.143–155.

Brewer, G.J. et al., 1993. Optimized survival of hippocampal neurons in B27-supplemented Neurobasal, a new serum-free medium combination. *Journal of neuroscience research*, 35(5), pp.567–76.

Bruus, H., 2014. ACOUSTOFLUIDICS : THEORY , SIMULATION , AND EXPERIMENT. In *18th International Conference on Miniaturized Systems for Chemistry and Life Sciences*. pp. 193–198.

Bruus, H., 2008. *Theoretical Microfluidics*, Oxford University Press.

Cate, D.M., Sip, C.G. & Folch, A., 2010. A microfluidic platform for generation of sharp gradients in open-access culture. *Biomicrofluidics*, 4(4), p.44105.

Chang, C. et al., 2014. A polydimethylsiloxane-polycarbonate hybrid microfluidic device capable of generating perpendicular chemical and oxygen gradients for cell culture studies. *Lab on a Chip*, 14, pp.3762–3772.

Chau, L., Doran, M. & Cooper-White, J., 2009. A novel multishear microdevice for studying cell mechanics. *Lab on a chip*, 9(13), pp.1897–902.

Chueh, B. et al., 2007. Leakage-Free Bonding of Porous Membranes into Layered Microfluidic Array Systems. *Analytical chemistry*, 79(9), pp.3504–3508.

Chung, B.G. et al., 2005. Human neural stem cell growth and differentiation in a gradient-generating microfluidic device. *Lab on a chip*, 5(4), pp.401–6.

Claverol-Tinturé, E. et al., 2005. Multielectrode arrays with elastomeric microstructured overlays for extracellular recordings from patterned neurons. *Journal of neural engineering*, 2(2), pp.L1–7.

Cooksey, G. a, Sip, C.G. & Folch, A., 2009. A multi-purpose microfluidic perfusion system with combinatorial choice of inputs, mixtures, gradient patterns, and flow rates. *Lab on a chip*, 9(3), pp.417–26.

Croft, W. et al., 2016. Ensemble encoding of dynamic stimuli in cellular calcium signals. *In Press*.

Delivopoulos, E., Minev, I.R. & Lacour, S., 2011. Evaluation of negative photo-patternable PDMS for the encapsulation of neural electrodes. In *5th IEEE International EMBS Conference on Neural Engineering*. pp. 490–494.

Delivopoulos, E., Murray, A.F. & Curtis, J.C., 2010. Effects of parylene-C photooxidation on serum-assisted glial and neuronal patterning. *Journal of biomedical materials research. Part A*, 94(1), pp.47–58.

Dinh, N.-D. et al., 2013. Microfluidic construction of minimalistic neuronal co-cultures. *Lab on a chip*, 13(7), pp.1402–12.

Duong, T.Q. et al., 2001. Extracellular Apparent Diffusion in Rat Brain. *Magnetic Resonance in Medicine*, 45, pp.801–810.

Eddings, M. a, Johnson, M. a & Gale, B.K., 2008. Determining the optimal PDMS–PDMS bonding technique for microfluidic devices. *Journal of Micromechanics and Microengineering*, 18(6), p.067001.

Fu, B., 2012. *A Configurable Real-Time Adaptive Imaging and Illumination System (PhD thesis)*. University of Nottingham, UK.

Fu, B., Pitter, M.C. & Russell, N.A., 2011. A reconfigurable real-time compressive-sampling camera for biological applications. *PloS one*, 6(10), p.e26306.

Gross, G.W., 1977. A new fixed-array multi-microelectrode system designed for long-term monitoring of extracellular single unit neuronal activity in vitro. *Neuroscience Letters*, 6(2-2), pp.101–105.

Gruart, A. et al., 2015. Functional basis of associative learning and their relationships with long-term potentiation evoked in the involved neural circuits: Lessons from studies in behaving mammals. *Neurobiology of learning and memory*, 124, pp.3–18.

Guenat, O.T. et al., 2006. Development of an Array of Ion-Selective Microelectrodes Aimed for the Monitoring of Extracellular Ionic Activities. *Analytical Chemistry*, 78(21), pp.7453–7460.

Harrison, R., 1907. Observations on the Living Developing Nerve Fiber. *Proceeding of the Society for Experimental Biology and Medicine*, 4, pp.140–143.

Hennemeyer, M. et al., 2008. Cell proliferation assays on plasma activated SU-8. *Microelectronic Engineering*, 85(5-6), pp.1298–1301.

Herzog, N. et al., 2014. RAPID DRUG DELIVERY TO IN VITRO NEURONAL CULTURES. In *18th International Conference on Minituarized Systems for Chemistry and Life Sciences*. San Antonio, Texas.

Huang, P.H. et al., 2014. TUNABLE MICROFLUIDIC PUMP ENABLED BY ACOUSTICALLY OSCILLATED SHARP-EDGES. In *18th International Conference on Miniaturized Systems for Chemistry and Life Sciences*. pp. 291–293.

Joanne Wang, C. et al., 2008. A microfluidics-based turning assay reveals complex growth cone responses to integrated gradients of substrate-bound ECM molecules and diffusible guidance cues. *Lab on a chip*, 8(2), pp.227–37.

Johnstone, A., 2011. *An Illumination System for Controlling Neural Activity (MSc thesis)*. University of Nottingham, UK.

De Jong, J., Lammertink, R.G.H. & Wessling, M., 2006. Membranes and microfluidics: a review. *Lab on a chip*, 6(9), pp.1125–39.

Kang, J.H., Um, E. & Park, J.-K., 2009a. Fabrication of a poly(dimethylsiloxane) membrane with well-defined through-holes for three-dimensional microfluidic networks. *Journal of Micromechanics and Microengineering*, 19(4), p.045027.

Kang, J.H., Um, E. & Park, J.-K., 2009b. Fabrication of a poly(dimethylsiloxane) membrane with well-defined through-holes for three-dimensional microfluidic networks. *Journal of Micromechanics and Microengineering*, 19(4), p.045027.

Kasthuri, N. et al., 2015. Saturated Reconstruction of a Volume of Neocortex. *Cell*, 162(3), pp.648–661.

Kebabian, J.W., Petzold, G.L. & Greengard, P., 1972. Dopamine-Sensitive Adenylate Cyclase in Caudate Nucleus of Rat Brain, and Its Similarity to the “Dopamine Receptor.” *Proceedings of the National Academy of Sciences of the United States of America*, 69(8), pp.2145–2149.

Kim, J., Surapaneni, R. & Gale, B.K., 2009. Rapid prototyping of microfluidic systems using a PDMS/polymer tape composite. *Lab on a chip*, 9(9), pp.1290–3.

Kim, L. et al., 2007a. A practical guide to microfluidic perfusion culture of adherent mammalian cells. *Lab on a chip*, 7(6), pp.681–94.

Kim, L. et al., 2007b. A practical guide to microfluidic perfusion culture of adherent mammalian cells. *Lab on a chip*, 7(6), pp.681–94.

Kim, T., Pinelis, M. & Maharbiz, M.M., 2009. Generating steep, shear-free gradients of small molecules for cell culture. *Biomedical microdevices*, 11(1), pp.65–73.

Kim, W.R. et al., 2014. Surface-printed microdot array chips for the quantification of axonal collateral branching of a single neuron in vitro. *Lab on a chip*, 14(4), pp.799–805.

Kleinfeld, D., 1988. Controlled Outgrowth of Dissociated Neurons on Patterned Substrates. *Journal of Neuroscience*, 8(11), pp.4098–4120.

Kleinfeld, D. & Sompolinsky, H., 1988. ASSOCIATIVE NEURAL NETWORK MODEL FOR THE GENERATION OF TEMPORAL PATTERNS. *Journal of Biophysics*, 54, pp.1039–1051.

Kolnik, M., Tsimring, L.S. & Hasty, J., 2012a. Vacuum-assisted cell loading enables shear-free mammalian microfluidic culture. *Lab on a chip*, 12(22), pp.4732–7.

Kolnik, M., Tsimring, L.S. & Hasty, J., 2012b. Vacuum-assisted cell loading enables shear-free mammalian microfluidic culture. *Lab on a chip*, 12(22), pp.4732–7.

Kondo, E. et al., 2014. Microfluidic perfusion cell culture system confined in 35 mm culture dish for standard biological laboratories. *Journal of bioscience and bioengineering*, 118(3), pp.356–8.

Koschwanez, J.H., Carlson, R.H. & Meldrum, D.R., 2009. Thin PDMS films using long spin times or tert-butyl alcohol as a solvent. *PloS one*, 4(2), p.e4572.

Kuczenski, B. et al., 2009. Probing cellular dynamics with a chemical signal generator. *PloS one*, 4(3), p.e4847.

Kuczenski, B., LeDuc, P.R. & Messner, W.C., 2007. Pressure-driven spatiotemporal control of the laminar flow interface in a microfluidic network. *Lab on a chip*, 7(5), pp.647–9.

Kuffler, S., Nicholls, J., & Martin, A., 1984. *From Neuron to Brain: A Cellular Approach to the Function of the Nervous System* 2nd ed., Sunderland, Massachusetts: Sinauer Associates Inc.

Kumamoto, J. et al., 2015. Effects of medium flow on axon growth with or without nerve growth factor. *Biochemical and Biophysical Research Communications*, 465(1), pp.26–29.

Kuryoz, P.Y., Poperenko, L. V. & Kravets, V.G., 2013a. Correlation between dielectric constants and enhancement of surface plasmon resonances for thin gold films. *Physica Status Solidi (a)*, 210(11), pp.2445–2455.

Kuryoz, P.Y., Poperenko, L. V. & Kravets, V.G., 2013b. Correlation between dielectric constants and enhancement of surface plasmon resonances for thin gold films. *Physica Status Solidi (a)*, 210(11), pp.2445–2455.

Kwiat, M. et al., 2012. Highly Ordered Large-Scale Neuronal Networks of Individual Cells − Toward Single Cell to 3D Nanowire Intracellular Interfaces. *Applied Materials and Interfaces*, 4, pp.3542–3549.

Lee, J.N. et al., 2004. Compatibility of Mammalian Cells on Surfaces of Poly (dimethylsiloxane). *Langmuir*, (20), pp.11684–11691.

Lee, K., He, J. & Wang, L., 2004. Benzocyclobutene (BCB) based neural implants with microfluidic channel. *Conference proceedings : ... Annual International Conference of the IEEE Engineering in Medicine and Biology Society. IEEE Engineering in Medicine and Biology Society. Conference*, 6, pp.4326–9.

Lee, P.J. et al., 2005. Nanoliter Scale Microbioreactor Array for Quantitative Cell Biology. *Biotechnology and bioengineering*, 94(1), pp.5–14.

Levinson, H.J., 2005. *Principles of Lithography* 2nd ed. H. J. Levinson, ed., Washington: SPIE Press.

Li, C. et al., 2004. Bidirectional Modification of Presynaptic Neuronal Excitability Accompanying Spike Timing-Dependent Synaptic Plasticity. *Neuron*, 41, pp.257–268.

Li, Z. et al., 2014. Syringe-pump-induced fluctuation in all-aqueous microfluidic system implications for flow rate accuracy. *Lab on a chip*, 14(4), pp.744–9.

Lin, Y. et al., 2013. Evaluating the Diffusion Coefficient of Dopamine at the Cell Surface During Amperometric Detection: Disk vs Ring Microelectrodes. *Analytical chemistry*, 85, pp.6421–6428.

Liu, M. et al., 2013. Galanin protects against nerve injury after shear stress in primary cultured rat cortical neurons. *PloS one*, 8(5), p.e63473.

Lochovsky, C., Yasotharan, S. & Günther, A., 2012. Bubbles no more: in-plane trapping and removal of bubbles in microfluidic devices. *Lab on a chip*, 12(3), pp.595–601.

Lovchik, R.D., Tonna, N., et al., 2010. A microfluidic device for depositing and addressing two cell populations with intercellular population communication capability. *Biomedical microdevices*, 12(2), pp.275–82.

Lovchik, R.D., Bianco, F., et al., 2010. Overflow microfluidic networks for open and closed cell cultures on chip. *Analytical chemistry*, 82(9), pp.3936–42.

Lovchik, R.D., Wolf, H. & Delamarche, E., 2011. High-grade optical polydimethylsiloxane for microfluidic applications. *Biomedical microdevices*, 13(6), pp.1027–32.

Lu, C. et al., 2012. Modeling Gas Transport and Reactions in Polydimethylsiloxane. In *TOUGH Symposium 2012*.

Luo, Y. & Zare, R.N., 2008. Perforated membrane method for fabricating three-dimensional polydimethylsiloxane microfluidic devices. *Lab on a chip*, 8(10), pp.1688–94.

Lutz, C. et al., 2008. Holographic photolysis of caged neurotransmitters. *Nature Methods*, 5(9), pp.821–827.

Majumdar, D. et al., 2011. Co-culture of neurons and glia in a novel microfluidic platform. *Journal of neuroscience methods*, 196(1), pp.38–44.

Marimuthu, M. & Kim, S., 2013. Pumpless steady-flow microfluidic chip for cell culture. *Analytical biochemistry*, 437(2), pp.161–3.

Martin, S.J., Grimwood, P.D. & Morris, R.G.M., 2000. S YNAPTIC P LASTICITY AND M EMORY : An Evaluation of the Hypothesis. *Annual Review Neuroscience*, (Hebb 1949), pp.649–711.

McAdams, E. et al., 2006. Characterization of gold electrodes in phosphate buffered saline solution by impedance and noise measurements for biological applications. In *28th IEEE EMBS Annual International Conference*. pp. 4594–4597.

Melai, J. et al., 2009. The electrical conduction and dielectric strength of SU-8. *Journal of Micromechanics and Microengineering*, 19(6), p.065012.

Meyvantsson, I. & Beebe, D.J., 2008. Cell culture models in microfluidic systems. *Annual review of analytical chemistry (Palo Alto, Calif.)*, 1, pp.423–49.

Millet, L.J. et al., 2010. Guiding neuron development with planar surface gradients of substrate cues deposited using microfluidic devices. *Lab on a chip*, 10(12), pp.1525–35.

References

Millet, L.J. et al., 2007. Microfluidic devices for culturing primary mammalian neurons at low densities. *Lab on a chip*, 7(8), pp.987–94.

Millet, L.J. & Gillette, M.U., 2012. New perspectives on neuronal development via microfluidic environments. *Trends in neurosciences*, 35(12), pp.752–61.

Monat, C., Domachuk, P. & Eggleton, B., 2007. Integrated optofluidics : A new river of light. *Nature Photonics*, 1(February), pp.106–114.

Morel, M. et al., 2012. Concentration landscape generators for shear free dynamic chemical stimulation. *Lab on a chip*, 12(7), pp.1340–6.

Multi Channel Systems, 2014. *USB-ME64-System Manual*,

Multichannel Systems, 2014. Microelectrode Array (MEA) Manual.

Nguyen, T.D. et al., 2013. Tension-induced neurite growth in microfluidic channels. *Lab on a chip*, pp.3735–3740.

Nielsen, L.J. et al., 2010. Dual fluorescent labelling of cellulose nanocrystals for pH sensing. *Chemical communications (Cambridge, England)*, 46(47), pp.8929–31.

Nikon Instruments, 2016. Microscope Objectives for Bioscience. , p.15.

Obara, M., Szeliga, M. & Albrecht, J., 2008. Regulation of pH in the mammalian central nervous system under normal and pathological conditions: facts and hypotheses. *Neurochemistry international*, 52(6), pp.905–19.

Ou, J., Ren, C.L. & Pawliszyn, J., 2010. A simple method for preparation of macroporous polydimethylsiloxane membrane for microfluidic chip-based isoelectric focusing applications. *Analytica chimica acta*, 662(2), pp.200–5.

Palyvoda, O., Chen, C.-C. & Auner, G.W., 2007. Culturing neuron cells on electrode with self-assembly monolayer. *Biosensors & bioelectronics*, 22(9-10), pp.2346–50.

Peck, R.A. & Martyniuk, J., 1995. Toward the ultimate metal microelectrode. *Journal of Neuroscience Methods*, 63, pp.175–183.

Priest, C., 2010. Surface patterning of bonded microfluidic channels. *Biomicrofluidics*, 4(3), p.32206.

Prucker, O. et al., 1999. Photochemical Attachment of Polymer Films to Solid Surfaces via Monolayers of Benzophenone Derivatives. *Journal of the American Chemical Society*, 121(38), pp.8766–8770.

Prucker, O. & Park, I., 1999. Photolithographic structuring of surface-attached polymer monolayers. *Materials Science and Engineering C*, 8-9, pp.291–297.

Rey, H.G. et al., 2015. Single-cell recordings in the human medial temporal lobe. *Journal of anatomy*, 227(4), pp.394–408.

Rhee, S.W. et al., 2005. Patterned cell culture inside microfluidic devices. *Lab on a chip*, 5(1), pp.102–7.

Ricks, C.B. et al., 2014. Extracellular matrices, artificial neural scaffolds and the promise of neural regeneration. *Neural regeneration research*, 9(17), pp.1573–7.

Roberts, J.G. et al., 2013. *Real-Time Chemical Measurements of Dopamine Release in the Brain* N. Kabbani, ed., Totowa, NJ: Humana Press.

Robinson, D.A., 1968. The Electrical Properties of Metal Microelectrodes. *Proceedings of the IEEE*, 56(6), pp.1065–1071.

Rolston, J.D., Gross, R.E. & Potter, S.M., 2009. A low-cost multielectrode system for data acquisition enabling real-time closed-loop processing with rapid recovery from stimulation artifacts. *Frontiers in neuroengineering*, 2(July), p.12.

Samel, B., Chowdhury, M.K. & Stemme, G., 2007. The fabrication of microfluidic structures by means of full-wafer adhesive bonding using a poly(dimethylsiloxane) catalyst. *Journal of Micromechanics and Microengineering*, 17(8), pp.1710–1714.

Shameli, S.M. et al., 2011. Fully integrated PDMS/SU-8/quartz microfluidic chip with a novel macroporous poly dimethylsiloxane (PDMS) membrane for isoelectric focusing of proteins using whole-channel imaging detection. *Electrophoresis*, 32(3-4), pp.333–9.

Shi, J. et al., 2007. Patterning Biomolecules with a Water-Soluble Release and Protection Interlayer. *Langmuir*, 23, pp.11377–11380.

Shleev, S. et al., 2005. Direct electron transfer between copper-containing proteins and electrodes. *Biosensors & bioelectronics*, 20(12), pp.2517–54.

Sip, C.G., Bhattacharjee, N. & Folch, A., 2014. Microfluidic transwell inserts for generation of tissue culture-friendly gradients in well plates. *Lab on a chip*, 14(2), pp.302–14.

Suzuki, M. et al., 2014. HIGH POWER MINIATURE PUMP FOR MICRONEEDLE BASED ON THREE-STAGE SUCTION USING CAPILLARY FLOW , ELECTRO-OSMOTIC FLOW , AND SUPER

ABSORBENT POLYMER. In *18th International Conference on Miniaturized Systems for Chemistry and Life Sciences*. pp. 2226–2228.

Tang, L. & Lee, N.Y., 2010. A facile route for irreversible bonding of plastic-PDMS hybrid microdevices at room temperature. *Lab on a chip*, 10(10), pp.1274–80.

Taylor, A.M. et al., 2010. Microfluidic local perfusion chambers for the visualization and manipulation of synapses. *Neuron*, 66(1), pp.57–68.

Taylor, A.M. et al., 2003. Microfluidic Multicompartment Device for Neuroscience. *Langmuir*, 19, pp.1551–1556.

Taylor, A.M. & Jeon, N.L., 2010. Micro-scale and microfluidic devices for neurobiology. *Current opinion in neurobiology*, 20(5), pp.640–7.

Théry, M., 2010. Micropatterning as a tool to decipher cell morphogenesis and functions. *Journal of cell science*, 123(Pt 24), pp.4201–13.

Thomas, C., 1972. Miniature Microelectrode Array to monitor Bioelectric Activity of Cultured Cells. *Experimental Cell Research*, 74(1), pp.61–66.

Thompson, C.S. & Abate, A.R., 2013. Adhesive-based bonding technique for PDMS microfluidic devices. *Lab on a chip*, 13(4), pp.632–5.

Toh, Y.C. & Voldman, J., 2010. MULTIPLEX MICROFLUIDIC PERFUSION IDENTIFIES SHEAR STRESS. In *14th International Conference on Miniaturized Systems for Chemistry and Life Sciences*. pp. 10–12.

Tong, Z. et al., 2015. A microfluidic neuronal platform for neuron axotomy and controlled regenerative studies. *RSC Adv.*, 5(90), pp.73457–73466.

Tovee, M.J., 1994. How fast is the speed of thought ? *Current Biology*, 4(12), pp.1125–1127.

Wang, L. et al., 2010. Chemical and physical modifications to poly(dimethylsiloxane) surfaces affect adhesion of Caco-2 cells. *Journal of biomedical materials research. Part A*, 93(4), pp.1260–71.

Wang, L. et al., 2009. Patterning bio-molecules for cell attachment at single cell levels in PDMS microfluidic chips. *Microelectronic Engineering*, 86(4-6), pp.1462–1464.

Webster, A. et al., 2007. The delivery of PEBBLE nanosensors to measure the intracellular environment. *Biochemical Society Transactions*, 35, pp.538–543.

Wheeler, B.B.C., Ieee, F. & Brewer, G.J., 2010. Designing Neural Networks in Culture. *Proceedings of the IEEE*, 98(3), pp.398–406.

Whitesides, G.M., 2002. Poly (dimethylsiloxane) as a Material for Fabricating Microfluidic Devices. *Accounts of chemical research*, 35(7), pp.491–499.

Whitesides, G.M. et al., 2001. Soft lithography in biology and biochemistry. *Annual review of biomedical engineering*, 3, pp.335–73.

Whitesides, G.M., 2006. The origins and the future of microfluidics. *Nature*, 442(7101), pp.368–73.

Wu, H.-W., Lin, C.-C. & Lee, G.-B., 2011. Stem cells in microfluidics. *Biomicrofluidics*, 5(1), p.13401.

Xu, S. et al., 2015. A rapid microfluidic technique for integrated viability determination of adherent single cells. *Analytical and bioanalytical chemistry*, 407(5), pp.1295–301.

Yagishita, S. et al., 2014. A critical time window for dopamine actions on the structural plasticity of dendritic spines. *Science*, 345(6204), pp.1616–1620.

Yamada, A. et al., 2009. A Rapid Microfluidic Switching System for Analysis at the Single Cellular Level. *IEEE Transactions on Nanobioscience*, 8(4), pp.306–311.

Yizhar, O. et al., 2011. Optogenetics in neural systems. *Neuron*, 71(1), pp.9–34.

Yoon, S.-H. & Mofrad, M.R.K., 2011. Cell adhesion and detachment on gold surfaces modified with a thiol-functionalized RGD peptide. *Biomaterials*, 32(30), pp.7286–96.

Young, E.W.K. & Beebe, D.J., 2010. Fundamentals of microfluidic cell culture in controlled microenvironments. *Chemical Society reviews*, 39(3), pp.1036–1048.

Zakaria, S. et al., 2014. The electrical breakdown of thin dielectric elastomers: thermal effects Y. Bar-Cohen, ed. , p.90562V.

Zhang, F. et al., 2006. Channelrhodopsin-2 and optical control of excitable cells. *Nature Methods*, 3(10), pp.785–792.

Zhang, Y.S. et al., 2014. A HIGHLY EFFICIENT BUBBLE TRAP FOR CONTINUOUS REMOVAL OF GAS BUBBLES FROM MICROFLUIDIC DEVICES. In *18th International Conference on Miniaturized Systems for Chemistry and Life Sciences*. pp. 730–732.

Zhang, Yulong et al., 2010. Application of SU-8 as the Insulator toward a Novel Planar Microelectrode Array for Extracellular Neural Recording. In *5th IEEE International Conference on Nano/Micro Engineered and Molecular Systems*. pp. 395–398.

Zhang, Z. et al., 2011. Sealing SU-8 microfluidic channels using PDMS. *Biomicrofluidics*, 5(4), pp.46503–465038.

Zheng, W. et al., 2010. A simple PDMS-based microfluidic channel design that removes bubbles for long-term on-chip culture of mammalian cells. *Lab on a chip*, 10(21), pp.2906–10.

Zhou, Y. & Danbolt, N.C., 2014. Glutamate as a neurotransmitter in the healthy brain. *Journal of neural transmission (Vienna, Austria : 1996)*, 121(8), pp.799–817.

Zhu, J. et al., 2012. Physiological oxygen level is critical for modeling neuronal metabolism in vitro. *Journal of neuroscience research*, 90(2), pp.422–34.

Ziółkowska, K., Kwapiszewski, R. & Brzózka, Z., 2011. Microfluidic devices as tools for mimicking the in vivo environment. *New Journal of Chemistry*, 35(5), p.979.

Abaci, H.E. et al., 2012. Microbioreactors to manipulate oxygen tension and shear stress in the microenvironment of vascular stem and progenitor cells. *Biotechnology and applied biochemistry*, 59(2), pp.97–105.

Albutt, D.J., 2013. *Surface Chemistry Modification of Glass and Gold for Low Density Neural Cell Culture (PhD thesis)*. University of Nottingham.

Aouani, H. et al., 2009. Crucial Role of the Adhesion Layer on the Plasmonic Fluorescence Enhancement. *American Chemical Society Nano Letters*, 3(7), pp.2043–2048.

Arbuthnott, G.W. & Wickens, J., 2007. Space, time and dopamine. *Trends in neurosciences*, 30(2), pp.62–9.

Bae, A.J., Beta, C. & Bodenschatz, E., 2009. Rapid switching of chemical signals in microfluidic devices. *Lab on a chip*, 9(21), pp.3059–65.

Baigl, D., 2012. Photo-actuation of liquids for light-driven microfluidics: state of the art and perspectives. *Lab on a chip*, 12(19), pp.3637–53.

Balasubramanian, S., Revzin, A. & Simonian, A., 2006. Electrochemical Desorption of Proteins from Gold Electrode Surface. *Electroanalysis*, 18(19-20), pp.1885–1892.

Barbulovic-Nad, I., Au, S.H. & Wheeler, A.R., 2010. A microfluidic platform for complete mammalian cell culture. *Lab on a chip*, 10(12), pp.1536–42.

Bartholomeusz, D.A., Boutté, R.W. & Andrade, J.D., 2005. Xurography : Rapid Prototyping of Microstructures Using a Cutting Plotter. *Journal of Microelectromechanical Systems*, 14(6), pp.1364–1374.

References

Beta, C. et al., 2007. Flow Photolysis for Spatiotemporal Stimulation of Single Cells translocation of fluorescent fusion proteins in chemotactic. *Analytical chemistry*, 79(10), pp.3940–3944.

Bi, G. & Poo, M., 2001. S YNAPTIC M ODIFICATION BY C ORRELATED A CTIVITY : Hebb ' s Postulate Revisited. *Annual Review Neuroscience*, 24, pp.139–166.

Bi, G. & Poo, M., 1998. Synaptic Modifications in Cultured Hippocampal Neurons : Dependence on Spike Timing, Synaptic Strength, and Postsynaptic Cell Type. *The Journal of Neuroscience*, 18(24), pp.10464–10472.

Biffi, E., Piraino, F., et al., 2012. A microfluidic platform for controlled biochemical stimulation of twin neuronal networks. *Biomicrofluidics*, 6(2), pp.24106–2410610.

Biffi, E., Menegon, A., et al., 2012. Validation of long-term primary neuronal cultures and network activity through the integration of reversibly bonded microbioreactors and MEA substrates. *Biotechnology and bioengineering*, 109(1), pp.166–75.

Björklund, A. & Dunnett, S.B., 2007. Dopamine neuron systems in the brain: an update. *Trends in neurosciences*, 30(5), pp.194–202.

Bliss, T. & Lomo, T., 1973. Long-Lasting Potentiation of Synaptic Transmission in the Dentate Area of the Anaesthetised Rabbit following Stimulation of the Perforant Path. *Journal of Physiology*, (232), pp.331–356.

Breier, J.M. et al., 2010. Neural progenitor cells as models for high-throughput screens of developmental neurotoxicity: state of the science. *Neurotoxicology and teratology*, 32(1), pp.4–15.

Brewer, G.J., 1997. Isolation and culture of adult rat hippocampal neurons. *Journal of neuroscience methods*, 71(August 1996), pp.143–155.

Brewer, G.J. et al., 1993. Optimized survival of hippocampal neurons in B27-supplemented Neurobasal, a new serum-free medium combination. *Journal of neuroscience research*, 35(5), pp.567–76.

Bruus, H., 2014. ACOUSTOFLUIDICS : THEORY , SIMULATION , AND EXPERIMENT. In *18th International Conference on Miniaturized Systems for Chemistry and Life Sciences*. pp. 193–198.

Bruus, H., 2008. *Theoretical Microfluidics*, Oxford University Press.

Cate, D.M., Sip, C.G. & Folch, A., 2010. A microfluidic platform for generation of sharp gradients in open-access culture. *Biomicrofluidics*, 4(4), p.44105.

Chang, C. et al., 2014. A polydimethylsiloxane-polycarbonate hybrid microfluidic device capable of generating perpendicular chemical and oxygen gradients for cell culture studies. *Lab on a Chip*, 14, pp.3762–3772.

Chau, L., Doran, M. & Cooper-White, J., 2009. A novel multishear microdevice for studying cell mechanics. *Lab on a chip*, 9(13), pp.1897–902.

Chueh, B. et al., 2007. Leakage-Free Bonding of Porous Membranes into Layered Microfluidic Array Systems. *Analytical chemistry*, 79(9), pp.3504–3508.

Chung, B.G. et al., 2005. Human neural stem cell growth and differentiation in a gradient-generating microfluidic device. *Lab on a chip*, 5(4), pp.401–6.

Claverol-Tinturé, E. et al., 2005. Multielectrode arrays with elastomeric microstructured overlays for extracellular recordings from patterned neurons. *Journal of neural engineering*, 2(2), pp.L1–7.

Cooksey, G. a, Sip, C.G. & Folch, A., 2009. A multi-purpose microfluidic perfusion system with combinatorial choice of inputs, mixtures, gradient patterns, and flow rates. *Lab on a chip*, 9(3), pp.417–26.

Croft, W. et al., 2016. Ensemble encoding of dynamic stimuli in cellular calcium signals. *In Press*.

Delivopoulos, E., Minev, I.R. & Lacour, S., 2011. Evaluation of negative photo-patternable PDMS for the encapsulation of neural electrodes. In *5th IEEE International EMBS Conference on Neural Engineering*. pp. 490–494.

Delivopoulos, E., Murray, A.F. & Curtis, J.C., 2010. Effects of parylene-C photooxidation on serum-assisted glial and neuronal patterning. *Journal of biomedical materials research. Part A*, 94(1), pp.47–58.

Dinh, N.-D. et al., 2013. Microfluidic construction of minimalistic neuronal co-cultures. *Lab on a chip*, 13(7), pp.1402–12.

Duong, T.Q. et al., 2001. Extracellular Apparent Diffusion in Rat Brain. *Magnetic Resonance in Medicine*, 45, pp.801–810.

Eddings, M. a, Johnson, M. a & Gale, B.K., 2008. Determining the optimal PDMS–PDMS bonding technique for microfluidic devices. *Journal of Micromechanics and Microengineering*, 18(6), p.067001.

Fu, B., 2012. *A Configurable Real-Time Adaptive Imaging and Illumination System (PhD thesis)*. University of Nottingham, UK.

References

Fu, B., Pitter, M.C. & Russell, N.A., 2011. A reconfigurable real-time compressive-sampling camera for biological applications. *PloS one*, 6(10), p.e26306.

Gross, G.W., 1977. A new fixed-array multi-microelectrode system designed for long-term monitoring of extracellular single unit neuronal activity in vitro. *Neuroscience Letters*, 6(2-2), pp.101–105.

Gruart, A. et al., 2015. Functional basis of associative learning and their relationships with long-term potentiation evoked in the involved neural circuits: Lessons from studies in behaving mammals. *Neurobiology of learning and memory*, 124, pp.3–18.

Guenat, O.T. et al., 2006. Development of an Array of Ion-Selective Microelectrodes Aimed for the Monitoring of Extracellular Ionic Activities. *Analytical Chemistry*, 78(21), pp.7453–7460.

Harrison, R., 1907. Observations on the Living Developing Nerve Fiber. *Proceeding of the Society for Experimental Biology and Medicine*, 4, pp.140–143.

Hennemeyer, M. et al., 2008. Cell proliferation assays on plasma activated SU-8. *Microelectronic Engineering*, 85(5-6), pp.1298–1301.

Herzog, N. et al., 2014. RAPID DRUG DELIVERY TO IN VITRO NEURONAL CULTURES. In *18th International Conference on Minituarized Systems for Chemistry and Life Sciences*. San Antonio, Texas.

Huang, P.H. et al., 2014. TUNABLE MICROFLUIDIC PUMP ENABLED BY ACOUSTICALLY OSCILLATED SHARP-EDGES. In *18th International Conference on Miniaturized Systems for Chemistry and Life Sciences*. pp. 291–293.

Joanne Wang, C. et al., 2008. A microfluidics-based turning assay reveals complex growth cone responses to integrated gradients of substrate-bound ECM molecules and diffusible guidance cues. *Lab on a chip*, 8(2), pp.227–37.

Johnstone, A., 2011. *An Illumination System for Controlling Neural Activity (MSc thesis)*. University of Nottingham, UK.

De Jong, J., Lammertink, R.G.H. & Wessling, M., 2006. Membranes and microfluidics: a review. *Lab on a chip*, 6(9), pp.1125–39.

Kang, J.H., Um, E. & Park, J.-K., 2009a. Fabrication of a poly(dimethylsiloxane) membrane with well-defined through-holes for three-dimensional microfluidic networks. *Journal of Micromechanics and Microengineering*, 19(4), p.045027.

Kang, J.H., Um, E. & Park, J.-K., 2009b. Fabrication of a poly(dimethylsiloxane) membrane with well-defined through-holes for three-dimensional microfluidic networks. *Journal of Micromechanics and Microengineering*, 19(4), p.045027.

Kasthuri, N. et al., 2015. Saturated Reconstruction of a Volume of Neocortex. *Cell*, 162(3), pp.648–661.

Kebabian, J.W., Petzold, G.L. & Greengard, P., 1972. Dopamine-Sensitive Adenylate Cyclase in Caudate Nucleus of Rat Brain, and Its Similarity to the "Dopamine Receptor." *Proceedings of the National Academy of Sciences of the United States of America*, 69(8), pp.2145–2149.

Kim, J., Surapaneni, R. & Gale, B.K., 2009. Rapid prototyping of microfluidic systems using a PDMS/polymer tape composite. *Lab on a chip*, 9(9), pp.1290–3.

Kim, L. et al., 2007a. A practical guide to microfluidic perfusion culture of adherent mammalian cells. *Lab on a chip*, 7(6), pp.681–94.

Kim, L. et al., 2007b. A practical guide to microfluidic perfusion culture of adherent mammalian cells. *Lab on a chip*, 7(6), pp.681–94.

Kim, T., Pinelis, M. & Maharbiz, M.M., 2009. Generating steep, shear-free gradients of small molecules for cell culture. *Biomedical microdevices*, 11(1), pp.65–73.

Kim, W.R. et al., 2014. Surface-printed microdot array chips for the quantification of axonal collateral branching of a single neuron in vitro. *Lab on a chip*, 14(4), pp.799–805.

Kleinfeld, D., 1988. Controlled Outgrowth of Dissociated Neurons on Patterned Substrates. *Journal of Neuroscience*, 8(11), pp.4098–4120.

Kleinfeld, D. & Sompolinsky, H., 1988. ASSOCIATIVE NEURAL NETWORK MODEL FOR THE GENERATION OF TEMPORAL PATTERNS. *Journal of Biophysics*, 54, pp.1039–1051.

Kolnik, M., Tsimring, L.S. & Hasty, J., 2012a. Vacuum-assisted cell loading enables shear-free mammalian microfluidic culture. *Lab on a chip*, 12(22), pp.4732–7.

Kolnik, M., Tsimring, L.S. & Hasty, J., 2012b. Vacuum-assisted cell loading enables shear-free mammalian microfluidic culture. *Lab on a chip*, 12(22), pp.4732–7.

Kondo, E. et al., 2014. Microfluidic perfusion cell culture system confined in 35 mm culture dish for standard biological laboratories. *Journal of bioscience and bioengineering*, 118(3), pp.356–8.

Koschwanez, J.H., Carlson, R.H. & Meldrum, D.R., 2009. Thin PDMS films using long spin times or tert-butyl alcohol as a solvent. *PloS one*, 4(2), p.e4572.

Kuczenski, B. et al., 2009. Probing cellular dynamics with a chemical signal generator. *PloS one*, 4(3), p.e4847.

Kuczenski, B., LeDuc, P.R. & Messner, W.C., 2007. Pressure-driven spatiotemporal control of the laminar flow interface in a microfluidic network. *Lab on a chip*, 7(5), pp.647–9.

Kuffler, S., Nicholls, J., & Martin, A., 1984. *From Neuron to Brain: A Cellular Approach to the Function of the Nervous System* 2nd ed., Sunderland, Massachusetts: Sinauer Associates Inc.

Kumamoto, J. et al., 2015. Effects of medium flow on axon growth with or without nerve growth factor. *Biochemical and Biophysical Research Communications*, 465(1), pp.26–29.

Kuryoz, P.Y., Poperenko, L. V. & Kravets, V.G., 2013a. Correlation between dielectric constants and enhancement of surface plasmon resonances for thin gold films. *Physica Status Solidi (a)*, 210(11), pp.2445–2455.

Kuryoz, P.Y., Poperenko, L. V. & Kravets, V.G., 2013b. Correlation between dielectric constants and enhancement of surface plasmon resonances for thin gold films. *Physica Status Solidi (a)*, 210(11), pp.2445–2455.

Kwiat, M. et al., 2012. Highly Ordered Large-Scale Neuronal Networks of Individual Cells − Toward Single Cell to 3D Nanowire Intracellular Interfaces. *Applied Materials and Interfaces*, 4, pp.3542–3549.

Lee, J.N. et al., 2004. Compatibility of Mammalian Cells on Surfaces of Poly (dimethylsiloxane). *Langmuir*, (20), pp.11684–11691.

Lee, K., He, J. & Wang, L., 2004. Benzocyclobutene (BCB) based neural implants with microfluidic channel. *Conference proceedings : ... Annual International Conference of the IEEE Engineering in Medicine and Biology Society. IEEE Engineering in Medicine and Biology Society. Conference*, 6, pp.4326–9.

Lee, P.J. et al., 2005. Nanoliter Scale Microbioreactor Array for Quantitative Cell Biology. *Biotechnology and bioengineering*, 94(1), pp.5–14.

Levinson, H.J., 2005. *Principles of Lithography* 2nd ed. H. J. Levinson, ed., Washington: SPIE Press.

Li, C. et al., 2004. Bidirectional Modification of Presynaptic Neuronal Excitability Accompanying Spike Timing-Dependent Synaptic Plasticity. *Neuron*, 41, pp.257–268.

Li, Z. et al., 2014. Syringe-pump-induced fluctuation in all-aqueous microfluidic system implications for flow rate accuracy. *Lab on a chip*, 14(4), pp.744–9.

Lin, Y. et al., 2013. Evaluating the Diffusion Coefficient of Dopamine at the Cell Surface During Amperometric Detection: Disk vs Ring Microelectrodes. *Analytical chemistry*, 85, pp.6421–6428.

Liu, M. et al., 2013. Galanin protects against nerve injury after shear stress in primary cultured rat cortical neurons. *PloS one*, 8(5), p.e63473.

Lochovsky, C., Yasotharan, S. & Günther, A., 2012. Bubbles no more: in-plane trapping and removal of bubbles in microfluidic devices. *Lab on a chip*, 12(3), pp.595–601.

Lovchik, R.D., Tonna, N., et al., 2010. A microfluidic device for depositing and addressing two cell populations with intercellular population communication capability. *Biomedical microdevices*, 12(2), pp.275–82.

Lovchik, R.D., Bianco, F., et al., 2010. Overflow microfluidic networks for open and closed cell cultures on chip. *Analytical chemistry*, 82(9), pp.3936–42.

Lovchik, R.D., Wolf, H. & Delamarche, E., 2011. High-grade optical polydimethylsiloxane for microfluidic applications. *Biomedical microdevices*, 13(6), pp.1027–32.

Lu, C. et al., 2012. Modeling Gas Transport and Reactions in Polydimethylsiloxane. In *TOUGH Symposium 2012*.

Luo, Y. & Zare, R.N., 2008. Perforated membrane method for fabricating three-dimensional polydimethylsiloxane microfluidic devices. *Lab on a chip*, 8(10), pp.1688–94.

Lutz, C. et al., 2008. Holographic photolysis of caged neurotransmitters. *Nature Methods*, 5(9), pp.821–827.

Majumdar, D. et al., 2011. Co-culture of neurons and glia in a novel microfluidic platform. *Journal of neuroscience methods*, 196(1), pp.38–44.

Marimuthu, M. & Kim, S., 2013. Pumpless steady-flow microfluidic chip for cell culture. *Analytical biochemistry*, 437(2), pp.161–3.

Martin, S.J., Grimwood, P.D. & Morris, R.G.M., 2000. S YNAPTIC P LASTICITY AND M EMORY : An Evaluation of the Hypothesis. *Annual Review Neuroscience*, (Hebb 1949), pp.649–711.

McAdams, E. et al., 2006. Characterization of gold electrodes in phosphate buffered saline solution by impedance and noise measurements for biological applications. In *28th IEEE EMBS Annual International Conference*. pp. 4594–4597.

Melai, J. et al., 2009. The electrical conduction and dielectric strength of SU-8. *Journal of Micromechanics and Microengineering*, 19(6), p.065012.

Meyvantsson, I. & Beebe, D.J., 2008. Cell culture models in microfluidic systems. *Annual review of analytical chemistry (Palo Alto, Calif.)*, 1, pp.423–49.

Millet, L.J. et al., 2010. Guiding neuron development with planar surface gradients of substrate cues deposited using microfluidic devices. *Lab on a chip*, 10(12), pp.1525–35.

Millet, L.J. et al., 2007. Microfluidic devices for culturing primary mammalian neurons at low densities. *Lab on a chip*, 7(8), pp.987–94.

Millet, L.J. & Gillette, M.U., 2012. New perspectives on neuronal development via microfluidic environments. *Trends in neurosciences*, 35(12), pp.752–61.

Monat, C., Domachuk, P. & Eggleton, B., 2007. Integrated optofluidics : A new river of light. *Nature Photonics*, 1(February), pp.106–114.

Morel, M. et al., 2012. Concentration landscape generators for shear free dynamic chemical stimulation. *Lab on a chip*, 12(7), pp.1340–6.

Multi Channel Systems, 2014. *USB-ME64-System Manual*,

Multichannel Systems, 2014. Microelectrode Array (MEA) Manual.

Nguyen, T.D. et al., 2013. Tension-induced neurite growth in microfluidic channels. *Lab on a chip*, pp.3735–3740.

Nielsen, L.J. et al., 2010. Dual fluorescent labelling of cellulose nanocrystals for pH sensing. *Chemical communications (Cambridge, England)*, 46(47), pp.8929–31.

Nikon Instruments, 2016. Microscope Objectives for Bioscience. , p.15.

Obara, M., Szeliga, M. & Albrecht, J., 2008. Regulation of pH in the mammalian central nervous system under normal and pathological conditions: facts and hypotheses. *Neurochemistry international*, 52(6), pp.905–19.

Ou, J., Ren, C.L. & Pawliszyn, J., 2010. A simple method for preparation of macroporous polydimethylsiloxane membrane for microfluidic chip-based isoelectric focusing applications. *Analytica chimica acta*, 662(2), pp.200–5.

Palyvoda, O., Chen, C.-C. & Auner, G.W., 2007. Culturing neuron cells on electrode with self-assembly monolayer. *Biosensors & bioelectronics*, 22(9-10), pp.2346–50.

Peck, R.A. & Martyniuk, J., 1995. Toward the ultimate metal microelectrode. *Journal of Neuroscience Methods*, 63, pp.175–183.

Priest, C., 2010. Surface patterning of bonded microfluidic channels. *Biomicrofluidics*, 4(3), p.32206.

Prucker, O. et al., 1999. Photochemical Attachment of Polymer Films to Solid Surfaces via Monolayers of Benzophenone Derivatives. *Journal of the American Chemical Society*, 121(38), pp.8766–8770.

Prucker, O. & Park, I., 1999. Photolithographic structuring of surface-attached polymer monolayers. *Materials Science and Engineering C*, 8-9, pp.291–297.

Rey, H.G. et al., 2015. Single-cell recordings in the human medial temporal lobe. *Journal of anatomy*, 227(4), pp.394–408.

Rhee, S.W. et al., 2005. Patterned cell culture inside microfluidic devices. *Lab on a chip*, 5(1), pp.102–7.

Ricks, C.B. et al., 2014. Extracellular matrices, artificial neural scaffolds and the promise of neural regeneration. *Neural regeneration research*, 9(17), pp.1573–7.

Roberts, J.G. et al., 2013. *Real-Time Chemical Measurements of Dopamine Release in the Brain* N. Kabbani, ed., Totowa, NJ: Humana Press.

Robinson, D.A., 1968. The Electrical Properties of Metal Microelectrodes. *Proceedings of the IEEE*, 56(6), pp.1065–1071.

Rolston, J.D., Gross, R.E. & Potter, S.M., 2009. A low-cost multielectrode system for data acquisition enabling real-time closed-loop processing with rapid recovery from stimulation artifacts. *Frontiers in neuroengineering*, 2(July), p.12.

Samel, B., Chowdhury, M.K. & Stemme, G., 2007. The fabrication of microfluidic structures by means of full-wafer adhesive bonding using a poly(dimethylsiloxane) catalyst. *Journal of Micromechanics and Microengineering*, 17(8), pp.1710–1714.

Shameli, S.M. et al., 2011. Fully integrated PDMS/SU-8/quartz microfluidic chip with a novel macroporous poly dimethylsiloxane (PDMS) membrane for isoelectric focusing of proteins using whole-channel imaging detection. *Electrophoresis*, 32(3-4), pp.333–9.

Shi, J. et al., 2007. Patterning Biomolecules with a Water-Soluble Release and Protection Interlayer. *Langmuir*, 23, pp.11377–11380.

Shleev, S. et al., 2005. Direct electron transfer between copper-containing proteins and electrodes. *Biosensors & bioelectronics*, 20(12), pp.2517–54.

Sip, C.G., Bhattacharjee, N. & Folch, A., 2014. Microfluidic transwell inserts for generation of tissue culture-friendly gradients in well plates. *Lab on a chip*, 14(2), pp.302–14.

Suzuki, M. et al., 2014. HIGH POWER MINIATURE PUMP FOR MICRONEEDLE BASED ON THREE-STAGE SUCTION USING CAPILLARY FLOW , ELECTRO-OSMOTIC FLOW , AND SUPER ABSORBENT POLYMER. In *18th International Conference on Miniaturized Systems for Chemistry and Life Sciences*. pp. 2226–2228.

Tang, L. & Lee, N.Y., 2010. A facile route for irreversible bonding of plastic-PDMS hybrid microdevices at room temperature. *Lab on a chip*, 10(10), pp.1274–80.

Taylor, A.M. et al., 2010. Microfluidic local perfusion chambers for the visualization and manipulation of synapses. *Neuron*, 66(1), pp.57–68.

Taylor, A.M. et al., 2003. Microfluidic Multicompartment Device for Neuroscience. *Langmuir*, 19, pp.1551–1556.

Taylor, A.M. & Jeon, N.L., 2010. Micro-scale and microfluidic devices for neurobiology. *Current opinion in neurobiology*, 20(5), pp.640–7.

Théry, M., 2010. Micropatterning as a tool to decipher cell morphogenesis and functions. *Journal of cell science*, 123(Pt 24), pp.4201–13.

Thomas, C., 1972. Miniature Microelectrode Array to monitor Bioelectric Activity of Cultured Cells. *Experimental Cell Research*, 74(1), pp.61–66.

Thompson, C.S. & Abate, A.R., 2013. Adhesive-based bonding technique for PDMS microfluidic devices. *Lab on a chip*, 13(4), pp.632–5.

Toh, Y.C. & Voldman, J., 2010. MULTIPLEX MICROFLUIDIC PERFUSION IDENTIFIES SHEAR STRESS. In *14th International Conference on Miniaturized Systems for Chemistry and Life Sciences*. pp. 10–12.

Tong, Z. et al., 2015. A microfluidic neuronal platform for neuron axotomy and controlled regenerative studies. *RSC Adv.*, 5(90), pp.73457–73466.

Tovee, M.J., 1994. How fast is the speed of thought ? *Current Biology*, 4(12), pp.1125–1127.

Wang, L. et al., 2010. Chemical and physical modifications to poly(dimethylsiloxane) surfaces affect adhesion of Caco-2 cells. *Journal of biomedical materials research. Part A*, 93(4), pp.1260–71.

Wang, L. et al., 2009. Patterning bio-molecules for cell attachment at single cell levels in PDMS microfluidic chips. *Microelectronic Engineering*, 86(4-6), pp.1462–1464.

Webster, A. et al., 2007. The delivery of PEBBLE nanosensors to measure the intracellular environment. *Biochemical Society Transactions*, 35, pp.538–543.

Wheeler, B.B.C., Ieee, F. & Brewer, G.J., 2010. Designing Neural Networks in Culture. *Proceedings of the IEEE*, 98(3), pp.398–406.

Whitesides, G.M., 2002. Poly (dimethylsiloxane) as a Material for Fabricating Microfluidic Devices. *Accounts of chemical research*, 35(7), pp.491–499.

Whitesides, G.M. et al., 2001. Soft lithography in biology and biochemistry. *Annual review of biomedical engineering*, 3, pp.335–73.

Whitesides, G.M., 2006. The origins and the future of microfluidics. *Nature*, 442(7101), pp.368–73.

Wu, H.-W., Lin, C.-C. & Lee, G.-B., 2011. Stem cells in microfluidics. *Biomicrofluidics*, 5(1), p.13401.

Xu, S. et al., 2015. A rapid microfluidic technique for integrated viability determination of adherent single cells. *Analytical and bioanalytical chemistry*, 407(5), pp.1295–301.

Yagishita, S. et al., 2014. A critical time window for dopamine actions on the structural plasticity of dendritic spines. *Science*, 345(6204), pp.1616–1620.

Yamada, A. et al., 2009. A Rapid Microfluidic Switching System for Analysis at the Single Cellular Level. *IEEE Transactions on Nanobioscience*, 8(4), pp.306–311.

Yizhar, O. et al., 2011. Optogenetics in neural systems. *Neuron*, 71(1), pp.9–34.

Yoon, S.-H. & Mofrad, M.R.K., 2011. Cell adhesion and detachment on gold surfaces modified with a thiol-functionalized RGD peptide. *Biomaterials*, 32(30), pp.7286–96.

Young, E.W.K. & Beebe, D.J., 2010. Fundamentals of microfluidic cell culture in controlled microenvironments. *Chemical Society reviews*, 39(3), pp.1036–1048.

Zakaria, S. et al., 2014. The electrical breakdown of thin dielectric elastomers: thermal effects Y. Bar-Cohen, ed. , p.90562V.

Zhang, F. et al., 2006. Channelrhodopsin-2 and optical control of excitable cells. *Nature Methods*, 3(10), pp.785–792.

Zhang, Y.S. et al., 2014. A HIGHLY EFFICIENT BUBBLE TRAP FOR CONTINUOUS REMOVAL OF GAS BUBBLES FROM MICROFLUIDIC DEVICES. In *18th International Conference on Miniaturized Systems for Chemistry and Life Sciences*. pp. 730–732.

Zhang, Yulong et al., 2010. Application of SU-8 as the Insulator toward a Novel Planar Microelectrode Array for Extracellular Neural Recording. In *5th IEEE International Conference on Nano/Micro Engineered and Molecular Systems*. pp. 395–398.

Zhang, Z. et al., 2011. Sealing SU-8 microfluidic channels using PDMS. *Biomicrofluidics*, 5(4), pp.46503–465038.

Zheng, W. et al., 2010. A simple PDMS-based microfluidic channel design that removes bubbles for long-term on-chip culture of mammalian cells. *Lab on a chip*, 10(21), pp.2906–10.

Zhou, Y. & Danbolt, N.C., 2014. Glutamate as a neurotransmitter in the healthy brain. *Journal of neural transmission (Vienna, Austria : 1996)*, 121(8), pp.799–817.

Zhu, J. et al., 2012. Physiological oxygen level is critical for modeling neuronal metabolism in vitro. *Journal of neuroscience research*, 90(2), pp.422–34.

Ziółkowska, K., Kwapiszewski, R. & Brzózka, Z., 2011. Microfluidic devices as tools for mimicking the in vivo environment. *New Journal of Chemistry*, 35(5), p.979.

10 Appendices

10.1 Full consumables / equipment / software list (Chapter 2 onwards)

10.1.1 Reagents used

Name	Company	Cat. No.
Neurobasal buffer solution	Invitrogen	21103-049
Neurobasal B27 supplement	Invitrogen	17504-044
Poly-L-Lysine 0.01% (PLL)	Sigma Aldrich	P4707
Penicillin-Streptomycin	Sigma Aldrich	G1146
L-Glutamine growth factor	Sigma Aldrich	G7513
11-amino-1-undecanethiol (AUT)	Sigma Aldrich	674397
ACS grade anhydrous Ethanol	Sigma Aldrich	458-600
(3-mercaptopropyl) trimethoxysilane (MPTS)	Sigma Aldrich	175617
Anhydrous Toluene	Sigma Aldrich	244511
Fluorescein	Sigma Aldrich	F-6377
(3-Aminopropyl) trimethoxysilane (APTMS)	Sigma Aldrich	281778
(3-Glycidyloxypropyl) trimethoxysilane (GPTMS)	Sigma Aldrich	440167
Poly [dimethysiloxane-co-(3-aminopropyl)-methysiloxane]	Sigma Aldrich	480304
SU-8 2050 photoresist	Microchemicals GmbH	Ordered by physics cleanroom
SU-8 2005 photoresist	Microchemicals GmbH	
BPR100 photoresist	Shipley	
AZ6612 photoresist	Microchemicals GmbH	
AZ400K MIF developer	Microchemicals GmbH	
AZ5214E Image Reverse photoresist	Microchemicals GmbH	

10.1.2 Consumables used

Name	Company	Cat. No.
Glass coverslips 19mm, grade 1,5	Glaswarenfabrik Karl Hecht GmbH & Co KG	1001/19_15
Poly(dimethylsiloxane)	Dow Corning	Sylgard 184
Polycarbonate porous membrane 0.1µm pore x 47mm	Whatman Cyclopore	7060-4701

Silicon Wafers [100]	Pi-Kem Ltd	n/a, to order
Oxygen N2 free	BOC Gases Ltd	UN1072
Nitrogen O2 free	BOC Gases Ltd	UN1066
CO2 vapour	BOC Gases Ltd	UN1013
5% CO2 / balance room air	BOC Gases Ltd	225742
Biopsy Punch	Harris Uni-Core	0.5, 1.5, 3mm

10.1.3 **Components and equipment**

Component	**Company**	**Model / Cat. No.**
Proportional Flow valves	Clippard	EV-PM-05-6025
	IMI Norgren Ltd	12-216C-04520 +EQIFIL+BED
Relief valves	IMI Norgren Ltd	1002/BM000
HPLC PEEK bulkheads	Thames Restek	VIZBU.5FPK
HPLC PEEK tubing	Kinesis	1568 / 1572
Pressure transducers	GE Druck	PMP 5074
Flow rate sensors	Elveflow, Elvesys	Mass flow sensor 2 (7µL/min)
	Sensirion AG	SLG1430-150
Pressure regulators	IMI Norgren Ltd	RM1L-NND-NCV
	IMI Norgren Ltd	11-818-100
	Proportion-Air	QVP1TFEE015
Micro electrode arrays	Multi-Channel Systems	200/30iR-Ti
		200/30iR-Ti-gr
Spin coater	SPS Europe	Spin150
Plasma Oven	Diener	Zepto
CCD Camera	Point Grey Research	Grasshopper 2
	Hamamatsu	Orca C11440-22CU
Inverted microscope	Brunel Microscopes	SP99F
	Nikon, Tokyo	Eclipse Ti-U
Dissection microscope	Brunel Microscopes	IMXZ
Power supply	Thurlby Thandar Instruments (TTi)	TTi PL303QMD-P
Data Acquisition Card	National Instruments	USB-6259
		USB-6008 / 6009
Syringe Driver	Cole-Palmer	789210C
Temperature controller	Warner Instruments	TC-434B
Plotter Cutter	Graphtec America	Silhouette Cameo

10.1.4 **Software used**

Name	**Company**	**Version**
LabVIEW	National Instruments	2012
COMSOL Multiphysics	COMSOL	4.4
Inventor Professional	Autodesk	2013
ImageJ	National Institutes of Health	FIJI

Silhouette Studio	Silhouette America	-
MatLab	Mathworks	R2015a
Eagle PCB Design	CADSoft USA	6.1.0

10.2 **COMSOL parameters used (chapter 3.1)**

Parameter	Denoted	Value (range)	Unit
Temperature (37C)	*T*	310	K
Flow Rate Q media	*Q*	1^{-10} to 1^{-12}	m^3/s
Density saltwater at 37C	*rho*	1019.2	Kg/m^3
Dynamic viscosity saltwater at 37C	*mu*	0.000749	Pa*s
Diffusion coefficient for dopamine in free media at 37C	*Ddopa*	6^{-10}	m^2/s
Diffusion coefficient for fluorescein in free media	*Dfluor*	3.7E-10	m^2/s
Backpressure	*Pback*	70	mbar

10.3 **Regression parameters (section 5.2.1.3)**

Ln (ω)	***Ln ($\bar{H}$)***
6.907	4.174
7.313	3.689
7.601	3.219

Table 23 Logarithmic values for parameters from Table 11

If $\ln \omega$ is denoted X and $\ln \bar{H}$ is denoted Y then

$$\bar{Y} = \alpha . \bar{X} + \ln k \qquad [30]$$

and

$$\alpha = \frac{\sum XY - (\frac{1}{n}) \sum X \sum Y}{\sum X^2 - (\frac{1}{n})(\sum X)^2} \quad [31]$$

where *n*= 3

$\sum XY$	80.28
$\sum X$	21.82
$\sum Y$	11.08
$\sum X^2$	158.97
$(\sum X)^2$	476.19
$\bar{Y}$	7.27

$\bar{X}$	3.69

Table 24 Summed products for RPM and height values

Thus α = -1.366

And $\ln k$ = 13.634; k = 834,696

$$\ln H = 13.634 - 1.366 \ln \omega \quad [32]$$

Modelling the values based on this equation:

ω (rpm)	Ln (ω)	Ln (H)	H (um)
750	6.6201	4.5844	97
1000	6.9078	4.1911	66
1250	7.1309	3.8861	49
1500	7.3132	3.6368	38
1750	7.4674	3.4261	31
2000	7.6009	3.2436	26
2250	7.7187	3.0826	22

Table 25 Modelled values for expected PDMS film height at various rpm

10.4 Hardware schematics

10.4.1 Original channel design: SU-8 geometries (section 2.4.1)

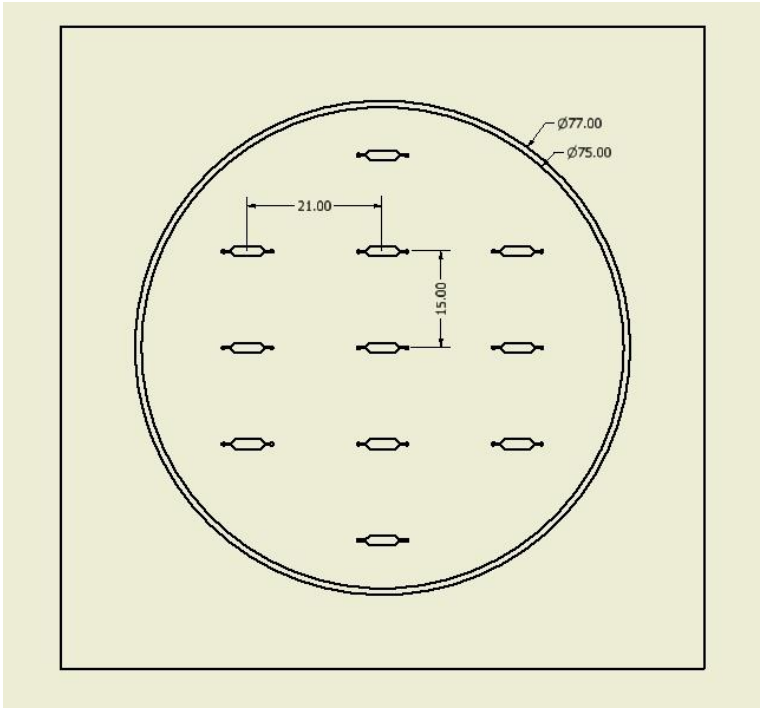

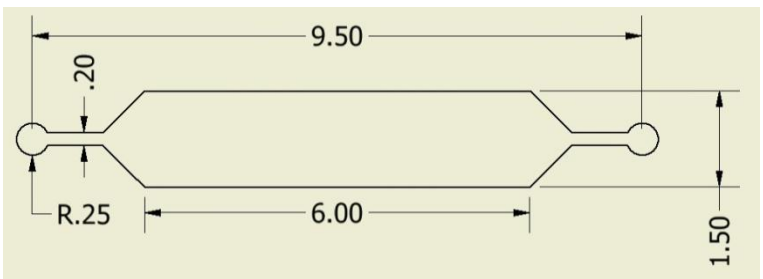

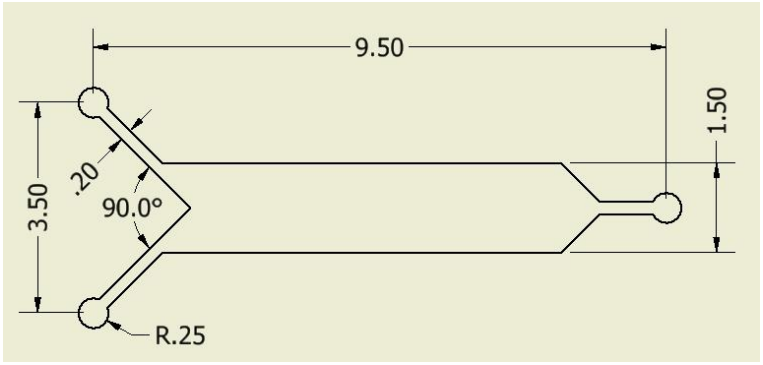

These dimensions must be converted to a photomask for subsequent photolithography

10.4.2 **Basic Xurographic geometries (section 2.5.6)**

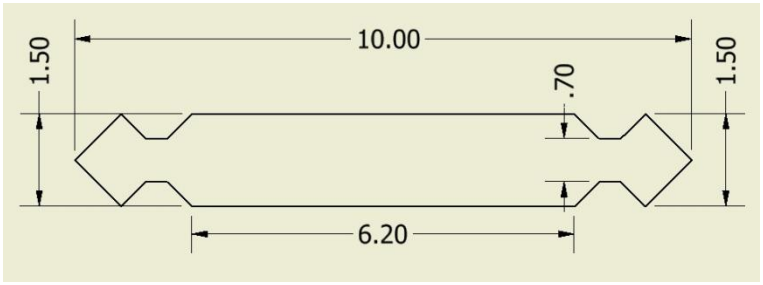

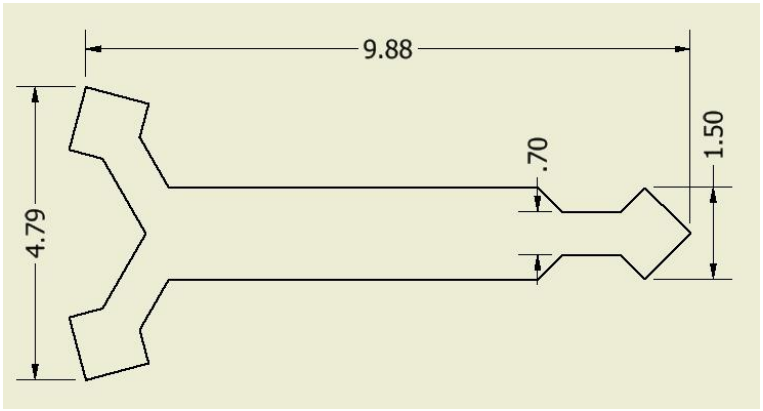

These are excised from tape layers as described in the methods section, having been designed in Autodesk Inventor and converted to .dxf format that the Silhouette Cameo can read.

10.4.3 **MEA channel mould (section 3.1.8.1)**

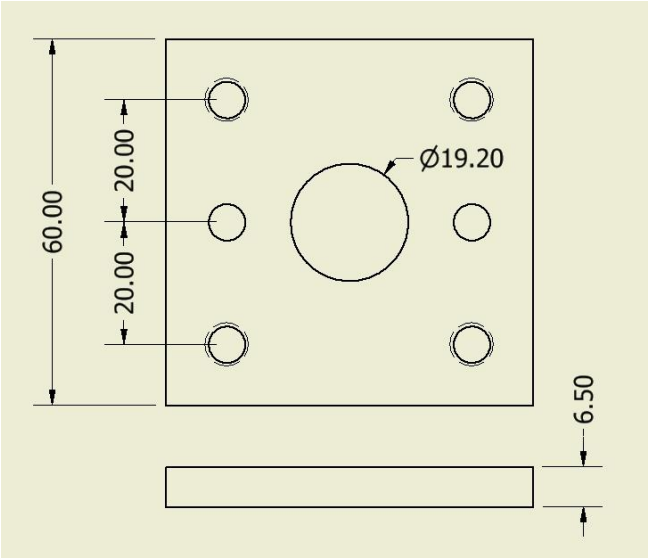

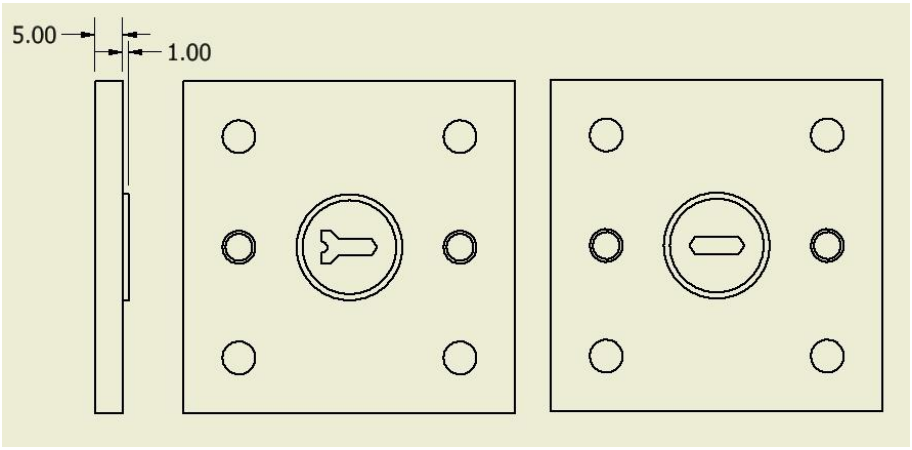

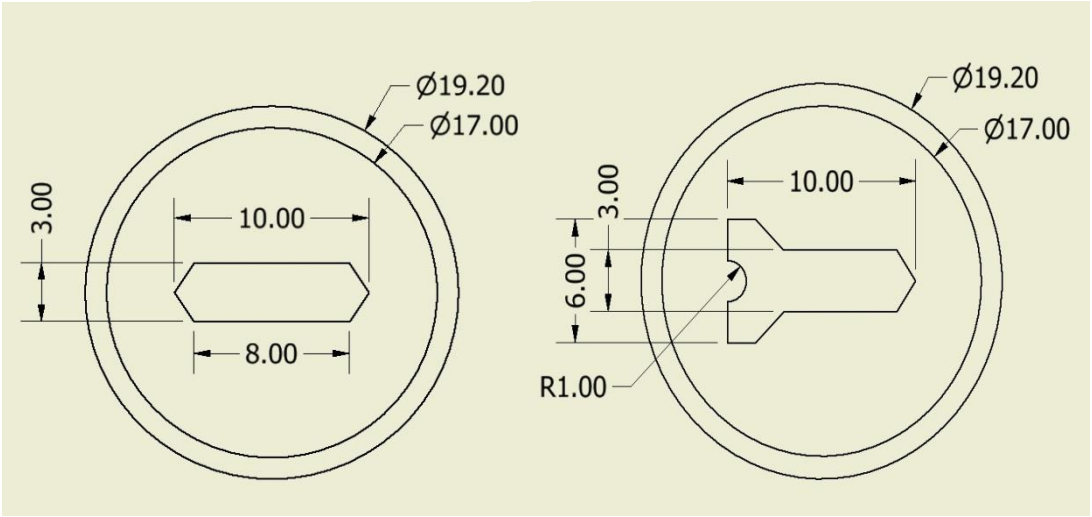

These are machined in aluminium and subsequently polished where the plates meet and where the channel surface will be in contact with PDMS.

10.4.4 Temperature clamp for coverslip microfluidic channels (section 4.5)

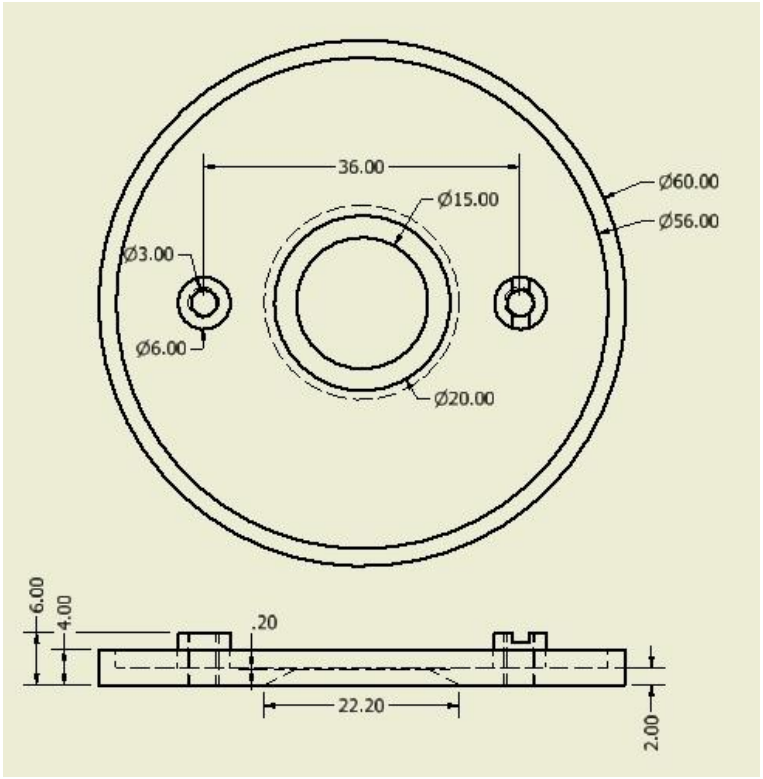

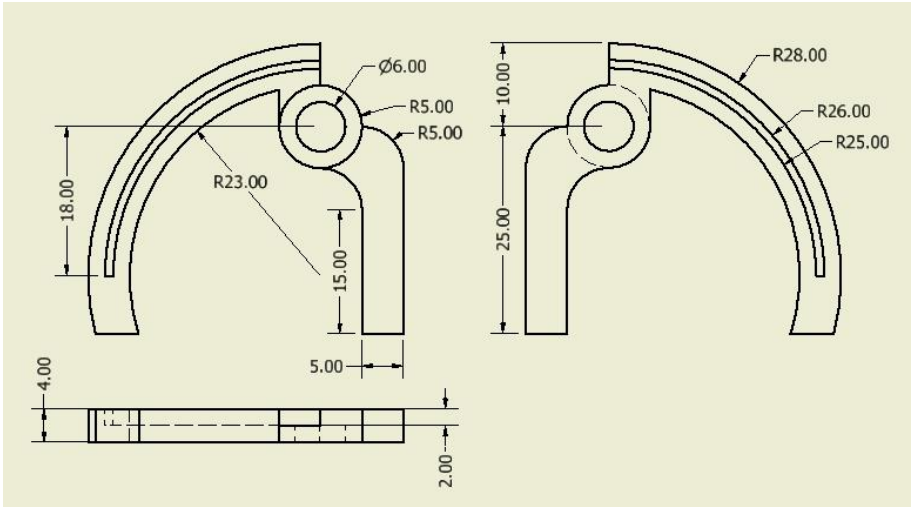

The Delrin base (top) and aluminium arms (bottom) were machined by the central Engineering Workshop

10.4.5 PCB interface with temperature clamp (7.1.4.5)

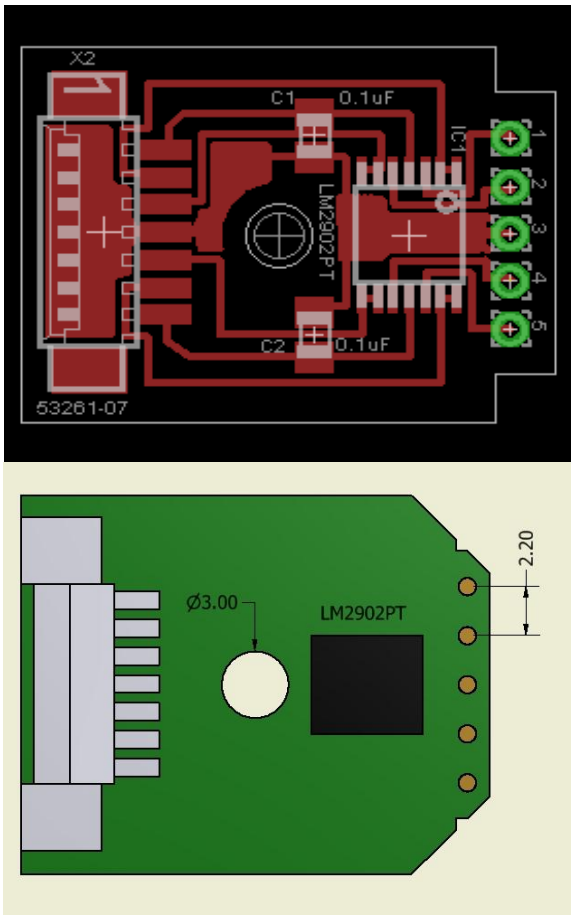

The schematic (left) was designed by Mr Gabriel Su and converted to a PCB by PCB Train™.

10.4.6 Simple photomasks: Crude spot and stripe (section 3.5.4 and section 5.1.2)

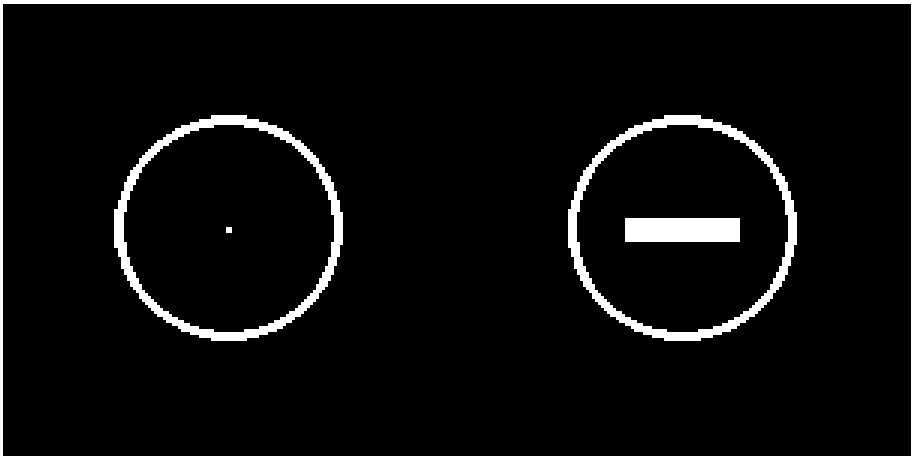

Masks made in acetate and ink; the spot is 500µm across and the stripe 3x10mm. The outer ring is 18.5mm and 19.5mm in diameter, to align with a 19mm coverslip.

10.4.7 **Original manifold schematic (section 4.4.2.3)**

Manifolds machined from Aluminium by Central Engineering Workshop

Schematics were designed with Autodesk Inventor Professional. All dimensions in mm

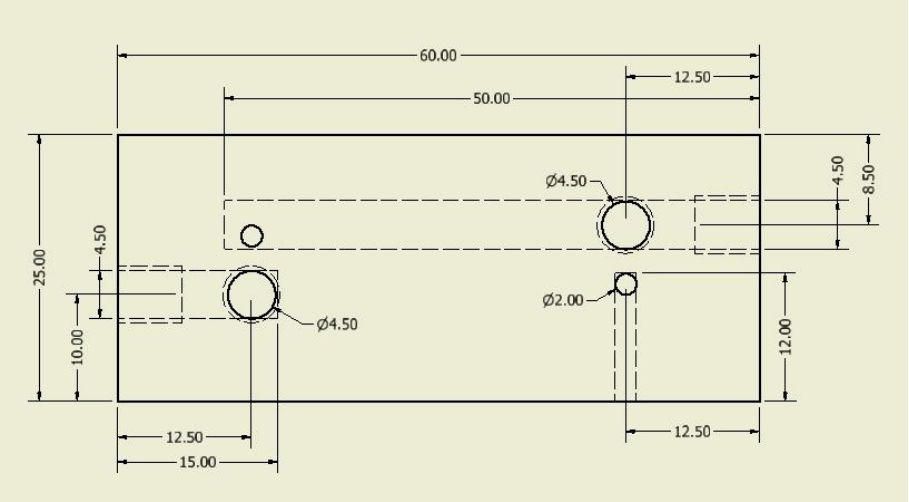

10.4.8 **Original power PCB schematic (section 4.4.2.3)**

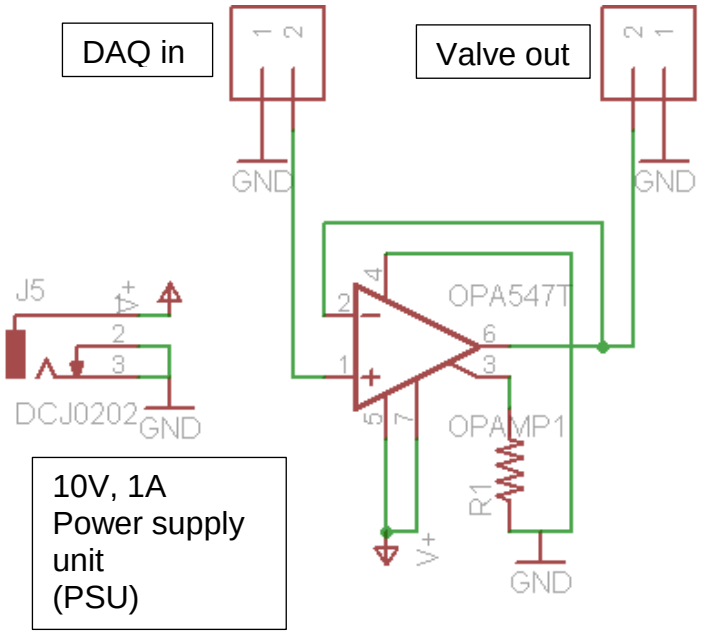

OPA547T operational amplifiers (op-amps) are used to repeat the voltage waveform from the NI USB-6008 DAQ (10mA output), and boost the output current to a level capable of actuating the Clippard EV-PM-05-6025 valves

Each manifold requires two amplifiers; there are thus 4X on the complete PCB. Each op-amp is bolted to a large form factor heat-sink, and has an external current load resistor (R1) which sets the current which can be drawn at the output. A value of 15.8kΩ was selected, for a current limit of 500mA (as each valve may draw up to 350mA, according to datasheet).

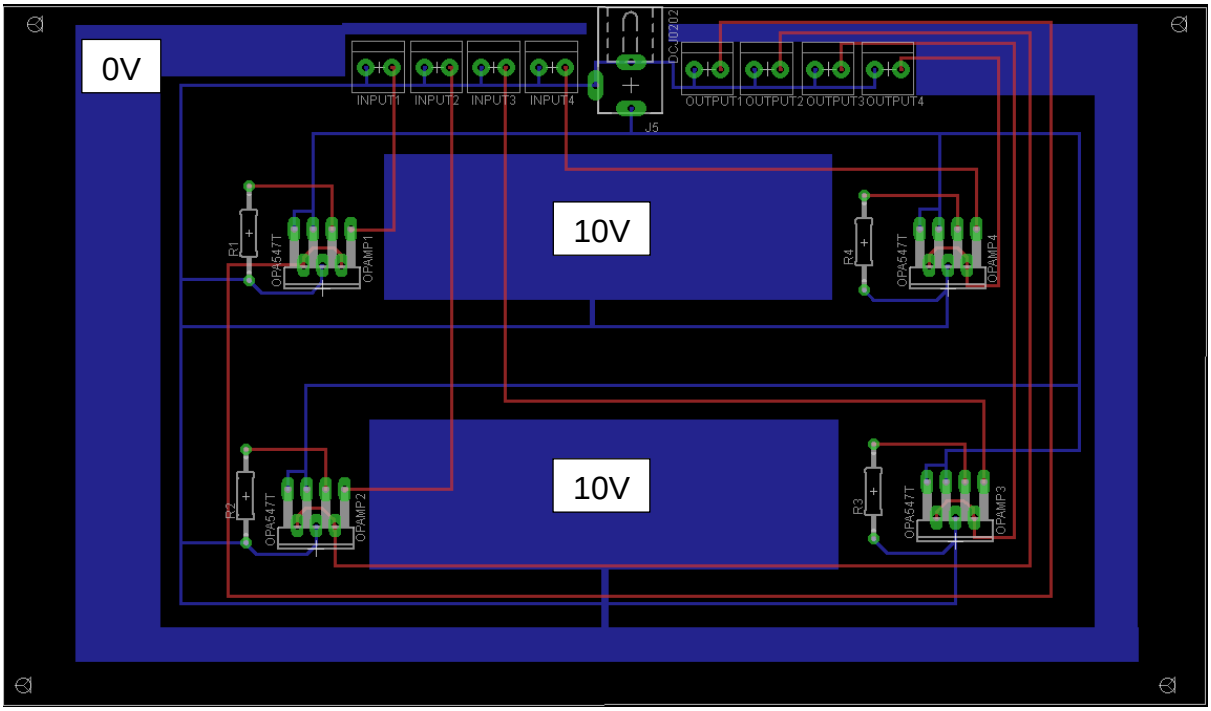

Circuit layout for a two-layer copper through-hole, rendered with Eagle PCB designer. Power planes (blue) across the entire PCB provide common reference voltages (10V and 0V) for each sub-circuit, while the signal lines (red) connect to the DAQ, valves, and load resistors.

10.4.9 Next generation manifold (Sorka Abanu) schematic (section 4.4.4.1)

Manifolds were machined from aluminium, as before. In order to accommodate the EQIFIL valves, which are a cartridge rather than screw fitting, a more complex cutting profile (Fitting D, see below) is necessary. The valves are held in place against internal pressure by M3 flathead screws, which tighten over flanges on the valve base. All dimensions are in mm.

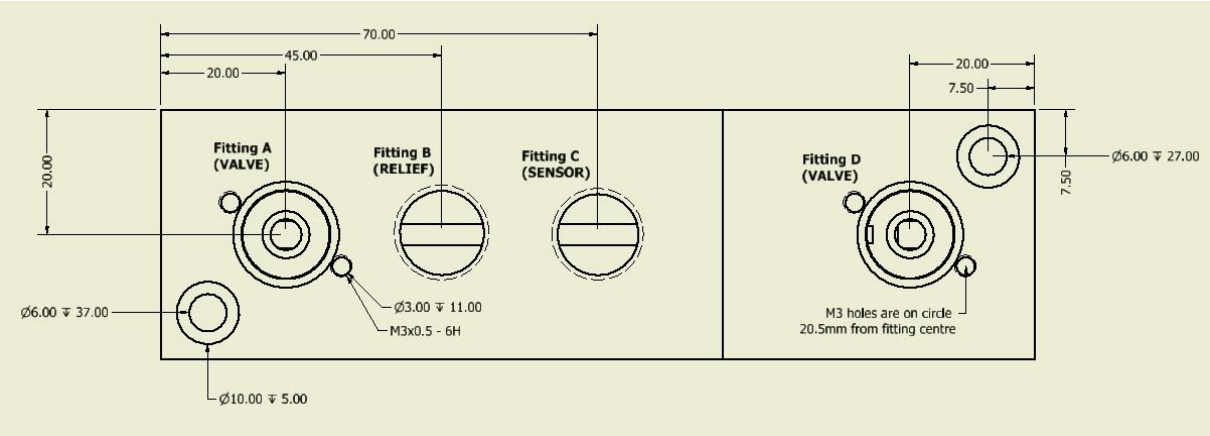

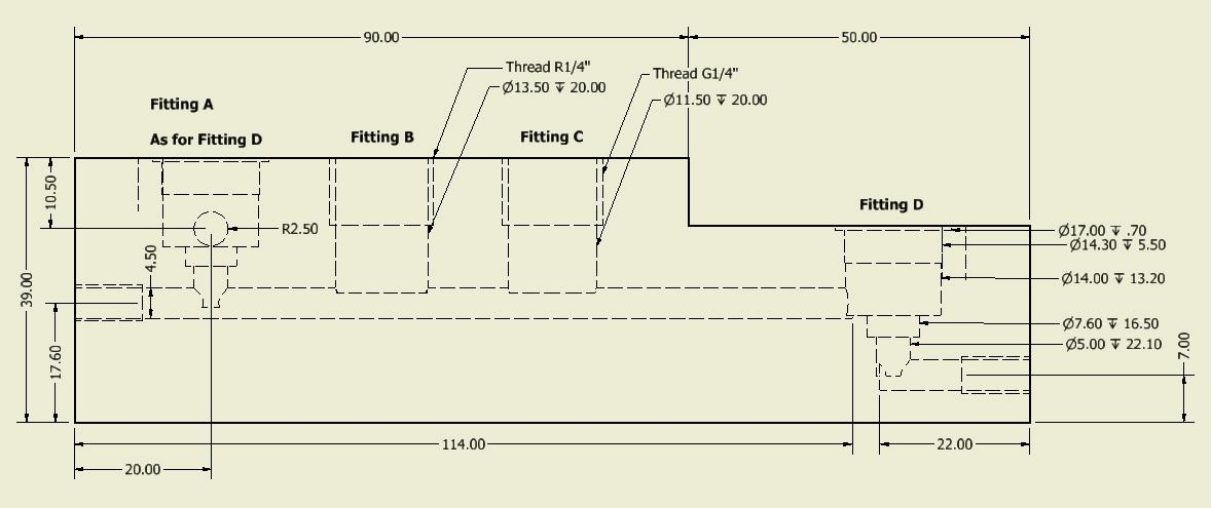

Note that the total volume of air controlled between the valves and acted upon by the pressure sensor is 9.4cm x 0.45cm diameter = 1.5cm^3 or 1.5mL.

10.4.10 **Next generation (Sorka Abanu) power PCB (section 4.4.4.1)**

Explanation of concept: the MOSFET picks up the PWM signal from the DAQ and permits the load to draw current. When the FET is off the capacitor discharges

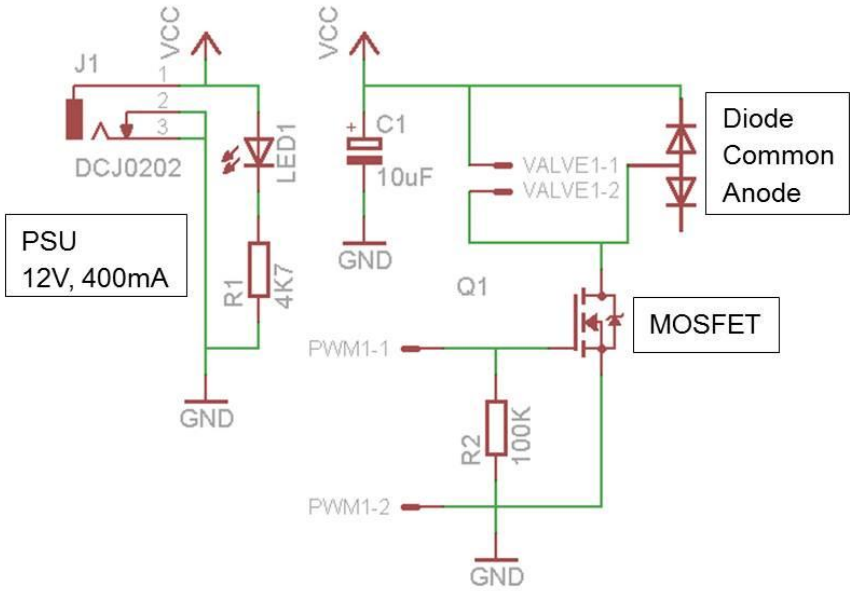

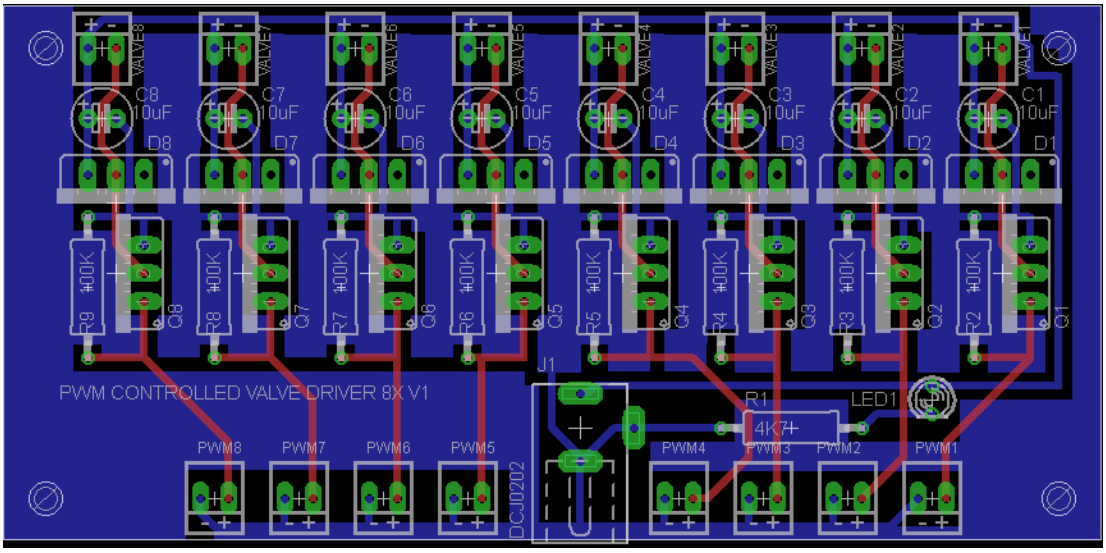

10.4.11 **Final generation manifold schematics (section 4.4.5)**

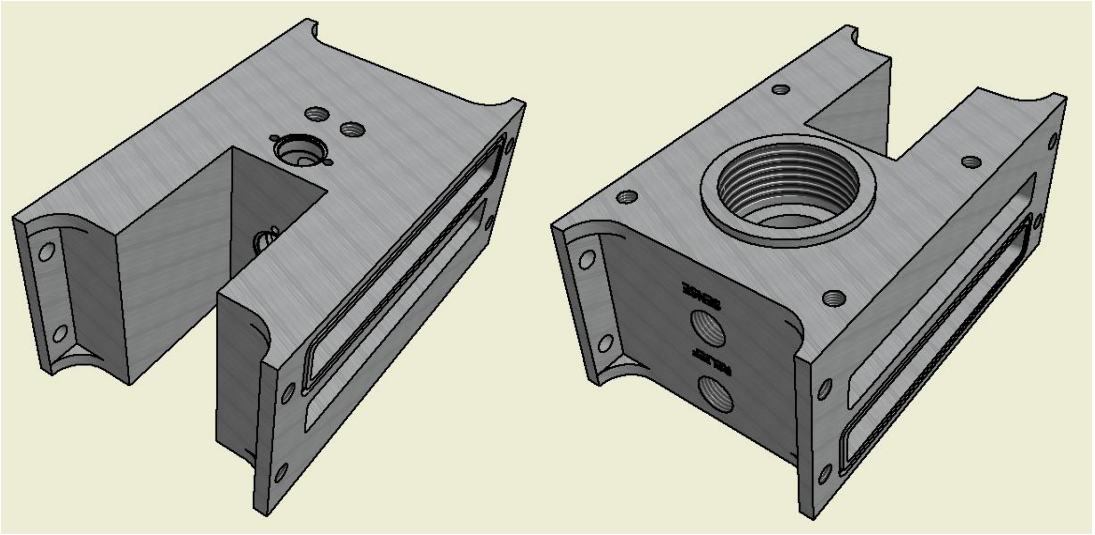

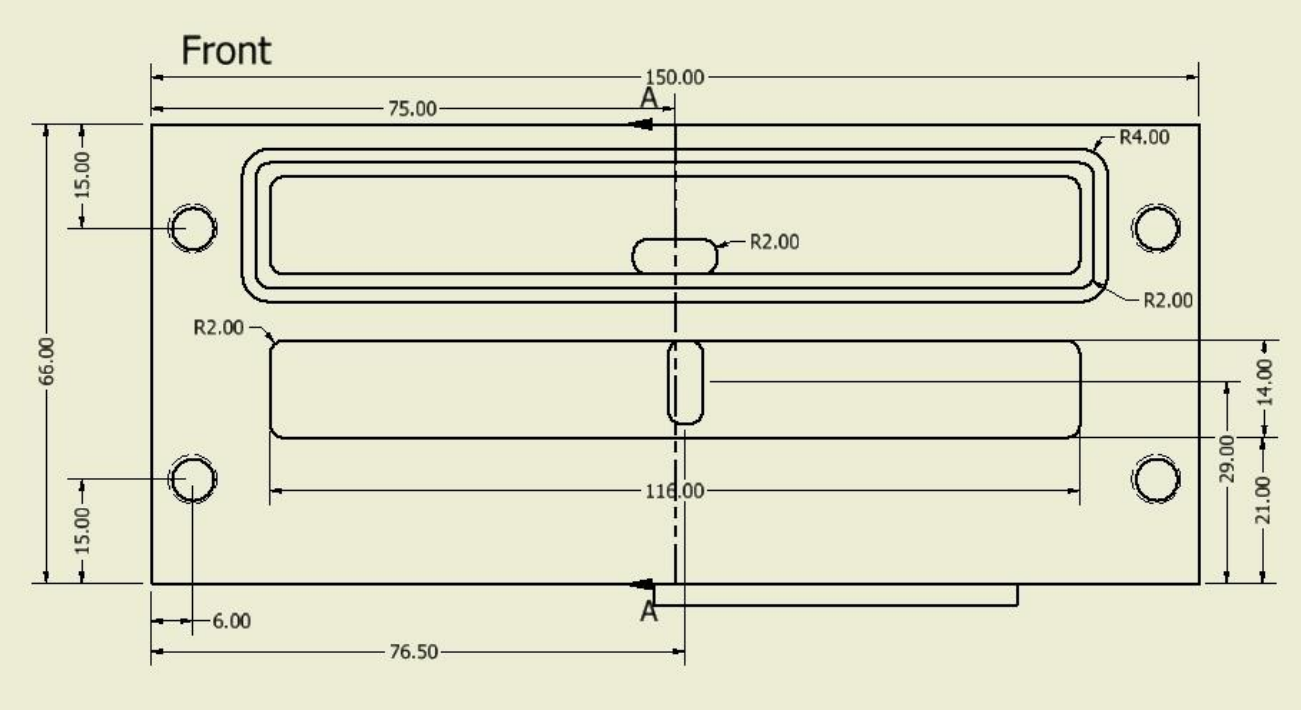

4X M6 bolts are used to clamp adjacent manifolds together, with O-rings set into the end faces of each section providing an airtight seal. The end plates for gas ingress and egress are similarly bolted on. This arrangement can in theory be expended to incorporate as many manifolds as is necessary.

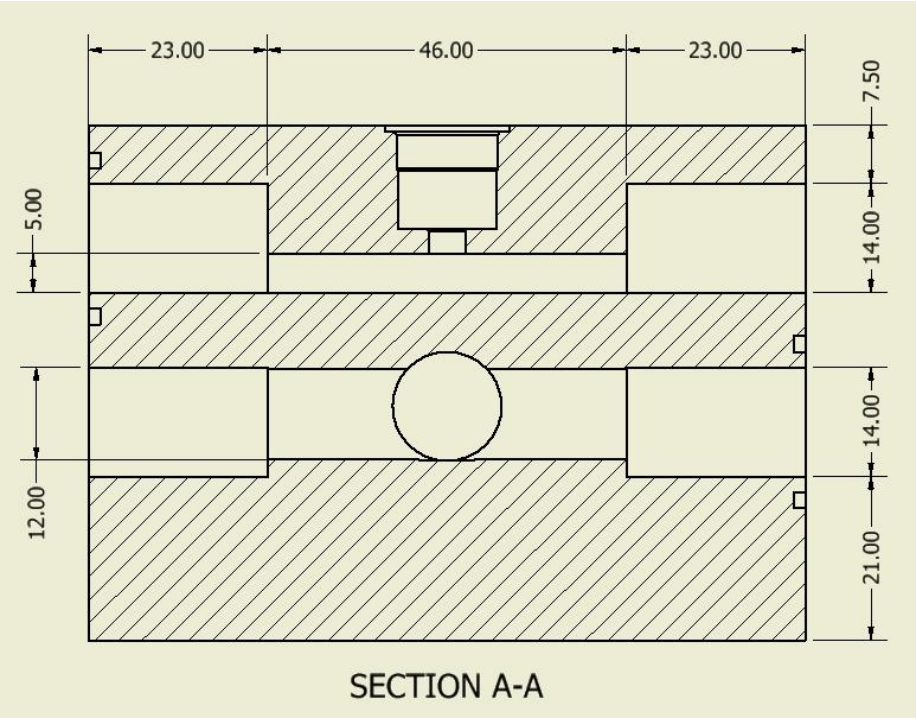

Cross section through the pressurisation valve fitting plane, showing how each valve links to the reservoirs either side and ultimately to the high and low pressure connectors

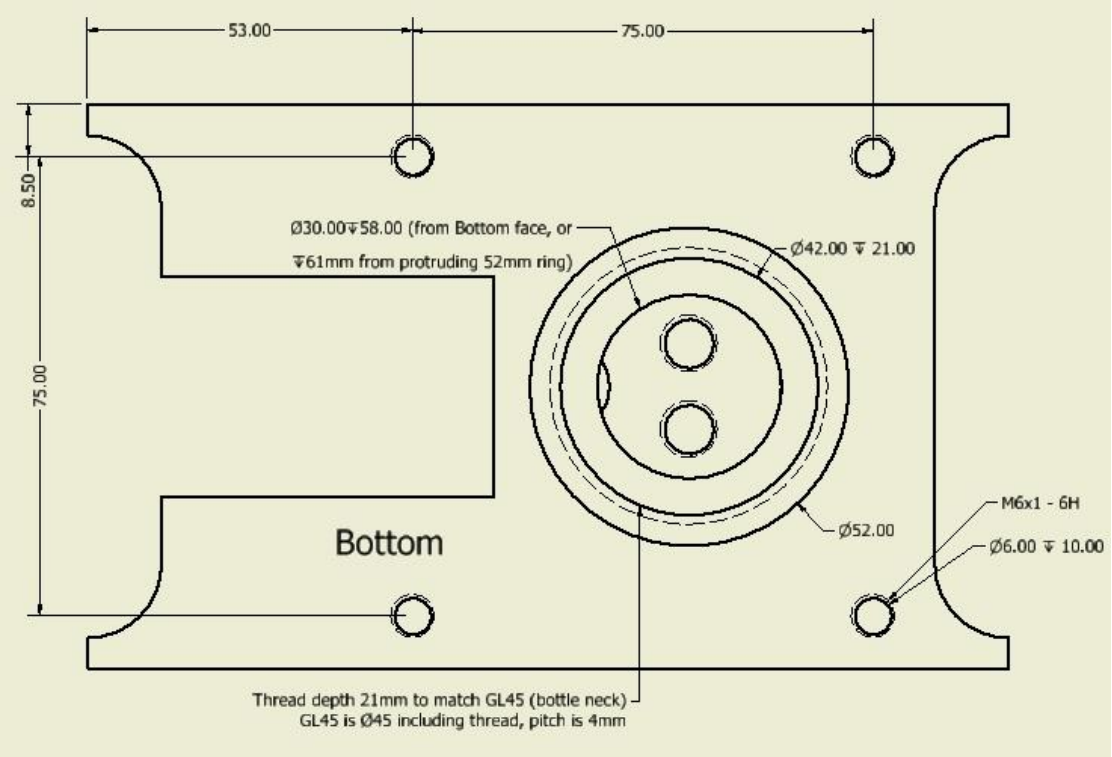

M6 holes for pillars on an *n*x25mm pitch permit the entire manifold assembly to be bolted to a standard optical breadboard, with sufficient clearance below the manifold for the pressure vessel to be readily attached and removed.

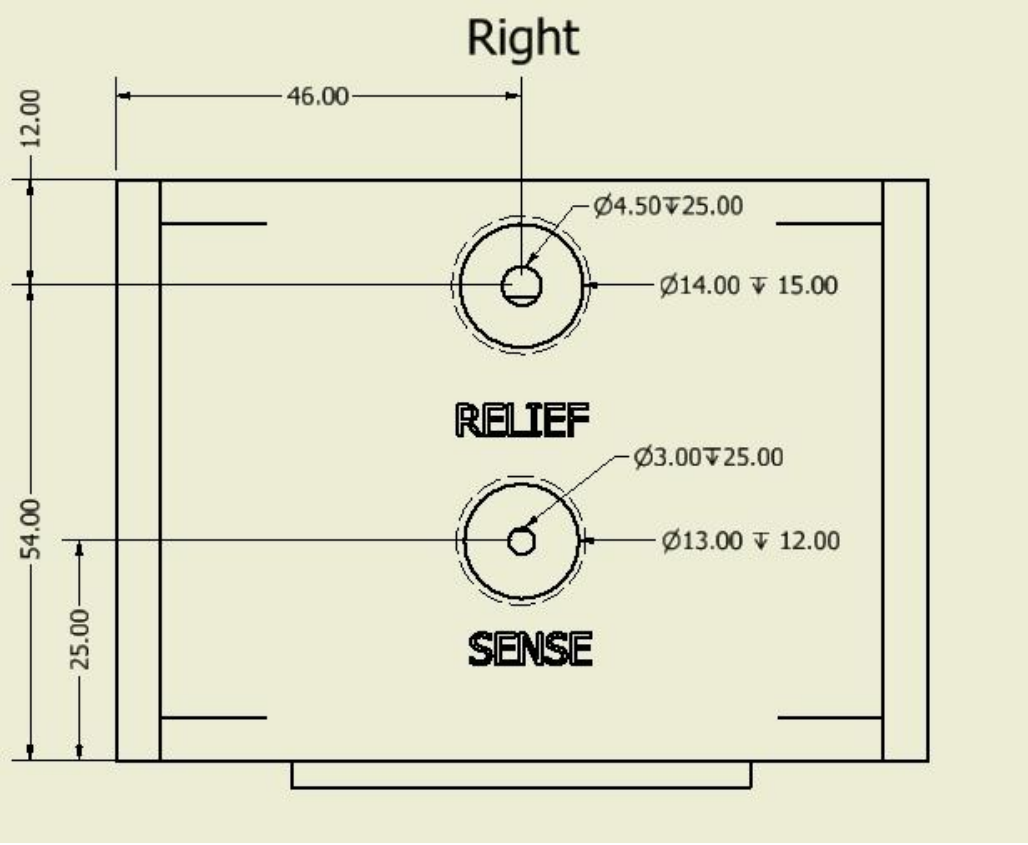

To facilitate ergonomic assembly of the screw fittings, which require a spanner to install and remove, the face for the relief and pressure sensing elements is not recessed.

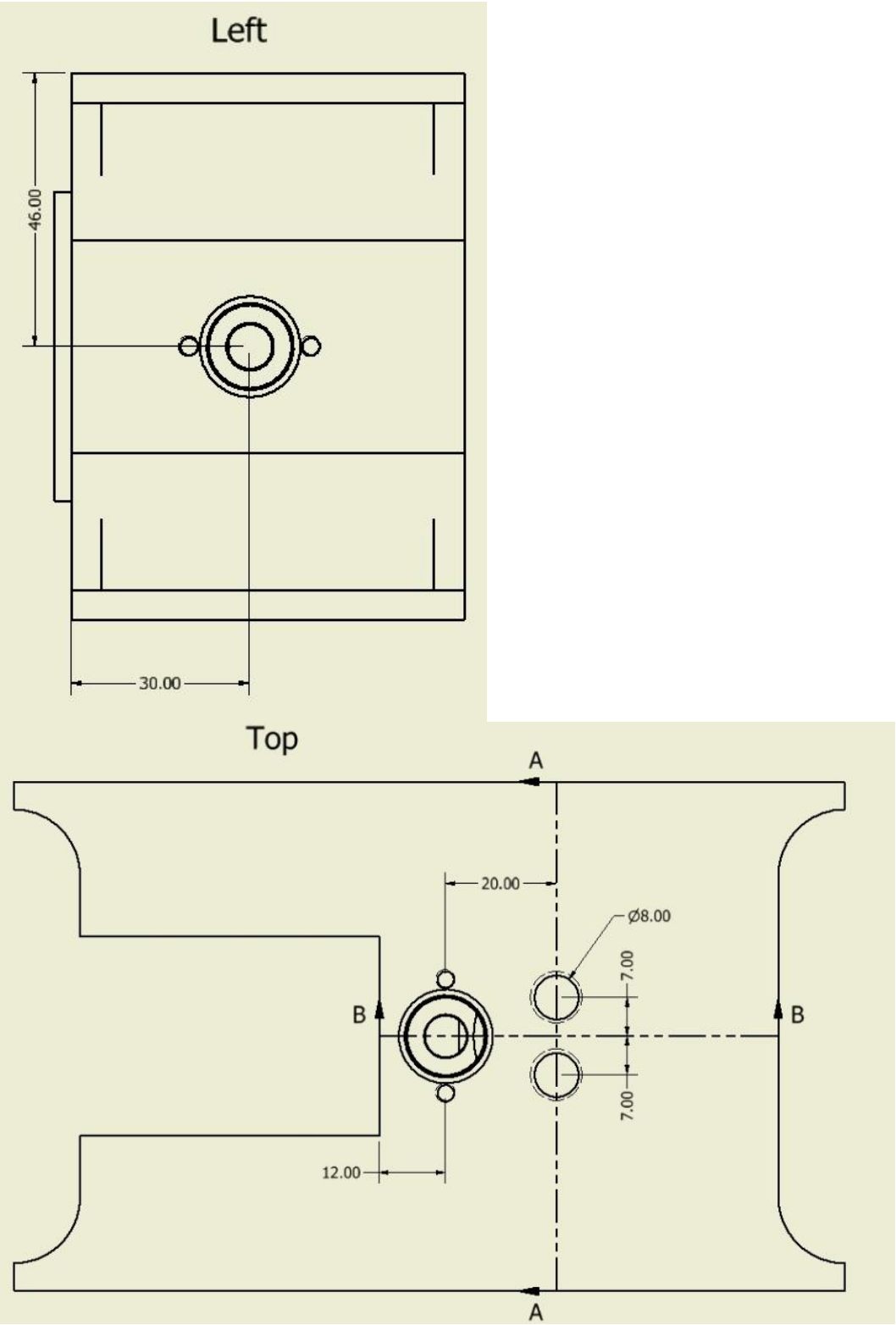

The valves (depressurisation, left, and pressurisation, top) have the same fittings as before. Two PEEK bulkheads as used with a Duran bottle lid are

directly installed into the manifold top. These can be blanked off if no flow is required, as for pressure testing.

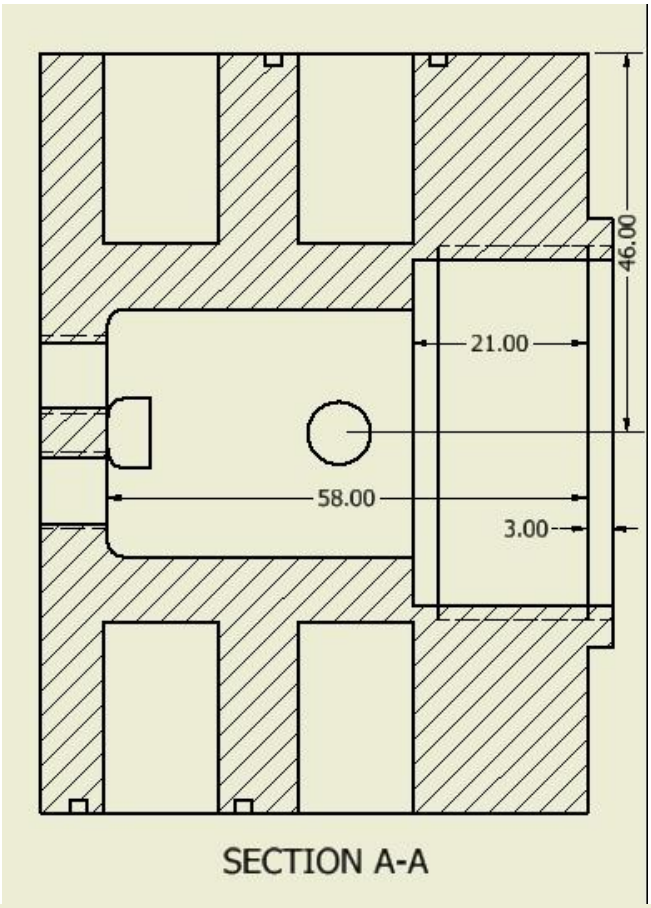

SECTION A-A

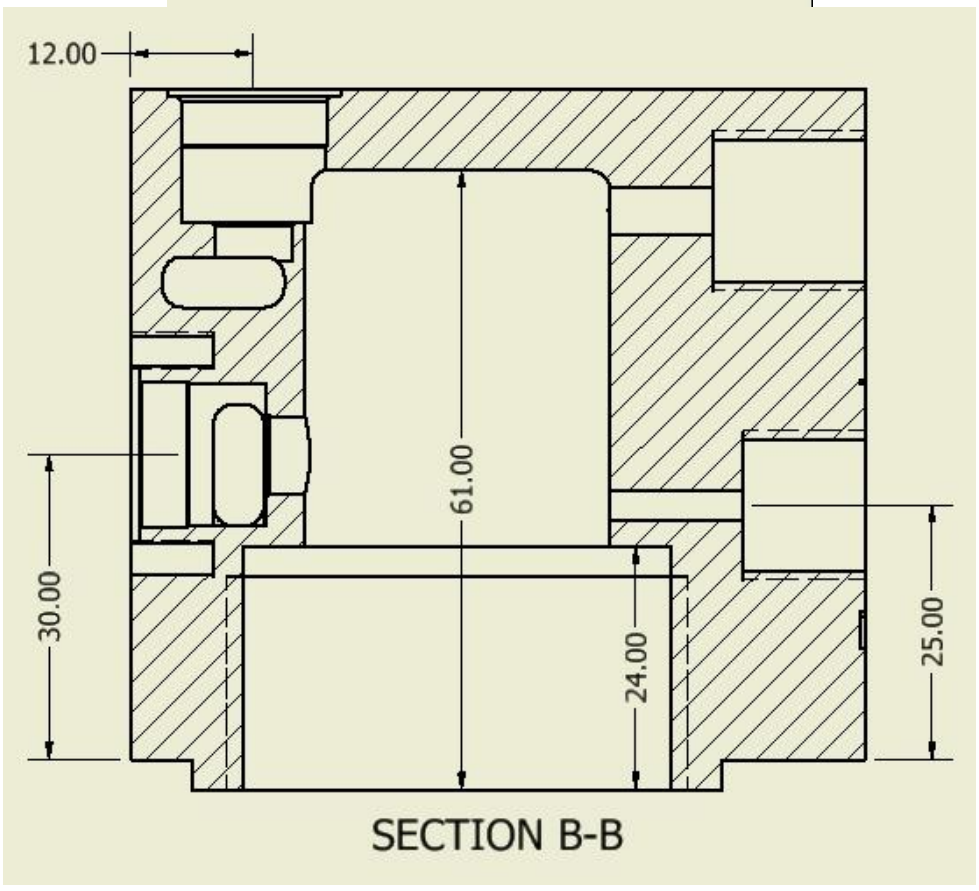

SECTION B-B

Now the minimum internal volume between the valves is the interior of the chamber (3.7cm x 3cm diameter = 26mm^3) plus the air volume in the Duran bottle (up to 100mL). This is rather larger than before, but the bottle volume is equivalent, and the time lag due to the increased chamber size is less than that induced by a two-stage system with separate manifold and pressure vessel. So the increase is useful for stability without compromising rapidity.

10.4.12 **Micro-well geometries in tape and alignment process (section 5.2.2.3)**

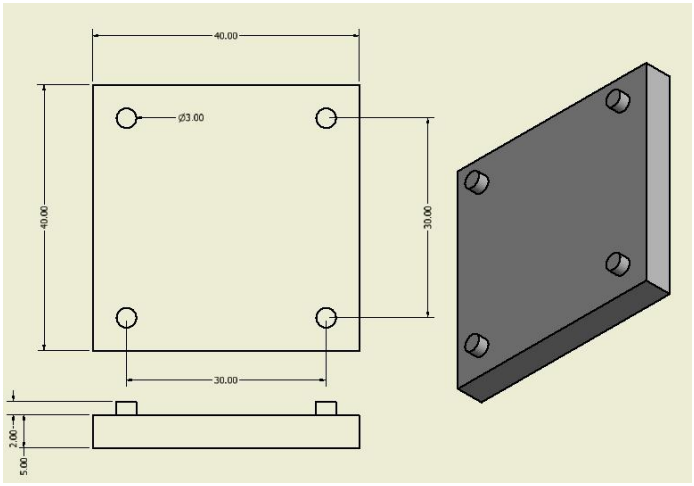

To facilitate accurate alignment of adjacent layers in excised tape, a platform with protruding 3mm pillars is used. The pillars locate each successive layer so that it can be correctly positioned with adjustment or lengthy setting up under a magnifying objective.

Every tape pattern cut has two or more 3.2 mm diameter holes which will line up with the pillars with a precision of around 0.2mm. This is not ideal but suffices for the large geometries intended. The additional diameter is to compensate for any inconsistency in cutting the compliant tape: when an exact 3mm circle is cut, the tape clashes with the pillar and assembly is not possible.

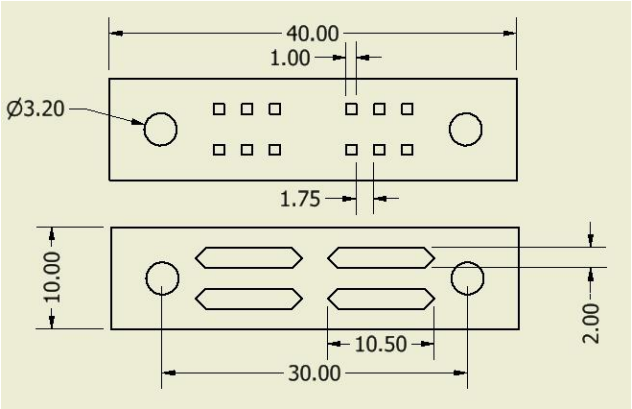

Here a set of 1x1mm wells is aligned with a typically sized cell compartment channel.

10.4.13 **Multilayer geometries for membrane inclusion (section 6.5.4.2)**

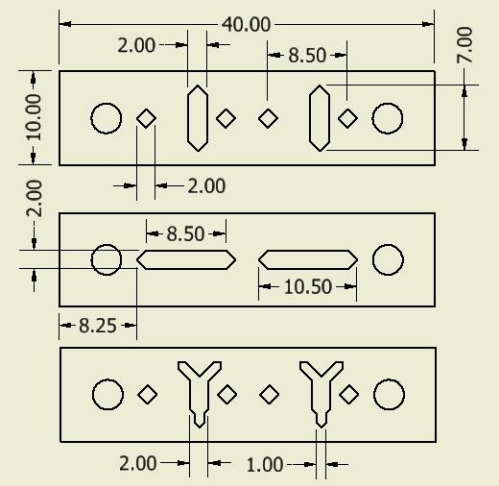

Top: A simple perfusion layer with gaps cut for connection through to the cell compartment layer (middle). Bottom: the perfusion layer can now incorporate laminar co-flows over a 2mmx2mm square, which is offset on the cell compartment to ensure it is over the MEA array.

10.4.14 **Electrode pattern photomasks and geometries (section 7.1.3)**

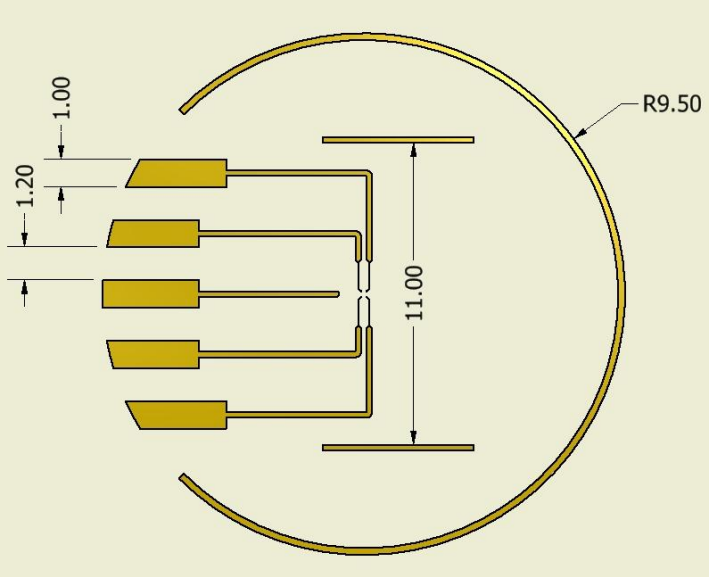

The gold planar pattern is evaporated 50nm as described in methods 2.3 and 2.4. An alignment pattern of two unconnected strips 11mm apart allows for interfacing with a PDMS block of similar dimensions, assisting in correct positioning of the microchannel.

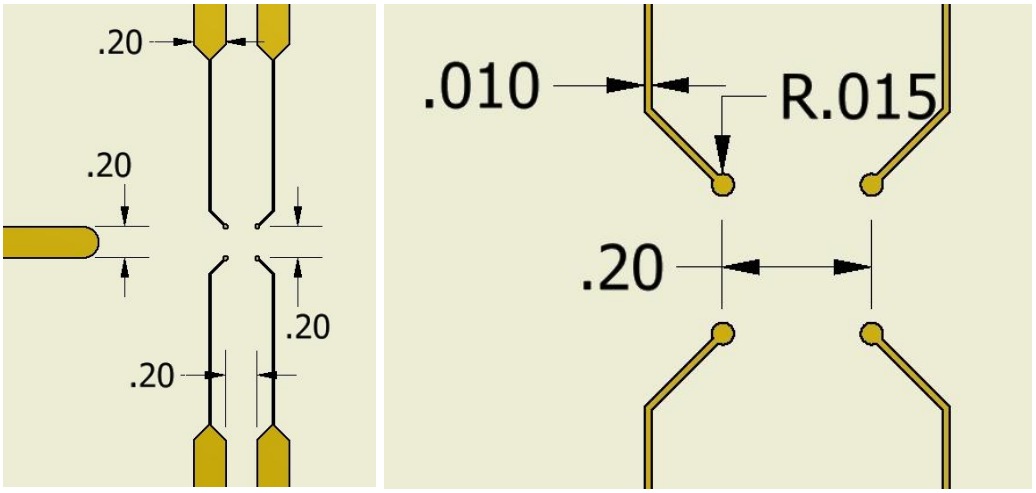

To match the electrode sizes of an MEA, the tracks are 10um across with 30um contacts in the region that will be under the channel, and are spaced 200um apart. The main tracks and reference electrode are 200um across. In retrospect it may have been better to keep the tracks thinner, so that the chance of photoresist bridging the tracks is reduced.